Flow Induced Noise from Turbulent Flow over Steps and Gaps

Matthew Ryan Catlett

Thesis submitted to the faculty of the Virginia Polytechnic Institute and State University
in partial fulfillment of the requirements for the degree of

Master of Science
in
Aerospace Engineering

William J. Devenport

Roger L. Simpson

Stewart Glegg

May 4th, 2010
Blacksburg, Virgnia

Keywords: wall jet, step noise, gap noise, surface pressure

Flow Induced Noise from Turbulent Flow over Steps and Gaps

Matthew Ryan Catlett

ABSTRACT

The existence of small surface discontinuities on a flow surface generate significant pressure fluctuations which can manifest as radiated far field sound and affect the fluctuating near wall pressure field exerted on the flow surface. A significant amount of research has been performed on various step and gap flows; however few have dealt with step heights that are small relative to the incoming boundary layer. Fewer still have been concerned with measuring the effect on the fluctuating wall pressure field or the radiated far field sound from these small surface discontinuities. This study presents the work aimed at scaling the radiated sound from small forward and backward steps, detailing the surface pressure field as a result of these steps, and detailing the far field sound radiated from gap configurations of similar dimension. These measurements were performed in the Virginia Tech Anechoic Wall Jet facility for step heights that ranged from approximately 10% to 100% of the incoming boundary layer height. The results show the influence of step height and boundary layer velocity on the far field sound from forward and backward steps. Very little directivity is seen for either source and the larger step heights considered in this study are shown to not be acoustically compact. A new mixed scaling normalization is proposed for the far field spectra from both types of step, which is shown to reliably collapse the data. Backward steps are shown to be much weaker producers of far field sound than a similarly sized forward step. The implications of this behavior are discussed with respect to the far field sound measured from various gap flows. The fluctuating wall pressure field was measured upstream and downstream of both step configurations. The data shows a slow recovery of the wall pressure field with lasting disturbances up to 100 step heights downstream of the step feature.

Acknowledgements

I want to thank my family for supporting me throughout my education. They have been there for me through all of this with their encouragement.

I will always be thankful to my advisor Dr. Devenport. My educational and professional development has progressed greatly under his direction. His work ethic and optimism are traits which I have tried to emulate and that I hope have rubbed off. I will always remember how he has shaped me as a student.

I would additionally like to thank my committee members Dr. Simpson and Dr. Glegg for their insight and assistance in this endeavor.

I would like to thank my friends and lab partners of Lab 7. I would like to specifically thank Dr. Aurelien Borgoltz, Nathan Alexander, Matt Rasnick, Ben Worrall, and Jon Forest. They have been there to provide direction, discuss ideas, and assist with measurements; all while remaining good friends.

Lastly, I would like to acknowledge the financial support of the Office of Naval Research through grant N00014-09-1-0315.

All photos in this thesis were taken by the author.

Thank you to everyone,

Ryan Catlett

List of Symbols

c	Speed of Sound
C_f	Skin Friction Coefficient
h	Step Height
f	Frequency
P_{ref}	Reference Pressure
R	Radius of Microphone Array
Re_δ	Reynolds Number based on Boundary Layer Thickness
Re_j	Reynolds Number based on Wall Jet Nozzle Height
Re_x	Reynolds Number based on Downstream Distance from Wall Jet Nozzle
U	Velocity Component along the x-axis
u	Fluctuating Velocity Component along the x-axis
U_j	Wall Jet Nozzle Exit Velocity
U_m	Local Maximum Velocity
U^*	Friction Velocity
w_a	Width of Gap Configuration A
w_b	Width of Gap Configuration B
w_c	Width of Gap Configuration C
x	Streamwise Distance from Wall Jet Nozzle
x_r	Reattachment Length
x_s	Distance from Wall Jet Nozzle Exit Plane to Step Feature
y	Normal Distance from Wall Jet Plate
$y_{1/2}$	Half Height of the Wall Jet
z	Spanwise Distance from Centerline of Wall Jet Plate
α	Ramp Angle
β	Tilt Angle
ρ	Density of Air
δ	Boundary Layer Height
ν	Kinematic Viscosity
λ	Acoustic Wavelength
τ_w	Wall Shear Stress
ω	Angular Frequency
Θ	Momentum Thickness
θ	Observation Angle
Φ	Power Spectral Density of either Radiated Far Field Noise or Surface Pressure

List of Figures

List of Tables

CHAPTER 1. INTRODUCTION

1.1 Motivation

The turbulent boundary layer developing over any vehicle will inevitably be disturbed by discontinuities along the surface of that vehicle. These discontinuities regularly appear as steps and gaps along the surface from skin panel joints or mismatches. Whether these features are intended or not, they can be a significant source of additional pressure fluctuation on the body which can be manifested as radiated noise. Additionally, these added pressure fluctuations from discontinuous surface features heavily influence the unsteady forcing on the surface structure, as well as the interaction with surface roughness and trailing edges, which in turn also generate noise and vibration. This thesis presents a study of the flow over surface steps and gaps which examine how these features radiate noise and how they influence the unsteady pressure fluctuations on the flow surface. The work of this study was conducted in the Virginia Tech Anechoic Wall Jet, which was built in 2005 and has well defined flow characteristics as detailed in recent publications.

1.2 Literature Review

There have been a considerable number of experiments concerned with the flow over forward and backward facing steps, as well as numerous gap flows. A recommended review and compilation of the numerous studies concerned with turbulent separated flow, including step flow, is provided by Simpson (1985). The purpose of this section is not to review this complete body of literature, but to focus on the studies that attempted far field noise and wall pressure measurements as a result of these surface discontinuities. Of those who have studied flow over steps and gaps, few have considered the radiated far field noise from these configurations. Fewer still were concerned with steps that are small relative to the incoming boundary layer height or their influence at a low Mach number. A review of these experiments is needed to define the conclusions and proposed theories regarding flow induced noise and effects on the wall pressure field from steps and gaps. This selection of studies has been made because they meet part of all of these criteria.

The work of Farabee and Zoccola (1998) studied the radiated sound from flow over both a forward and backward step in a low noise wind tunnel with a directional microphone system. The step heights and freestream velocities were similar to the ones of this study. A backward step of 1.27 cm and two forward steps of 0.76 and 1.4 cm were tested at freestream velocities of 25.5 and 40.7 m/s. The flow parameters for this study are referenced from the previous work of Farabee and Casarella (1986), which will be discussed later in this review; however the boundary layer thickness was approximately 3 cm for the backward step at the slowest velocity condition. They were unable to distinguish any spectral levels above the background for their backward step. However, they were successful in attaining far field spectra above the background for both forward steps at both freestream velocities. They speculate that the radiated sound from the backward step is significantly weaker than a similarly sized forward step. This has been seen and confirmed by more recent studies. They show a weak dependence on

step height for the far field spectra of the two forward step heights considered. Additionally, they show that the far field spectra is almost uniformly shifted upward across the entire frequency range for a given step height and increasing freestream velocity. The directional microphone used in this study was positioned normal to the flow surface containing the step feature. The collected data contradicted the previous model of Howe (1989) that the noise field acted as a streamwise aligned dipole. That type of model would predict zero noise radiation normal to the flow surface, which was not borne out in this experiment. Farabee and Zoccola (1998) conclude that the source location of the noise induced by the forward facing step originates in the immediate vicinity of the step. Additionally, they show that the sound scales on the seventh power of velocity and that the streamwise distribution is slightly skewed in the upstream direction.

Jacob *et al.* (2001) studied the aerodynamics and the radiated acoustics from various backward steps in an acoustically treated plane wall jet facility. Multiple step heights were considered between 1 and 6 cm for jet exit velocities between 60 and 140 m/s. For the jet exit velocity of 130 m/s, the boundary layer height and wall jet half height are quoted as 0.88 cm and 7 cm respectively. Multiple far field microphones were used at locations forming a streamwise circular arc centered about the step. The behavior of the far field spectra is presented for these multiple observation angles showing little effects of directivity and a weak dependence on step height for a constant observation angle and local maximum velocity.

They identify the acoustic source near the edge of the step by showing this as the most turbulent region. They continue to claim the source's location as approximately two step heights downstream in the reattachment region behind the step. A scaling on velocity to the power 6.2 is presented. Lastly, the oscillations of the shear layer behind the step are claimed to not significantly affect the far field measurements.

The work of Leclercq *et al.* (2001) included studies of the aerodynamics, wall pressure field, and acoustics of a forward-backward facing step pair. This forward-backward facing step pair formed a block and was immersed in the flow through an acoustically treated channel. The freestream velocity was 50 m/s, the step height of both steps was 5 cm, and the length separating the two steps was 50 cm. The incoming boundary layer thickness is given as approximately 3.5 cm. In this configuration, they state that the flow about the forward step (the leading feature) behaves in the typical manner described in past literature. This is characterized by a smaller separation zone reaching about 0.8 h in front of the step and a larger separation zone directly behind the exposed corner of the step reaching about 3.2 h downstream. The flow accelerates over the step with a significant increase in turbulence levels being seen on top of the step. However, the flow behavior of the backward step is strongly affected by the wake and lasting perturbations of the upstream forward step. They state a reduced reattachment length downstream of the backward step (as opposed to backward step only configuration) and a modified wall pressure field showing evidence of the structures generated by the upstream forward step flow.

Their findings present the lengths of the separation zones resulting from the steps. In front of the forward step a separation bubble is formed which detaches from the 0.8 step heights ahead of the step. The separated flow above the forward step caused by the sharp corner is seen to reattach 3.2 step heights downstream. Lastly, the separated flow

behind the backward step reattaches approximately 3.5 step heights downstream. All of these values agree reasonably well with past literature, though it should be noted that reattachment lengths have been shown to depend on flow conditions and experimental configurations.

Measurements of the wall pressure field behind the forward step show elevated spectral levels directly behind the step that fall with distance downstream but persist well beyond flow reattachment. The wall pressure field behind the backward step exhibits a somewhat different behavior. Inside of the recirculation zone the wall pressure spectra is seen to have highly elevated low frequency levels and greatly reduced high frequency levels which affect the slope of the spectra. At locations outside of separation the low frequency maxima are seen to fall with downstream distance and more closely resemble the wall pressure field under a flat plate turbulent boundary layer.

Leclercq *et al.* (2001) also state that the local maximum wall pressure field levels are found at flow reattachment. Consistent with the acoustic results of Farabee and Zoccola (1998), they find that the forward step generates stronger perturbations in the flow than the backward step. This is true acoustically, but also in terms of velocity fluctuations and wall pressure fluctuation levels. Lastly, using source localization they identify the location of the acoustic source for the forward step as the immediate vicinity of the exposed corner which corresponds with the location of maximum turbulence levels.

It is understood at this time that the works of Jacob *et al.* (2001) and Leclercq *et al.* (2001) are the only two experimental studies presenting far field sound measurements from backward facing steps.

Addad *et al.* (2003) mirrored the experimental configuration of Leclercq *et al.* (2001) and performed a computational study of this arrangement. A large eddy simulation (LES) was performed over the domain which is shown to agree well with the experimental results. The acoustic source term determined by the LES was then input to an acoustic propagation computation. In contrast to the aerodynamic data, discrepancies exist between the experimental and computational sound results. The far field noise was stated to be over estimated by several dB. They state possible explanations for this; mainly discrepancies in the experimental conditions. This is notable in that computational models exist that predict the aerodynamics of step flow well, but computational models for the acoustics of these configurations is not fully developed.

Becker *et al.* (2005) studied the aerodynamics, wall pressure field, and radiated noise from a forward facing step in an anechoic wind tunnel. Three separate freestream velocities of 35, 20, and 10 m/s were studied on a 12 mm forward step. Unfortunately, no boundary layer heights or description of the incoming flow is given for the flow conditions of this study. Using a far field microphone positioned normally to the flow surface and centered on the step they register broad signal to noise ratios relative to a smooth plate (no step) background between frequencies of 1 – 10 kHz. They quote a scaling of the radiated sound on the sixth power of velocity, suggesting the behavior of a dipole. This study generally agrees with and supports the work of Farabee and Zoccola (1998), and Leclercq *et al.* (2001) in the nature of the far field spectra and the measured turbulence levels around a forward step.

By using a traversed hot-wire probe, they show the fluctuations in the velocity field in front of and behind the forward step. In this way they highlight the locations and

magnitude of the greatest velocity fluctuations generated by the step. The separated region and upstream recirculation bubble are both identified as areas of local maximum turbulence with the downstream flow separation producing the largest fluctuations.

Notably, this study also attempts a numerical approach to the flow over a forward step using a finite element analogy of Lighthill's (1952) analogy for the acoustic field and LES for the flow field. Unfortunately, the presented acoustic calculations do not align with the experimental results, despite fairly consistent predictions of the aerodynamic behavior.

The computation work of Ji and Wang (2008) concerns the radiated sound from both a forward and backward step, as well as how the fluctuating wall pressure field is affected by these discontinuous surface features. This study looks to mirror the experimental work of Farabee and Cassarella (1986), which is quite similar to the conditions of the study presented in this thesis. The Reynolds number based on step height and freestream velocity for these calculations is 21,000, and the Reynolds number based on inlet momentum thickness is 4,100. The boundary layer height at the beginning of the computational domain is 1.6 step heights. Again, LES was performed for the aerodynamics and Lighthill's acoustic analogy was used to predict the generated sound.

A reattachment length of approximately 6 step heights downstream was seen behind the backward step. The extent of the forward separation bubble and the separated region on top of the forward step was less than one step height and approximately 3 step heights, respectively. The comparison of the computed and corresponding experimental wall pressure spectra around both forward and backward steps show good agreement, with the exception of early fall off of the computed spectra at high frequency. This is identified as characteristic of LES due to limited grid resolution. Data for the fluctuating wall pressure field exhibit a slow downstream recovery away from the step for both types of step configuration.

Certain assumptions were made in the calculations performed to predict the far field sound. Quadrupole contributions were neglected, leaving only dipole behavior resulting in no radiated sound normal to the flow surface. This is in contradiction to experimental results. The assumption that the step source is acoustically compact was made, which is valid for much of the frequency range. At high frequency the acoustic wavelengths are on the order of the step heights rendering this assumption less valid. With these assumptions, predicted spectra do show similarity to the experimental results.

Higher far field spectra levels were predicted for a forward step when compared to the same size backward step across the full frequency range. While there is no direct comparison, this is consistent with past experimental data. The forward step is found to generate louder sound for two reasons. First, the acoustic source terms generated by the forward step are larger in magnitude than those for the backward step. Additionally, the source terms are located closer to the exposed corner of the step surface for the forward step than they are for the backward step. In this way, the source terms of the forward step are more heavily weighted by the Green's function. These results are in agreement with Farabee and Zoccola (1998), and Leclercq *et al.* (2001) in showing that the forward step produces stronger far field noise than a similar backward step and the nature of the wall pressure field as a result of the presence of either step feature.

The work of Farabee and Cassarella (1986) was used as a baseline in order to help chose the conditions of the current study. Their work looks at the wall pressure spectrum

measured in front of and behind a forward step and behind a backward step. The conditions for this work were a step height of 1.27 cm and a freestream velocity of approximately 25 m/s. The fluctuating wall pressure data is compared with the spectrum from an undisturbed flat plate exhibiting the spectral behavior of the wall pressure field as a result of these surface discontinuities.

Directly behind a backward step inside of the separation zone, the wall pressure spectra are seen to be elevated by as much as 20 dB at low frequency and suppressed by at least the same amount at high frequency when compared to the equilibrium spectra for a smooth wall. Downstream of flow reattachment, the elevated low and mid frequency perturbations persist while the high frequency content of the spectra returns to near equilibrium levels. These perturbations are seen to diffuse with distance downstream, appearing to return to the equilibrium levels. Elevated low frequency content was seen to remain in the wall pressure spectra behind a backward step up to the furthest measurement location of 72 step heights downstream.

For measurement locations in front of a forward step, the step is seen to have a measurable effect on the wall pressure field at 6 step heights upstream. From that location and approaching the step, the low frequency spectral levels rise and high frequency levels fall relative to the smooth wall spectra. The wall pressure spectra measured at locations behind the forward step are all elevated above the equilibrium spectra. The step spectra are seen to relax and diffuse back to the equilibrium spectra with downstream distance. High frequency collapse is witnessed at approximately 6 step heights downstream, though low frequency levels remain elevated. Up to the furthest measurement location of 36 step heights downstream, the low frequency spectral levels remain approximately 10 dB above that of the equilibrium smooth wall.

Efimtsov (1999) and Efimtsov (2000) studied the surface pressure fluctuations around a series of forward and backward facing steps which were small in comparison to the boundary layer thickness. The data set incorporates Mach numbers between 0.05 and 2.5 and step height to displacement thickness ratios of 0.1 to 1.5. The forward step data only show wall pressure measurements made in front of the step. The forward step is seen to affect the wall pressure field at up to 7 step heights upstream with the spectra becoming more pronounced as the step face is approached and measurements are taken inside of the forward separation bubble. At low frequency, the differences between the smooth wall and step spectra are seen to exceed 20 dB. Potential normalizations are presented for the surface pressure data which collapse the spectra fairly well over the wide range of conditions studied.

The backward step data show wall pressure measurements made behind the step. Measurements locations include those inside of the separated region behind the step and once the flow has reattached. At downstream distances of less than one step height the wall pressure spectra is elevated at low frequency by over 10 dB and suppressed at high frequency by as much as 20 dB when compared to a no step condition. Beneath the separated flow at approximately 3 step heights downstream, much of the wall pressure spectra over low to mid frequency are elevated by more than 10 dB and still suppressed at high frequency. The most intense pressure fluctuations are seen at 5 step heights downstream of the step with the step spectra as much as 20 dB above smooth wall conditions. Presumably this is the location of flow reattachment. Further downstream, the wall pressure spectra is seen to slowly recover back to the conditions of a smooth wall

turbulent boundary layer, though the spectra are still elevated by approximately 10 dB at 20 step heights downstream. This data is generally consistent with the trends presented by Farabee and Casarella (1986), though the flow conditions vary widely. Unfortunately, a lack of velocity data defining the boundary conditions and clarity in the presented data make direct comparison difficult.

A review of the studies concerned with radiated far field noise and the fluctuating wall pressure field around small surface steps has been presented. Numerous studies have been conducted on step flows due to their canonical relevance to separated flow; however few studies have measured the far field sound from step flows. Of these, there is little to no acoustic data for forward or backward steps that are small relative to the incoming boundary layer height and little is known about the influence of step height on the far field spectra. Therefore no clear scaling of the far field spectra exist for either forward or backward steps. Measurements of the fluctuating wall pressure field around steps are more abundant; however, again few are concerned with small steps relative to the boundary layer height which is of particular importance in this study. Additionally, there exists limited knowledge of the full downstream extent of the influence of forward or backward steps on the wall pressure field.

1.3 Objectives

This study is concerned with the radiated acoustics and influence on the fluctuating wall pressure field from surface discontinuities. The far field spectra as well as the fluctuating wall pressure field around these surface features were measured for both possible step configurations, forward and backward. In all, six step heights were considered for each configuration. The far field spectra were measured for three different gap configurations, again, each consisting of the same set of step heights. These step heights cover a broad range in terms of percentage of the incoming boundary layer thickness; from 10% to over 100%. The objectives of this study are:

- Characterize the radiated far field noise and wall pressure spectra for forward and backward steps for multiple step heights that vary between 10% to over 100% of the incoming boundary layer thickness
- Analyze how the far field and wall pressure spectra scale with step height and local maximum velocity for forward and backward step configurations
- Present and assess new far field scaling for the radiated sound from forward and backward steps
- Analyze flow reattachment downstream of backward steps in terms of reattachment length to determine its influence on the wall pressure spectra
- Characterize the far field spectra for gap configurations that incorporate the same broad set of step heights
- Determine the relationship between sound radiated from steps and gaps of similar geometry

CHAPTER 2. APPARATUS AND INSTRUMENTATION

2.1 Virginia Tech Wall Jet

Data for this study was collected in the Virginia Tech Anechoic Wall Jet Facility which is detailed in Figures 2.1 through 2.3. In this facility a Cincinnati Fan variable speed centrifugal fan with model number HP-8D20 is housed inside of a casing constructed of medium density fiberboard, MDF, and pushes air into a settling chamber consisting of acoustically treated baffles. The fan is detached from the settling chamber with the air being delivered through SSA-8 steel discharge silencer and then a large flexible hose. The acoustic baffles in the settling chamber work to prevent direct radiation of acoustic waves emanating from the fan. The settling chamber is constructed of MDF with square steel tubing along the outside for support as the settling chamber pressurizes during operation.

The air from the settling chamber is pushed through a designed contraction, variable height nozzle and out onto a flat, rectangular, 1,524 mm wide, 3,058 mm long, 9.5 mm thick aluminum plate. The wall jet plate is supported by steel framework that is secured to the cement floor of the laboratory. The nozzle dimensions were kept constant throughout this study at 12.7 mm height and 1,206 mm width. The undisturbed flow over the plate consists of a fully developed wall jet with a two dimensional core that remains some 800 mm wide and 1850 downstream of the nozzle.

The entire wall jet flow is housed inside of a removable acoustic enclosure of dimension 2.13 by 2.43 by 4.06 m. This enclosure is constructed of MDF and square steel tubing, in a similar fashion as the settling chamber. All walls and the ceiling of this enclosure are covered with acoustic foam. The side walls and ceiling are covered in 89 mm egg crate foam. The front and back walls are covered in 457 mm foam wedges. Part of this enclosure includes an acoustically treated baffle positioned above the jet exit that extends over the wall jet plate to shield far field microphones from direct jet noise produced at the nozzle exit. The baffle is covered in the same 89 mm egg crate foam as the walls of the acoustic enclosure.

The trailing edge of the wall jet plate is rounded with a plexi-glass radius with dimension of 100 mm attached in order to promote Coanda effect and to avoid edge effects that could cause scattering and noise at the end of the wall jet plate. The air from the wall jet flow exits the acoustic enclosure through space along the floor of the enclosure and diffuses into the laboratory.

A Setra 239 pressure transducer was used to determine the stagnation pressure inside of the settling chamber. The range of this transducer was $\pm$ 2.5 psid (error of $\pm$ 0.14% full scale). The resulting error in the nozzle exit velocity is $\pm$1.1%, $\pm$0.5%, and $\pm$0.3% for nozzle exit velocities of 30, 45, and 60 m/s, respectively. The settling chamber pressure minus the static pressure at the wall jet nozzle sets the wall jet nozzle velocity. A pressure port was located inside of the settling chamber and a static port was placed directly beside the wall jet nozzle exit outside of the flow. The temperature was recorded with an Omega DP80 thermistor system (error of $\pm 0.1^{o}$F) with the probe placed directly beside the wall jet nozzle exit and outside of the flow.

Figure 2.1 provides a schematic of the facility and Figure 2.2 provides a schematic more specifically of the wall jet nozzle and acoustic baffle. Figure 2.3 gives a

view from the back of the facility looking at the wall jet nozzle which also includes the dimensions of the rectangular wall jet plate.

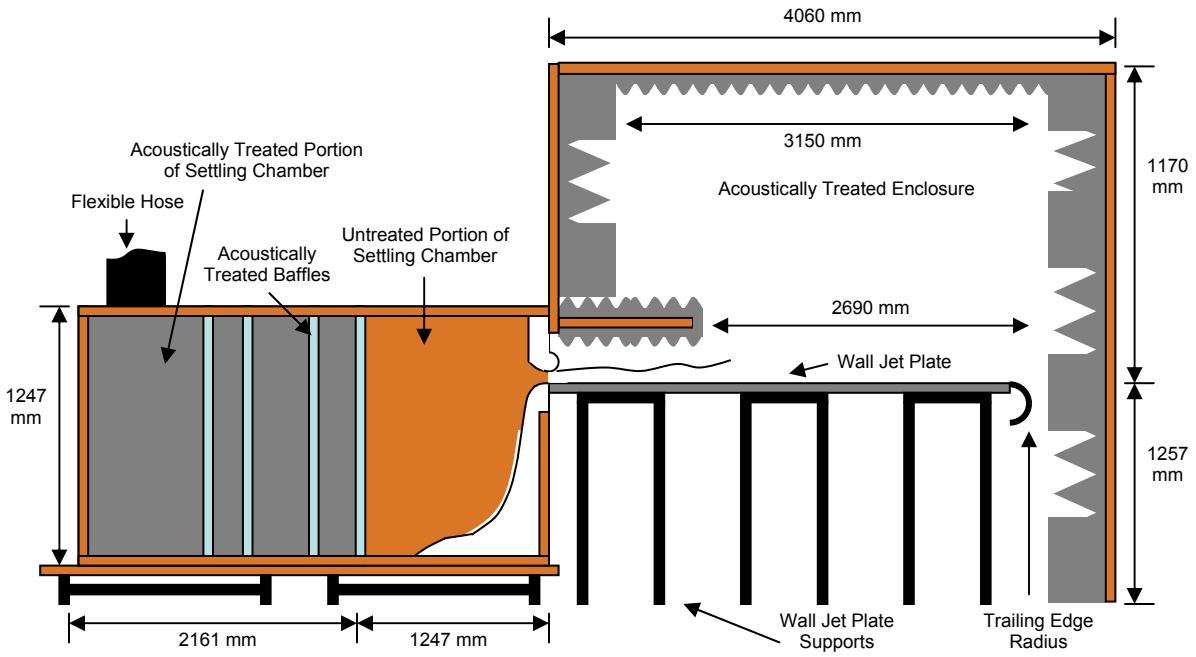

Figure 2.1. Schematic View of the Virginia Tech Anechoic Wall Jet Facility

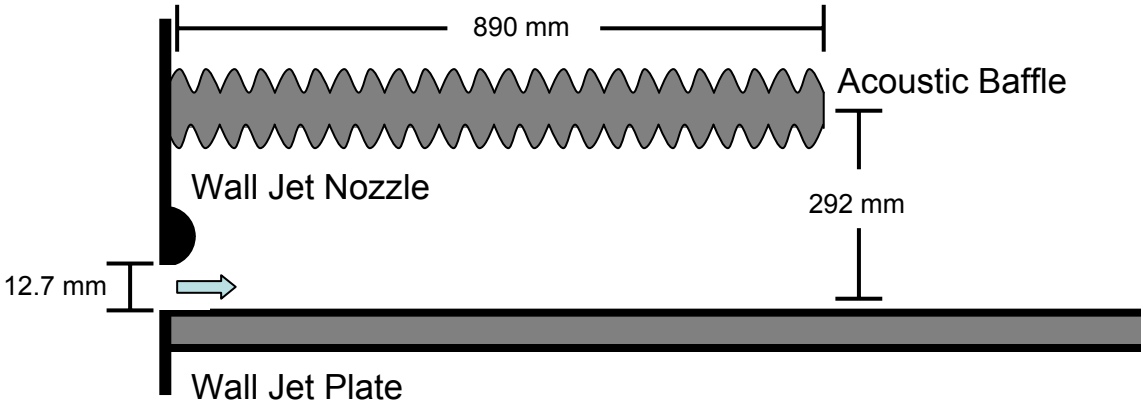

Figure 2.2. Closer Side View Schematic of the Anechoic Wall Jet Facility

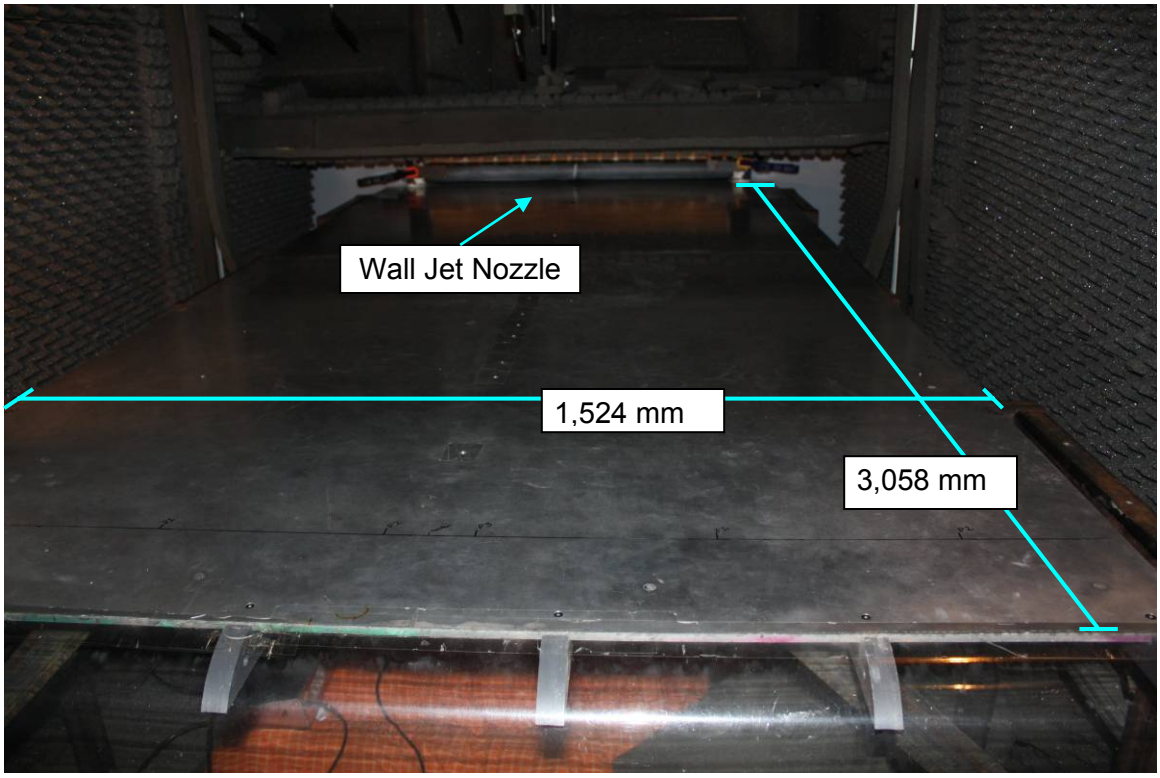

Figure 2.3. Virginia Tech Anechoic Wall Jet

The work of Grissom (2007), Grissom *et al.* (2007), and Smith *et al.* (2008) provides a detailed description of this facility's aerodynamic and acoustic characteristics. The work of Alexander *et al.* (2009) was also performed in this facility and provides additional detail into its characteristics.

A visual representation of the coordinate system adopted for this study is provided by Figure 2.4. The origin of the system is located in the plane of the wall jet nozzle at the mid span location and on the leading surface of the wall jet plate. The positive x direction is defined parallel with the flow moving downstream along the plate. The positive y coordinate is defined as being normal to the wall jet plate. Finally the positive z coordinate is in the direction dictated by a positive right handed coordinate system. The definition of the observer angle, θ, and tilt angle, β, used to define the position of the far field microphones used in this study is also presented in this figure.

Both angles θ and β are defined relative to the location of the leading feature of the step or gap being examined. The location of the leading feature of the steps or gaps, x_s, was held constant throughout this study at 1,372 mm downstream of the wall jet nozzle. The specific observer angles that were chosen for this study will be discussed later in this chapter; however the tilt angle for all of the far field microphones was kept constant at 90^o so that the microphones were normal to the centerline of the wall jet plate.

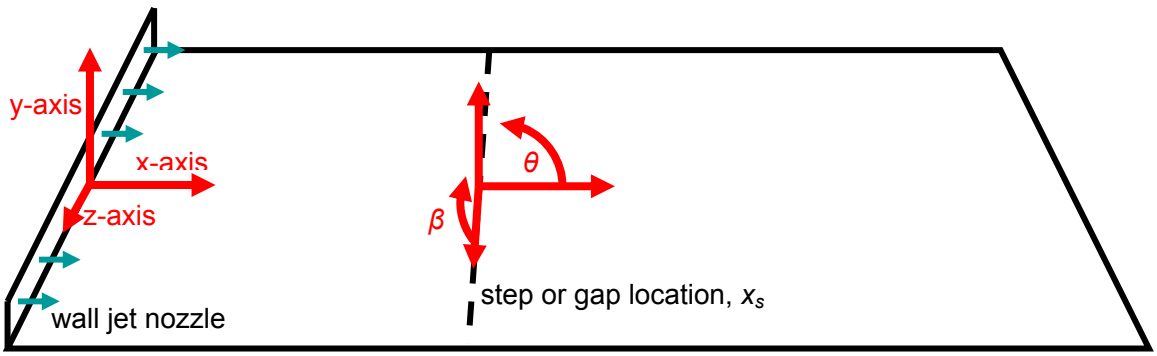

Figure 2.4. Coordinate System Utilized in the Wall Jet

2.2 Steps and Gaps

Five distinct varieties of two-dimensional step and gap configuration were examined in this study. All considered configurations were two-dimensional in that they extended across the entire span of the wall jet plate. The two possible step configurations were considered; a forward and backward step. Both of these step configurations consisted of six different step heights. The step heights considered were 1.5, 3.0, 4.6, 6.1, 11.7 and 18.0 mm. Three types of gap configuration were considered and are labeled Gap A, B and C for short. Figures 2.5 through 2.9 provide a visual depiction of all five of these configurations.

In general, all of the gap configurations are created by an 11.7 mm backward step followed by different forward steps at varying locations. The Gap A configuration places an 11.7 mm forward step at four distinct downstream locations relative to the location of the upstream backward step. These distances are 5.85, 11.7, 23.4, and 93.6 mm, corresponding to 0.5, 1, 2, and 8 step heights gap separation. Both steps that produce this gap configuration are the same height. The Gap A configuration is also referred to as the set of symmetric gaps.

The Gap B and C configurations place the full set of six forward step heights at two separate locations downstream of the backward step. Gap B corresponds to a closer forward step location of 11.7 mm downstream of the backward step (or 1 backward step height). Gap C corresponds to a further location of 93.6 mm downstream of the backward step (or 8 backward step heights). The Gap B configuration is also referred to as the set of asymmetric narrow gaps, while the Gap C configuration is also referred to as the set of asymmetric wide gaps. Figure 2.10 provides a schematic view of all of these configurations.

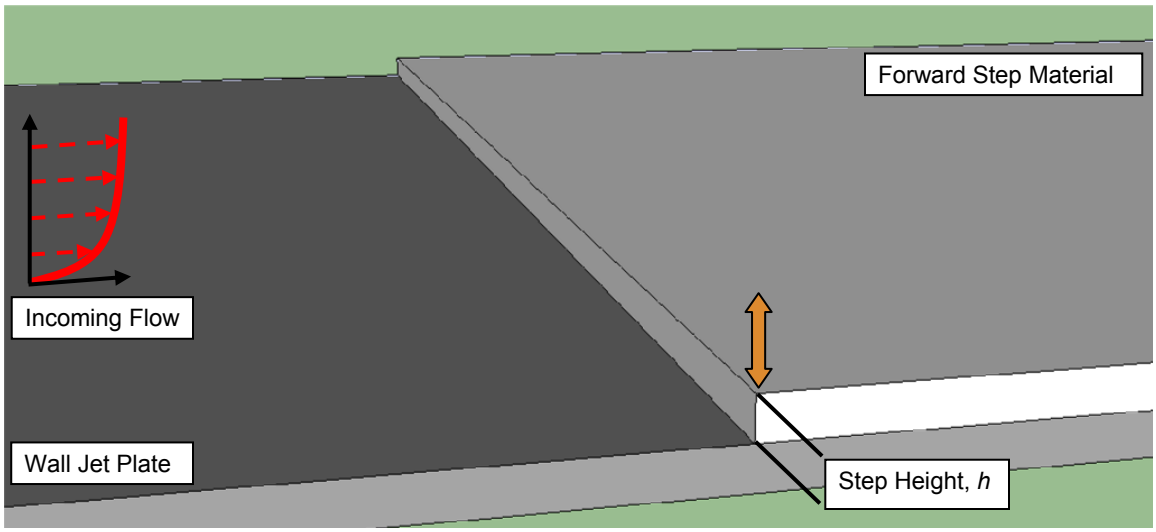

Figure 2.5. Forward Step Schematic

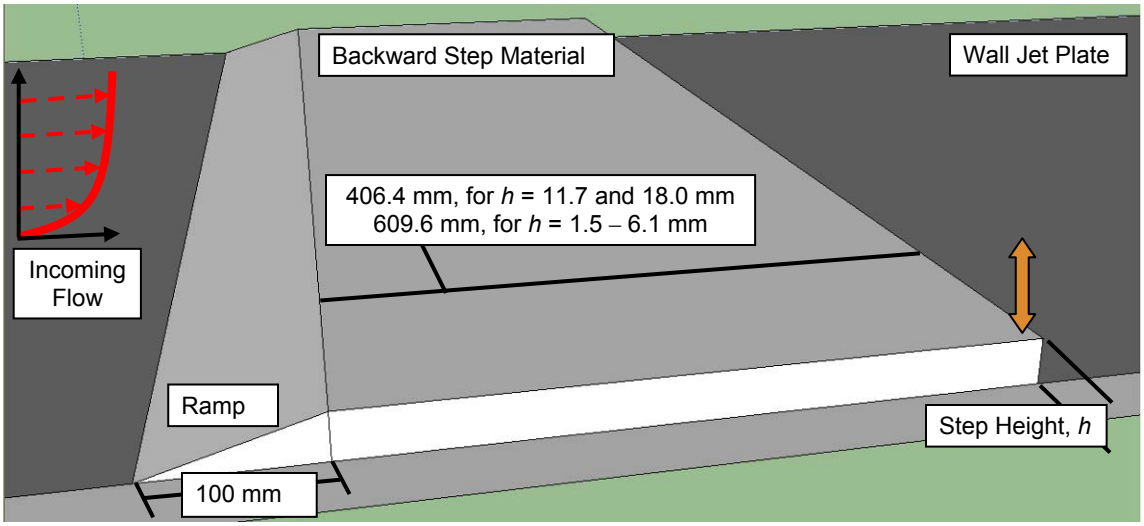

Figure 2.6. Backward Step Schematic

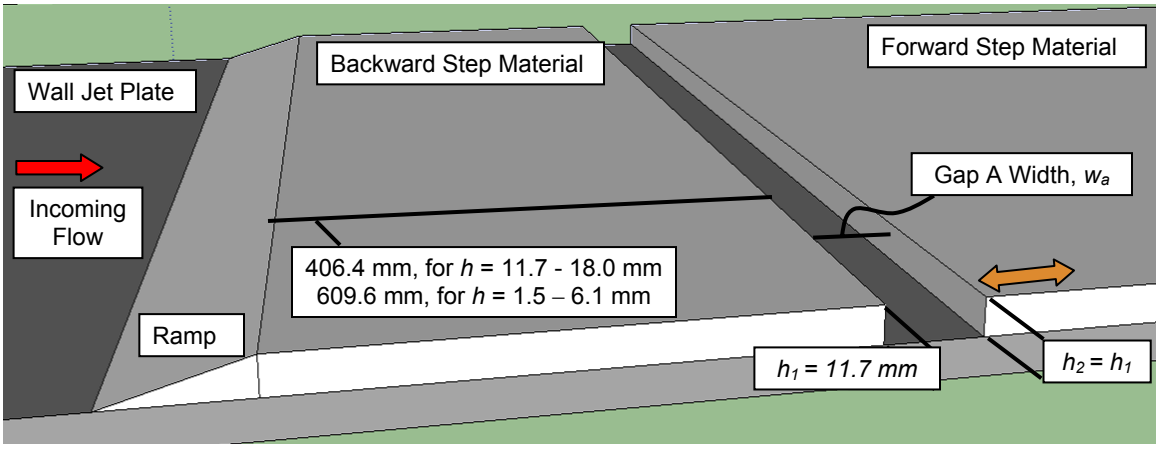

Figure 2.7. Symmetric Gap Schematic

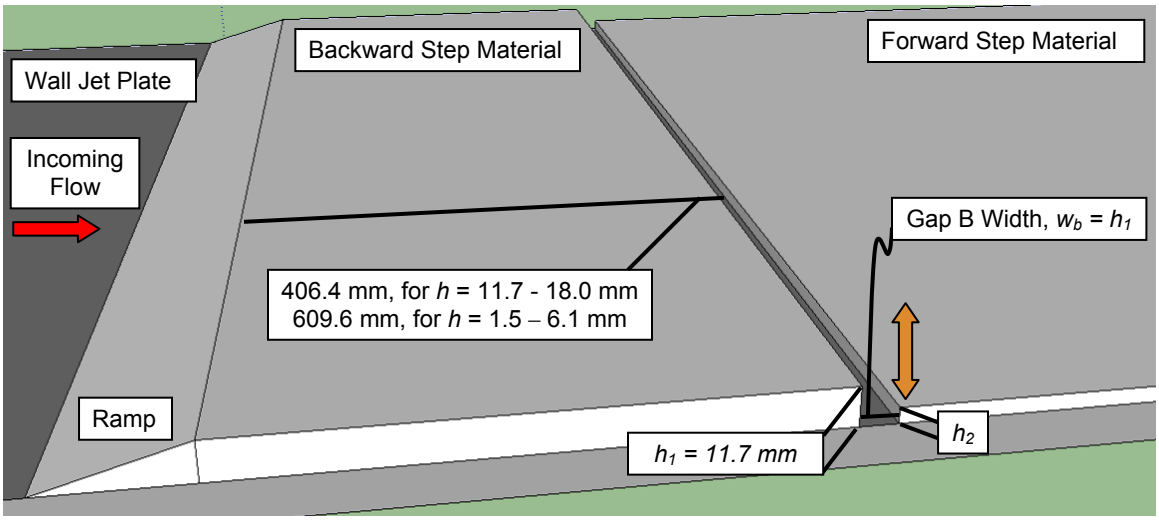

Figure 2.8. Asymmetric Narrow Gap Schematic

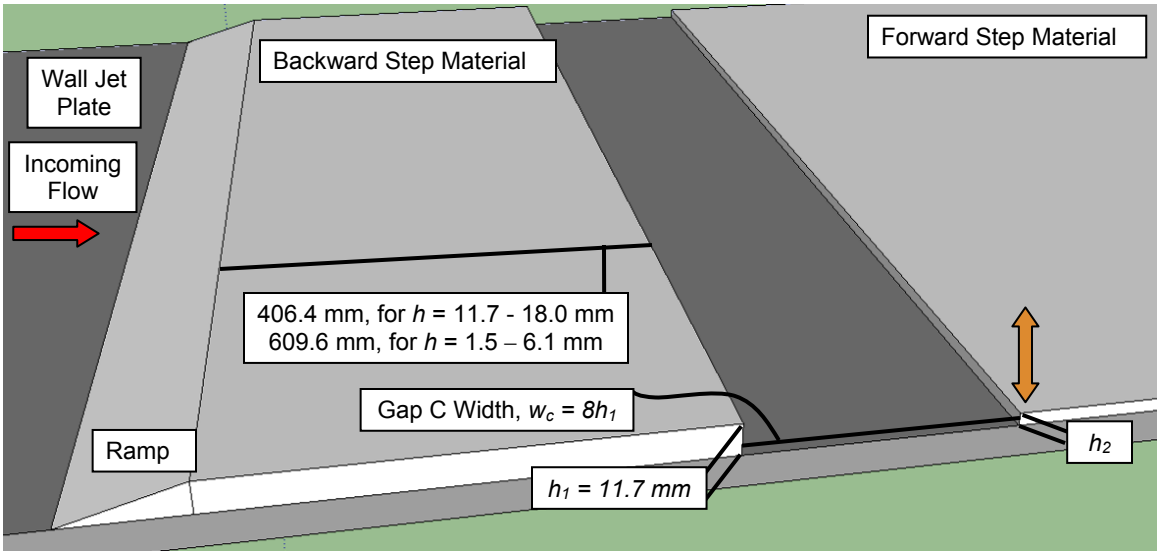

Figure 2.9. Asymmetric Wide Gap Schematic

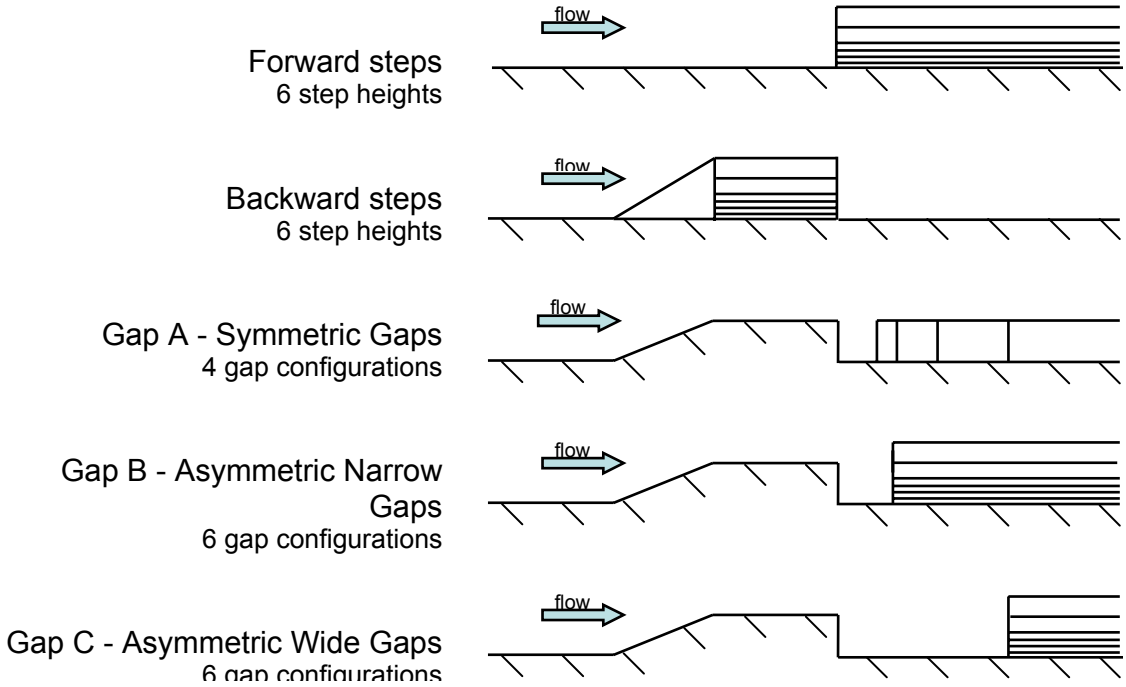

Figure 2.10. Visual Depiction of All Step and Gap Configurations

Two separate thicknesses of Lexan sheet were used to create the six different step heights used for the various step and gap configurations. Up to four thin Lexan sheets of 1.5 mm thickness were stacked on top of each other to create the forward and backward steps of 1.5, 3.0, 4.6, and 6.1 mm. The number of sheets utilized depended on the desired step height. Each of these sheets spanned the entire width of the wall jet plate and had a running length of 609.6 mm. Silicon sealant was used between each of the sheets and the sheet to plate connection across the entire edge that constituted the step. This was done

to ensure the integrity of the step feature and prevent any entrainment of the air impinging on the face of the step.

Forward and backward 11.7 mm steps were created using a Lexan sheet of the same thickness that was just slightly wider than the wall jet plate by 38.1 mm on each side. The running length of this sheet was 406.4 mm. The 18 mm forward and backward steps were created be raising this same sheet on the appropriate sized shims. Again, Silicon sealant was used to seal the Lexan to the wall jet plate and create a sealed step surface.

For all forward steps, the elevated step surface produced by the Lexan was continued from the step location to the end of the wall jet plate (some 1.7 m downstream) where it was then ramped back down to the wall jet plate. This downward ramp at the end of the plate had a height corresponding to the specific step height being tested and a running length of approximately 100 mm. It was located at the very end of the wall jet plate where the local velocity is greatly reduced by the decay of the wall jet. This position is also as far from the microphone array as possible.

Backward steps were created by placing the Lexan sheets in front of the step location with a forward ramp between the wall jet plate and the elevated surface. This ramp, fabricated from Lexan was located with its leading edge 662 mm downstream of the wall jet nozzle for the four smallest step heights, and 866 mm downstream of the wall jet nozzle for the two larger step heights. This difference is due to the different running lengths of the two types of Lexan sheets used. Again, the ramp had the necessary height for the step being tested and had a running length of 100 mm.

Table 2.1 provides the ramp angle, α, that is implied for each step height due to the geometry previously stated. The intent of these ramps was to smooth over the unwanted forward steps and eliminate or severely reduce their effect on the incoming flow. As will be discussed in the results section, this was necessarily not the case with evidence showing the some of the effects of these ramps.

Step Height, h	1.5 mm	3.0 mm	4.6 mm	6.1 mm	11.7 mm	18.0 mm
Ramp Angle, α	0.86^o	1.7^o	2.6^o	3.5^o	6.7^o	10.4^o

Table 2.1. Implied Ramp Angles for each Step Height

The gap configurations considered in this study are a combination of the backward and forward steps and are created in the same way as their individual components. All material used to create the step and gap configurations were clamped to the wall jet plate along the span-wise edges of the plate. Additionally, all joints between sheets, ramps, or the wall jet plate, except features that constituted the steps, were taped over to avoid additional noise sources or flow entrainment.

Preliminary measurements were made to show (a) that the clamps holding the various sheets at the span-wise edges of the plate did not produce measureable sound and (b) that the portions of the steps and gaps immersed in the wall jet outside of the two dimensional core did not contribute significantly to the radiated sound. The results of these measurements are presented in the Smooth Plate Wall Jet Properties section of Chapter 3.

2.3 Far Field Microphone Instrumentation

The microphones used in this study were ½ inch model 4190 B&K free field microphones. These are notable for having a high sensitivity and a flat frequency response to over 20 kHz. A B&K Nexus 2690 four channel amplifier was used with these microphones. Before digitizing the microphone signals, they were band pass filtered between 250 Hz and 20 kHz. These signals were then read by an Agilent E1432 16-bit digitizer. The spectra presented in this study were measured by averaging 1000 records of 2048 samples collected at 51,200 Hz for each condition.

The acoustic measurements made in this study were performed with four microphones located in a stream-wise circular arc centered on the location x_s, at the base of the steps. The arc of microphones was located outside of the flow in the far-field. The microphones were secured to an acoustically treated support structure located outside of the flow that arches over the wall jet plate. The microphones were held by acoustically treated microphone stands, one of which can be seen in Figure 2.11. A view of the entire microphone arc, as well as the acoustically treated support structure, can be seen in Figure 2.12. A schematic view of the far field microphone experimental setup is provided by Figure 2.13.

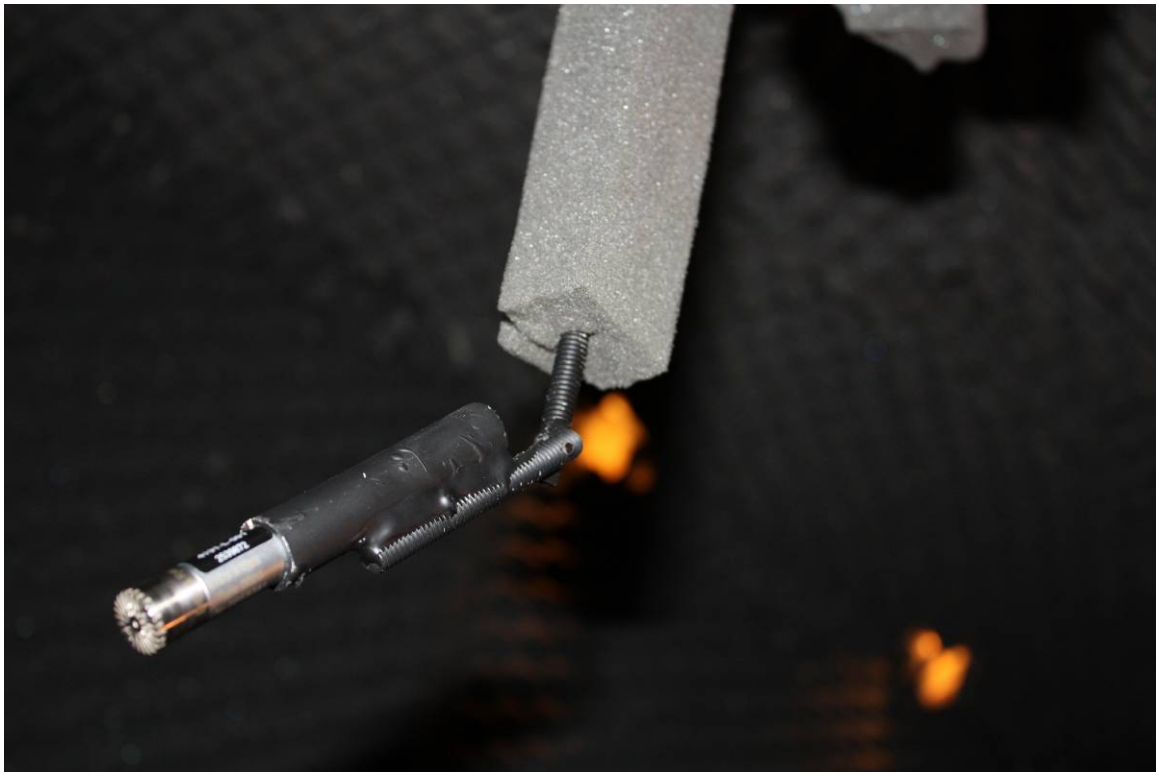

Figure 2.11. A Close View of a Single Microphone in an Acoustically Treated Stand

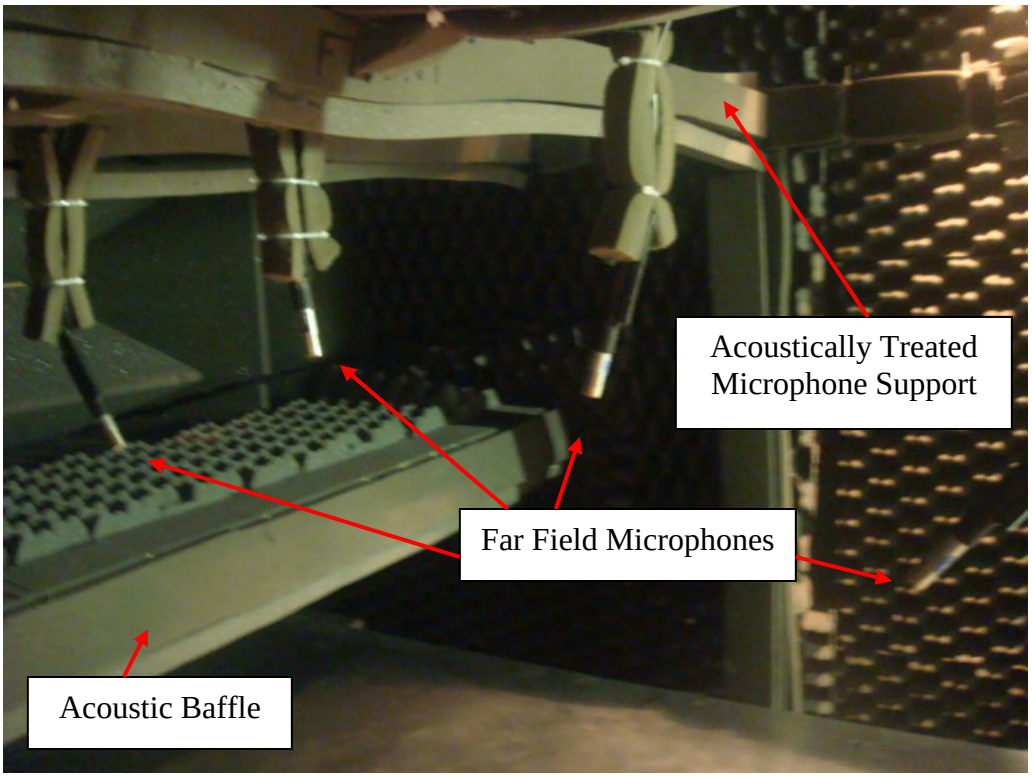

Figure 2.12. Acoustically Treated Far Field Microphone Array

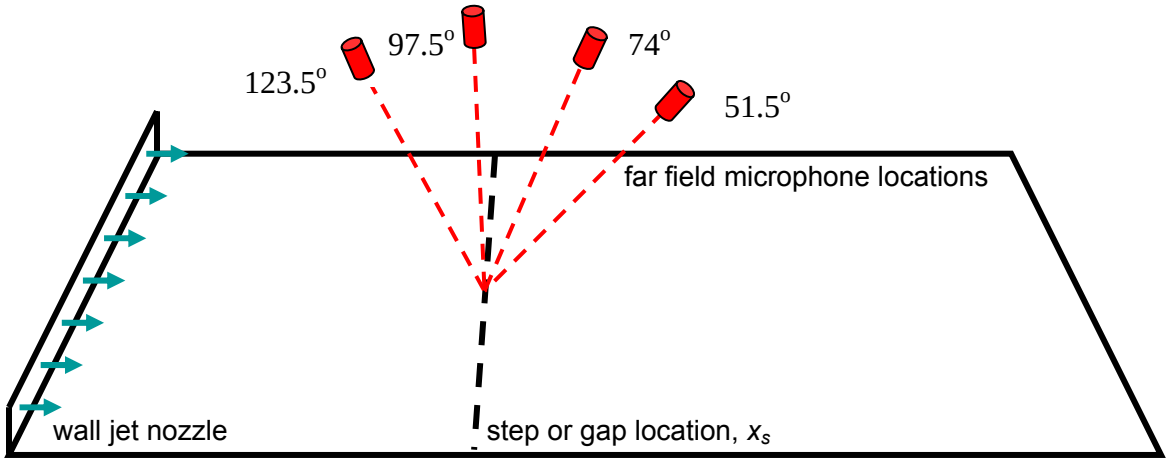

Figure 2.13. Schematic of Far Field Microphone Array

Nominally, two microphones were placed downstream, one microphone was placed normal to, and one microphone was placed upstream of the step location along a circular arc. As mentioned previously, the microphones were positioned along the centerline of the wall jet plate in a stream-wise circular arc. In this way each microphone had a unique observation angle, θ; however the tilt angle, β, was kept constant at 90° for all four microphone locations.

Each microphone was located a distance R = 577.5 $\pm$ 2.5 mm away from the base of the step location x_s. The microphones were located at observer angles of θ = 51.5^o, 74^o, 97.5^o, 123.5^o; with an uncertainty of 0.5^o applying to all angles.

2.4 Wall Pressure Microphone Instrumentation

The fluctuating wall pressure measurements were performed with a set of three Sennheiser KE-4-211-2 electret condenser microphones each with a nominal sensitivity of 10 mV/Pa. These microphones were modified with smaller pinholes taking the factory aperture of 1 mm down to ¼ mm in order to increase the spatial resolution of the surface pressure spectra. Disks of 0.26 mm thick and 5.0 mm diameter brass shim stock were machined and then secured to the microphones with epoxy so that the machined ¼ mm pinholes were located overtop of the factory microphone apertures. A close up view of the microphone face and a schematic cross section of an installed microphone is shown in Figures 2.14 and 2.15 respectively.

Figure 2.14. Close View of Near Field Wall Pressure Microphones

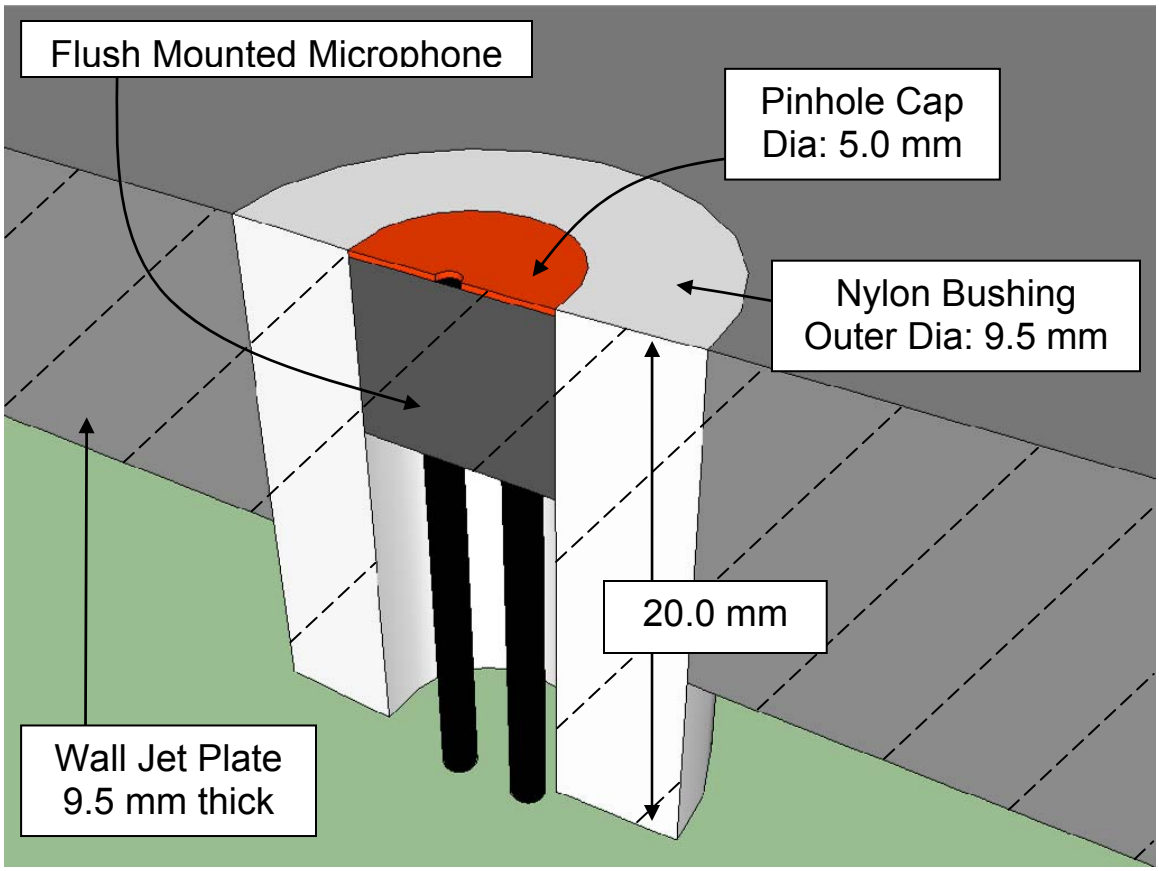

Figure 2.15. Schematic Cut-Away of the Near Field Microphone Installation

These microphones were flush mounted to the plane of the wall jet plate through holes drilled in the surface. A cylindrical, hollow, nylon spacer was used to house each of the microphones and to help secure the microphones to the underside of the wall jet plate. This spacer had an outer diameter of 9.5 mm, an inner diameter of 5.0 mm and a length of 20.0 mm. The microphones were secured to the nylon bushings and the bushings to the underside of the wall jet plate by hot glue which allowed secure placement during testing, but also easy removal for relocating microphones and changing step or gap configurations.

Three measurement locations were taken in front of all of the forward steps and six locations were taken behind all of the backward steps. For two of the forward and backward step heights, surface pressure measurements were taken both in front of and behind the steps, thus utilizing all nine locations. The step heights for which this larger data set was collected were for both steps of 1.5 and 11.7 mm. No fluctuating surface pressure measurements were taken for any gap configurations.

The holes through which these microphones are mounted are at fixed locations on the wall jet plate. For the constant step and microphone locations, the non-dimensional distance, x/h, between the microphone and the step is completely dependent on which of the step heights is being tested. In this way, the measurement locations for the smallest step are relatively further away than the measurement locations for the largest step.

The distance from the origin located at the wall jet nozzle to all of these positions, as well as to the step or gap location, x_s, is provided in Table 2.2. Also for clarity, a schematic view of these locations relative to the wall jet nozzle and the step location on the wall jet plate is provided by Figure 2.16.

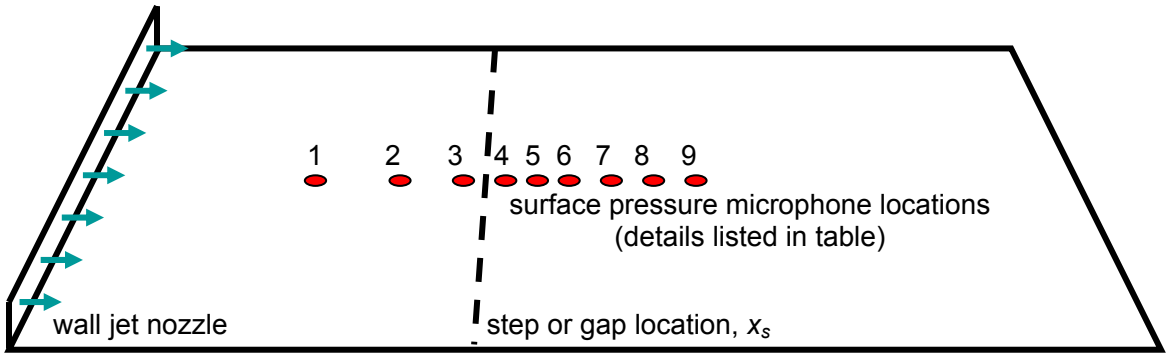

Figure 2.16. Schematic of Surface Pressure Microphone Locations

Distance from Origin to Surface Pressure Microphone Locations and Step Location [mm]									
1	2	3	step, x_s	4	5	6	7	8	9
819.2	1,124	1,353	1,372	1,403	1,429	1,454	1,505	1,556	1,607

Table 2.2. Measurement Locations of Surface Pressure Microphones Relative to the Nozzle Exit and Step or Gap Location

The calibration of these microphones was performed through comparison against a B&K 1/8th inch microphone for white noise generated by an Agilent VXI data acquisition system and a University Sound ID60C8 speaker. The calibrations were performed in the anechoic enclosure of the wall jet facility. The speaker emitting white noise was positioned on the acoustic shelf of the enclosure and each of the microphones was placed on a stand aligned with the speaker approximately 2.5 m away. The aluminum plate of the wall jet and the stand used to hold the microphones were covered with acoustic foam throughout each calibration. A view of the calibration setup inside of the anechoic enclosure is provided by Figure 2.17.

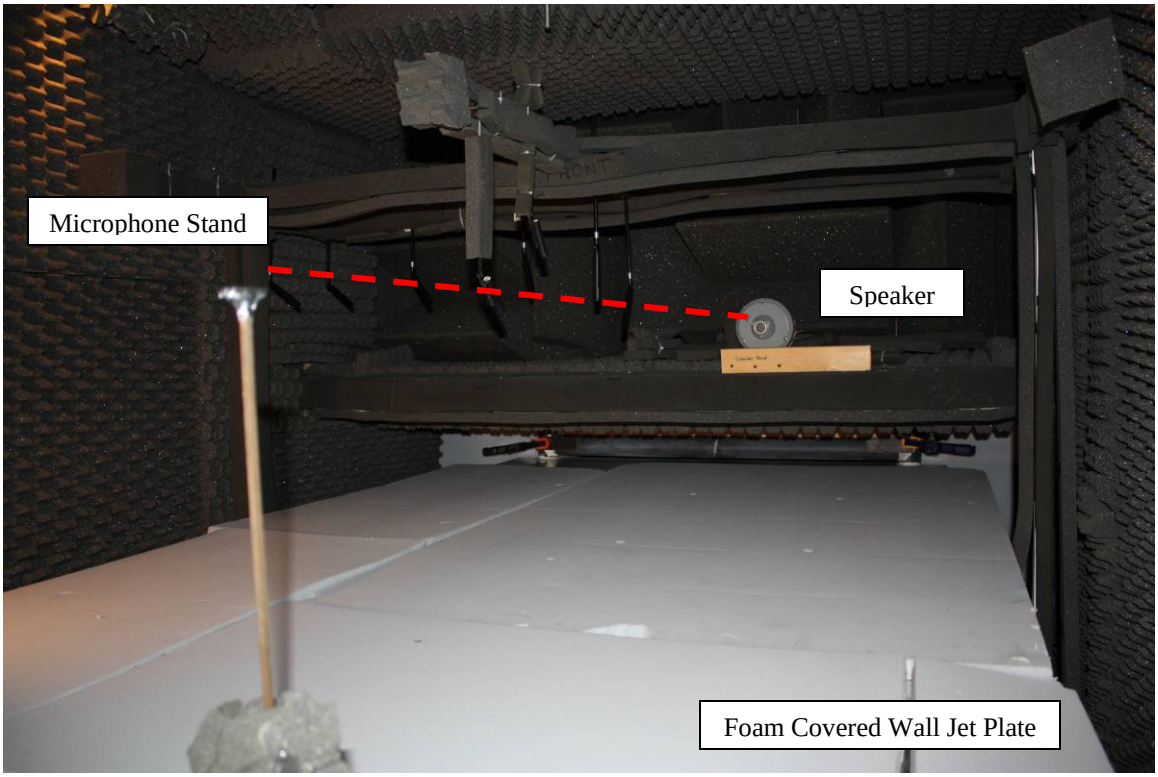

Figure 2.17. Set Up for Calibration of Near Field Surface Pressure Microphones

The collection of the fluctuating wall pressure data set occurred during multiple sessions and therefore multiple microphone calibrations were taken and used depending on when the data was collected. Typically, no more than two weeks were allowed to elapse between when data was collected and its corresponding calibration was taken. A typical calibration showing the curves for the three surface microphones is given in Figure 2.18. This calibration is typical with the same general microphone behavior seen for all calibrations.

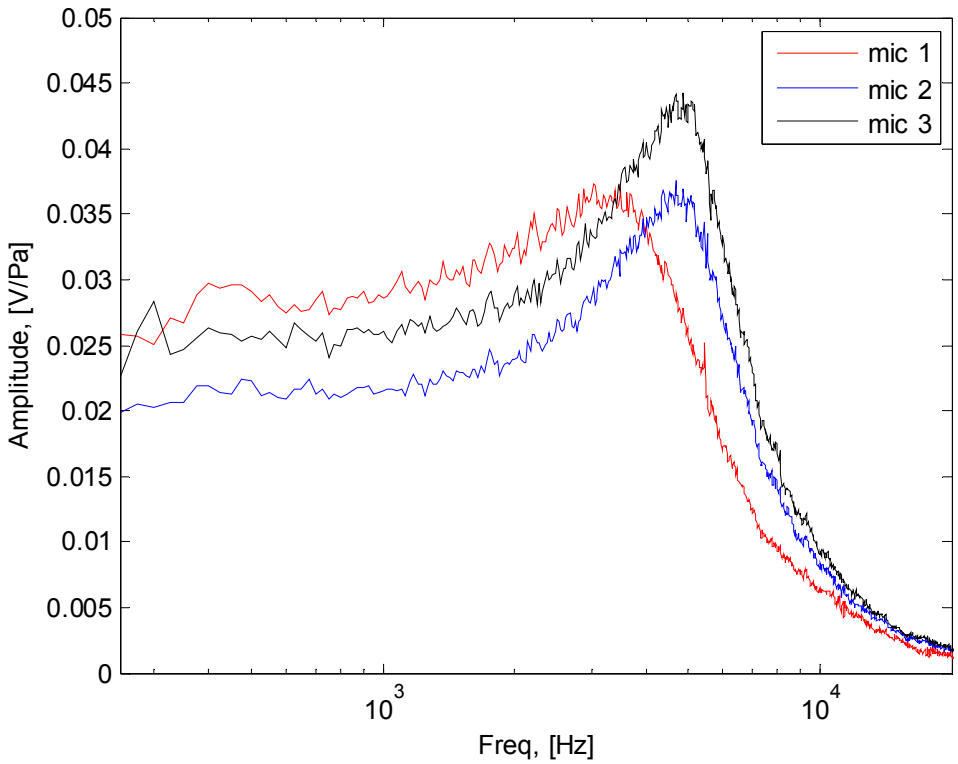

Figure 2.18. Typical Calibration Curves for Flush Mounted Sennheiser Microphones with ¼ mm Pinholes

The power for these microphones was provided by a 5V DC power supply. The signals were amplified by a gain of 2.5 from amplifiers that were made in-house by Mish (2003). These signals were then low pass filtered at 20 kHz and read by the same Agilent system as the far field microphone data with an identical collection scheme.

2.5 Oil Flow Visualization Instrumentation

An oil flow visualization technique was utilized behind the largest five of the six backward step configurations considered in this study in order to define the reattachment lengths of the resulting shear layers. The surface oil mixture consisted of titanium dioxide, kerosene, and oleic acid which were combined at approximately 15 to 5 to 2 parts per volume. This ratio was used a guideline to begin, but was constantly tweaked so as to yield the best visual results.

The mixture was applied to flat black contact paper which was adhesively secured to the flow surface behind the backward step configurations. A roughly square patch of contact paper approximately 0.5 m per side was centered behind the backward step configurations. The oil used for the flow visualization was then thinly painted onto the contact paper surface with a foam brush. Strokes parallel with the flow direction were used so that brush strokes did not influence the results of this method.

With the oil mixture applied to the surface, the wall jet tunnel was quickly brought up to the fastest run condition of a jet exit velocity of 60 m/s. The tunnel was run until the kerosene had enough time to evaporate, leaving the suspended titanium dioxide

on the surface to reveal the flow features. Excess surface oil which was blown down the wall jet plate during these tests was wiped away. The run time for each test was approximately five minutes. Each backward step configuration tested was run multiple times in order to optimize the oil mixture for the best visual results and to ensure the consistency of the results.

At the conclusion of each run, the flow pattern was archived by a camera (details). The camera was placed on a tripod and the pictures were taken from the same location relative to the backward steps. A small ruler was placed next to the flow pattern in each picture. These pictures were then post-processed using visual tools allowing the reattachment lengths to be determined by using the ruler as a reference.

Two visual techniques were used to determine the reattachment lengths from this method. The first technique utilized a wide view of the entire oil flow patch in which the vanishing point of the image was established. Lines were drawn from the vanishing point through the flow features determined by the oil flow visualization and then through the reference ruler. This method showed the two dimensional behavior of the flow over the tested area. The second visual technique was simply analyzing close up direct overhead views of the flow patterns with straight lines and the ruler as a reference. The results from both methods were very consistent with each other. The presented results of the following chapter are averaged results from both of these methods.

2.6 Discussion of Experimental Presentation Conventions

In order to isolate the far field sound produced by the various step and gap configurations of this study, the background facility noise levels have been subtracted from the measured sound spectra for each condition. Background measurements for the forward step configurations were made with all hardware removed from the wall jet plate. The far field spectra were then measured for this smooth plate condition at all nozzle exit velocities. Background measurements for all backward steps and gap configurations included the forward ramps used to create each backward step and gap, with additional material added downstream to create an uninterrupted flow surface from the ramp to the end of the wall jet plate of height corresponding to each step height. This elevated surface was created for each considered step height and used as the background measurement to determine the subtracted far field spectra for each possible step height at all of the nozzle exit velocities.

The method for determining the subtracted far field spectra consisted of comparing the smooth plate baseline spectra with those measured for each step and gap configuration. Wherever the signal to noise ratio between the measured spectra and the baseline spectra was greater than or equal to 1 dB the smooth plate spectra was subtracted from the step or gap spectra. For instances when the two spectra coincide to with in 1 dB, that data is rejected and no data is presented. The subtracted far field spectra defined in this way was then put into SPL which is how all far field data is presented. Figure 2.19 provides a brief example of this method for a forward step, backward step, and a gap configuration in order to give insight into effects on the spectra.

The method for determining the uncertainty in the subtracted spectra comes from the work in Devenport *et al.* (2010). The method combines the statistical uncertainty of the measured spectra with the uncertainty in the radiated far field sound as a function of

the uncertainty in the wall jet exit velocity. All spectral measurements were taken using 1000 samples, which result in a relative statistical uncertainty of 0.0632. When combined, using a root sum square, with a 2% microphone bias uncertainty, the spectral uncertainty becomes 0.0663. This is then combined, with a root sum square, with the uncertainty in the radiated sound which is controlled by the uncertainty in the wall jet nozzle exit velocity. The uncertainty in the subtracted spectra is based on this total relative uncertainty and the signal to noise ratio (SNR) between the two spectra being subtracted. Table 2.3 presents the uncertainty in a subtracted spectral measurement for the fastest wall jet nozzle exit velocity of 60 m/s with different SNR's.

Relative Uncertainty in U_j = 60 m/s		0.003		
Total Relative Uncertainty		0.0680		
SNR	1	2	5	10
Uncertainty in Substracted Spectra [dB]	4.22	2.18	1.043	0.760

Table 2.3. Uncertainty in the Subtracted Far Field Spectra for Specified SNR's

As can be seen, a large uncertainty is present for the subtracted spectra when the SNR is only 1dB which is the limiting case for any data to be presented. This usually arises at the lowest frequencies on the limits of the presented spectra. The spectra are seen to cut in and out and at times appear very jagged. This behavior is indicative of the uncertainty at these locations. For many cases the SNR is well above 5 and even 10 dB over much of the frequency range resulting in an uncertainty at or below 1 dB.

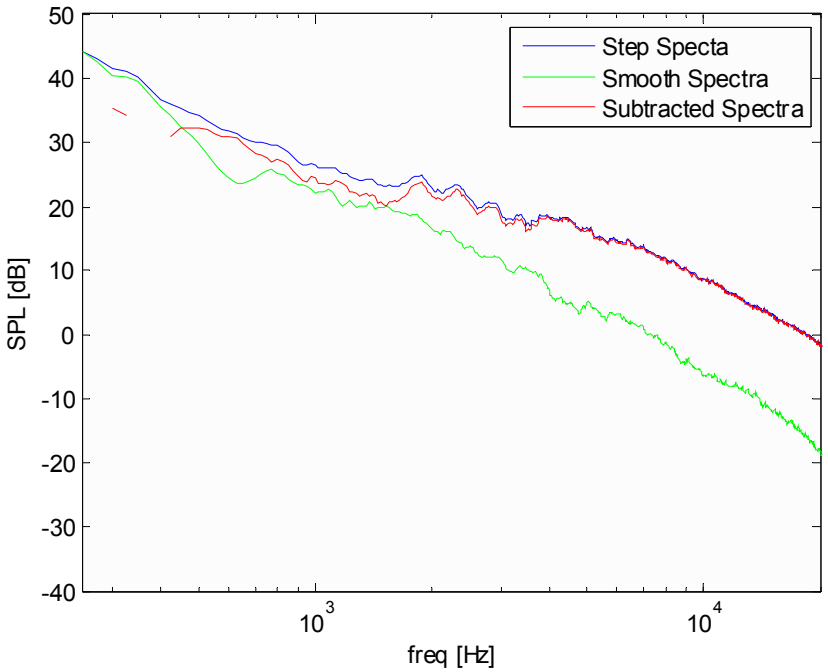

Figure 2.19 a

Figure 2.19 a-c. Example of the Method to Determine the Subtracted Far Field Spectra at U_j = 60m/s and θ = 123.5°; a) forward step, b) backward step, c) gap

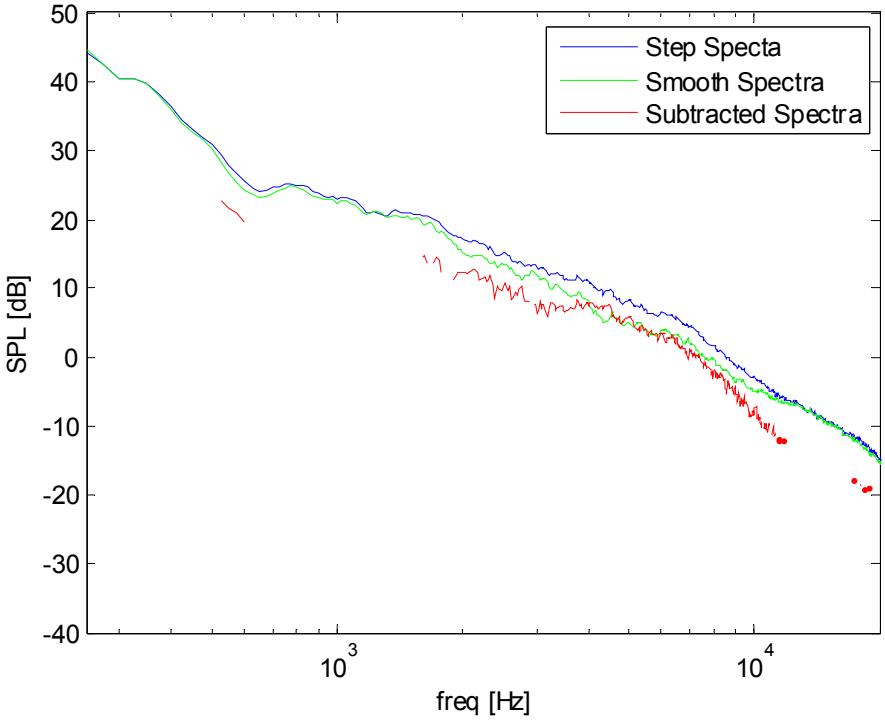

Figure 2.19 b

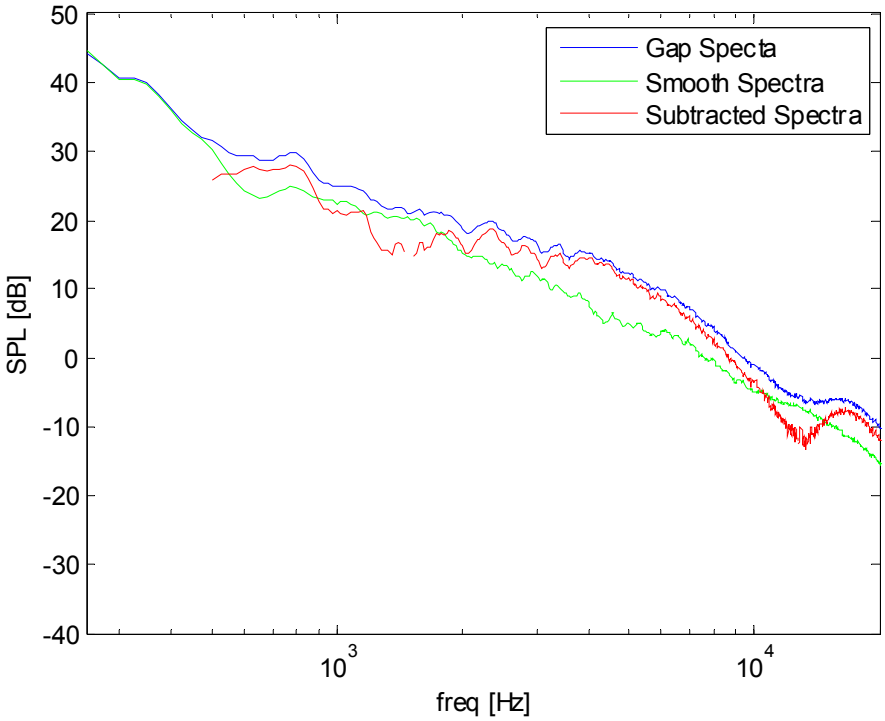

Figure 2.19 c

Figure 2.19 a-c. Example of the Method to Determine the Subtracted Far Field Spectra at U_j = 60m/s and θ = 123.5°; a) forward step, b) backward step, c) gap

The surface pressure spectra in this study are also presented in SPL format with normalization on the standard value of $(20e6)^2$ Pa^2/Hz. No subtraction of spectra is done for this data. The smooth plate spectra are presented along side each measured step spectra. All presented spectra are accompanied by the corresponding flow conditions; often defined in the title of each graph and figure caption.

CHAPTER 3. EXPERIMENTAL RESULTS AND ANALYSIS

3.1 Smooth Plate Wall Jet Properties

Numerous previous studies have been performed in the Virginia Tech Anechoic Wall Jet facility. Of those prior studies, many of the goals and results have been concerned with measuring and characterizing the flow properties of the wall jet over its entire operating range. A major result of these past studies is the existence of a two dimensional flow core coming from this wall jet that is well behaved and that extends far downstream on the wall jet plate. The flow of this two dimensional core may be described by algebraic relations which are functions of the nozzle exit velocity, nozzle height, and fluid properties. This study takes advantage of this result and assumes these relations, which are detailed in Devenport *et al.* (2010), in order to describe the flow properties throughout the domain.

The stream-wise development of the two dimensional core conforms well to the self-similarity relations of Narasimha *et al.* (1973) and Wygnanski (1992). As a result, the boundary layer edge velocity, U_m, displacement thickness, δ^*, and wall jet half height, $y_{1/2}$, can be calculated for streamwise positions throughout the plate for a smooth undisturbed surface from the following relations:

$$\frac{U_m}{U_j} = A_u \,\mathrm{Re}_j^{\,n+1}\,\mathrm{Re}_x^{\,n} \quad , \quad \frac{\delta^*}{b} = A_\delta \,\mathrm{Re}_j^{\,m-2}\,\mathrm{Re}_x^{\,m} \quad , \quad \frac{y_{1/2}}{b} = A_{y1/2}\,\mathrm{Re}_j^{\,p-2}\,\mathrm{Re}_x^{\,p}$$

Re_j is a Reynolds number determined by the nozzle height, b, and wall jet nozzle exit velocity, U_j. Re_x is a Reynolds number determined by the downstream location taken from the nozzle exit, x, and the wall jet nozzle exit velocity, U_j. The coefficients A_u, A_δ, $A_{y1/2}$, m, n, and p are constants which have been determined experimentally from previous studies to have values of 4.97, 0.01560, 0.074, 0.888, -0.512, and 1.014, respectively.

Secondary calculations are also provided in order to define the boundary layer thickness, δ, and momentum thickness, Θ. These relations are presented below and incorporate numerical constants that were determined experimentally.

$$\delta = 15.449\delta^* \quad , \quad \Theta = 0.7405\delta^*$$

The data collected in this study were for three nozzle exit velocities of 30, 45, and 60 m/s. The leading step feature for either the steps or gaps was in all cases placed 1,372 mm downstream of the nozzle; the location referred to as the step location, x_s. Estimated boundary layer parameters and Reynolds numbers based on boundary layer thickness and local maximum velocity for the undisturbed boundary layer at this location are given below in Table 3.1. Uncertainty estimates for these parameters are presented in Table 3.2 with the uncertainty for the wall jet exit velocity coming from discussion in Chapter 2 and the uncertainty for U_m/U_j and δ^* coming from comparison of experimental and calculated values.

U_j [m/s]	U_m [m/s]	δ [mm]	δ^* [mm]	Θ [mm]	Re_δ
30	10.7	20.6	1.34	0.989	13,040
45	15.8	18.8	1.22	0.903	17,580
60	21.0	17.7	1.14	0.847	21,990

Table 3.1. Selected Wall Jet Properties for the considered Nozzle Exit Velocities at the Step Location, x_s

U_j [m/s]	ΔU_j		$\Delta U_m / U_j$	$\Delta \delta^*$
30	$\pm$ 1.1 %		$\pm$ 6 %	$\pm$ 11 %
45	$\pm$ 0.5 %		$\pm$ 6 %	$\pm$ 11 %
60	$\pm$ 0.3 %		$\pm$ 6 %	$\pm$ 11 %

Table 3.2. Error Estimates for Wall Jet Properties

Table 3.3 lists the step heights, h, and the corresponding step to undisturbed boundary layer height ratios, h/δ, for all three nozzle exit velocity conditions of U_j = 30, 45, and 60 m/s with the step positioned at the fixed x_s location. As can be seen, five of the six step heights are significantly smaller than the boundary layer height at the x_s location for all three of the velocity conditions. The largest step height of 18.0 mm is approximately equal to the boundary layer height at this location for the fastest condition.

A major objective of this work is understanding the acoustic and flow behavior for steps of a small percent of the boundary layer height. The step heights studied in this work performed in the Virginia Tech Anechoic Wall Jet cover a wide range of step to boundary layer height ratios, from approximately 100% to below 10% of the incoming boundary layer.

	U_j = 60 m/s	U_j = 45 m/s	U_j = 30 m/s
Step Height, h [mm]	h/δ	h/δ	h/δ
1.5	0.0849	0.0796	0.0727
3.0	0.170	0.159	0.145
4.6	0.260	0.244	0.223
6.1	0.345	0.324	0.296
11.7	0.662	0.621	0.567
18.0	1.02	0.955	0.872

Table 3.3. Step Height to Boundary Layer Height Ratios for the considered Nozzle Exit Velocities

As previously stated, the streamwise development of the wall jet flow is seen to be self-similar within the two dimensional core. In this way, boundary layer profiles taken at various streamwise positions and wall jet nozzle exit velocities normalize on each other. Figure 3.1 provides a graph of this normalization. The local velocity, U, normalized on the local maximum velocity, U_m, is plotted versus distance away from the wall, y, normalized on the local boundary layer height, δ.

This plot incorporates the normalization of 12 separate boundary layer profiles taken at different streamwise locations and for different wall jet nozzle exit velocities. The flow conditions and measurement locations of the data set shown are very comparable to those of this study; incorporating the same range of nozzle exit velocities and similar streamwise positions. It should be noted that the flow in this facility does not have a typical freestream and that the boundary layer height is defined as the height in the y direction at which the local maximum velocity occurs. Characteristically of a wall jet flow, above the boundary layer height the velocity profile is seen to bend back. This behavior is presented in the normalized profiles seen in Figure 3.2 where $y_{1/2}$ is the wall jet half height. Additionally, Figure 3.2 presents normalized profiles detailing the turbulence levels seen in the flow. These figures were taken with permission from Devenport *et al.* (2010).

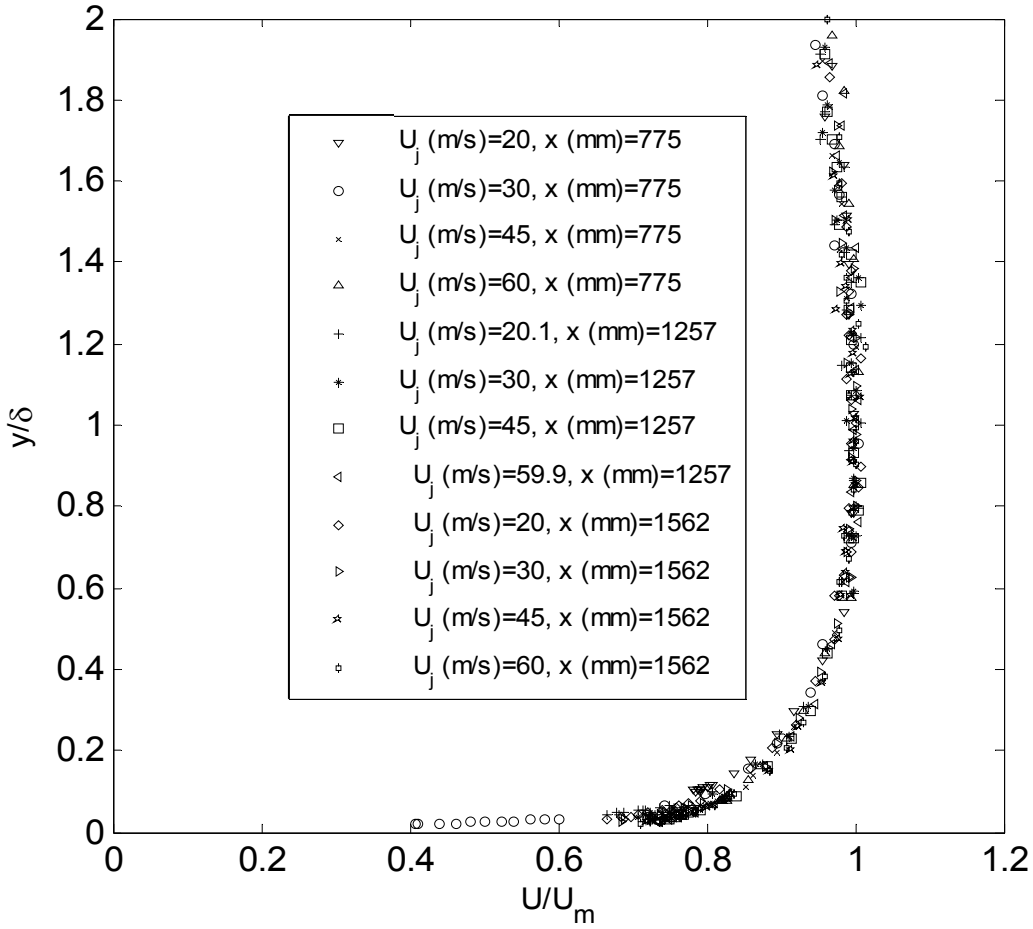

Figure 3.1. Self Similar Velocity Profiles Measured in the Virginia Tech Anechoic Wall Jet Facility, used with permission of Dr. William J. Devenport (2010)

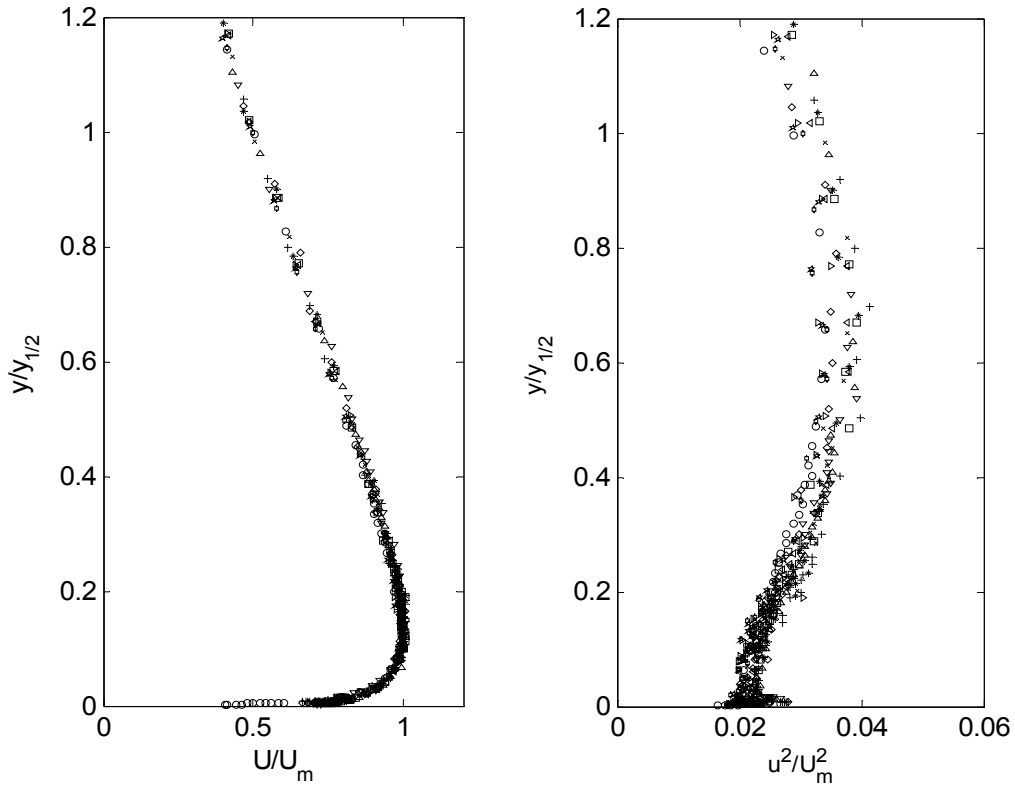

Figure 3.2. Self Similar Half Height and Turbulence Profiles Measured in the Virginia Tech Anechoic Wall Jet Facility, used with permission of Dr. William J. Devenport (2010)

Figures 3.3 and 3.4 provide the normalized smooth plate wall pressure spectra taken at the nine measurement locations considered in this study. Two different normalizations are presented, both of which are slight variants of those suggested by Farabee and Casarella (1991). The wall shear stress, τ_w, and friction velocity, U^*, both come from estimates of the skin friction coefficient, C_f, which is based on the experimental fit of the wall jet data, using the correlation of Bradshaw and Gee (1962). The relation to estimate C_f is given below with the numerical constants determined experimentally and the Reynolds number based on boundary layer height and local maximum velocity.

$$C_f = 0.0315\,\mathrm{Re}_\delta^{-0.182}$$

Detailed measurements of the wall pressure fluctuation spectrum were made along the plate centerline for the undisturbed wall jet. The description of these measurements is provided in section 2.4. Figure 3.3 normalizes the smooth wall spectra on the outer flow variables U_m, δ, and τ_w. Figure 3.4 normalizes the smooth wall spectra on the inner flow variables U^*, ν, and τ_w. Guides with slopes of ω^{-1} and ω^{-5} have been

overlain on the normalizations, in accordance with the results of Goody and Simpson (2000).

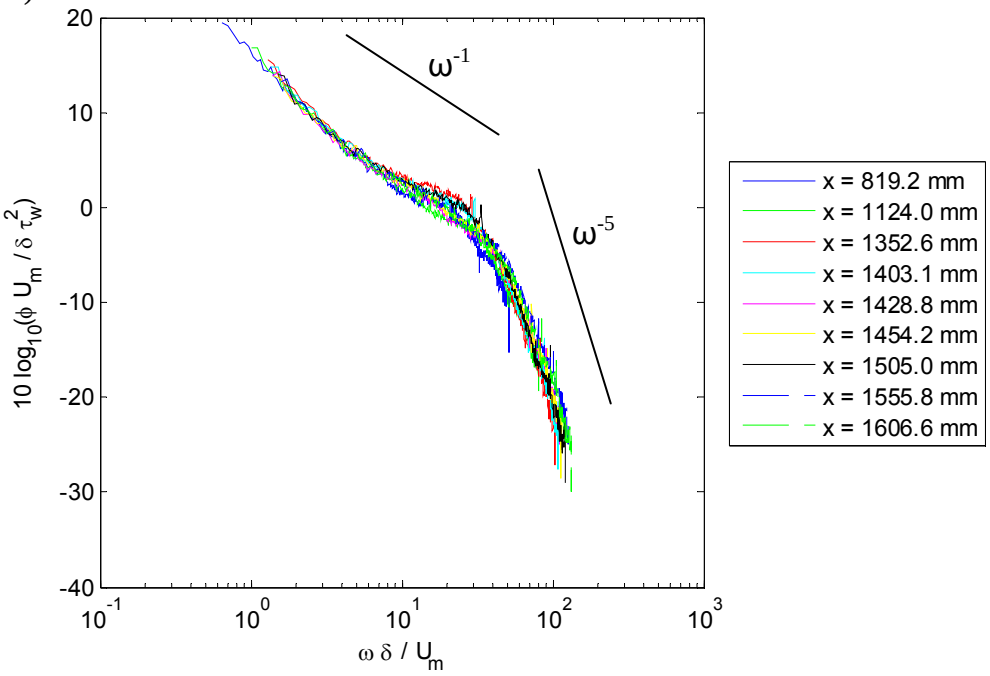

Figure 3.3. Fluctuating Wall Pressure Measurements on the Smooth Wall Jet Plate Normalized on Outer Flow Variables at U_j = 60 m/s

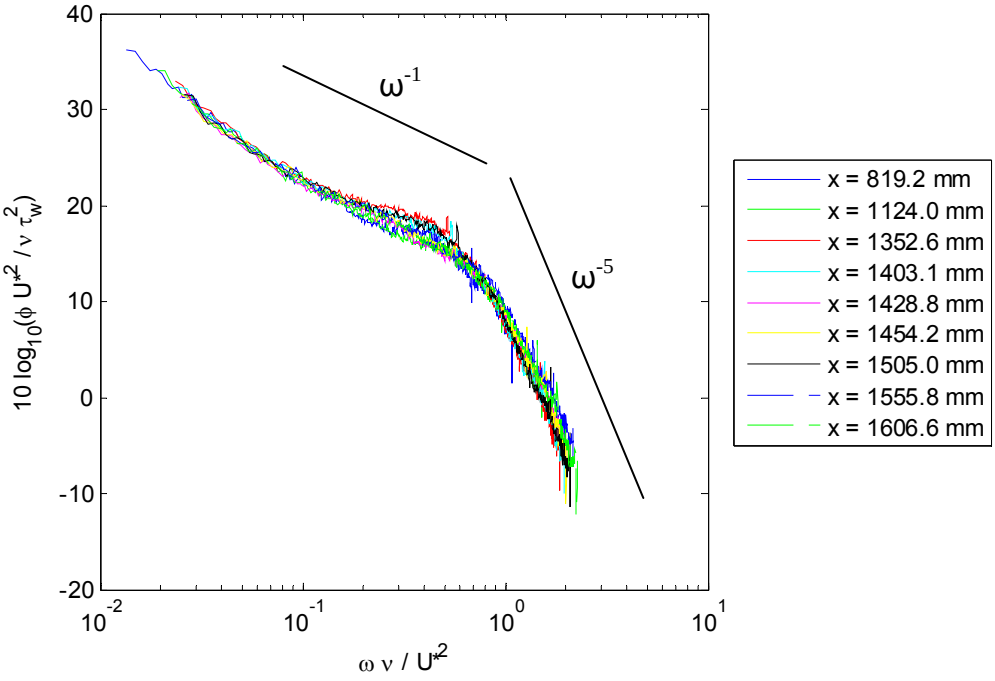

Figure 3.4. Fluctuating Wall Pressure Measurements on the Smooth Wall Jet Plate Normalized on Inner Flow Variables at U_j = 60 m/s

As can be seen, both normalizations collapse the near field spectra well. The exception in both normalizations is around the non-dimensional middle frequency regions where the different spectra spread out. This is located at values of approximately 20 and 0.4 for the outer and inner variable normalizations. The maximum here is approximately 3.5 dB for the outer flow normalization and approximately 3 dB for the inner flow variable normalization.

As stated in section 2.2, measurements were made to show (a) that the clamps holding the various sheets used to form the steps and gaps at the span-wise limits of the plate did not produce measureable sound and (b) that the portions of the steps and gaps immersed in the wall jet outside of the two dimensional core did not contribute significantly to the radiated sound. These measurements are used to further describe the behavior of the smooth plate wall jet.

The first statement was assessed by comparing the spectra from the far field for an entirely clean wall jet plate to the measured spectra when multiple clamps were placed along the edges of the plate at locations similar to where they were for the step or gap configurations. Figure 3.5 shows the measured far field spectra at a wall jet exit velocity of 60 m/s for the smooth wall jet plate and for when clamps are placed on the outer edges of the wall jet plate. As can be seen, the measured spectra for the two conditions are essentially identical implying that the clamps are not sources of flow induced noise and do not contribute the background noise of the facility.

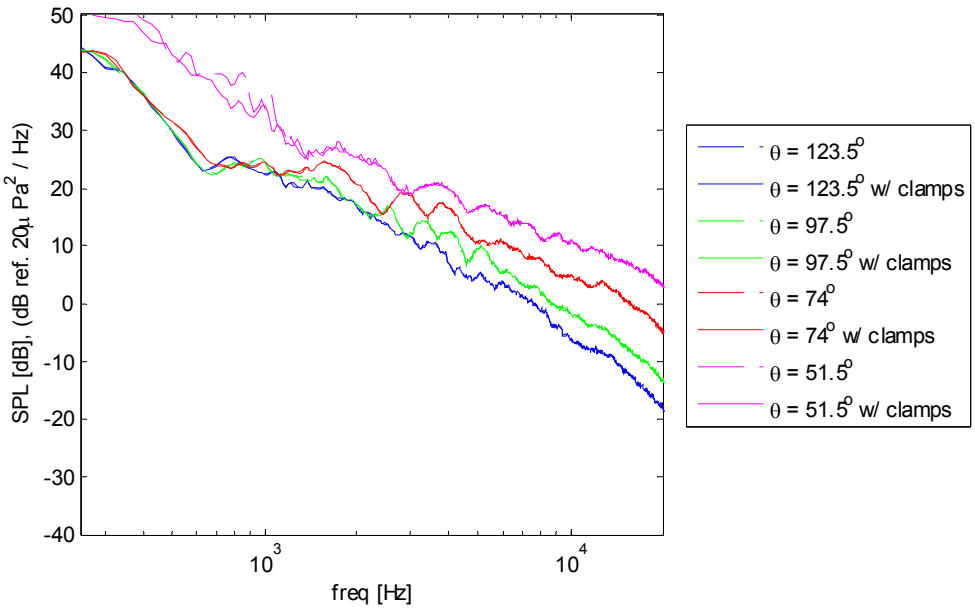

Figure 3.5. Comparison of Far Field Spectra for Smooth Wall Jet Plate with and without Clamps on the Outer Edges at U_j = 60 m/s

The assessment of the effects of three-dimensional flow over the span-wise extremities of the step and gap configurations on the sound recorded at the microphone locations was made by comparing the far field spectra from a typically installed forward step of 11.7 mm step height to when the outer edges of the same forward step were masked. Tape was placed over the outer 200 mm on either side of the plate in a wedge

shape in order to mask the step and prevent any flow induced sound from these regions. This masking of the outer 200 mm on either side of the wall jet plate covers most of the shear region of the wall jet. The two dimensional core is estimated to be 600 mm wide at this streamwise location of the step.

Figure 3.6 shows the measured far field spectra at a wall jet exit velocity of 60 m/s for the 11.7 mm forward step with its outer edges masked and unmasked in the manner just described. The lack of influence on the flow induced far field sound from the shear flow outside of the two dimensional core of the wall jet is evident by the coincidence of the dashed and solid spectra representing the two conditions.

These results and those showing the lack of influence of the clamps on the outer edges of the smooth wall jet plate demonstrate that the far field sound is dominated by the two dimensional core of the wall jet flow. As can be seen, neither feature on the extremities of the wall jet had a noticeable impact on the measured far field spectra.

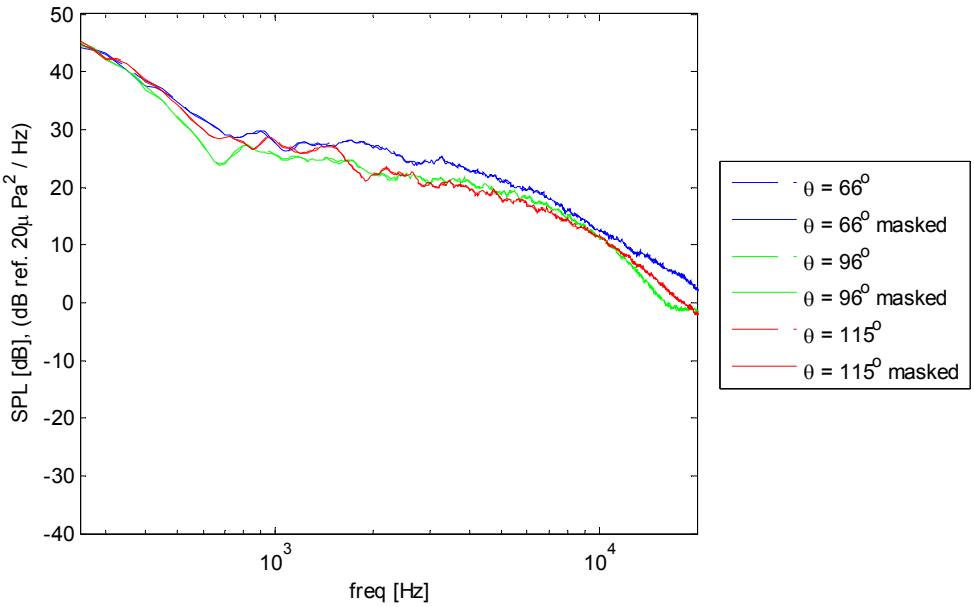

Figure 3.6. Comparison of Far Field Spectra for an 11.7 mm Forward Step with its Edges Masked and Unmasked at U_j = 60 m/s

3.2 Forward Steps

This section presents and discusses the results for the flow over the multiple forward steps considered in this study. The following subsections will concentrate on the far field radiated noise followed by the effects of the steps on the wall pressure field.

The flow over a forward step is characterized by the separated flow that occurs at the open corner of the step. A recirculation zone exists directly behind the forward step which terminates with flow reattachment occurring downstream of the step. The distance to flow reattachment is not a steady value and fluctuates with in a small region as the shear layer impinges on the flow surface. Additionally, a separation bubble exists in front of the step. Figure 3.7 highlights this behavior with a schematic representation of a typical forward step immersed in flow. These characteristics will be examined in the following subsections and estimations of the lengths of these separation zones and their impact on the flow will be presented and compared to that given in the literature.

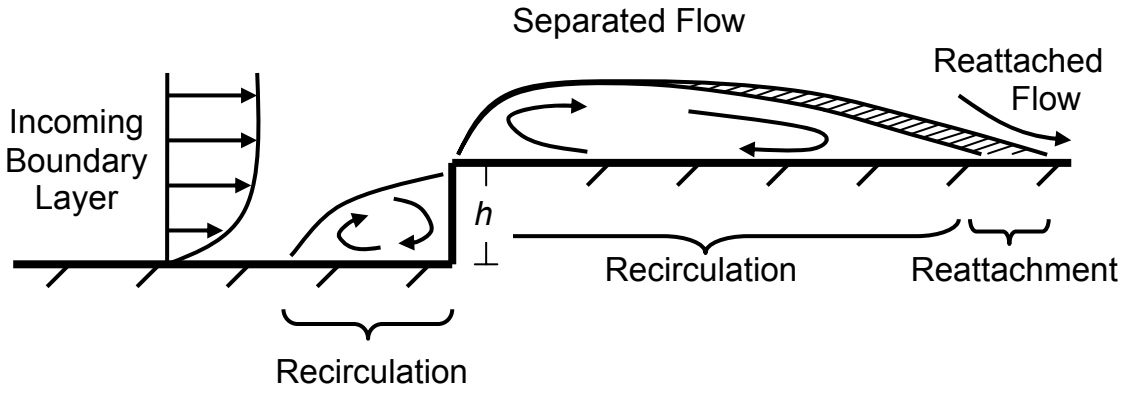

Figure 3.7. Schematic Representation of the Flow over a Forward Facing Step

3.2.1 Far Field

The radiated far field sound that emanates from forward steps immersed in turbulent flow was studied for six different step heights, at four stream-wise observation angles, and at three different local maximum velocities. All of the definitions and conventions described in Chapter 2 are assumed in the presentation of this data. All figures for this subsection are presented at the end of the subsection.

The far field spectra for all six step heights, at the four observation angles for a wall jet exit velocity of 60 m/s are presented in Figure 3.8. It should be noted that the far field microphones are placed in a circular arc at constant distance, *R*, relative to the step. In this way, any changes between spectra for a specified step height and nozzle velocity condition will highlight the directivity of the source.

For the most upstream observation angle, the spectra are structured in a cascade with spectral levels rising with step height almost over the entire frequency range. All step heights produce a measurable signal over much of the frequency range, except the two smallest steps which are limited to the mid to high frequency range. A clear dependence on step height is witnessed.

Over much of the frequency range, the spectra maintain a constant separation relative to each other. This behavior begins to break down at high frequency where the spectra from the two largest step heights of 11.7 and 18 mm are seen to bend down and drop to or below the levels of the other spectra. To give an idea of how the spectra depend on step height, the following Table 3.4 gives the spectral level, in dB, for each forward step at a frequency of 3 kHz at an observation angle of 123.5°.

h [mm]	1.5	3.0	4.6	6.1	11.7	18.0
SPL @ 3 kHz [dB]	7.27	10.6	13.8	14.8	17.3	21.4

Table 3.4. Sound Pressure Level at a Frequency of 3 kHz for set of Forward Steps

As can be seen in the table above, the approximate doublings of the step height from 1.5 mm to 3.0 mm to 6.1 mm to 11.7 mm each produces an approximate doubling of measured SPL at 3 kHz (an increase of 3 dB). Again, this behavior is not entirely consistent over the full frequency range, but does provide insight into the influence of step height on the far field sound.

Looking at the spectra for the next two most upstream observation angles of 97.5° and 74° begins to show the directivity of this sound source. There are numerous notable features when compared to the spectra of the most upstream observation angle. First, the frequency limit at which the measured step spectra rise above the background is a much stronger function of step height. This is seen as the frequency at which each spectrum begins, with the largest step height registering data over the largest frequency range. The behavior of this signal cut-in above the background is generally smooth with changing step height and consistent between the two observation angles of θ = 97.5° and 74°. It can be seen that the rise in dB level with step height is generally consistent with what was observed for the most upstream observation angle.

The most interesting features of these spectra are the dips seen in the spectra of the two largest step heights at high frequency. The spectra are seen to roll off and scallop resulting in significant falls in dB level over certain frequencies. This behavior is believed to be a feature of this flow and not introduced error from microphone hardware or placement. The reality of this behavior is justified by its consistent existence at multiple flow speeds for the given observation angles and its nonexistence at the most upstream observation angle for the same step heights. Also, while not explicitly discussed in past studies, this spectral behavior is witnessed in the data of past studies (Farabee and Zoccola (1998), Becker *et al.* (2005)). The scalloping behavior is seen to drop the affected spectra by as much as 6 dB in the most extreme case of these findings.

By studying the spectra from the middle two observation angles, it is seen that each of these dips are centered on consistent frequencies. These frequencies can be converted to wavelengths using the simple relation:

$$\lambda = c / f$$

It becomes immediately apparent that the frequencies at which spectral fall off are centered correspond to wavelengths that are multiples of the step heights being considered.

Results of this type would suggest that deconstructive interference of the sound source is occurring at these frequencies. This lends considerable evidence to the source location being in the immediate proximity of the exposed corner of the forward step. Assuming a reflective flow surface, any sound waves radiated from a source that travel down towards the surface would reflect back through the source and into the far field interfering with itself at frequencies corresponding to wavelengths that are multiples of $\lambda/2$ of the source's height away from the surface.

Tables 3.5 and 3.6 present the results of this type of analysis using the symbols f_d and λ_d as the frequency and wavelength where the deconstructive interference is centered as determined by inspection of the graphs. For the largest step height of 18.0 mm, a second dip is seen in the spectra at the highest frequencies and this is specified in Table 3.6 with a subscript 2 in order to distinguish these values from the set of values that correspond to the first spectral dip.

Forward Step, h = 11.7 mm, U_{exit} = 60 m/s			
θ [deg]	f_d [Hz]	λ_d [mm]	λ_d / 2 [mm]
97.5	$10^{4.16}$ ~ 14,500	23.8	11.9
74	$10^{4.11}$ ~ 12,900	26.7	13.35

Table 3.5. Deconstructive Interference seen for an 11.7 mm Forward Step Immersed in Flow

Forward Step, h = 18.0 mm, U_{exit} = 60 m/s						
θ [deg]	f_d [Hz]	λ_d [mm]	λ_d / 2 [mm]		f_{d2} [Hz]	λ_{d2} [mm]
97.5	$10^{3.95}$ ~ 8,910	38.6	19.3		$10^{4.23}$ ~ 16,980	20.3
74	$10^{3.92}$ ~ 8,320	41.4	20.7		$10^{4.2}$ ~ 15,850	21.7

Table 3.6. Deconstructive Interference seen for an 18.0 mm Forward Step Immersed in Flow

The interference patterns from both steps identify a source location at a height away from the wall that is slightly higher than the corresponding step height. As identified by past studies, this region in the vicinity of the step is an area of maximum turbulence levels as the flow accelerates over the step. This would suggest that these turbulent fluctuations would be the source terms for the radiated sound. This is in agreement with source localization data presented by Leclercq *et al.* (2001).

Extending this analysis provides reasoning why no spectral dips are seen in the spectra for the smaller step heights. If the source is located at a distance away from the surface that is approximately equal to the step height, then deconstructive interference would occur at frequencies that are higher then resolved in this data, and are therefore not present.

Lastly, the behavior of the far field spectra for the smallest and therefore most downstream observation angle of 51.5^o only qualitatively exhibit the features that have been discussed for the other observation angles. Overall levels and cut-in frequencies both remain functions of step height and dips in the spectra are observed in approximately the same way as for the other observation angles. However, for

measurements at this observation angle the background noise from the facility begins to contaminate the measurements and alter the smooth features seen at the other observation angles. Jet noise from the wall jet nozzle not being reliably shielded by the acoustic baffle and infrequent flow impingement on the microphone head both contribute to the overall increase in background noise at this measurement location.

The same type of far field measurements at the same four observation angles and for all step heights was made for wall jet exit velocities of 45 and 30 m/s. This data is presented in Figure 3.9 for U_{exit} = 45 m/s and Figure 3.10 for U_{exit} = 30 m/s.

Generally, the same behavior is witnessed for a wall jet exit velocity of 45 m/s as to the 60 m/s case, except that these spectra are shifted downward corresponding to slower flow conditions, resulting in lower background levels and a weaker source strength. The specific effects of flow speed will be discussed later in this section, but in general there is very little difference in the spectral behavior or signal to noise ratios at this condition as opposed to the faster condition. The cascading effect of step height on overall levels, the effect of step height on cut-in frequency, and the spectral dips are all present in this set of data.

The far field spectra for the complete set of forward steps immersed in wall jet flow for the slowest wall jet exit velocity of 30 m/s exhibit most of the same features and behavior as seen for the faster conditions; however at even weaker signal to noise ratios. The best measurement angle in terms of signal to noise ratio for this configuration is the largest and most upstream of 123.5^o. The next two of 97.5^o and 74^o reach the noise floor of the background at high frequency while the spectra remain very similar, as was seen for the faster flow conditions. The most downstream observation angle of 51.5^o still registers meaningful signals above the background, though they are weaker than for the previous conditions and reach the noise floor at an even lower frequency.

Notably, only the initial behavior of the spectral dip is seen for the largest step height at this condition. This behavior which was evident at faster flow conditions for the two largest step heights is not resolved at this slower condition because the source is drowned out by the background.

Figure 3.11 presents the far field spectra for the 1.5 and 11.7 mm forward steps at the most upstream observer angle of 123.5^o as a function of the three wall jet nozzle exit velocities. Parts of the spectra for the 1.5 mm forward step are missing due to background levels; however complete spectra over much of the frequency range are seen for the 11.7 mm forward step. Table 3.7 provides the spectral levels in dB at a specific frequency of 3 kHz for the two forward step heights and three nozzle exit velocities.

SPL @ 3 kHz [dB]	U_j = 30 m/s	U_j = 45 m/s	U_j = 60 m/s
h = 1.5 mm	-14.7	-0.622	7.27
h = 11.7 mm	-4.30	8.98	17.3

Table 3.7. Sound Pressure Level at 3 kHz for two Forward Steps with varying Nozzle Exit Conditions

The far field spectra are seen to shift upward with velocity with only a slight dependence on frequency being witnessed at high frequency. A number of the features of the spectra for each velocity condition are consistent with frequency suggesting that they

are not characteristics of the flow, but rather influenced by the experimental setup. At these conditions and for these step heights, the far field spectra are seen to scale on approximately the 7th power of velocity; the same scaling that was determined by Farabee and Zoccola (1998).

Figure 3.12 presents the far field spectra for the 1.5 and 11.7 mm forward steps for a wall jet exit velocity of 60 m/s as a function of the four observer angles considered. These views highlight any characteristics of the directivity of this sound source. No distinguishable data exists for the most downstream observer angle for the smaller step of 1.5 mm. Reasons for this were previously discussed. Data from the other observer angles show that the weakest signal in terms of level is seen at 97.5^o. The other two angles record approximately equal levels despite the spectrum for the 74^o observer angle having a reduced frequency range. This is presumably due to the background levels of the facility since the more upstream microphone is better shielded than the downstream microphone. Previous theories on step noise use the model of a streamwise aligned dipole for the source. This type of model implies varying sound levels with observer angle and would result in no radiated sound normal to the flow surface. A model of this type would predict that the spectra at observation angles of 97.5^o and 74^o would be approximately 12.5 and 6 dB below the spectrum taken at an observation angle of 123.5^o respectively. This type of model is not supported by these experimental results; except possibly at the lowest discernable frequencies. The spectral data is sparse, but below frequencies of 2 kHz this type of model could be relevant.

The spectra for the larger step height of 11.7 mm cover a larger frequency range for all of the observer angles. These spectra closely coincide with each other over much of their range and exhibit weak directivity over the mid to high frequencies. As previously discussed, the spectral dips are seen clearly in this view. This view shows that the frequency at which these dips are centered is slightly shifted from each other (values given in Table 3.5). It is believed that this is a result of the difference in observation angle. The distance from the sound source to the flow surface is slightly longer as viewed from the observation angle of 74^o than 97.5^o. This would result in interference occurring at a different wavelength, and therefore centered on a different frequency, which is seen in the data.

This description would account for the lack of a spectral dip seen in the most upstream observation angle. Interference at this observer angle would occur from wavelengths reflecting off of the face of the step and back into the far field. For a source located in the immediate vicinity of the exposed corner of the step, this distance is much shorter than for the other observer angles, resulting in interference at higher frequencies than resolved in this data. The spectrum for the most downstream observer angle of 51.5^o cuts out over the frequency range where the other spectra fall, because this signal drops back to the level of the facility background.

An effort to normalize the spectra of the far field sound from each forward step for the three velocity conditions is presented in Figures 3.13 through 3.18. The normalization is made on step height, h, and local maximum velocity, U_m, in the following way:

$$\frac{fh}{U_m} \text{ vs. } 10\log_{10}\left(\frac{\phi c^2}{\rho^2 {U_m}^5 h}\right)$$

Each plot shows the spectra for a specific step height at an observation angle of 123.5^o for the three wall jet nozzle exit velocities considered in this study. It should be noted that data at dimensional frequencies above 20 kHz have been cut off in the same way that they are not presented in the earlier dimensional spectra. Additionally, the size of the decade spacing of the axes remains the same in each figure for easier comparison. The *x*-axis of the figures for the two largest step heights have been shifted to higher non-dimensional frequencies in order to completely show the data, but the decade spacing remains the same.

For each specific step height, the normalization reliably collapses the three spectra, with the best results occurring for the two fastest velocity conditions. A difference in frequency dependence is seen for the slowest velocity condition at mid to high frequency contributing to its deviation from the other two spectra. The normalized spectra are seen to be shifted to higher non-dimensional frequencies as step height is increased. Figure 3.19 shows this trend by comparing the normalized spectra for each step height, but only at the fastest velocity condition. Again, all of this data is for an observation angle of 123.5^o.

Viewed in this way, all of the spectra are shifted along the *x*-axis depending on step height; however the spectral levels along the *y*-axis appear to be relatively unaffected by step height. At this velocity condition all of these step flows are experiencing the same boundary layer height. Taking this into account, a new normalization is presented with boundary layer height replacing step height as the length scale along the *x*-axis of the normalization. This mixed scaling takes the following form:

$$\frac{f\delta}{U_m} \text{ vs. } 10\log_{10}\left(\frac{\phi c^2}{\rho^2 {U_m}^5 h}\right)$$

This normalization is presented in Figure 3.20 for the set of six step heights at the fastest velocity condition and for an observation angle of 123.5^o. As can be seen this normalization reliably collapses the data for these conditions over the middle frequencies with a slight fanning out of the spectra over high frequency. There does not appear to be a specific correlation on step height for how the spectra deviate. A normalization of this type implies the importance of both the step height and boundary layer height as important length scales to be considered in these flows.

Figures 3.21, 3.22, and 3.23 show this normalization applied to the spectra for the other observation angles for the set of six steps at the fastest velocity condition. This normalization scheme does not collapse the data as well at these observation angles as it did for the more upstream observation angle of 123.5^o. One clear reason for this is the dips seen in the spectra for the largest two step heights due to deconstructive interference of the source (i.e. the non-compactness of the step). These spectral dips not only create local minima in the spectra, but alter the overall slope of the spectra at high frequency so that they fall off faster than for the smaller steps.

3.2.2 Summary of Far Field Results

The radiated far field sound from a set of six forward steps was studied at three velocity conditions for four observation angles. The far field spectra are shown to be highly dependent on step height and local maximum velocity. The dependence on step height is discussed, with SPL generally doubling with a doubling in step height. The spectra at multiple velocity conditions show consistent behavior with local maximum velocity corresponding to different source strengths. A velocity scaling of approximately velocity to the 7^{th} power is seen for this data. Little directivity of the sound source is witnessed, with the exception of dips seen in the spectra for the largest steps which correspond to deconstructive interference occurring from the sound reflecting off of the flow surface. The frequency at which this interference occurs allows the distance of the source away from the wall to be determined. This distance corresponds to a value that is slightly larger than the step height, which has been identified in past studies as a region of local maximum turbulence levels. This data supports the idea that the acoustic source of flow over a forward step is a result of the turbulent fluctuations located in the immediate vicinity of the exposed corner of the step. A new mixed scaling, which involve step height and boundary layer height as scaling parameters, is introduced which collapse the data well for observation angles that are not affected by deconstructive interference.

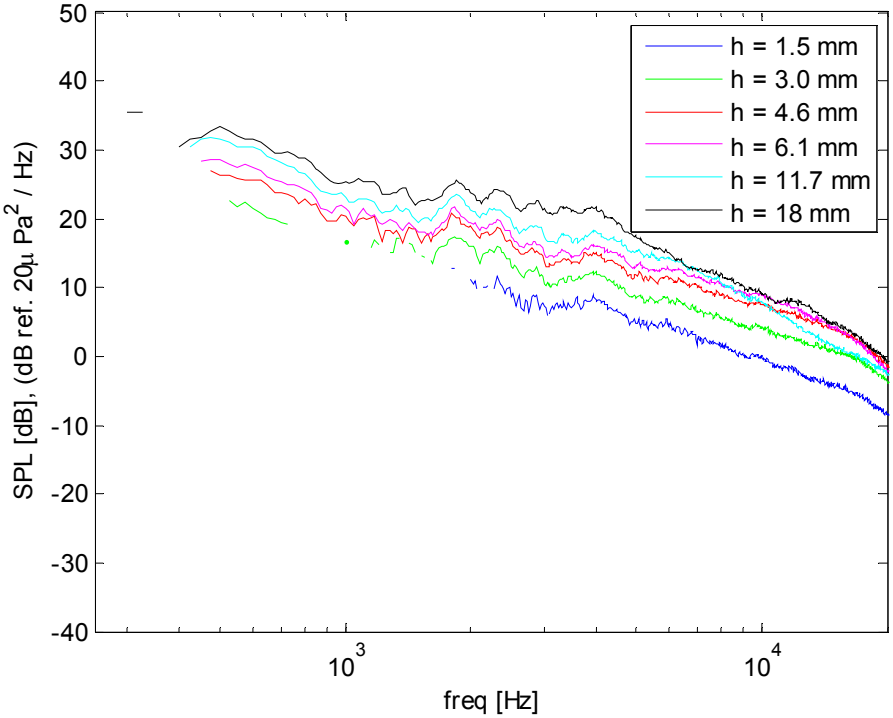

Figure 3.8 a

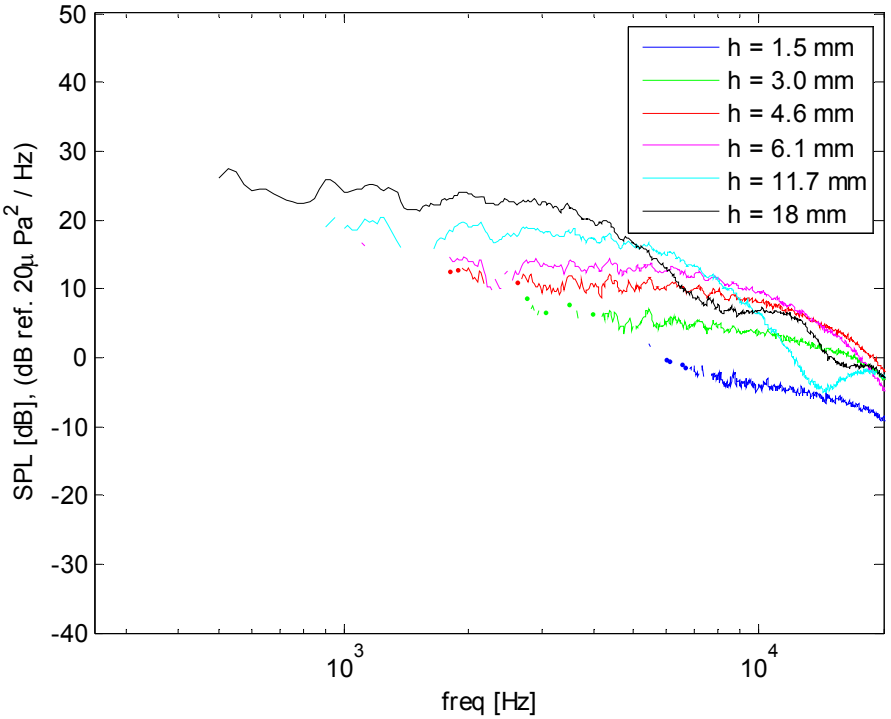

Figure 3.8 b

Figure 3.8 a-d. Far Field Acoustics from Forward Steps at U_j = 60 m/s at the considered Observation Angles; a) θ = 123.5° b) θ = 97.5° c) θ = 74° d) θ = 51.5°

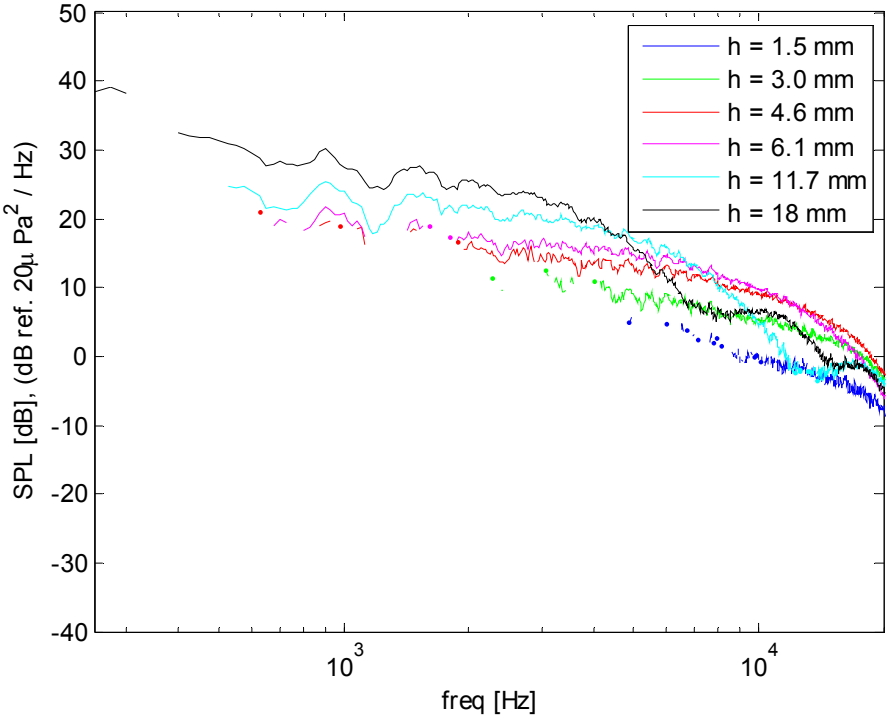

Figure 3.8 c

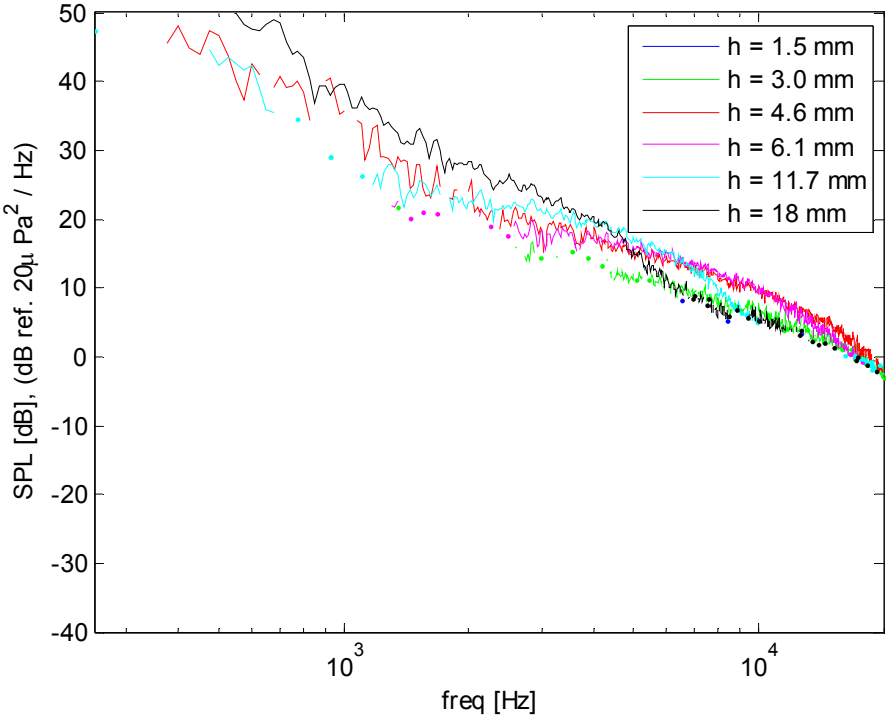

Figure 3.8 d

Figure 3.8 a-d. Far Field Acoustics from Forward Steps at U_j = 60 m/s at the considered Observation Angles; a) θ = 123.5° b) θ = 97.5° c) θ = 74° d) θ = 51.5°

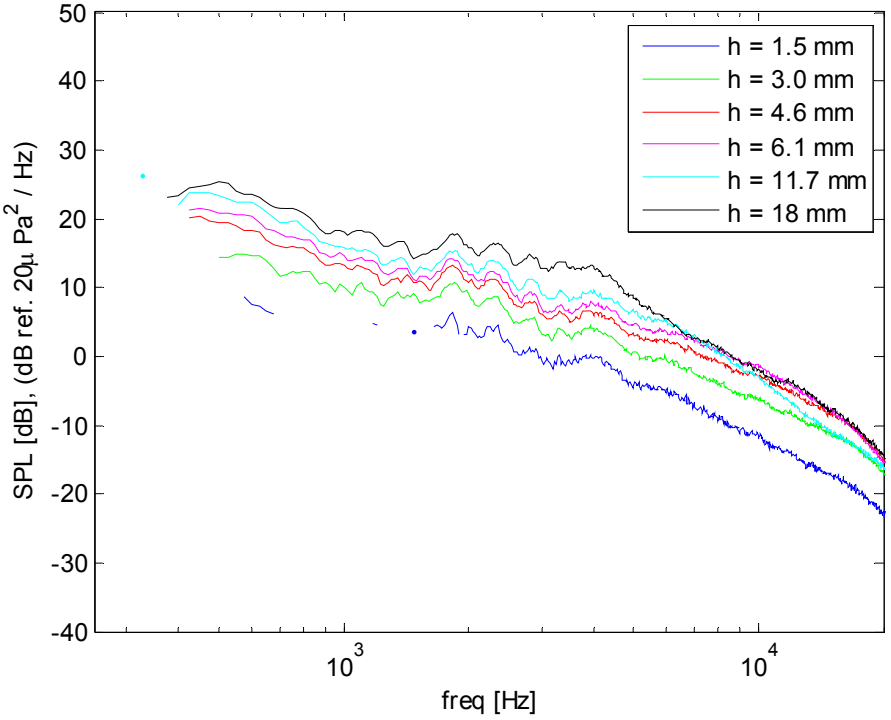

Figure 3.9 a

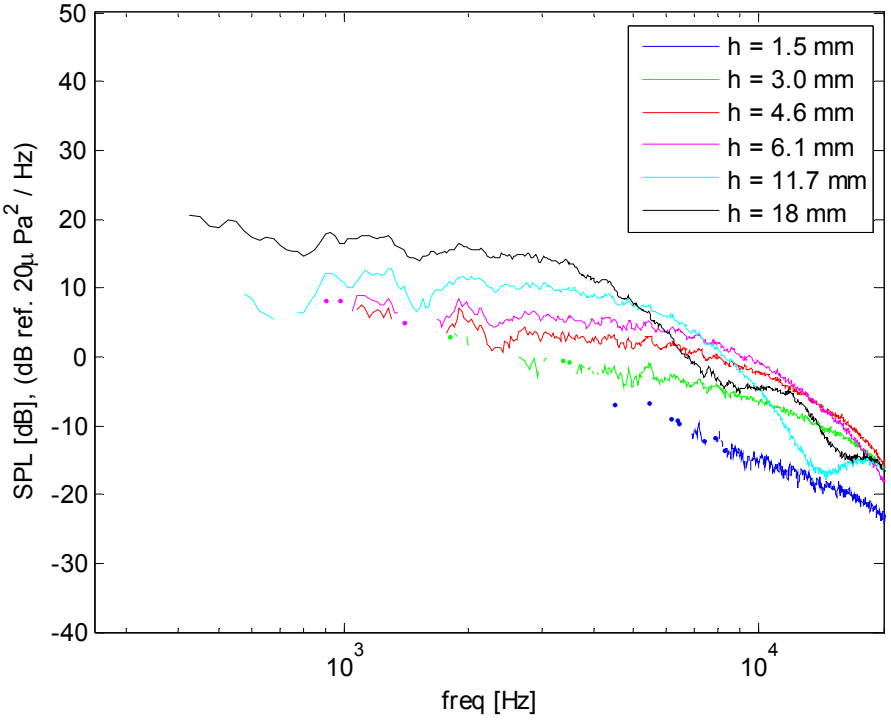

Figure 3.9 b

Figure 3.9 a-d. Far Field Acoustics from Forward Steps at U_j = 45 m/s at the considered Observation Angles; a) θ = 123.5° b) θ = 97.5° c) θ = 74° d) θ = 51.5°

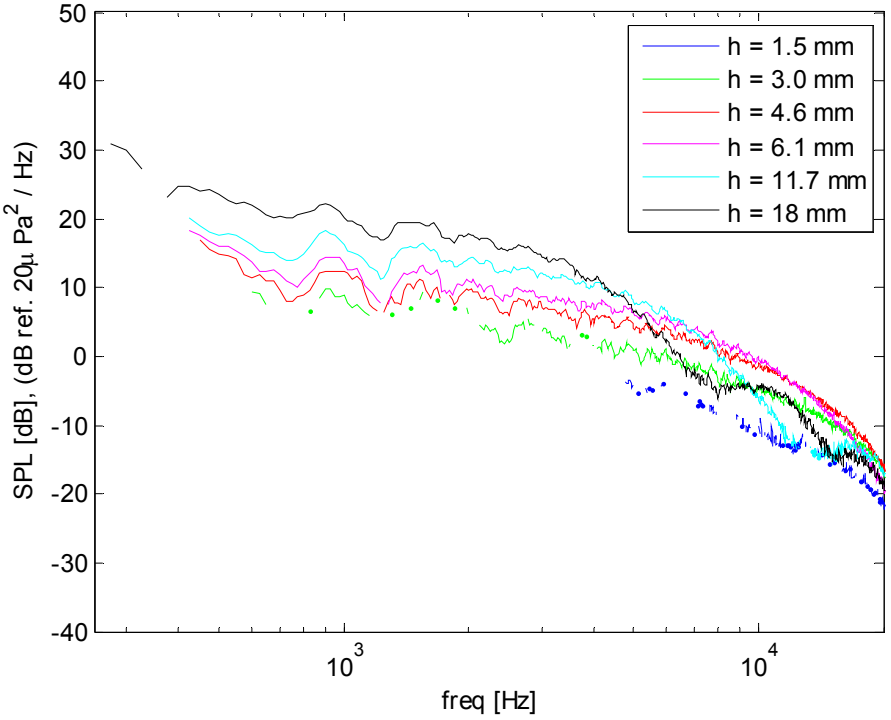

Figure 3.9 c

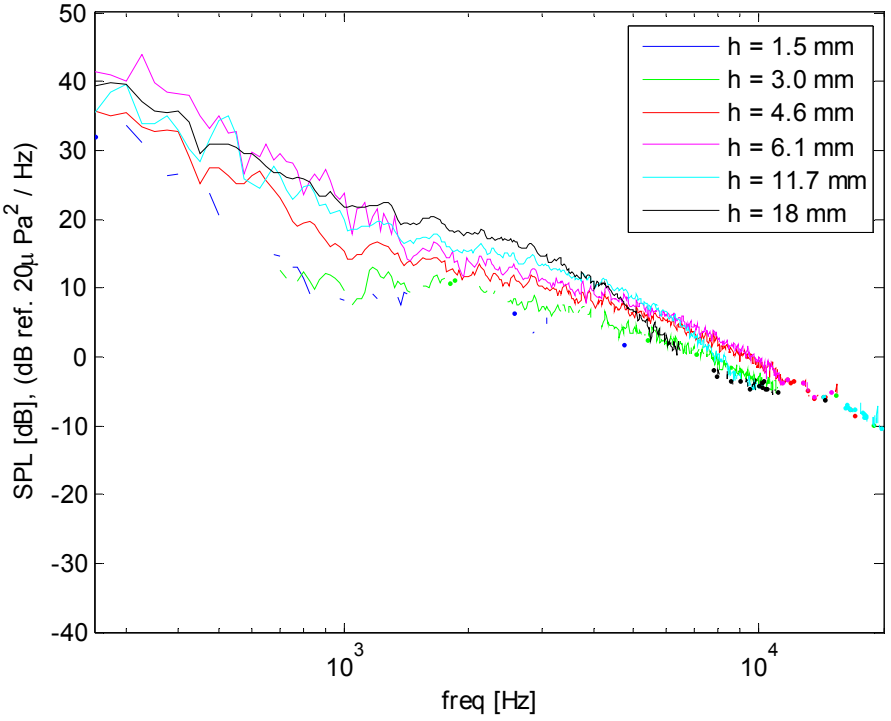

Figure 3.9 d

Figure 3.9 a-d. Far Field Acoustics from Forward Steps at U_j = 45 m/s at the considered Observation Angles; a) θ = 123.5° b) θ = 97.5° c) θ = 74° d) θ = 51.5°

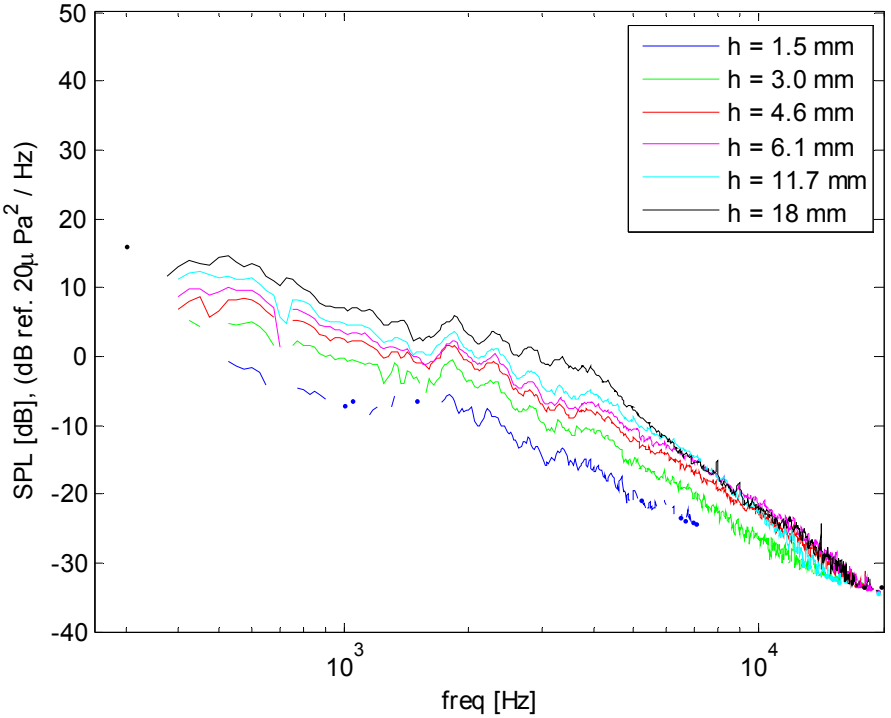

Figure 3.10 a

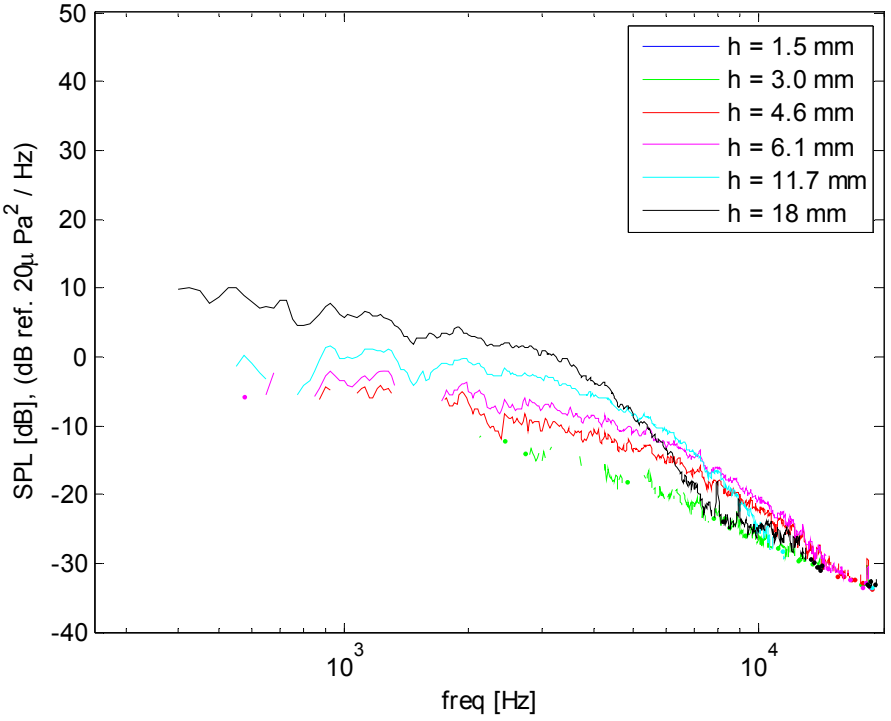

Figure 3.10 b

Figure 3.10 a-d. Far Field Acoustics from Forward Steps at U_j = 30 m/s at the considered Observation Angles; a) θ = 123.5° b) θ = 97.5° c) θ = 74° d) θ = 51.5°

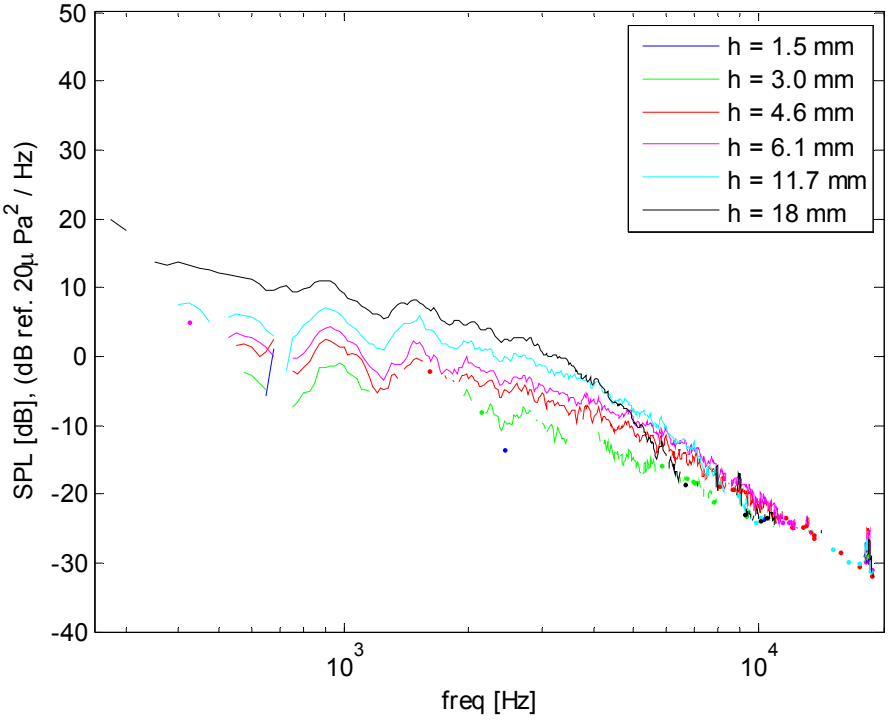

Figure 3.10 c

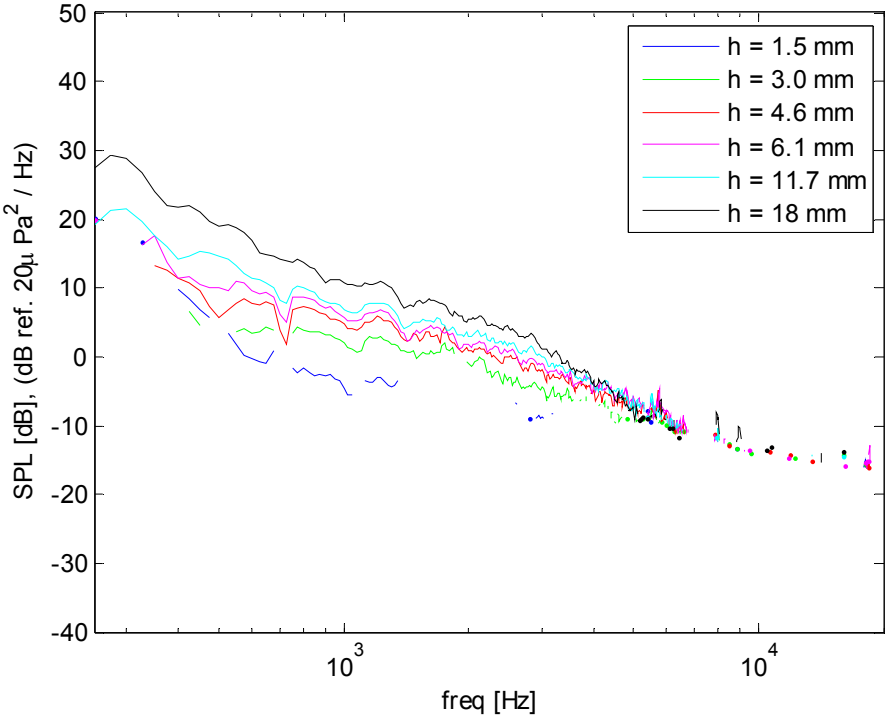

Figure 3.10 d

Figure 3.10 a-d. Far Field Acoustics from Forward Steps at U_j = 30 m/s at the considered Observation Angles; a) θ = 123.5° b) θ = 97.5° c) θ = 74° d) θ = 51.5°

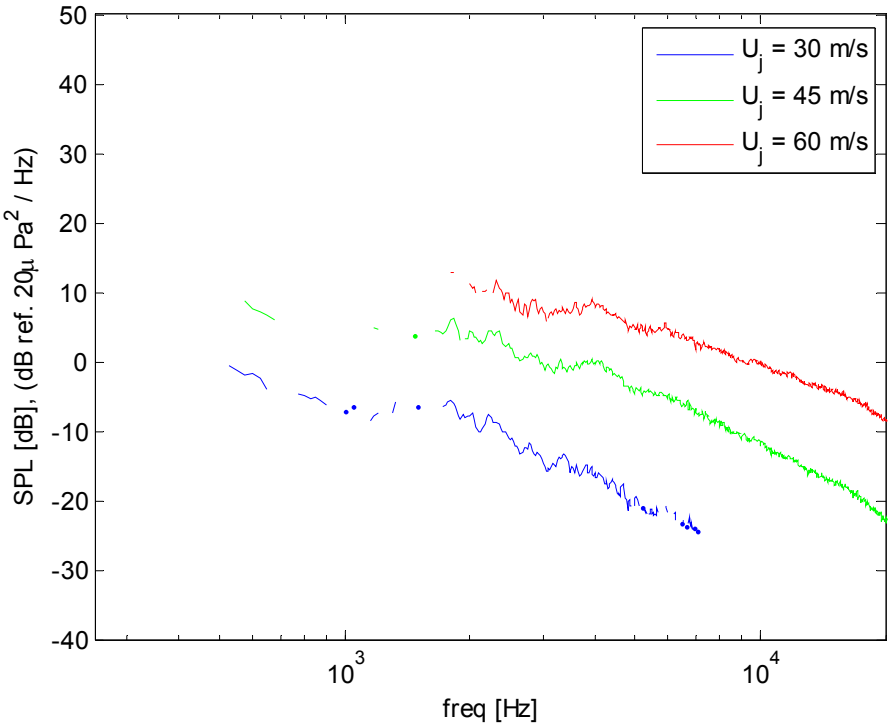

Figure 3.11 a

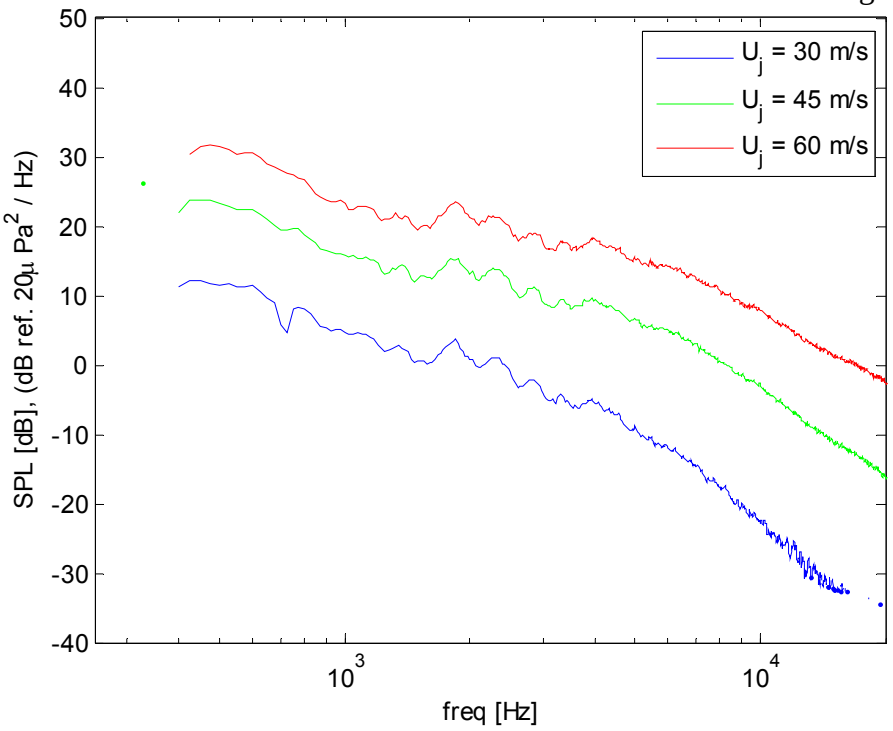

Figure 3.11 b

Figure 3.11 a-b. The Dependence of Far Field Sound on Jet Exit Velocity from different Forward Steps at $\theta = 123.5^{o}$; a) h = 1.5 mm b) h = 11.7 mm

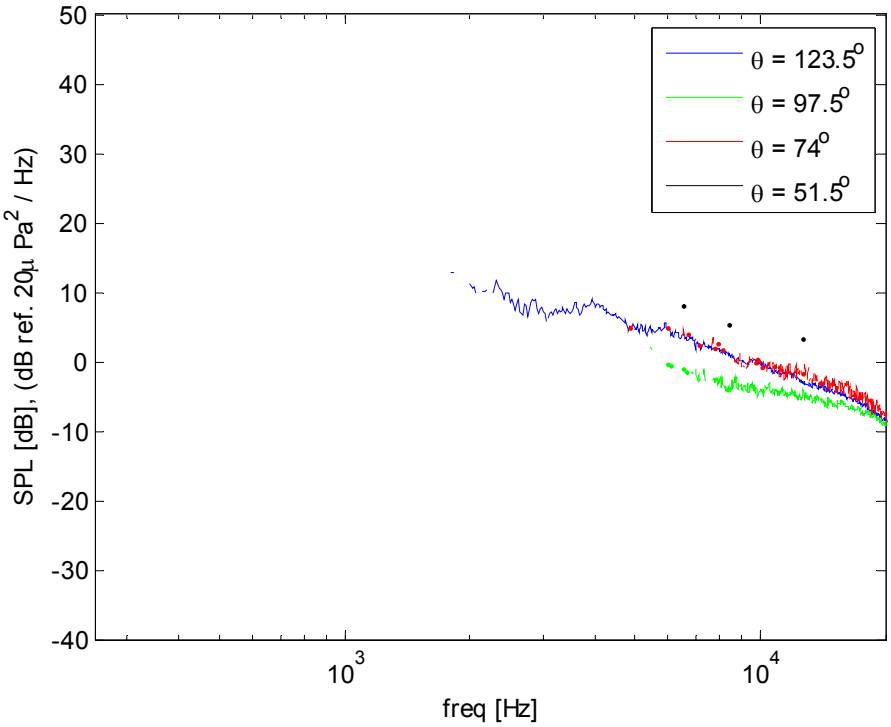

Figure 3.12 a

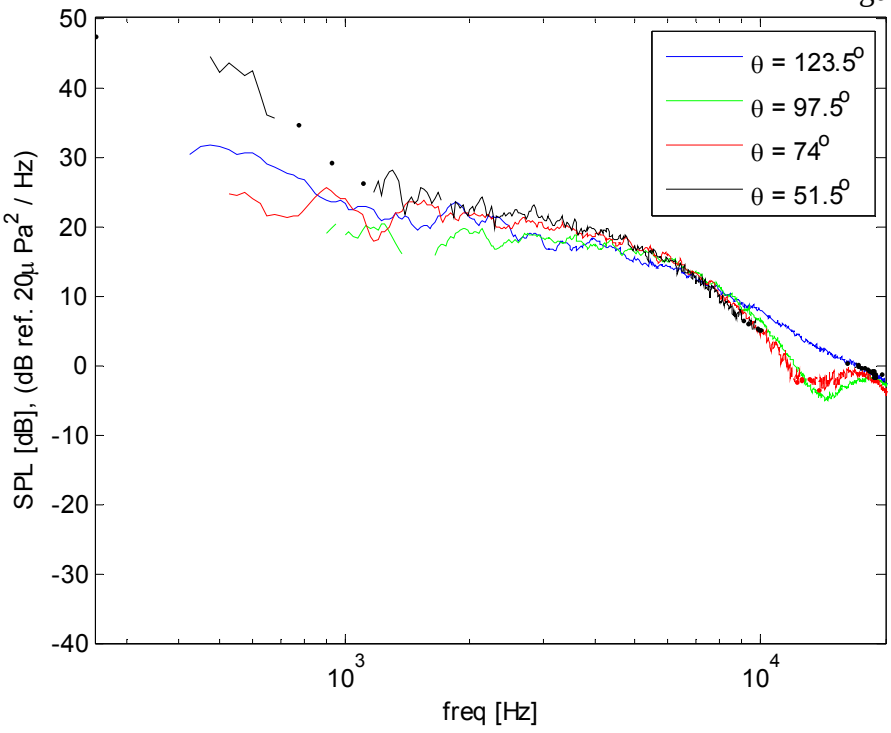

Figure 3.12 b

Figure 3.12 a-b. Directivity of the Radiated Far Field Sound from different Forward Steps at U_j = 60 m/s; a) h = 1.5 mm b) h = 11.7 mm

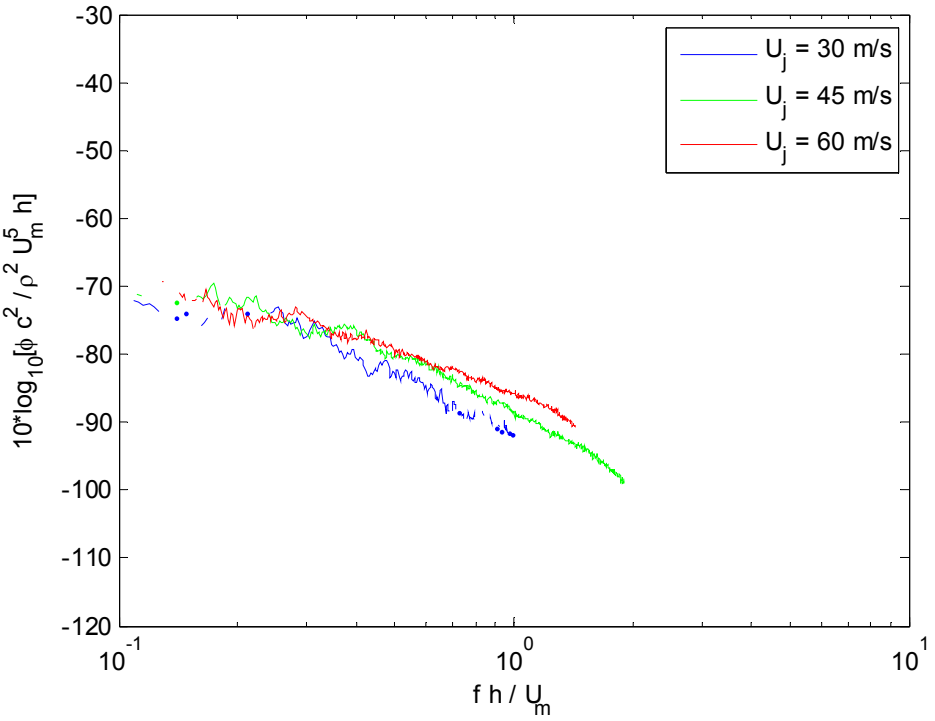

Figure 3.13. Far Field Spectra Normalization for the 1.5 mm Forward Step at $\theta = 123.5^{o}$

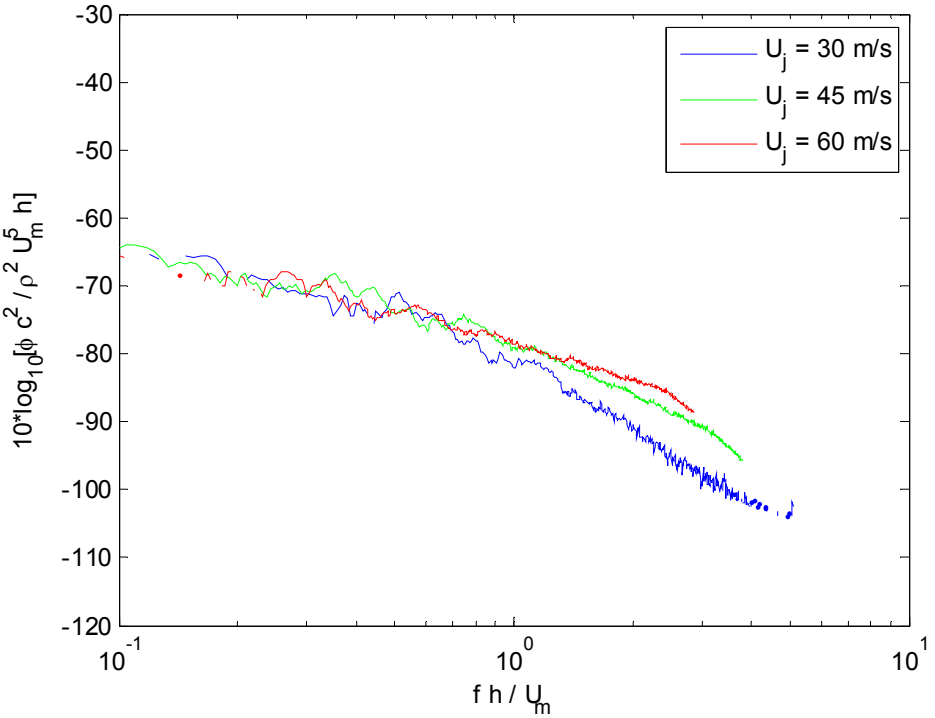

Figure 3.14. Far Field Spectra Normalization for the 3.0 mm Forward Step at $\theta = 123.5^{o}$

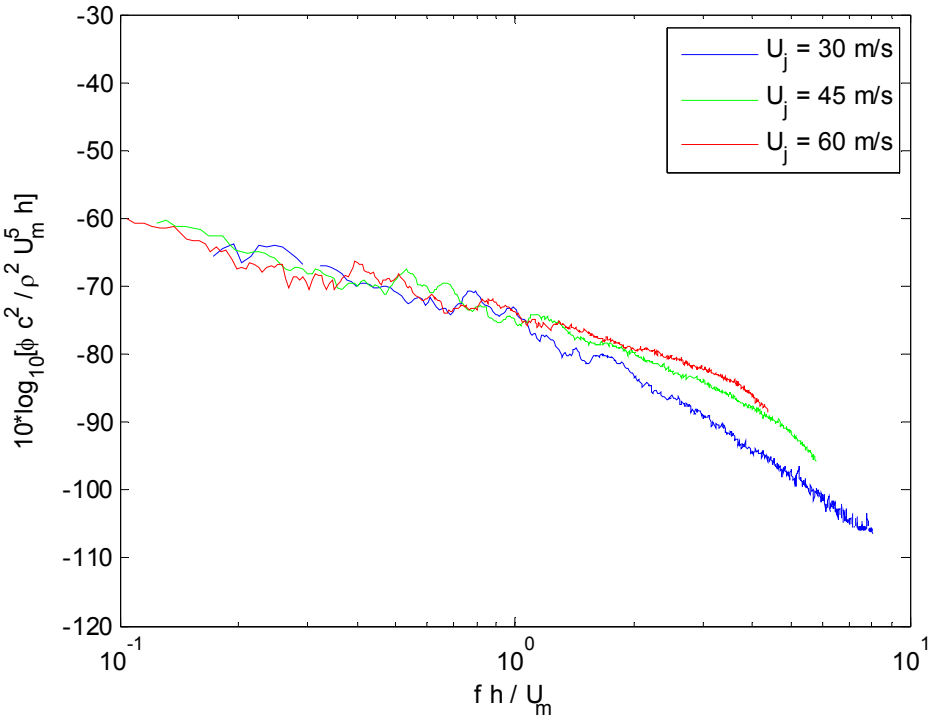

Figure 3.15. Far Field Spectra Normalization for the 4.6 mm Forward Step at $\theta = 123.5^{o}$

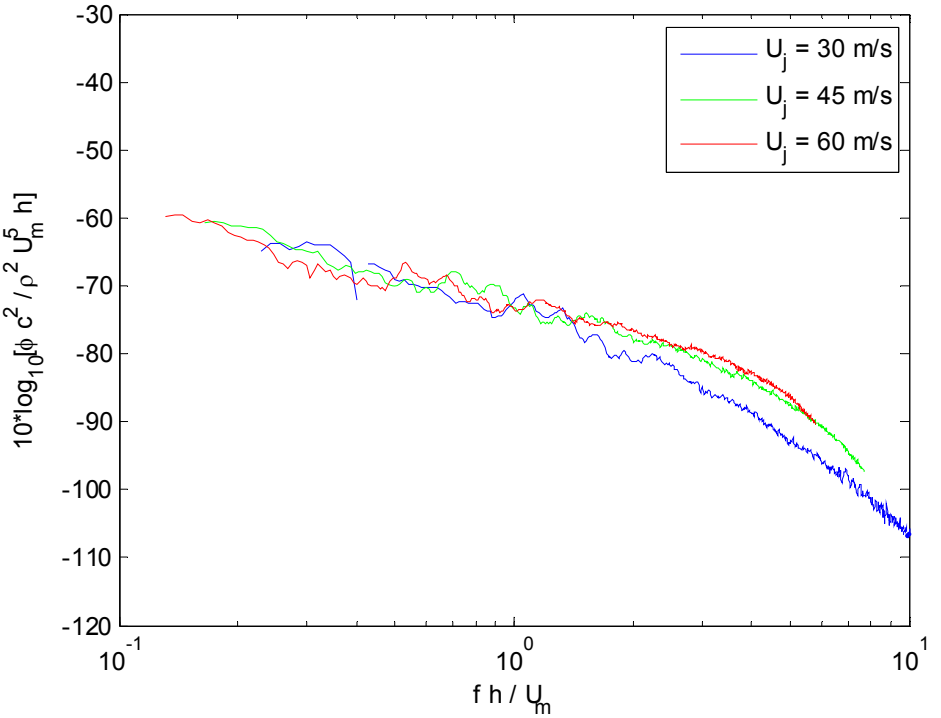

Figure 3.16. Far Field Spectra Normalization for the 6.1 mm Forward Step at $\theta = 123.5^{o}$

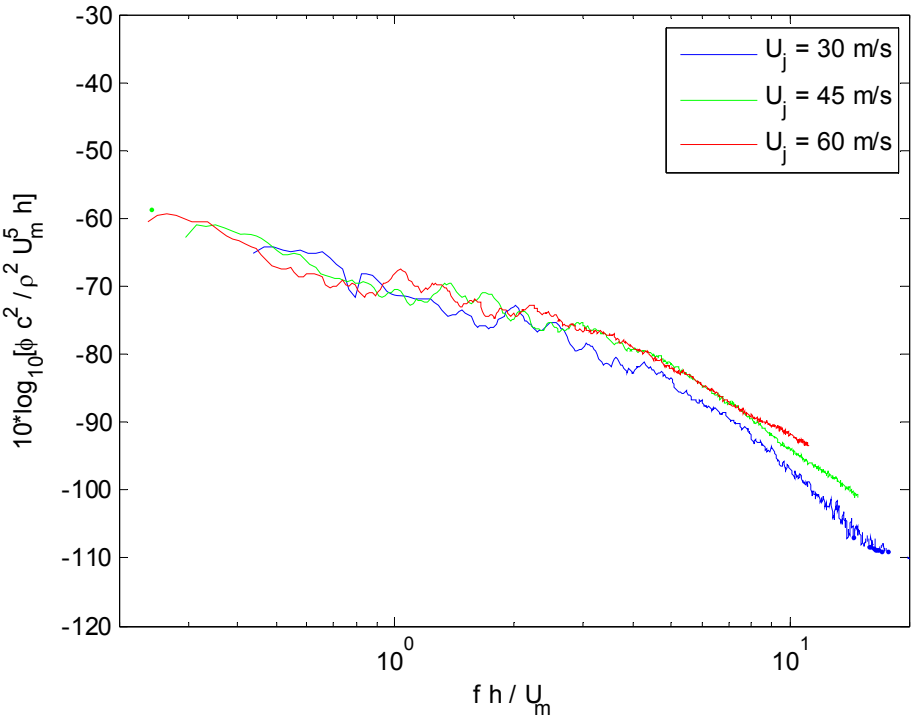

Figure 3.17. Far Field Spectra Normalization for the 11.7 mm Forward Step at θ = 123.5°

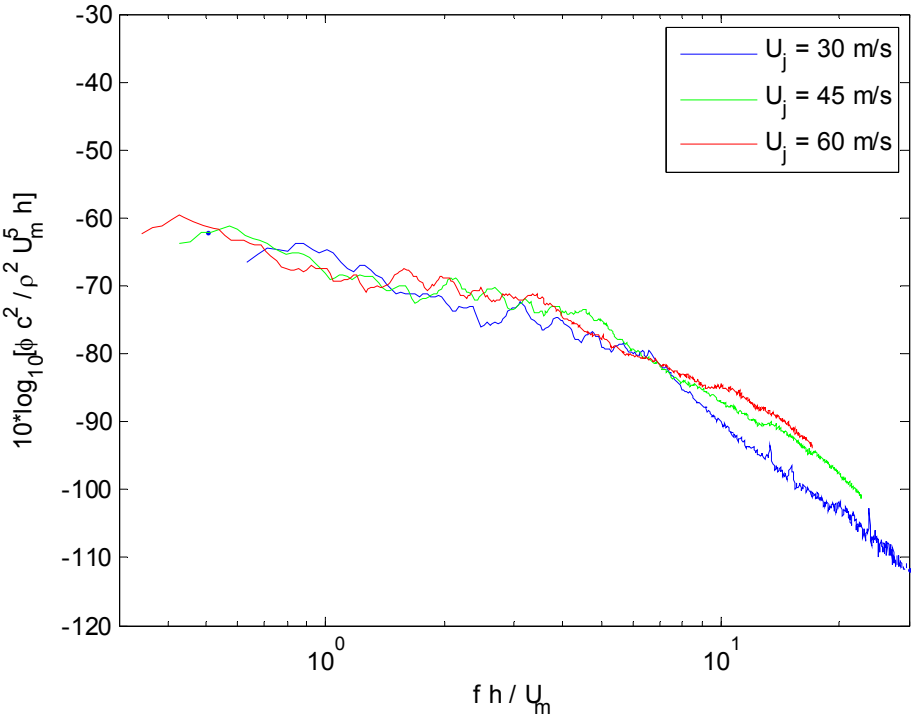

Figure 3.18. Far Field Spectra Normalization for the 18.0 mm Forward Step at θ = 123.5°

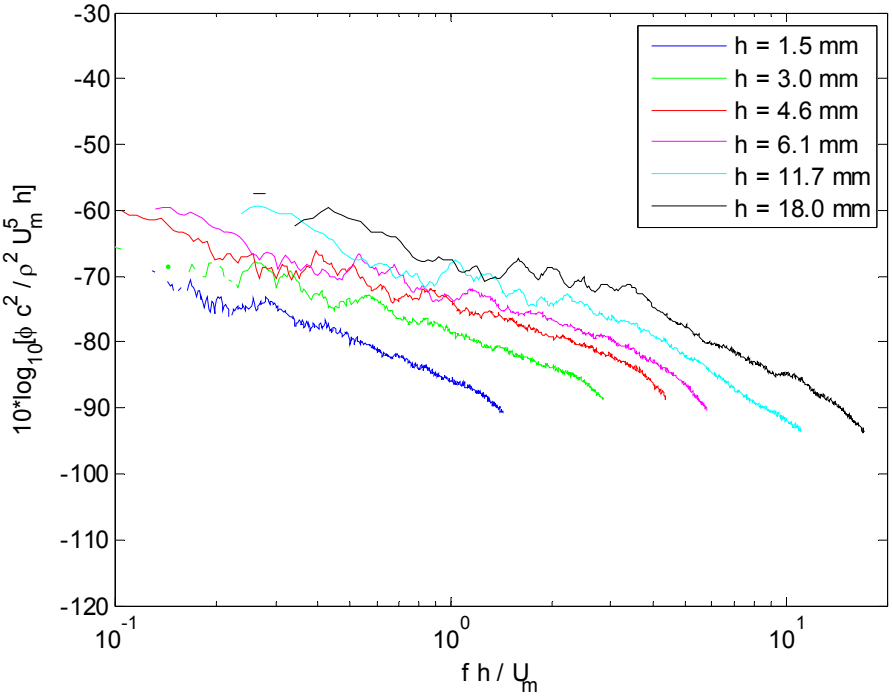

Figure 3.19. Normalized Far Field of all Forward Steps at U_j = 60 m/s and θ = 123.5°

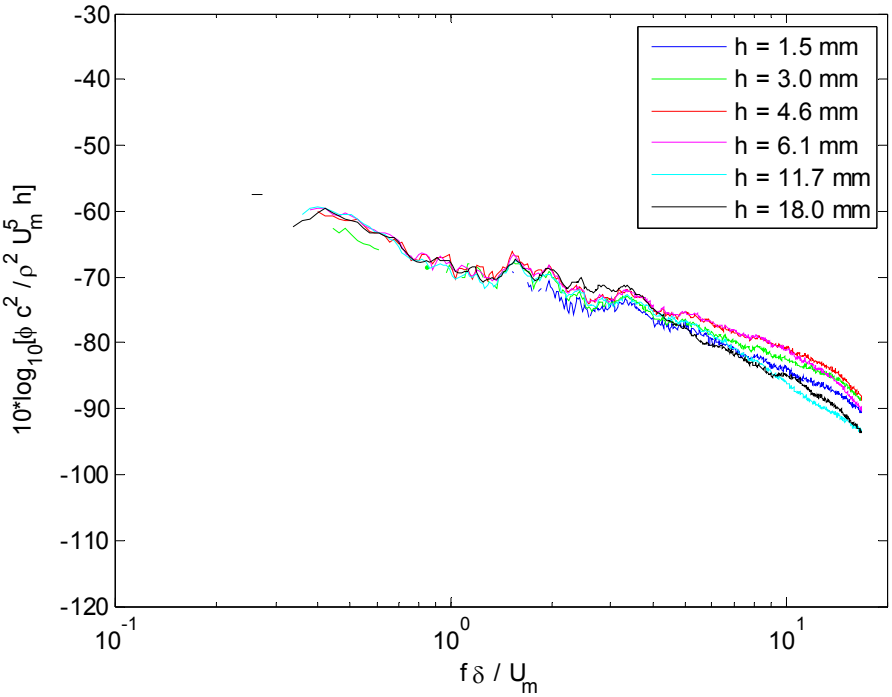

Figure 3.20. Mixed Scaling Normalization of Far Field from all Forward Steps at U_j = 60 m/s and θ = 123.5°

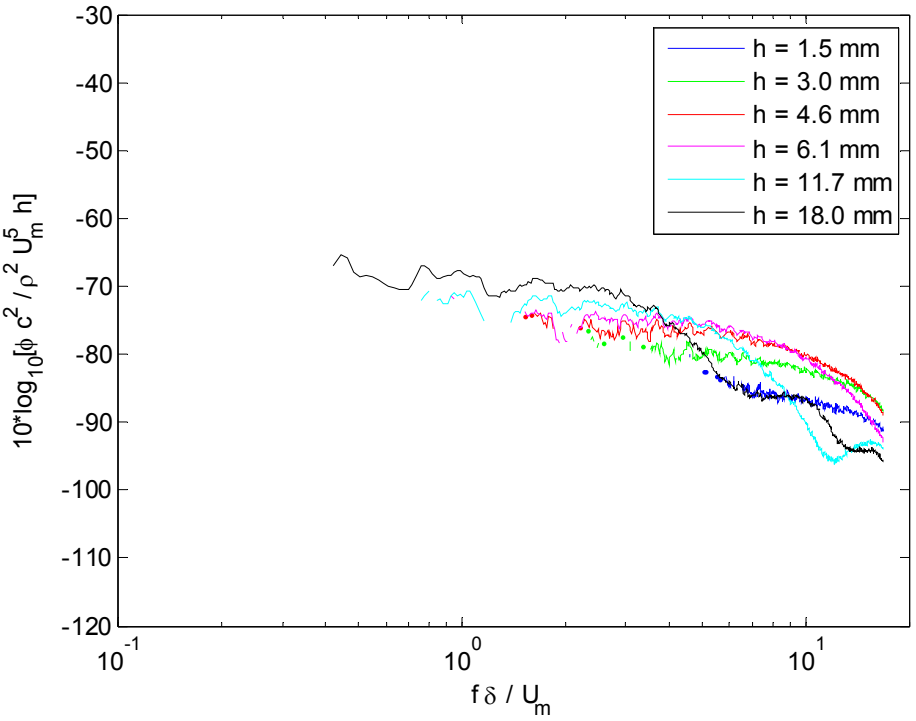

Figure 3.21. Mixed Scaling Normalization of Far Field from all Forward Steps at U_j = 60 m/s and θ = 97.5°

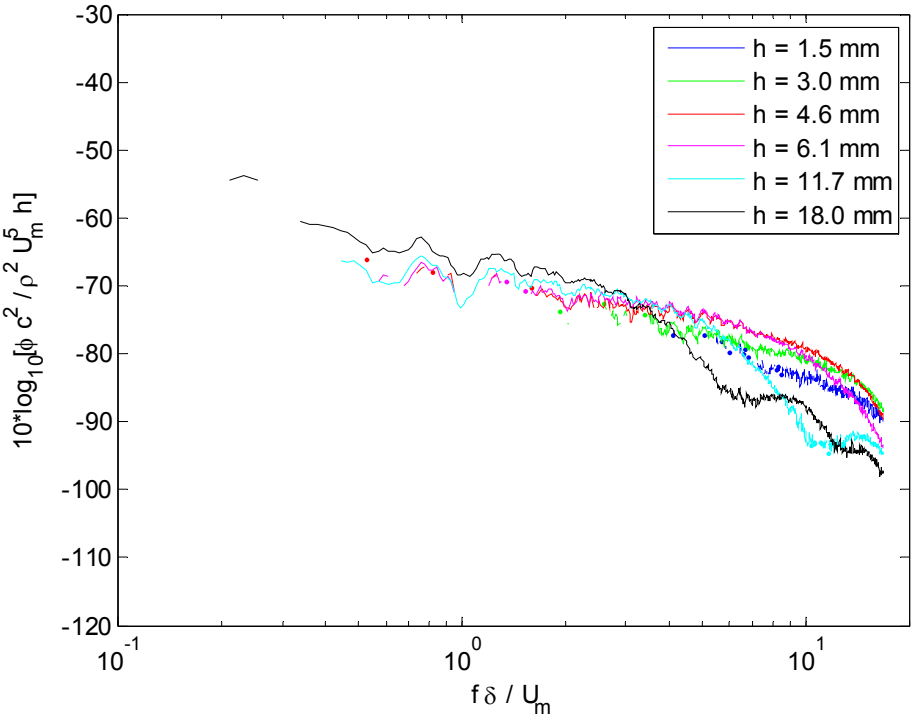

Figure 3.22. Mixed Scaling Normalization of Far Field from all Forward Steps at U_j = 60 m/s and θ = 74°

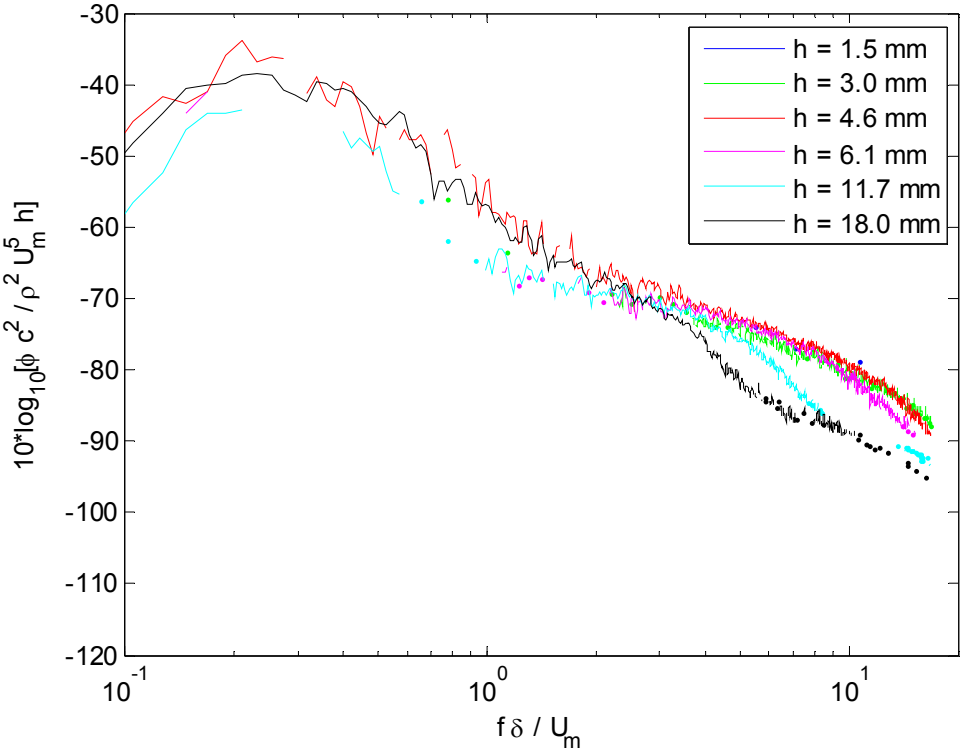

Figure 3.23. Mixed Scaling Normalization of Far Field from all Forward Steps at U_j = 60 m/s and θ = 51.5°

3.2.3 Fluctuating Wall Pressure

The effects of the presence of the forward steps on the fluctuating wall pressure field was examined at locations in front of and behind the set of six forward steps at three wall jet exit velocities. With measurement locations detailed in Chapter 2, the wall pressure field was measured at three locations upstream of all six forward steps of the studied set. Additionally, the wall pressure field was measured at six locations downstream of two forward steps of step height 1.5 mm and 11.7 mm. All of these spectral measurements are compared against the corresponding smooth plate spectra measured at the same location for an undisturbed flow surface. All figures for this subsection are presented at the end of the subsection. The distance from the measurement location to the step feature, $(x-x_s)$, has been normalized on the corresponding step height and is present in the legend of each graph.

Figures 3.24, 3.25, and 3.26 present the wall pressure data in front of the set of forward step heights at the three wall jet exit velocities. This data is taken at a single measurement location which is normalized on the incoming boundary layer height. Only data collected at the closest measurement location to the step collected wall pressure spectra that differed from the clean plate spectra for all step heights. All spectra for all step heights measured at the two further upstream measurement locations coincided with the clean plate spectra.

Figure 3.24 presents the wall pressure spectra for the closest measurement location to the step location for all step heights at the fastest nozzle exit velocity condition. The wall pressure spectrum in front of the smallest forward step of 1.5 mm is undisturbed from that of the smooth plate at this location. This measurement was taken at a location 12.7 step heights in front of the step. The implication of this data is that the furthest reach of any effect on the wall pressure field by this step is restricted to less than approximately 13 step heights upstream of the step. This is consistent with the accepted knowledge of flow over a forward step present in the literature.

The forward step of 3.0 mm does have a measurable influence on the wall pressure field at the closest location which is 6.4 step heights upstream. The step spectra is slightly elevated at low to mid frequency and slightly depressed at mid to high frequency as compared to the smooth wall spectra. A frequency of approximately 3,300 Hz is where the spectra changes from elevated to depressed. This location of 6.4 step heights upstream corresponds with the very beginning of the accepted location of the frontal recirculation zone that exists in front of a forward step. The behavior of the spectra in this region will be further explored with the data collected for the larger step heights, as those locations probe closer to a forward step in terms of step height distance.

For the step height of 4.6 mm, the measurement location of 4.1 step heights in front of the step exhibits similar behavior as seen for the further upstream location and smaller step of 3.0 mm; however the difference between the spectra is greater. This step spectrum is more elevated and more depressed with respect to the smooth plate spectra when compared with the previous measurement. The frequency at which this step spectrum switches from elevated to depressed is approximately 3,000 Hz.

The step spectra for the 6.1 mm forward step measured at a location 3.1 step heights in front of the step exhibits a slightly more pronounced difference away from the smooth plate spectra than at measurement locations further upstream due to the smaller step height. These measurements suggest that as a forward step is approached from the upstream direction the fluctuating wall pressure field starts to experience stronger contributions from low frequency content and less from high frequency when compared to a no step situation. These effects are seen to begin at the front of the forward separation bubble and to become more pronounced as the step is approached. The frequency at which this step spectra switches from elevated at low frequency to depressed at high frequency is approximately 2,600 Hz.

The spectral behavior seen for the 11.7 mm step height at this measurement location is consistent with the behavior discussed earlier. The low frequency content remains elevated and the high frequency remains depressed to that of the smooth plate spectra. These differences are also more pronounced than those seen at measurement locations which are further from the step face in terms of step height distance. As the step is approached it is becoming more apparent that the high frequency features of the

flow are being affected more than the features at the lower frequencies. The approximate frequency at which the step spectra switch from being elevated to depressed in comparison with the smooth spectra is 2,100 Hz.

The closest non-dimensional measurement location for the forward step configuration is located 1.1 step heights in front of an 18.0 mm step and continues to exhibit the trend that has been shown for the other step heights. The low frequency content of the step spectra remains elevated over the corresponding smooth plate. A slight difference is now witnessed, in that middle and high frequency features of the step spectra are depressed below that of the smooth plate. Also, in terms of spectral levels the elevated and depressed behavior is the most extreme when compared to the other configurations. This is consistent with the previous data, showing that the difference between the step and smooth plate spectra continually become more pronounced as the step is approached. The frequency from where the behavior of the step spectra switches from elevated to depressed is approximately 1,300 Hz in this instance.

Figures 3.25 and 3.26 present this same type of data for the full set of forward step heights at wall jet nozzle exit velocities of 45 and 30 m/s, respectively. The same general trends are witnessed for the two slower speeds; however with lower spectral levels due to the slower flow conditions. The spectra for these conditions show a spectral rise at high frequency which is especially apparent at the slowest velocity condition. This behavior is a result of the pinhole caps placed on the microphones and the inability of the microphones to resolve these frequencies due to hitting the electrical noise floor; it is not linked with the behavior of the flow. In order to avoid confusion, the affected parts of the spectra have been dimmed, but are still visible, such that they appear lighter in color than the rest of the spectra.

The frequencies at which the measured step spectra change from being elevated above to depressed below the smooth plate spectra is being termed the cross frequency in this discussion. The cross frequencies were determined for measured spectra in front of the forward steps by inspection for each step height and velocity condition and are presented in Figure 3.27. There are five data points at each velocity condition because the wall pressure spectrum in front of the 1.5 mm forward step coincides with the smooth plate.

This parameter describes what turbulent features of the flow are being exacerbated and which are being suppressed by the presence of the step as the flow interacts with the wall. This is relevant to understanding the fluctuating pressure field exerted on the wall by the flow as well as how the wall pressure field reacts to and develops in the presence of a forward step. The *x*-axis of this plot is logarithmic, and when shown in this way, the data for each velocity condition fall to approximately straight lines. Trend lines fit to the data are present alongside the data and show that the cross frequency varies smoothly with distance in front of the step. These fits to the experimental data are shown below:

$$60 \text{ m/s} : \text{Cross Frequency} = 1089 \ln(x - x_s) + 1378$$

$$45 \text{ m/s} : \text{Cross Frequency} = 738 \ln(x - x_s) + 1008$$

$$30 \text{ m/s} : \text{Cross Frequency} = 518 \ln(x - x_s) + 621$$

Figure 3.28 presents the wall pressure spectra measured at six locations behind both a 1.5 and 11.7 mm forward step at a wall jet exit velocity of 60 m/s. These measurements were taken at the same location on the wall jet plate, but are located at different non-dimensional distances downstream of the step due to the varying step height.

Notable disturbances from the smooth plate measurements persist behind the 1.5 mm forward step up to 55 step heights downstream. These minor disturbances are not present at the lowest frequencies, but exist over much of the mid frequency range. The frequency at which the maximum disturbance is centered is seen to shift to higher frequency with distance downstream. This could be evidence of larger turbulent eddies dissipating into smaller eddies as the flow moves downstream of the wall disturbance.

The wall pressure field appears to return to equilibrium smooth plate values at a location 88.8 step heights downstream of the step; however there is no way of determining when this occurs between the locations of 55.0 and 88.8 step heights downstream for this data set. Interestingly, further downstream at locations over 100 step heights downstream of the forward step the wall pressure spectrum is seen to slightly drop below the smooth plate spectra at high and over some mid frequencies. This would suggest that the wall pressure field does not return to equilibrium in a monotonic fashion. The wall pressure field undershoots the smooth plate spectral equilibrium at high frequency supporting the idea of oscillatory convergence. Unfortunately it is not known what happens even further downstream for this configuration; whether the wall pressure field returns to the smooth plate spectra or settles on a new equilibrium. It is believed that for a classic freestream flow, the original wall pressure equilibrium would be eventually restored; however this assumption is not as easily made for a wall jet flow. The furthest downstream measurement for the 1.5 mm forward step was located 157 step heights away from the step feature and while the low frequency and much of the mid frequency content of the step spectrum had returned to the wall pressure spectrum measured without the step, the high frequency levels had not fully recovered.

The locations for the measurements taken behind an 11.7 mm forward step range from 2.7 to 20.1 step heights downstream of the step and all measured spectra deviate from those of the corresponding smooth plate. The first three spectra of 2.7, 4.9 and 7.1 step heights downstream are all elevated above their corresponding smooth plate values across the entire frequency range. At low frequency the step spectra is elevated by at least 10 dB. This elevated behavior slowly diminishes with downstream distance.

The step spectra measured at 7.1 step heights downstream is seen to just recover to the smooth plate spectra in the high frequency bend at roughly 8,000 Hz. This recovery is further witnessed at the next downstream measurement location of 11.4 step heights as more of the high frequency is recovered to that of the smooth plate spectra.

At the farther downstream location of 15.8 step heights, the low frequency elevation of the step spectra remains and exhibits a slow and smooth recovery back to the smooth plate values. Interestingly however, the high frequency values of the step spectra drop below that of the smooth plate. At the farthest measurement location of 20.1 step heights downstream similar behavior is witnessed. The low frequency step spectral values smoothly and slowly recover back to the smooth plate values. The higher frequency values of the step spectra, are still depressed, but are seen to be gradually recovering to the smooth plate values.

This behavior reinforces the idea of a downstream oscillatory recovery as also seen behind the smallest 1.5 mm forward step. There are similarities and differences though between the behaviors seen for these two configurations. Both exhibit a slow and what appears to be monotonic recovery back to the smooth plate over the low and much of the middle frequencies. Both also exhibit an oscillatory recovery back to the smooth plate spectral values over the high frequency.

A notable difference between the measured wall pressure field behind the 11.7 and 1.5 mm forward steps is the scale over which they take place. The same type of behavior is seen to take place for both step heights, but it occurs over different non-dimensional distances in terms of step height. The fact that the measurements and steps for each configuration are located at physically the same locations on the wall jet plate could support the idea that absolute distance downstream of the step could be more important than first anticipated. It is only the changing step height that accounts for the varying downstream non-dimensional distance.

Figures 3.29 and 3.30 present the fluctuating wall pressure field measured at the six locations behind the 1.5 and 11.7 mm forward steps for wall jet exit velocity of 45 and 30 m/s, respectively. The same general trends are witnessed for the two slower speeds; however with lower spectral levels due to the slower flow conditions. The high frequency spectral rise resulting from aliasing of the signal has again been dimmed out in order to distinguish it as not a property of the flow.

3.2.4 Summary of Fluctuating Wall Pressure Results

In summary, the fluctuating wall pressure field was measured in front of and behind a set of forward facing steps in order to determine the effects of the presence of the steps on the wall pressure field and their downstream influence. The forward-most influence of the step has been seen to correspond with the beginning of the initial separation bubble located upstream of the step. As the step is approached from an upstream location, the fluctuating wall pressure spectra is seen to drop below the undisturbed wall pressure spectrum at high frequency and rise above it at low frequency. The levels of the measured spectrum are exacerbated as the non-dimensional distance to the step is shortened and traverses through the forward separation bubble. Additionally, the frequency at which the measured spectrum is seen to switch from being below to above the undisturbed wall pressure spectrum is seen to drop as the step is approached. This behavior has been modeled by fits to the experimental data for each velocity condition.

The downstream influence of the 1.5 mm forward step was seen to affect the wall pressure field by as much as 150 step heights downstream. Initially this disturbance is seen as an elevated wall pressure spectrum over the mid frequencies. A slow recovery is seen to persist up to approximately 90 step heights downstream. At locations further downstream of the step, the measured spectra were seen to drop below the high frequency levels of the undisturbed wall spectrum.

The downstream influence of the 11.7 mm forward step was only measured to a location 20 step heights downstream. The measured spectra at the three closest locations of 2.7, 4.9, and 7.1 step heights are elevated above the undisturbed wall spectrum at all frequencies with the levels falling with downstream distance. High frequency

coincidence of the two spectra is seen at 11.4 step heights, while the slow recovery over the low frequency persists. Further downstream, the slow recovery back to the smooth wall levels of the low frequency content remains, but a slight drop in levels at high frequency is witnessed.

The high frequency suppression seen downstream of the two step heights occurs for measurements taken at the same physical locations, but that are at very different non-dimensional distances in terms of step height. This behavior suggests a possible oscillatory convergence of the high frequency content back to the undisturbed levels or a settling to a new equilibrium for the high frequency. To conclude either result requires more data for the other step heights and measurement locations that extend further downstream. The low and mid frequency content of the step spectra, however, is seen to monotonically relax back to the undisturbed wall spectral values.

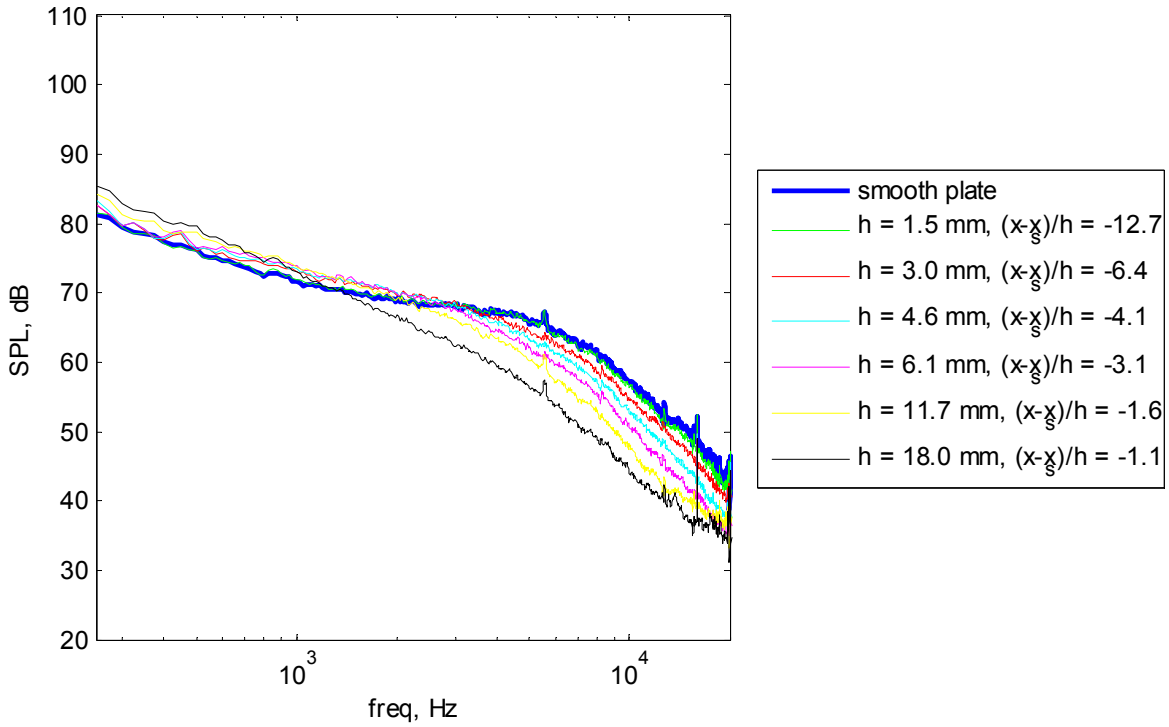

Figure 3.24. Wall Pressure Spectra at $(x_s\text{-}x) / \delta = 1.07$ for all Step Heights at $U_j = 60$ m/s

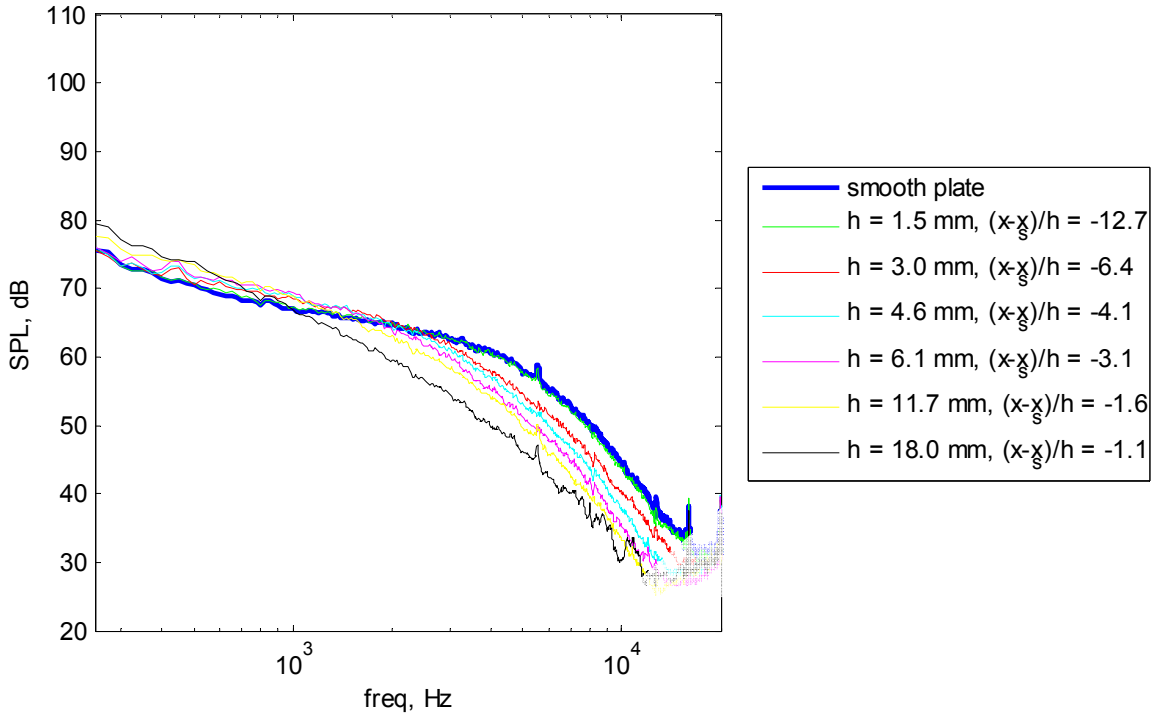

Figure 3.25. Wall Pressure Spectra at $(x_s\text{-}x) / \delta = 1.01$ for all Step Heights at $U_j = 45$ m/s

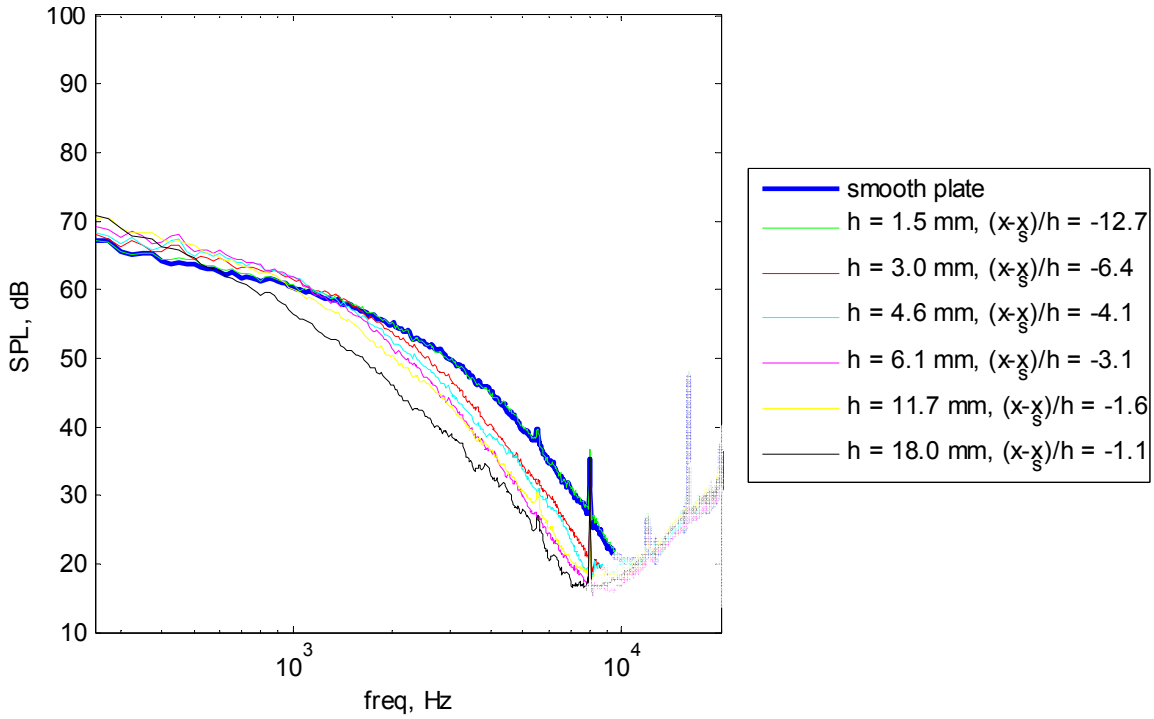

Figure 3.26. Wall Pressure Spectra at $(x_s\text{-}x) / \delta = 0.92$ for all Step Heights at $U_j = 30$ m/s

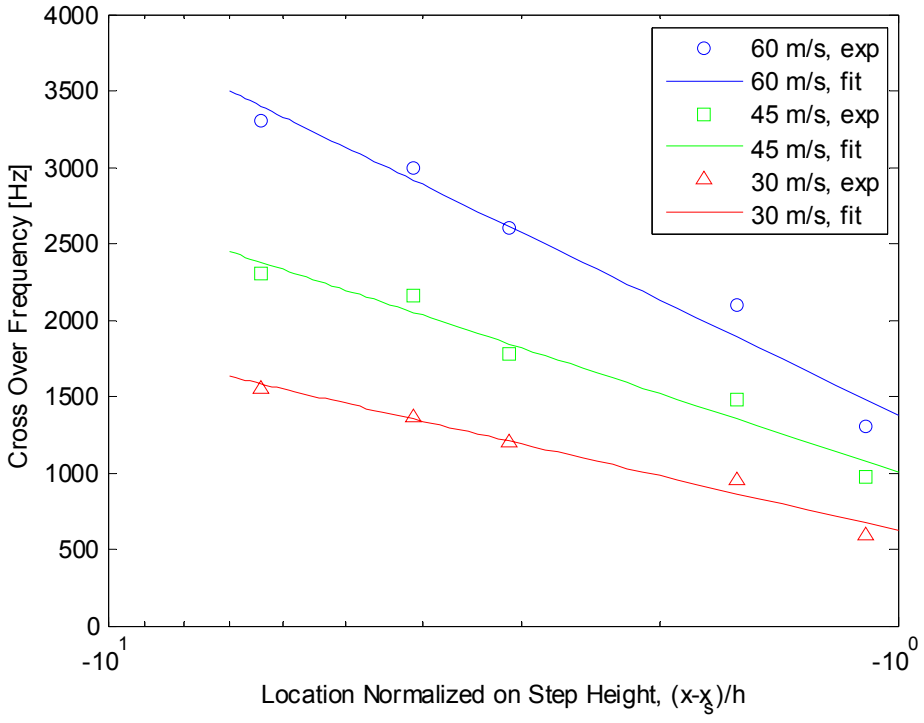

Figure 3.27. Spectral Cross Over Frequency for Locations in front of a Forward Step

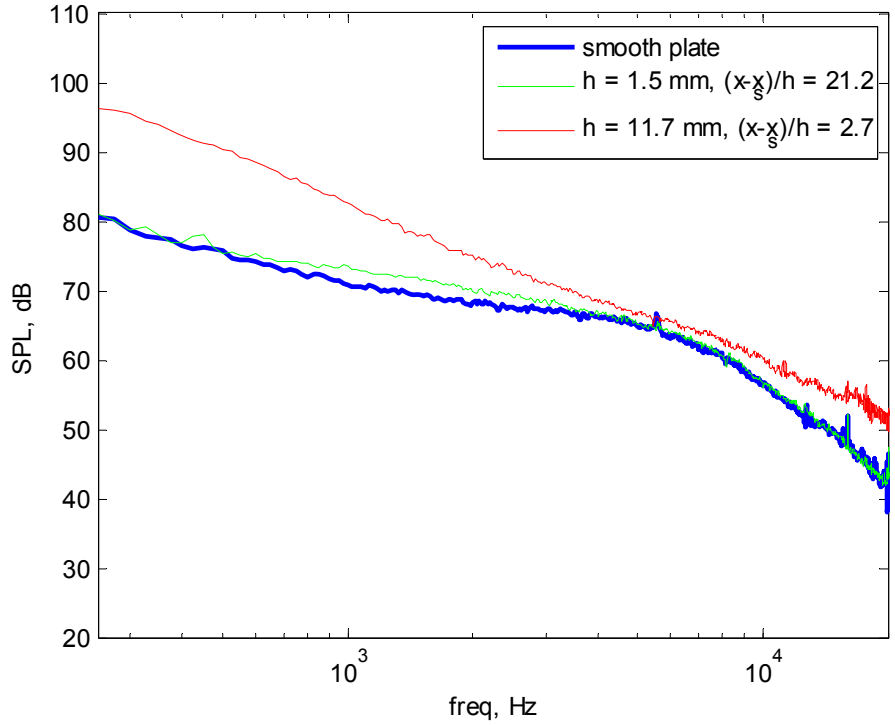

Figure 3.28 a

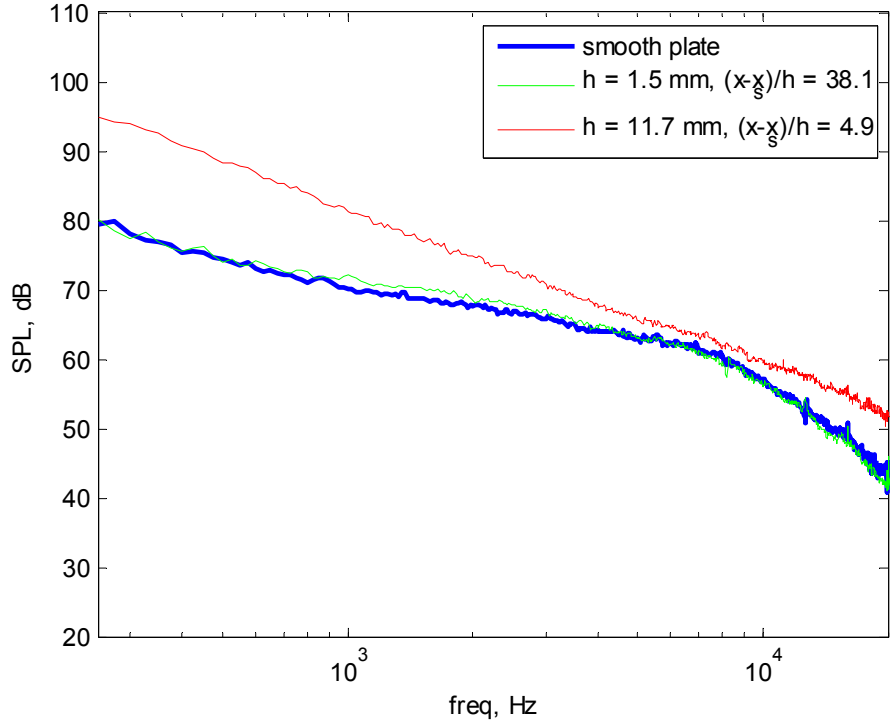

Figure 3.28 b

Figure 3.28 a-f. Wall Pressure Measurements behind a 1.5 and 11.7 mm Forward Step at U_j = 60 m/s

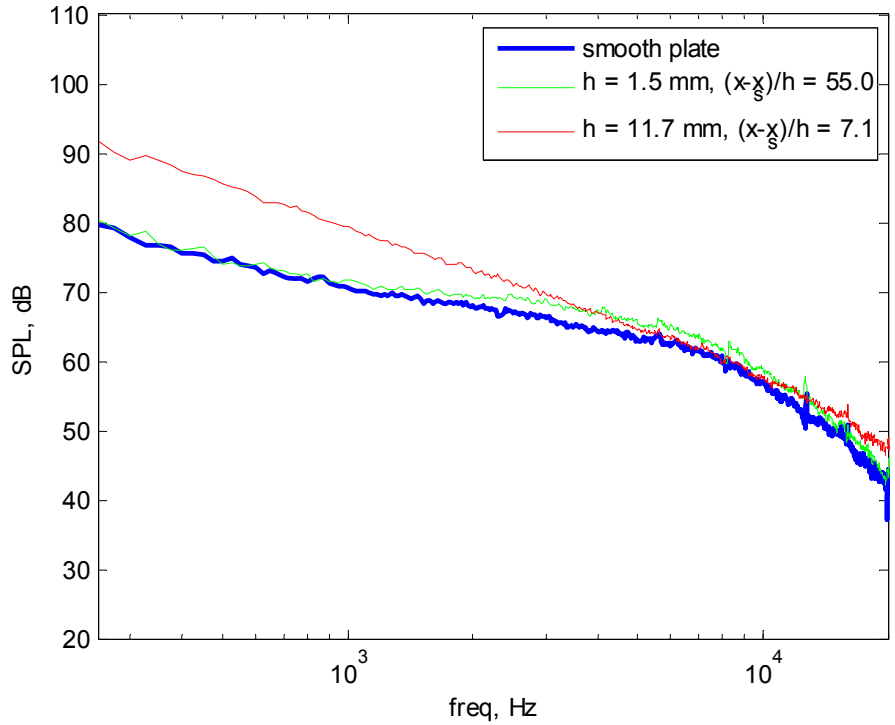

Figure 3.28 c

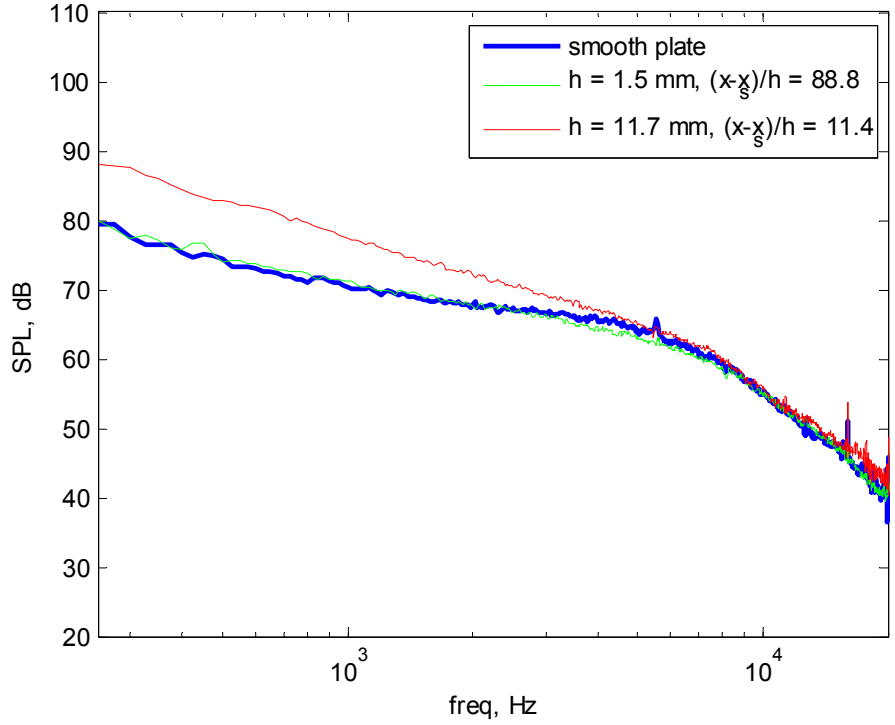

Figure 3.28 d

Figure 3.28 a-f. Wall Pressure Measurements behind a 1.5 and 11.7 mm Forward Step at U_j = 60 m/s

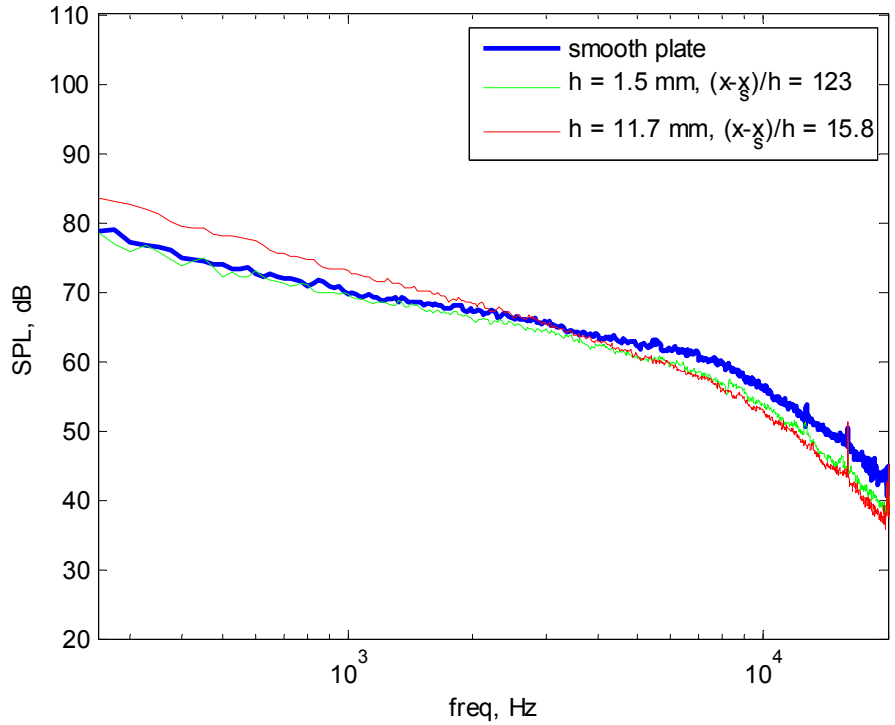

Figure 3.28 e

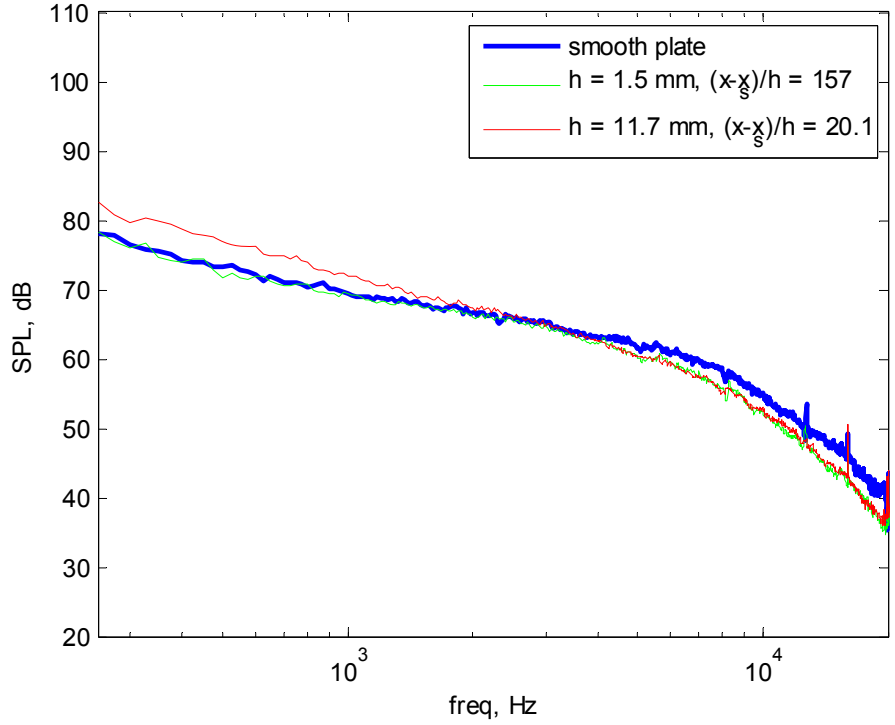

Figure 3.28 f

Figure 3.28 a-f. Wall Pressure Measurements behind a 1.5 and 11.7 mm Forward Step at U_j = 60 m/s

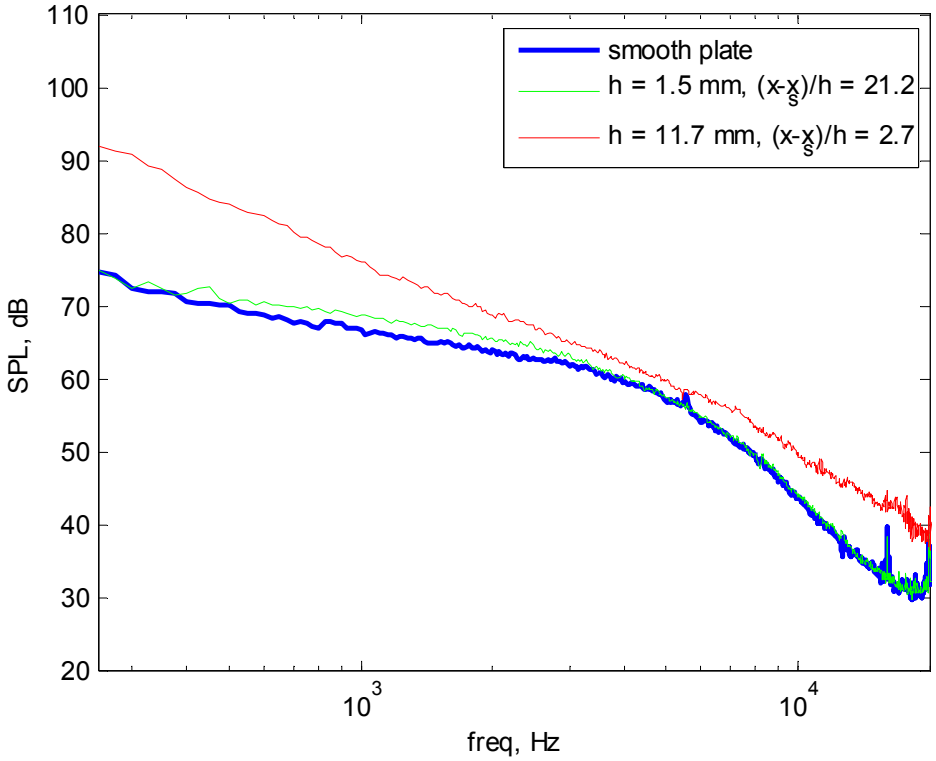

Figure 3.29 a

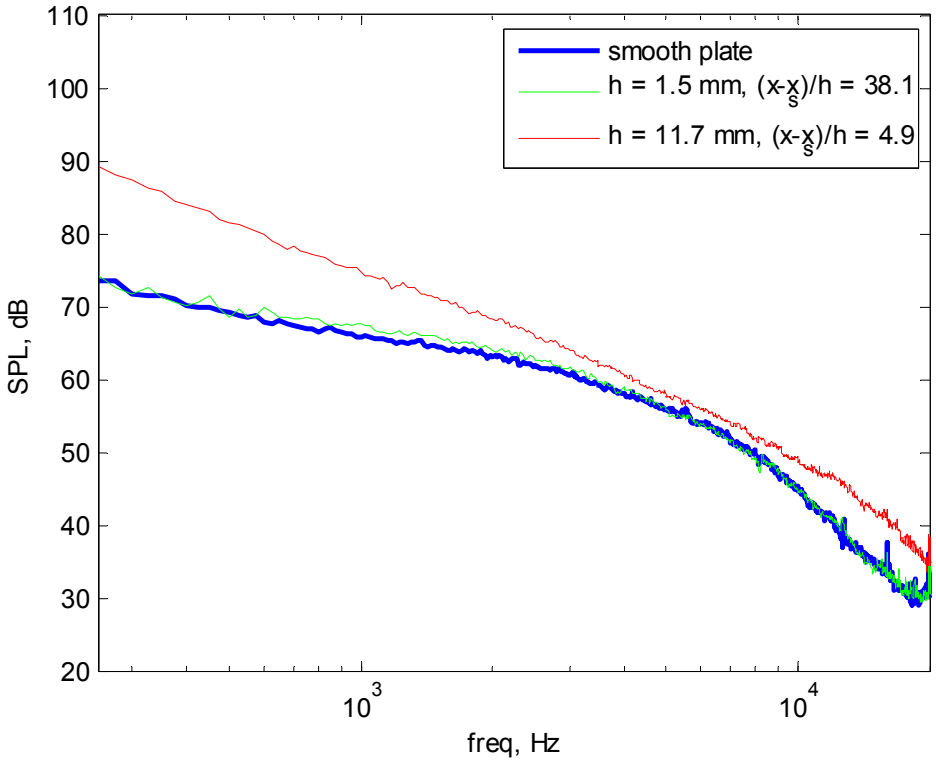

Figure 3.29 b

Figure 3.29 a-f. Wall Pressure Measurements behind a 1.5 and 11.7 mm Forward Step at U_j = 45 m/s

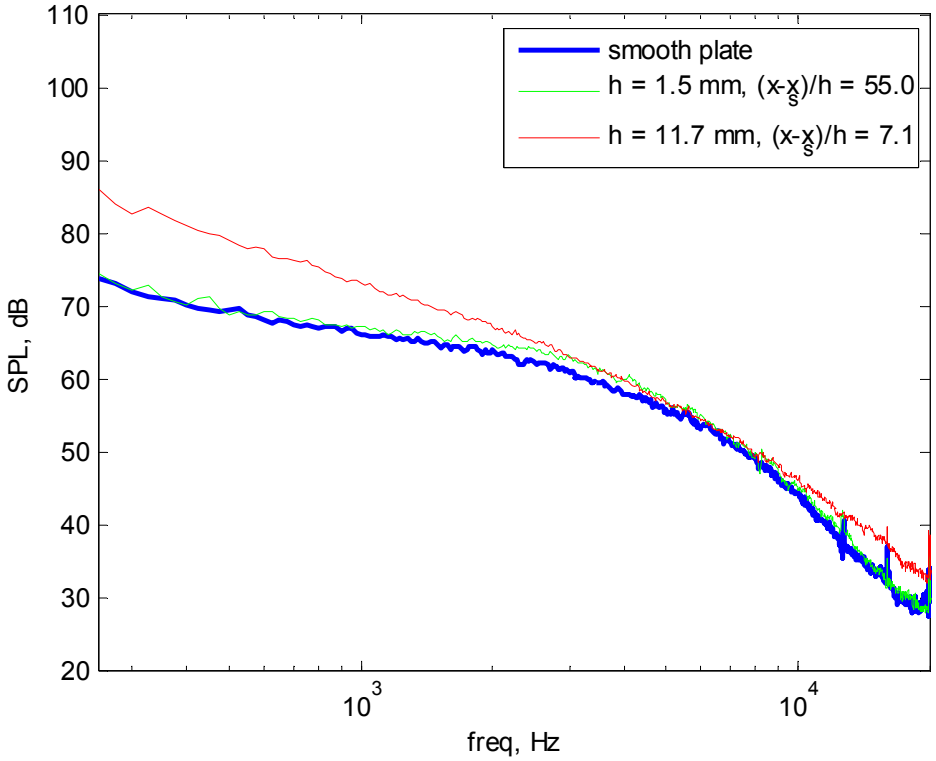

Figure 3.29 c

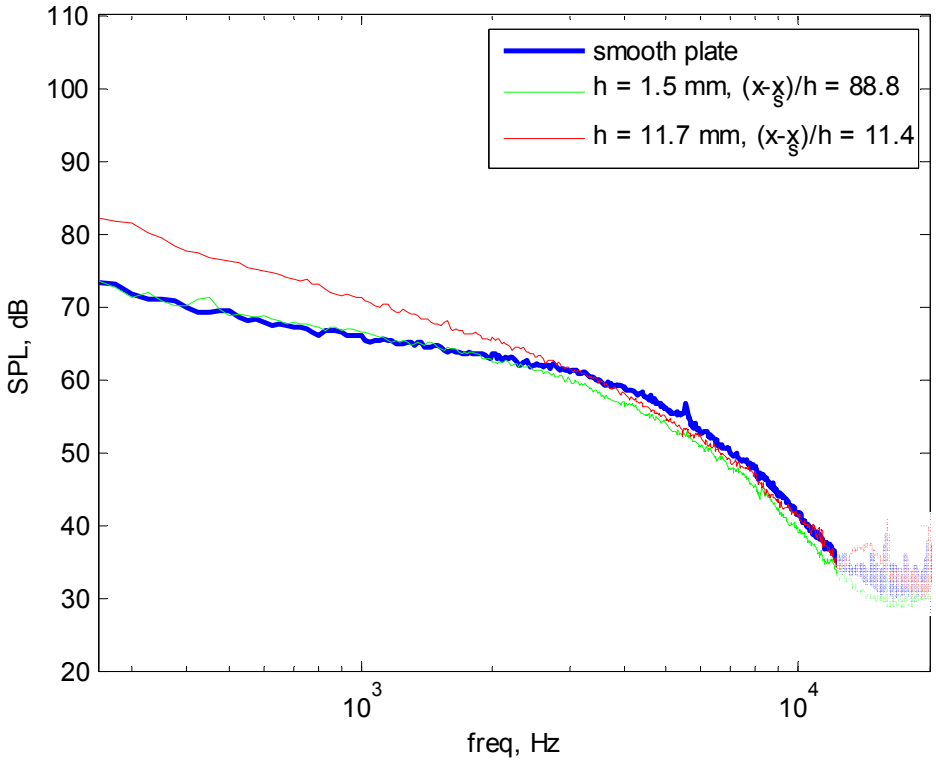

Figure 3.29 d

Figure 3.29 a-f. Wall Pressure Measurements behind a 1.5 and 11.7 mm Forward Step at U_j = 45 m/s

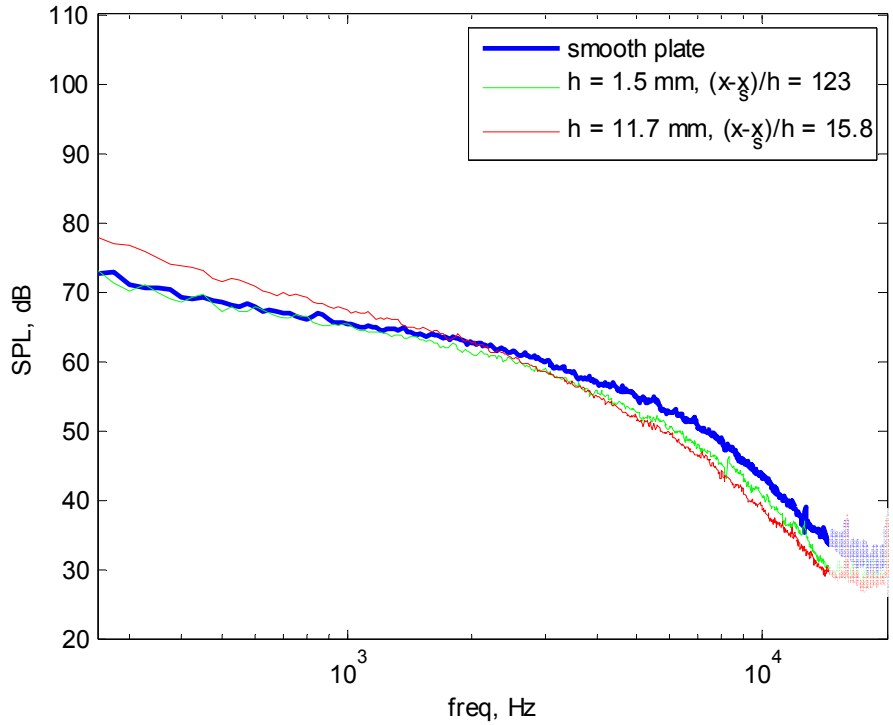

Figure 3.29 e

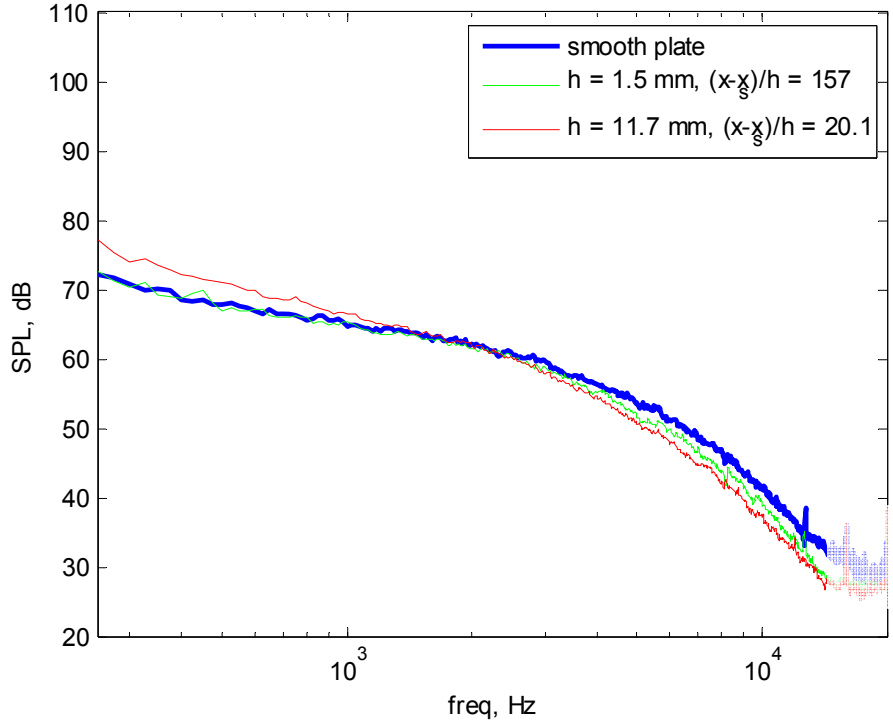

Figure 3.29 f

Figure 3.29 a-f. Wall Pressure Measurements behind a 1.5 and 11.7 mm Forward Step at U_j = 45 m/s

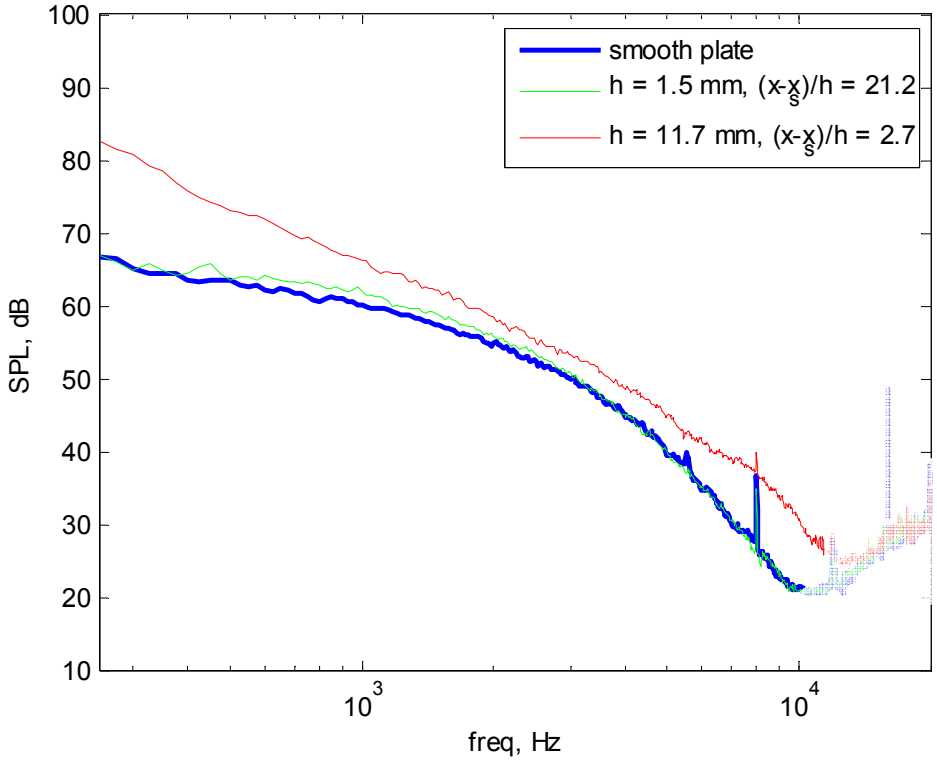

Figure 3.30 a

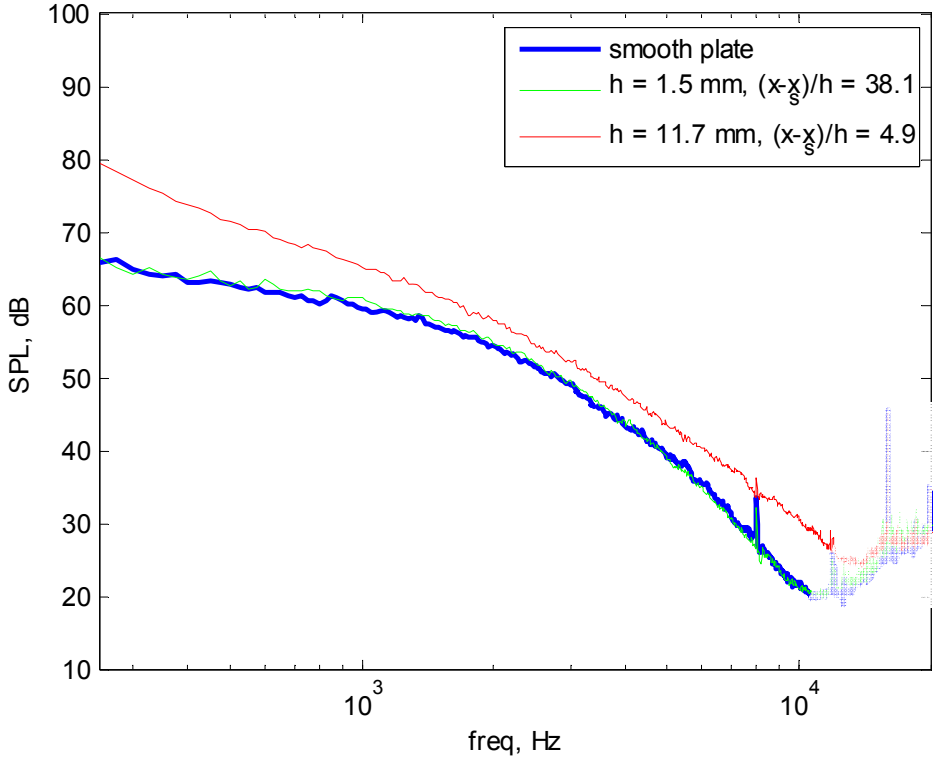

Figure 3.30 b

Figure 3.30 a-f. Wall Pressure Measurements behind a 1.5 and 11.7 mm Forward Step at U_j = 30 m/s

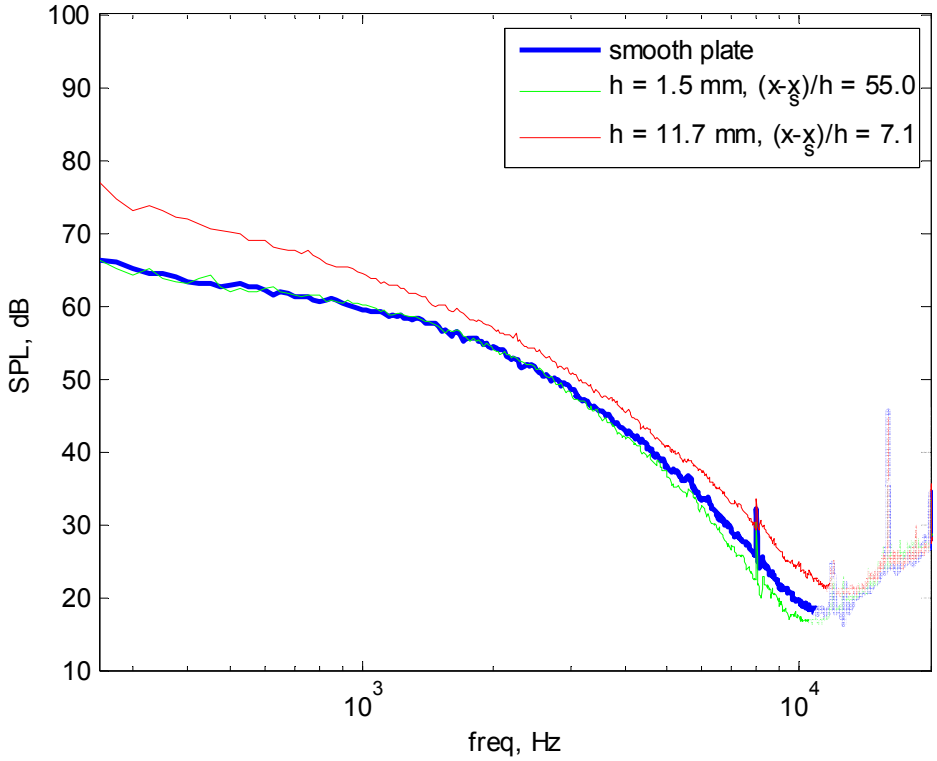

Figure 3.30 c

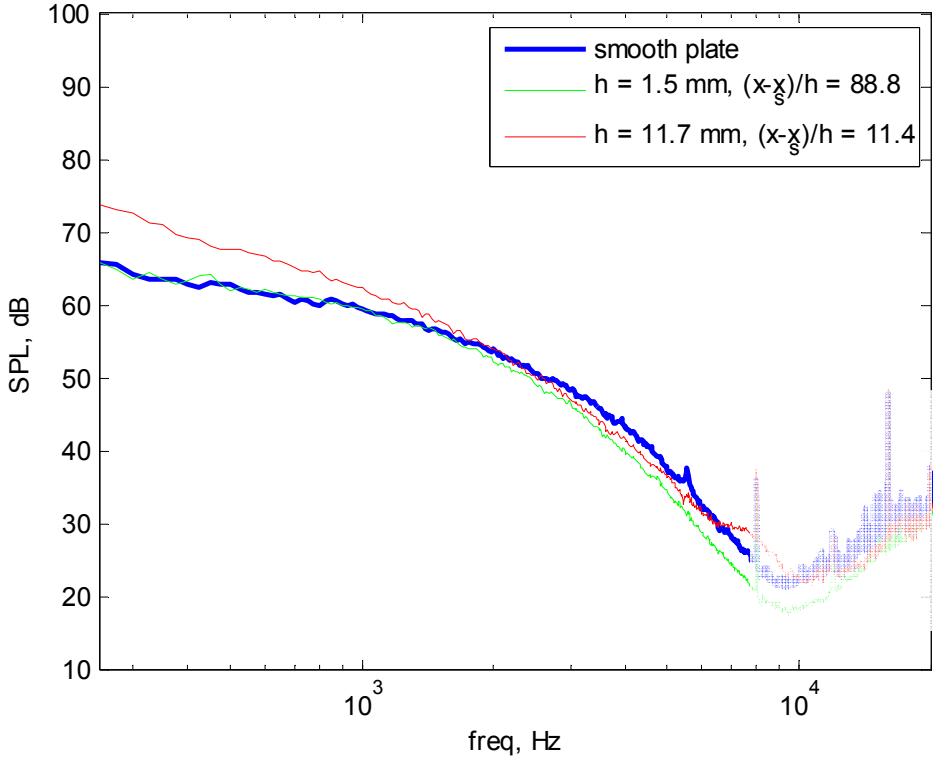

Figure 3.30 d

Figure 3.30 a-f. Wall Pressure Measurements behind a 1.5 and 11.7 mm Forward Step at U_j = 30 m/s

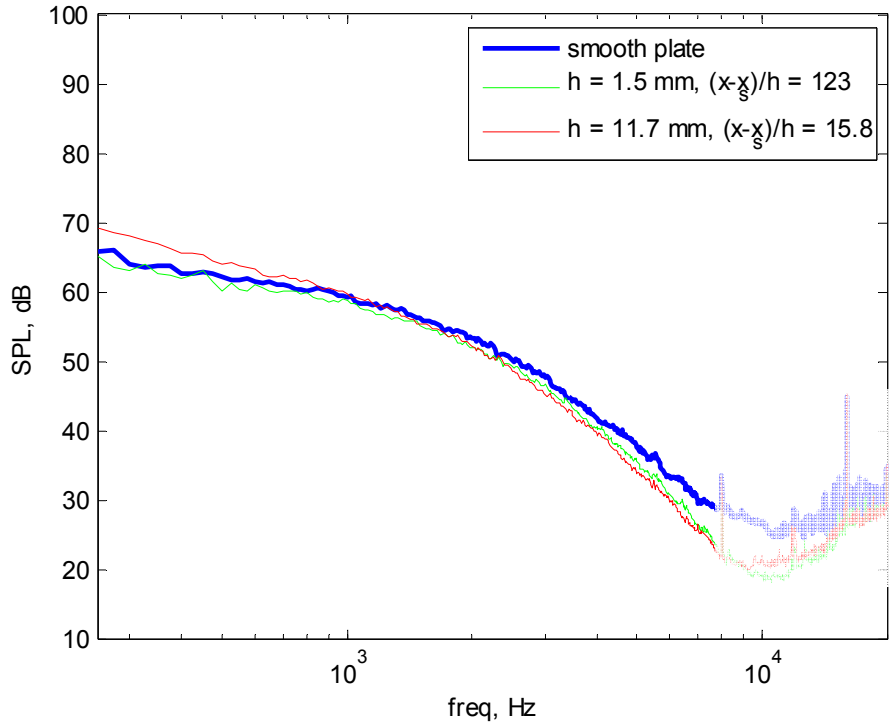

Figure 3.30 e

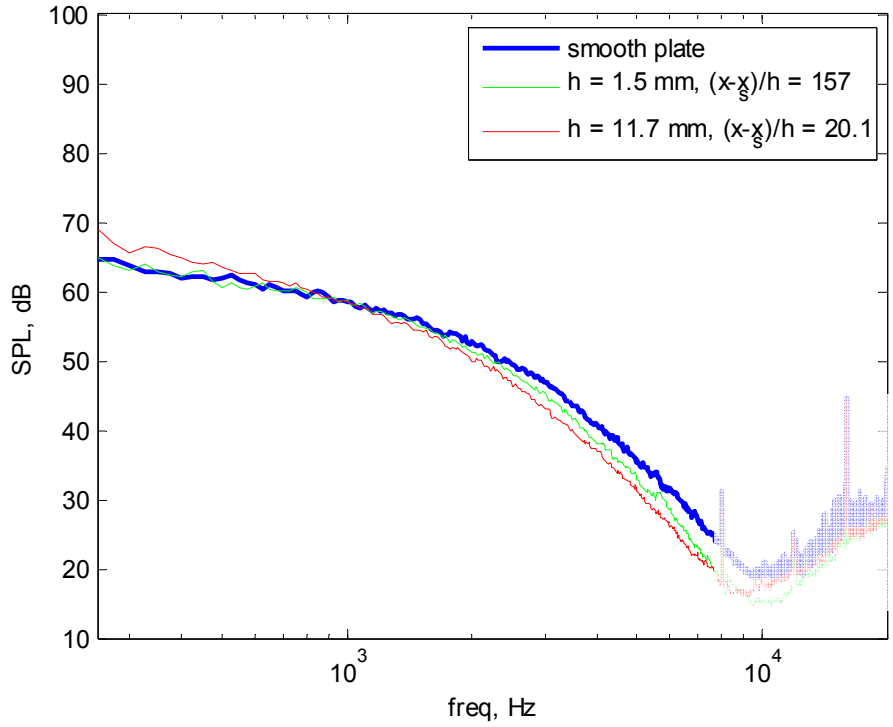

Figure 3.30 f

Figure 3.30 a-f. Wall Pressure Measurements behind a 1.5 and 11.7 mm Forward Step at U_j = 30 m/s

3.3 Backward Steps

This section presents and discusses the results for the flow over the multiple backward steps considered in this study The following subsections will concentrate on the oil flow visualization performed behind the backward steps, then the far field radiated noise, followed by the effect of the steps on the wall pressure field.

The flow behind a backward step is characterized by a shear flow that separates at the open corner of the step. A recirculation zone exists directly behind the backward step which terminates with flow reattachment occurring shortly downstream of the step. The distance to flow reattachment is not a steady value and fluctuates with in a small region as the shear layer impinges on the flow surface. Figure 3.31 highlights this behavior with a schematic representation of a typical backward step flow. Estimations of the lengths of the separation zones will be presented and compared to values from the literature in the subsequent sections.

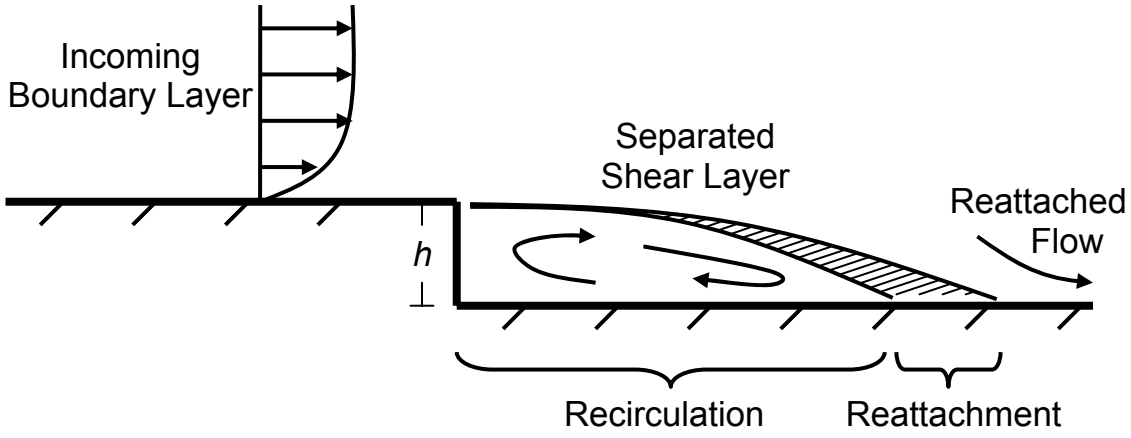

Figure 3.31. Schematic Representation of the Flow Over a Backward Facing Step

3.3.1 Oil Flow Visualization

Oil flow visualization was used behind five of the six backward steps considered in this study in order to study the recirculation zone and to determine the average reattachment lengths behind the steps. Oil flow visualization was not attempted on the smallest step height of 1.5 mm because of the very small size of the step and the inability to resolve a reattachment length so near to the step feature. Figure 3.32 below provides the widest views and completely shows the extent of the patches used for the flow visualization over the various steps. The width of the applied oil mixture spanned almost the entire approximately 0.5 m wide patch of contact paper placed behind the steps in the center of the wall jet.

The views shown are from the set of best results for each step configuration. While only one image is shown here per set and for each step configuration, multiple sets were collected for all five of the backward step configurations. At least three runs per

step configuration were completed in order to ensure consistency of the results and to obtain the best visual results.

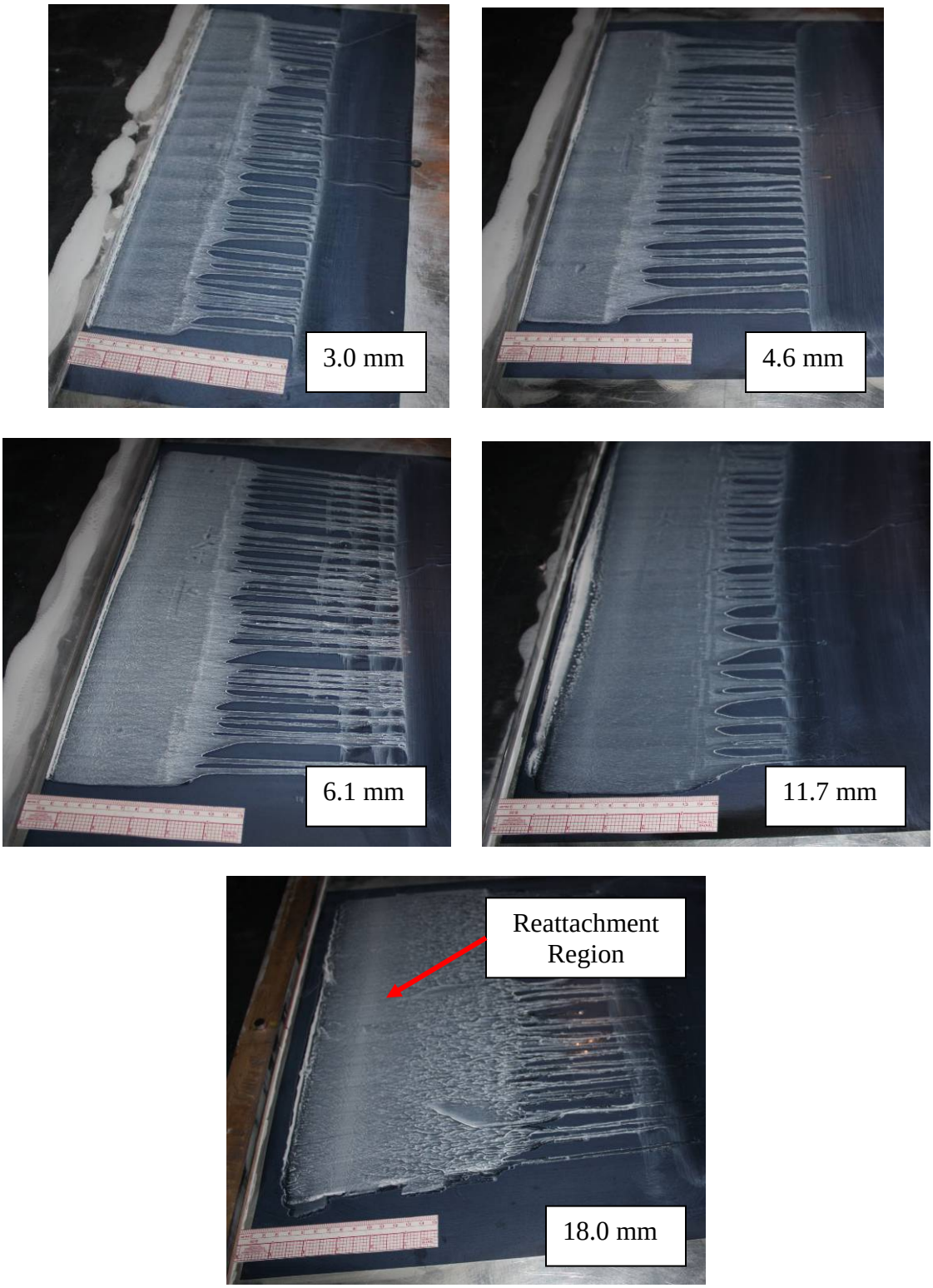

Figure 3.32. Surface Oil Flow Visualization behind Five of the Six Backward Steps

Some of the detail provided by the flow visualization is not clearly visible in these extended views; however it can be seen that the reattachment length is uniform in the spanwise direction parallel with the step. The behavior of how the flow reattaches is found by examining the zoomed views of the pictures of the flow visualization to determine where the flow switches from reversed upstream to downstream movement.

Figure 3.33 provides a close up view of the typical detail given by the oil flow visualization technique. Specifically, this is a view of the reattachment behind the 18.0 mm backward step. It can be seen that there clearly exists a region close to the step where the flow is reversed, as evident by the streaking of the titanium dioxide in the oil flow. Further downstream it is evident that the flow has reattached by the streaks directed downstream. A region in which flow reattachment occurs is also clearly visible. The region of reattachment appears to have a well defined width and to be two dimensional in the spanwise direction. It is apparent that downstream of this region the flow has reattached back to the wall jet plate.

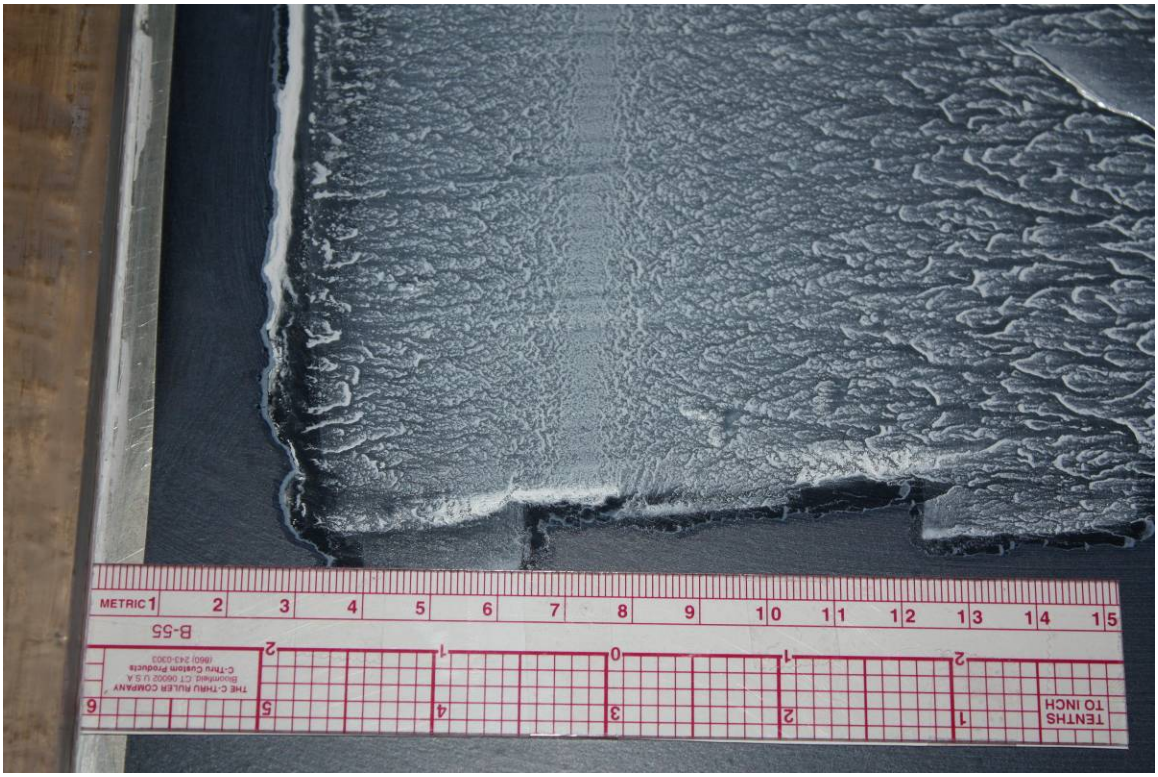

Figure 3.33. Close View of the Typical Detail Attained from the Oil Flow Visualization Technique

From the techniques described in Chapter 2, the average reattachment lengths have been determined as a function of step height. Table 3.8 lists the results for the reattachment lengths as determined visually and Figure 3.34 provides graphs of both reattachment length, x_r, and reattachment length normalized on step height, x_r / h, as a function of step height.

Step Height, h [mm]	Average Reattachment Length, x_r [cm]	x_r / h
3.0	1.65	5.50
4.6	2.6	5.65
6.1	3.18	5.20
11.7	5.53	4.72
18.0	7.28	4.04

Table 3.8. Reattachment Lengths of Separated Flow behind Backward Steps

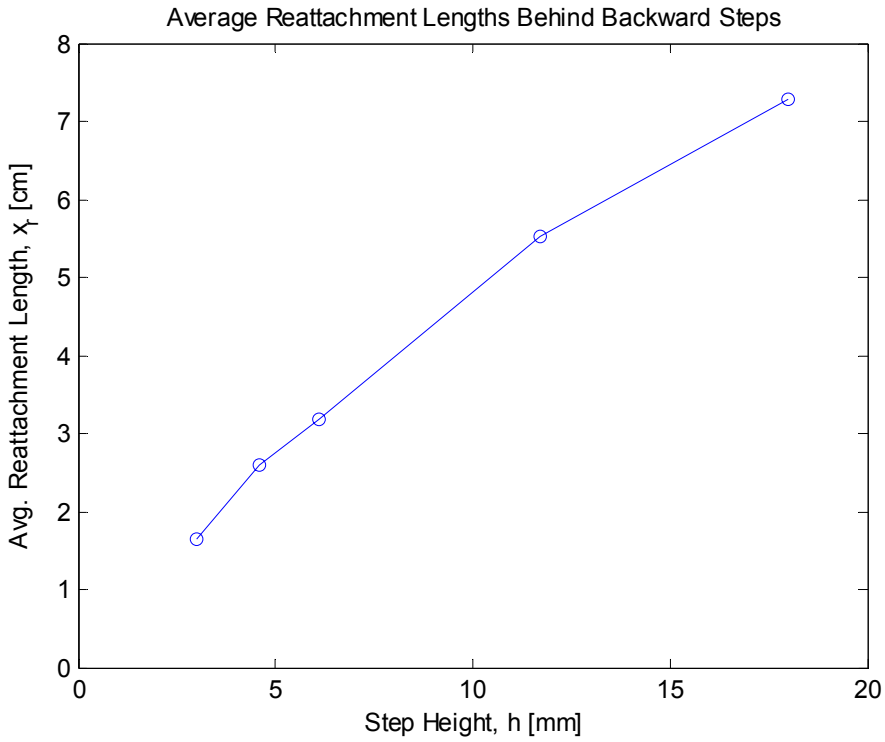

Figure 3.34 a

Figure 3.34 a-b. Reattachment Lengths of Separated Flow behind Backward Steps a) Dimensional Reattachment Length b) Reattachment Normalized on Step Height

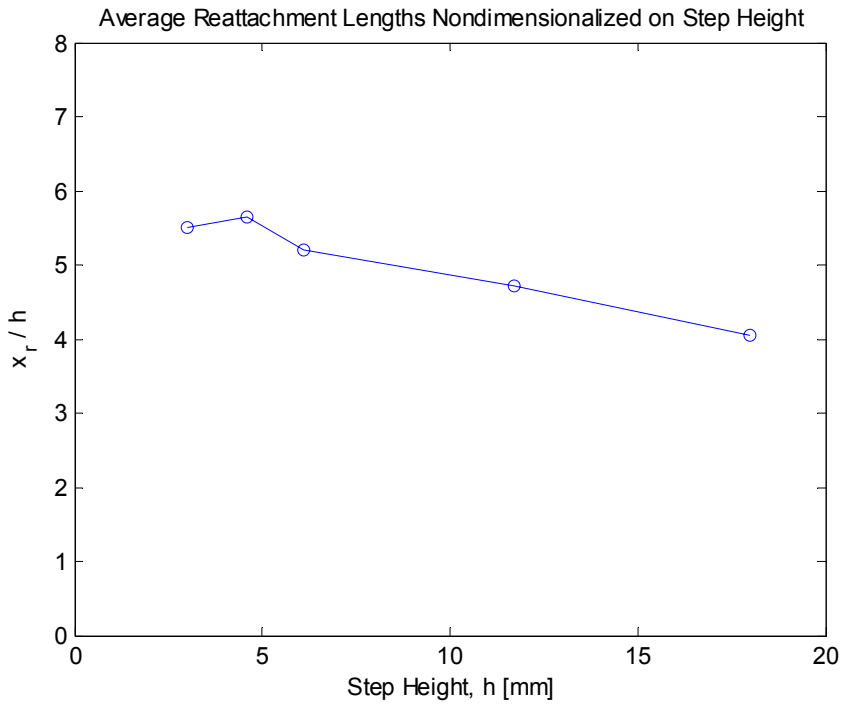

Figure 3.34 b

Figure 3.34 a-b. Reattachment Lengths of Separated Flow behind Backward Steps a) Dimensional Reattachment Length b) Reattachment Normalized on Step Height

As illustrated in Table 3.8 and Figure 3.34, the reattachment lengths behind the backward steps studied here exhibit a smooth dependence on step height. As expected the absolute length to flow reattachment increases with step height. However it is shown that this relation is not constant with step height. Normalized on the step height considered, the separated flow behind the larger steps reattaches closer to the step than for the smaller steps in this set. Overall, a gradual decline in reattachment length normalized on step height is seen as step height is increased. The flow downstream of the smallest backward step of 3.0 mm reattaches 5.5 step heights downstream while the flow downstream of the largest backward step of 18.0 mm reattaches after approximately 4 step heights.

This data generally agrees with the accepted knowledge of flow reattachment lengths behind backward steps; however differences do exist. Farabee and Casarella (1986) quote a reattachment length of approximately 6 step heights for a freestream flow over a backward step, while Jacob *et al.* (2001) quote a reattachment length of 3 step heights for their wall jet flow over a backward step. Past studies identify the reattachment length is highly dependent on flow and turbulence conditions. The lengths determined in this study are in between this range.

It should be noted that the reattachment lengths were only studied for a single wall jet nozzle exit velocity and that the in-flow parameters at the step are not as well defined due to the addition of the forward ramp needed to create the .backward steps. Additionally, these results are influenced by the use of a wall jet flow with a large mixing layer present on top of the near wall flow as opposed to a typical freestream.

3.3.2 Far Field

The radiated sound from the backward steps was studied for six different step heights, at four stream-wise observation angles, and at three different local maximum velocities. All of the definitions and conventions described in Chapter 2 are assumed in the presentation of this data. All figures for this subsection are presented at the end of the subsection.

The far field spectra for all six step heights, at the four observation angles for a wall jet exit velocity of 60 m/s are presented in Figure 3.35. As can be seen, only the two most upstream observation angles of 123.5^o and 97.5^o measure significant flow induced noise above that of the facility background.

The registered signal at high frequency for the 6.1 mm step at an observation angle of 74^o is believed to be an experimental error in the setup of the step configuration. This is supported by the lack of measured spectra for the other step heights. This same error is believed to have affected the data for the two upstream observations angle as well. The far field spectra for this step height are elevated above the others and do not appear to follow the same trend as the other spectra. Coupled with the unusual signal measured at an observation angle of 74^o, it is believed that more measurements are needed at this condition in order to accept or reject this behavior and to draw any conclusions from the data at this step height.

Excluding this one exception, no meaningful far field spectra were measured for any step height for the two downstream observation angles due to the sparse nature of the signals. These signals are essentially indistinguishable from the background noise of the facility. While unfortunate, this behavior is consistent with what has been experienced in past experiments. Farabee and Zocola (1998) and Leclercq *et al.* (2001) show that the radiated far field is much weaker from backward steps as compared to similarly sized forward steps. This backward step behavior coupled with higher background levels present at these downstream observation angles would explain the lack of signal at these locations.

The two upstream observation angles of 123.5^o and 97.5^o both show data for much of the set of backward step heights, although at much weaker signal to noise ratios when compared to the same data for the set of forward steps. This weaker signal above the background of the facility is evident by the jagged nature of the spectra resulting in greater uncertainty.

For the most upstream observation angle a weak dependence on step height is seen for the overall levels of the far field spectra. All of the spectra bunch together in a band (excluding the 6.1 mm backward step) that is much less dependent on step height than the same forward steps. This could be an effect of these signal to noise ratios also being much smaller than for the forward steps; effectively shadowing the step relationship that could be determined with a quieter background. The cut-in frequency for the spectra is however strongly dependent on step height.

Analyzing the rise in spectral level with step height is more difficult for this data due to the sparseness of the data and limited frequency range. All spectra fall into a band which is consistently 6 dB wide across the frequency range. This is significant considering the range of step heights being considered. This behavior highlights the physical difference between the flow induced noise from backward steps as opposed to

forward steps and suggests that the backward step noise is produced by a different mechanism.

Upon closer inspection, the far field spectra for the two largest step heights show similar behavior of dips in the spectra as witnessed for the forward steps. For the 18 mm step height, this is seen by the cutting in and out of the spectra which is where the signal drops back to the level of the background. A similar, though less obvious dip is seen for the 11.7 mm step at a higher frequency. Under the same premise as the discussion for the forward steps, this behavior is believed to be a result of deconstructive interference occurring for the source as sound is reflected off of the flow surface. The source localization of Leclercq *et al.* (2001) provide evidence that the source from the backward step is a result of the turbulence created by the separated flow beginning at the edge of the step. With a source located in the proximity of the step edge, it would follow that similar deconstructive interference would occur for this source as it did for the forward steps.

The analysis of the behavior of the radiated sound from the backward steps is identical to that of the forward steps, except that these signals and spectral dips are not as well defined as those of the forward steps. Instead of the far field spectra dipping but always remaining above the background, as for the forward steps, these spectra fall back to the background levels making identification of the frequency at which deconstructive interference is occurring much less certain. Considering this discrepancy, estimates of the frequencies and resulting wavelengths is not made, but are seen to be generally consistent with the expected values based on the two largest step heights.

Figures 3.36 and 3.37 provide the same far field spectra for the full set of backward steps and four observation angles for wall jet exit velocities of 45 and 30 m/s, respectively. All of the same general descriptions apply to this data, noting the difference in spectral levels and signal quality as a result of the slower flow conditions.

Figure 3.38 presents the far field spectra for the 11.7 mm backward step at the most upstream observer angle of 123.5^{o} as a function of the three wall jet nozzle exit velocities. Parts of the spectra are missing due to coincidence with the background levels. Table 3.9 provides the spectral levels in dB at a specific frequency of 3 kHz for the 11.7 mm backward step at the three nozzle exit velocities.

SPL @ 3 kHz [dB]	U_j = 30 m/s	U_j = 45 m/s	U_j = 60 m/s
h = 11.7 mm	-12.0	1.00	6.45

Table 3.9. Sound Pressure Level at 3 kHz for an 11.7 mm Backward Step with varying Nozzle Exit Conditions

This rise with velocity is seen to shift the spectra upward in level as well as slightly to higher frequency. The velocity scaling of this data is not as clear as for the forward steps; however the far field spectra for this configuration appear to scale on the 6^{th} power of velocity. This is consistent with work of Jacob *et al.* (2001) that show a power dependence on velocity to 6.2 at a similar observation angle; however this is not constant with observation angle. It should be noted that this is different than the 7^{th} power scaling seen for the forward steps.

Figure 3.39 presents the spectra for the 11.7 mm backward step at the fastest wall jet nozzle exit velocity of 60 m/s for the set of four observation angles. As previously discussed, essentially no distinguishable signal is recorded for the two downstream observation angles. The spectra for the two upstream observation angles band together quite well; to within 2 dB over their range. Though limited to two observation angles this shows the lack of source directivity for the flow induced noise from a backward step.

The same normalization scheme as was presented for forward steps was attempted on the far field sound from these backward steps. The normalization is made on step height, h, and local maximum velocity, U_m, in the following way:

$$\frac{fh}{U_m} \text{ vs. } 10\log_{10}\left(\frac{\phi c^2}{\rho^2 {U_m}^5 h}\right)$$

Figures 3.40 through 3.44 shows the spectra for a specific step height at an observation angle of 123.5^o for the three wall jet nozzle exit velocities considered in this study. It should be noted that data at dimensional frequencies above 20 kHz have been cut off in the same way that they are not presented in the earlier dimensional spectra. Additionally, the size of the decade spacing of the axes remains the same in each figure for easier comparison. The x-axis of the figures for the two largest step heights have been shifted to higher non-dimensional frequencies in order to completely show the data, but the decade spacing remains the same.

This normalization was not performed on the smallest step height of 1.5 mm because this step only registered far field data at the fastest velocity condition, making normalization less useful. For the other step heights, the normalization reliably collapses the spectra at the various velocity conditions. The data for the 3.0 and 4.6 mm backward steps is sporadic because of the low signal to noise ratios of these signals as a result of the weaker sources associated with backward steps. The normalizations for larger steps of 6.1, 11.7, and 18.0 all collapse the spectra for all three velocity conditions. Interestingly, the normalization of the 6.1 mm backward step appears to be effective at collapsing the spectra despite the unusual behavior described at the beginning of this section. The data for this step height still deserves scrutiny though.

The normalized spectra are seen to be shifted to higher non-dimensional frequencies as step height is increased. Figure 3.45 shows this trend by comparing the normalized spectra for each step height, but only at the fastest velocity condition. Again, all of this data is for an observation angle of 123.5^o.

A slightly altered form of this normalization was attempted by replacing step height, h, with boundary layer height, δ, as the length scale along the x-axis of the normalization. This mixed scaling normalization takes the following form:

$$\frac{f\delta}{U_m} \text{ vs. } 10\log_{10}\left(\frac{\phi c^2}{\rho^2 {U_m}^5 h}\right)$$

This normalization is presented in Figure 3.46 for the five step heights at the fastest velocity condition and for an observation angle of 123.5^o. In a similar fashion as for the forward steps, this normalization collapses what data is present over the middle

frequencies while the higher frequency levels fan out with step height. It is seen that the deconstructive interference reduces the quality of this normalization at high frequency as the spectra dip and fan out. The mixed scaling normalized spectra for the observation angle of 97.5^o are presented in Figure 3.47 with the same general description applying to these curves. The other two observation angles are not presented because of the lack of significant data.

Figure 3.48 presents the far field spectra from an 11.7 mm forward and backward step at the fastest wall jet nozzle exit velocity of 60 m/s and an observation angle of 123.5^o. This figure illustrates the difference in source strength between the two step configurations. The spectra of both steps maintain an approximately constant spacing of 10 dB between them, except where the backward step spectra bends down at high frequency which is a result of the subtraction scheme utilized in the presentation of this data as the spectra drops back to the background levels of the facility. This agrees with the calculated results of Ji and Wang (2008) which predict the same spacing of one decade between the spectra from a forward and backward step. This is also qualitatively in agreement with Farabee and Zoccola (1998) who found their forward steps to be approximately 5 dB above the background of their facility, but could not measure sound from a backward step.

3.3.3 Summary of Far Field Results

In summary, the radiated far field sound from a set of six backward steps was studied at three velocity conditions for four observation angles. The far field spectra are shown to be dependent on local maximum velocity; however only weakly dependent on step height. This is in contrast to what was seen for forward steps. The spectra for all step heights at a given velocity condition all remain with in an approximate 6 dB band. A velocity scaling of approximately velocity to the 6^{th} power is seen for this data, which is again different than what was seen for forward steps. Essentially no directivity is witnessed in sound source; however this was limited to only two observation angles. No distinguishable data above that of the background was collected for the two downstream observation angles. The same deconstructive interference is witnessed in these spectra as was for forward steps, but the effect is much less drastic as these signal to noise ratios are smaller. As opposed to the dips seen in the forward steps, the deconstructive interference causes the radiated sound to fall back to the levels of the background resulting in the presented spectra to cut out over these frequencies. The distance of the source away from the wall that is implied by this interference place the source at a distance approximately equal to the step height. Past studies have shown that directly behind the backward step is an area of local maximum turbulence as a result of the separation that occurs off of the step. Additionally, it has been shown that these turbulence levels are weaker than the corresponding fluctuations caused by the flow over a similarly sized forward step. It follows that this turbulence produces the acoustic source for the flow over a backward step which is weaker than a similarly sized forward step. When comparing the far field spectra from the same size forward and backward step at the same velocity condition and observation angle, it was found that the forward step spectra maintains a constant 10 dB rise over that of the backward step, clearly showing the difference in source strength. A mixed scaling normalization which employs step height and boundary layer height as

length scales is presented which appear to reliably collapse the data, though spread is seen at high frequency due to deconstructive interference of the source.

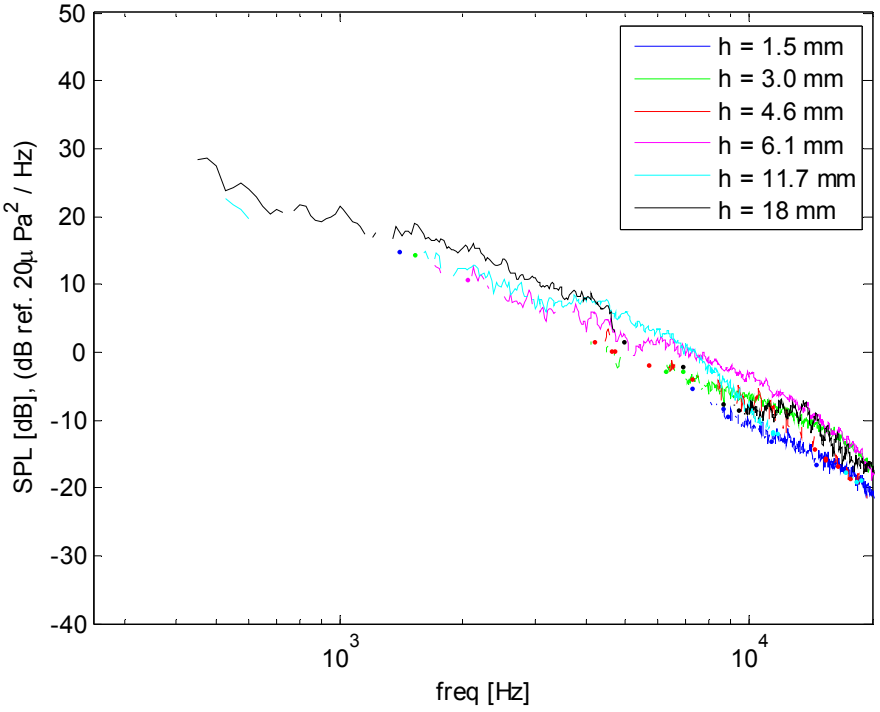

Figure 3.35 a

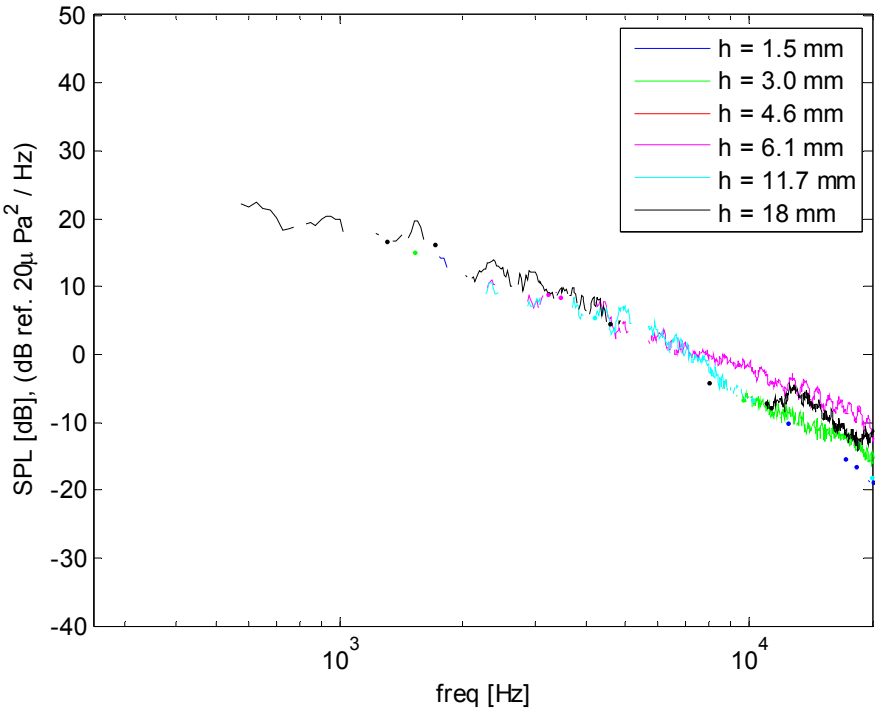

Figure 3.35 b

Figure 3.35 a-d. Far Field Acoustics from Backward Steps at U_j = 60 m/s at the considered Observation Angles; a) θ = 123.5° b) θ = 97.5° c) θ = 74° d) θ = 51.5°

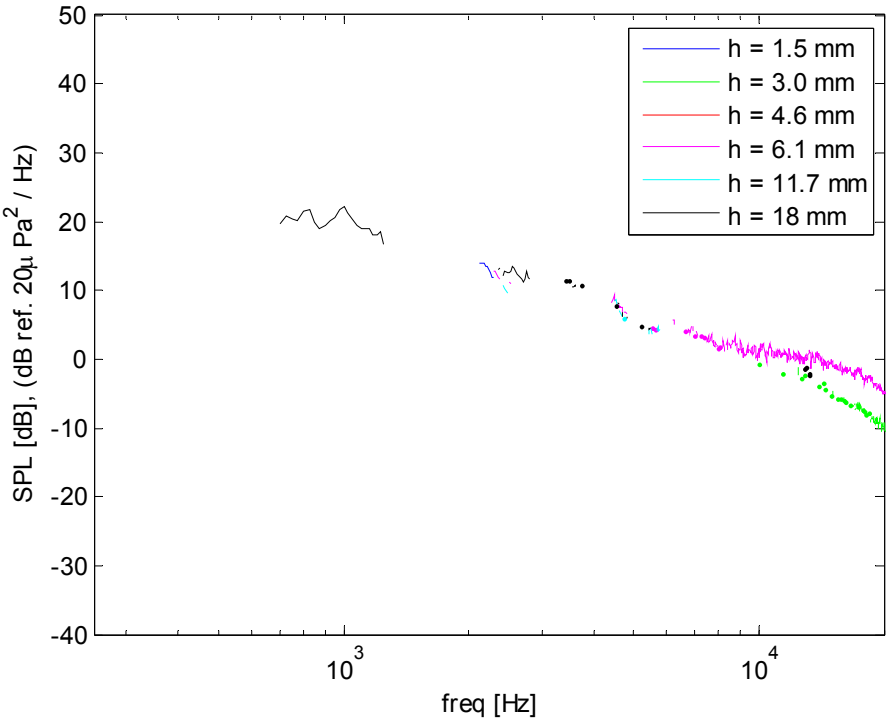

Figure 3.35 c

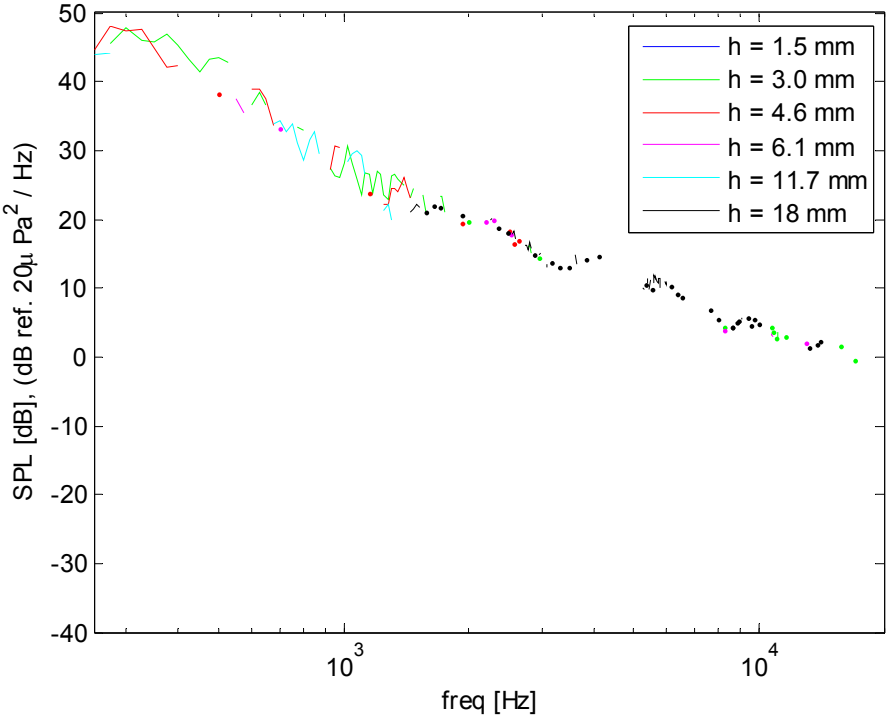

Figure 3.35 d

Figure 3.35 a-d. Far Field Acoustics from Backward Steps at U_j = 60 m/s at the considered Observation Angles; a) θ = 123.5° b) θ = 97.5° c) θ = 74° d) θ = 51.5°

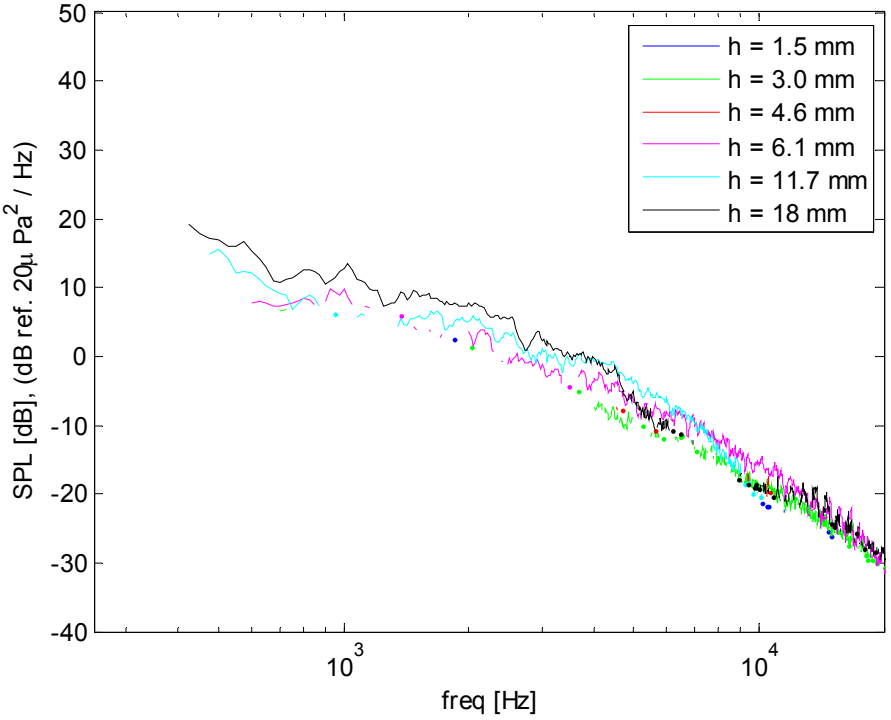

Figure 3.36 a

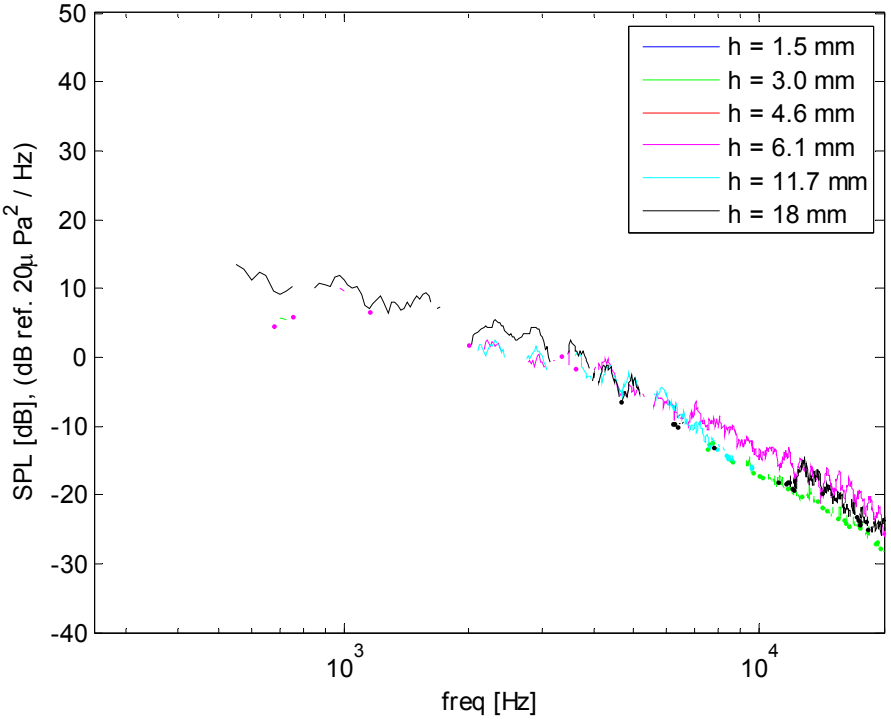

Figure 3.36 b

Figure 3.36 a-d. Far Field Acoustics from Backward Steps at U_j = 45 m/s at the considered Observation Angles; a) θ = 123.5° b) θ = 97.5° c) θ = 74° d) θ = 51.5°

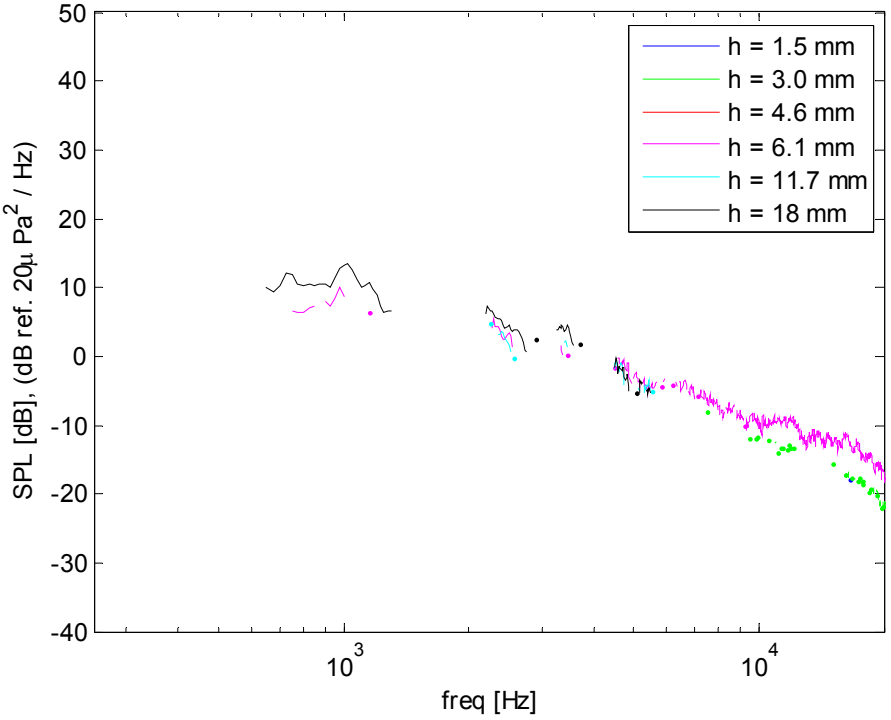

Figure 3.36 c

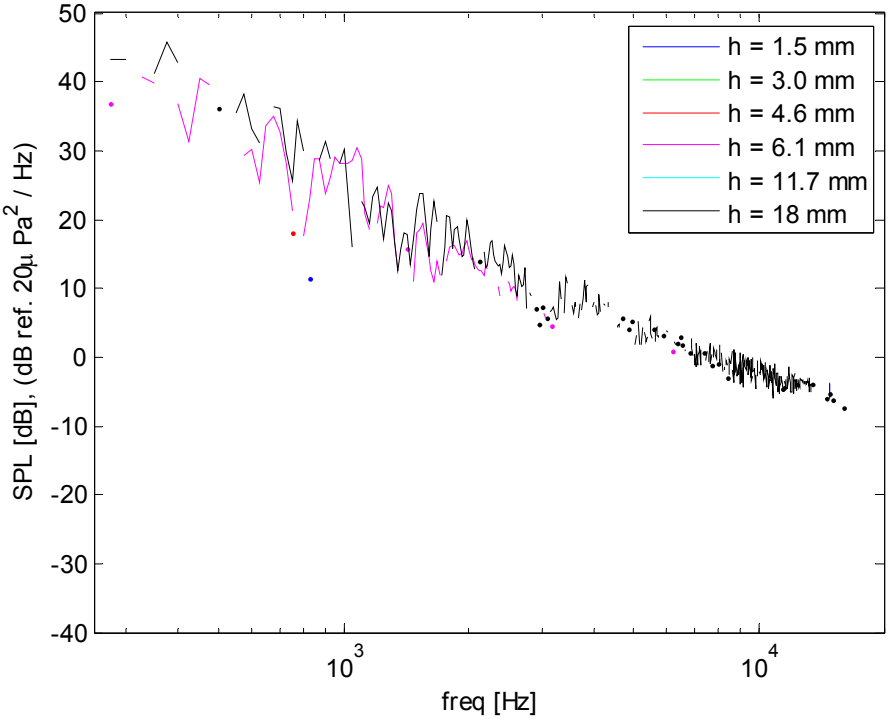

Figure 3.36 d

Figure 3.36 a-d. Far Field Acoustics from Backward Steps at U_j = 45 m/s at the considered Observation Angles; a) θ = 123.5° b) θ = 97.5° c) θ = 74° d) θ = 51.5°

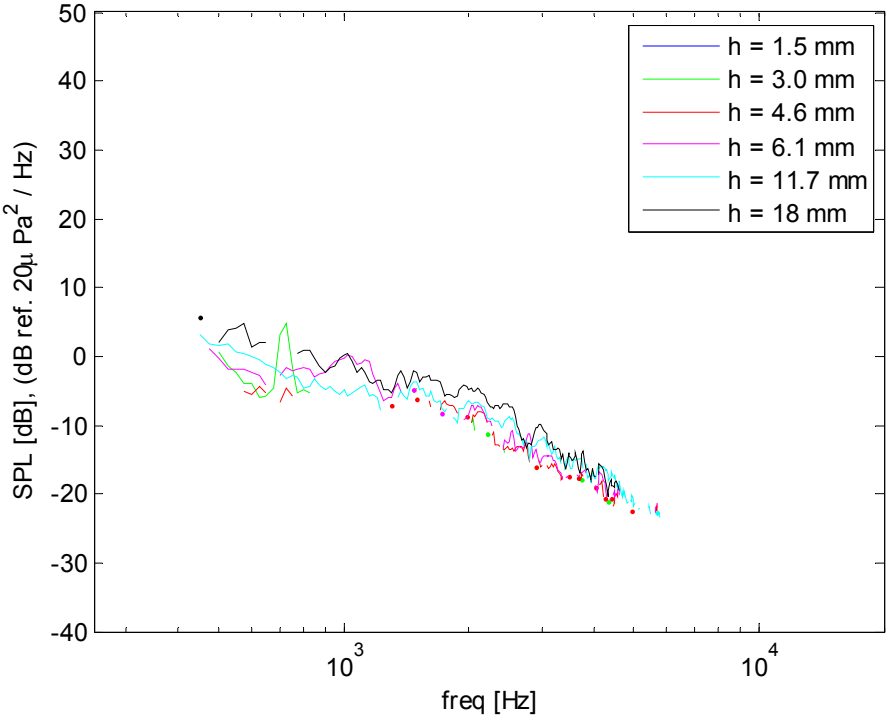

Figure 3.37 a

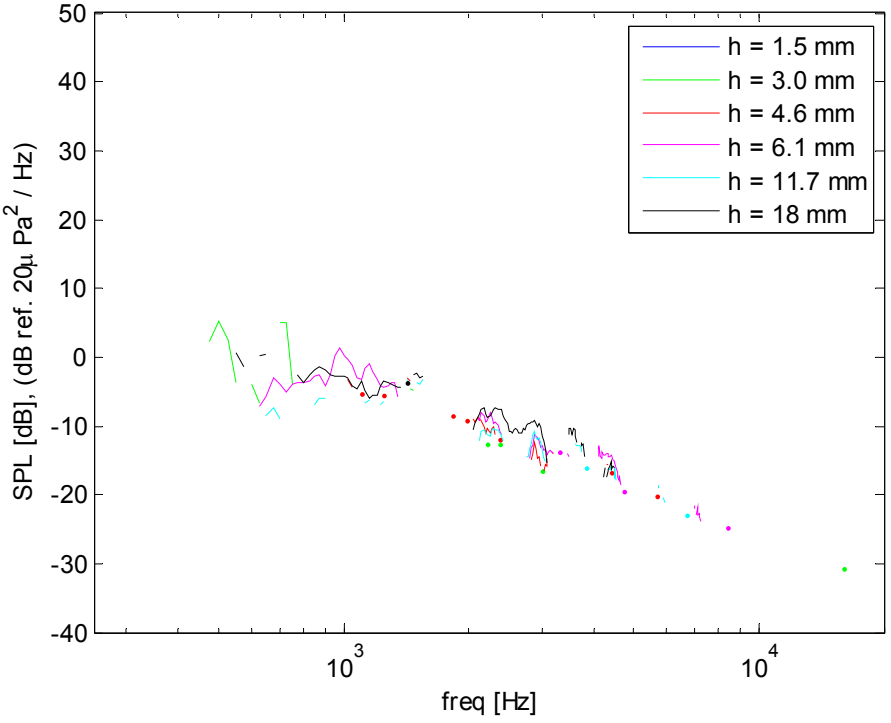

Figure 3.37 b

Figure 3.37 a-d. Far Field Acoustics from Backward Steps at U_j = 30 m/s at the considered Observation Angles; a) θ = 123.5° b) θ = 97.5° c) θ = 74° d) θ = 51.5°

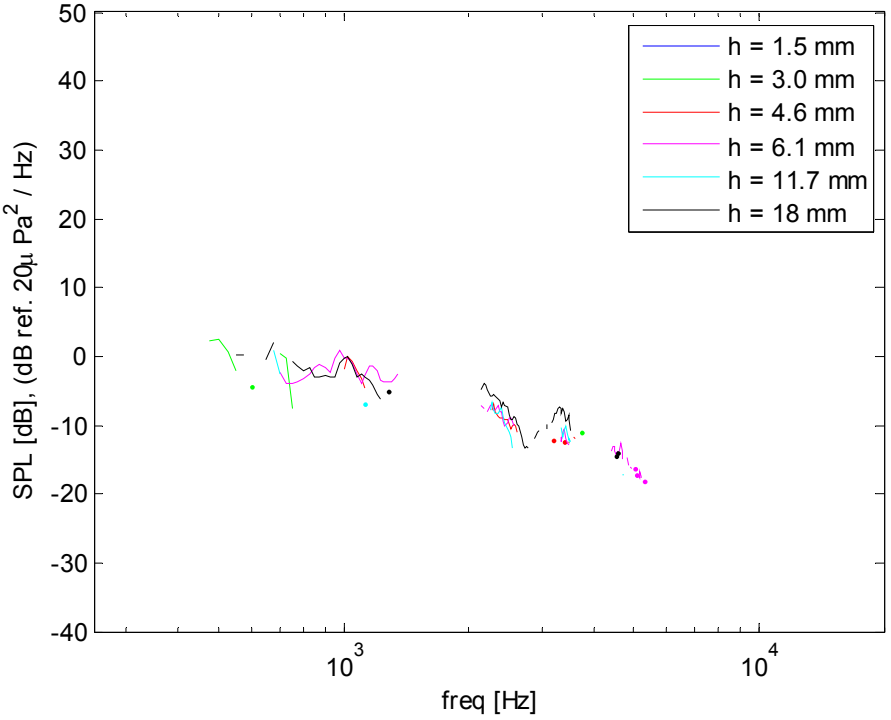

Figure 3.37 c

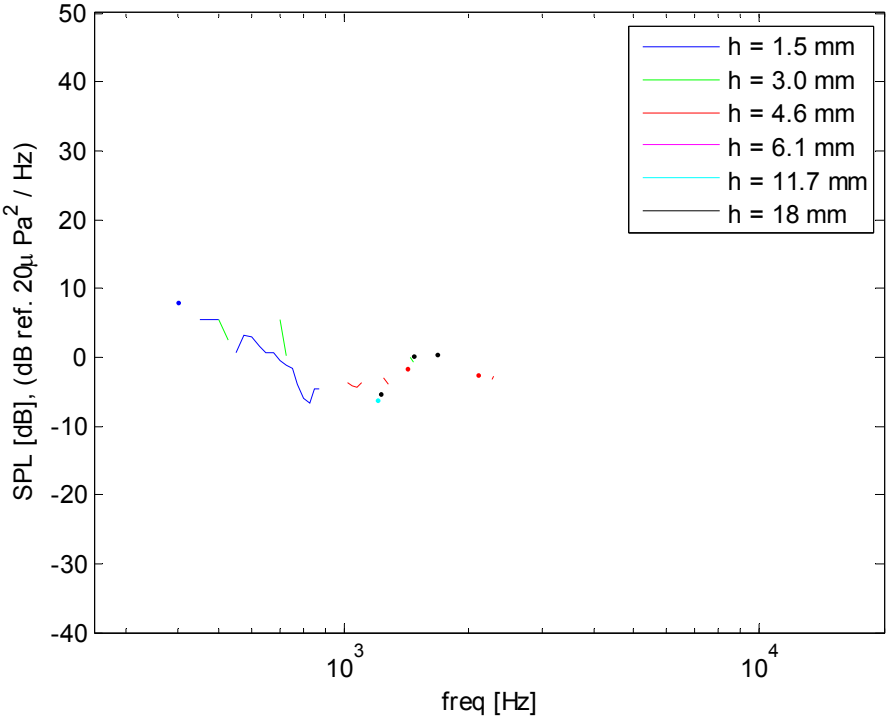

Figure 3.37 d

Figure 3.37 a-d. Far Field Acoustics from Backward Steps at U_j = 30 m/s at the considered Observation Angles; a) θ = 123.5° b) θ = 97.5° c) θ = 74° d) θ = 51.5°

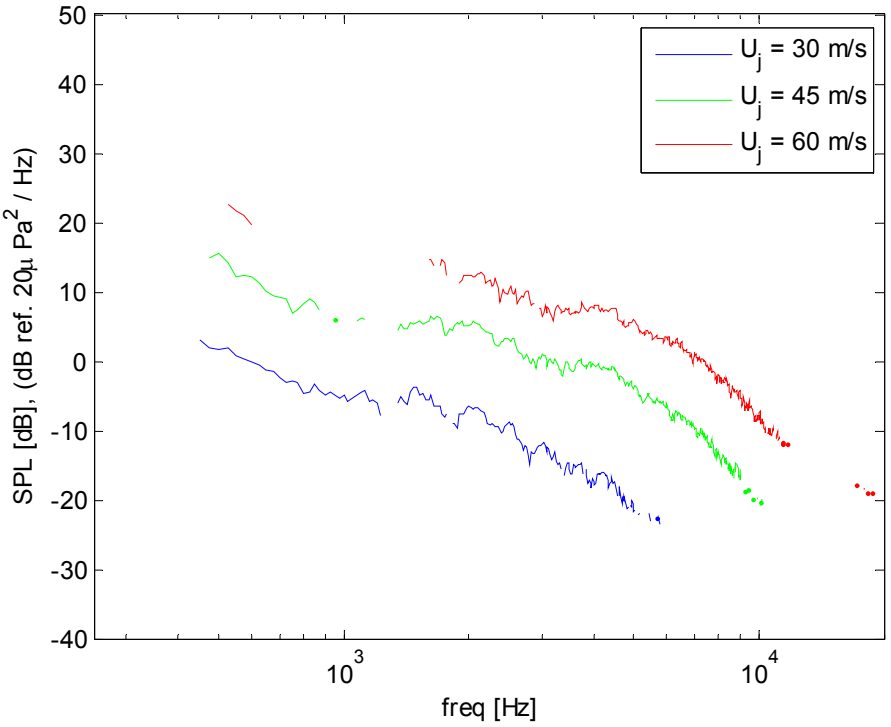

Figure 3.38. The Dependence of Far Field Sound on Jet Exit Velocity from an 11.7 mm Backward Step at θ = 123.5°

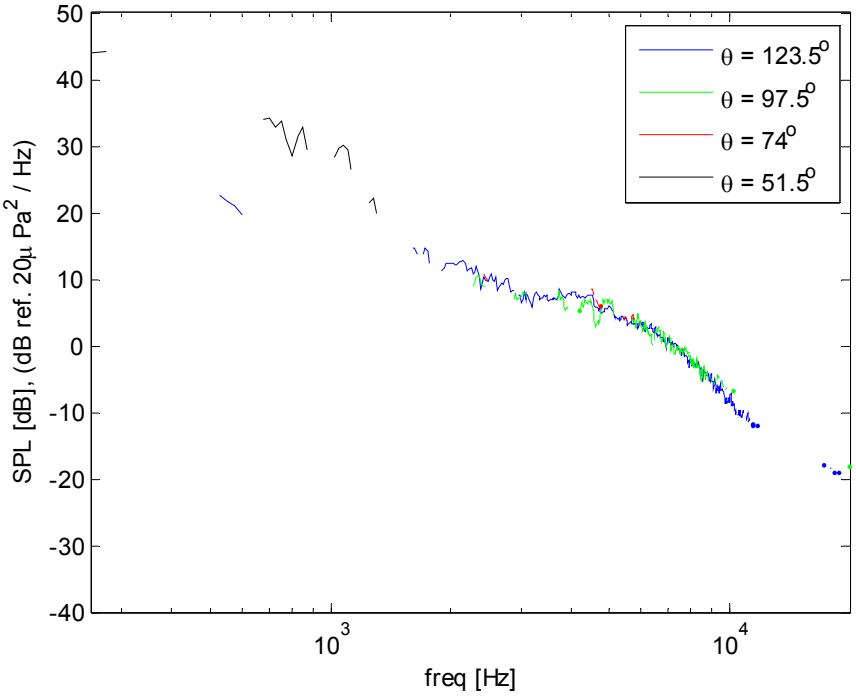

Figure 3.39. Directivity of the Radiated Far Field Sound from an 11.7 mm Backward Step at U_j = 60 m/s

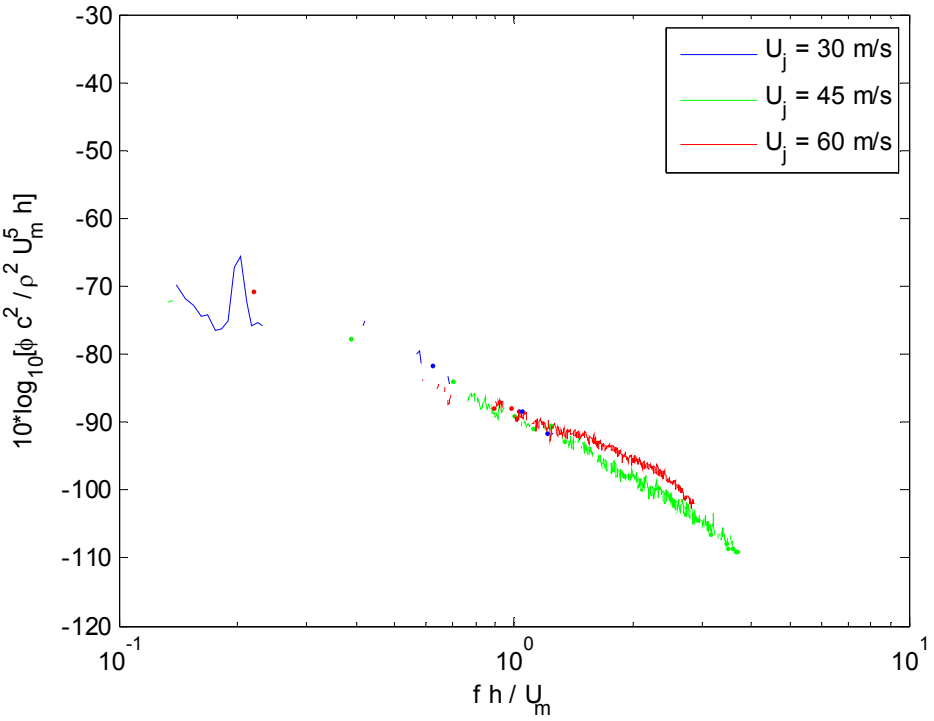

Figure 3.40. Far Field Spectra Normalization for the 3.0 mm Backward Step at $\theta = 123.5^{o}$

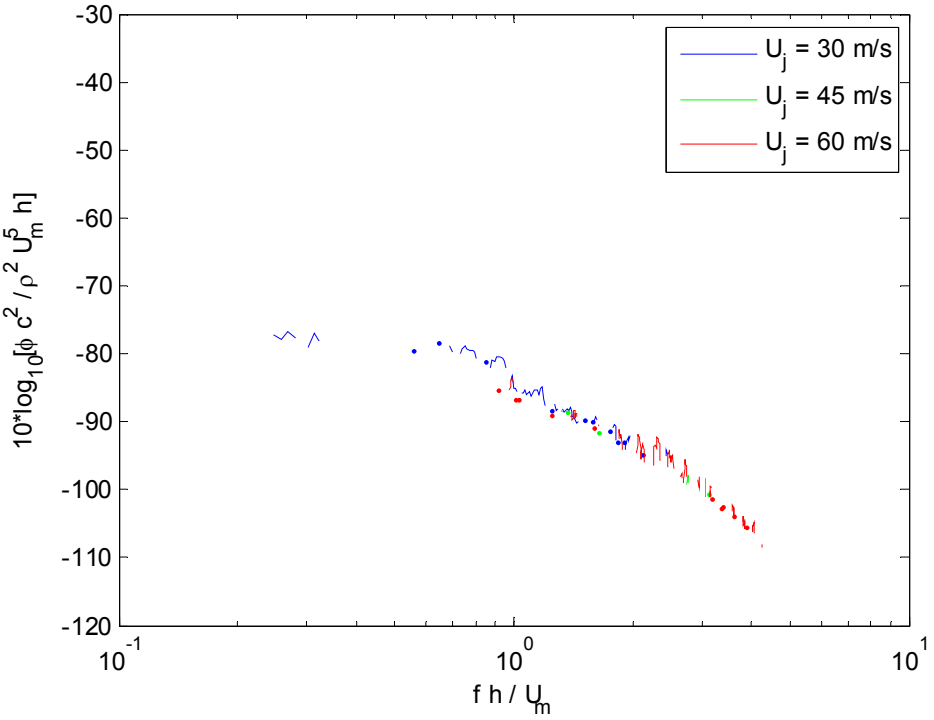

Figure 3.41. Far Field Spectra Normalization for the 4.6 mm Backward Step at $\theta = 123.5^{o}$

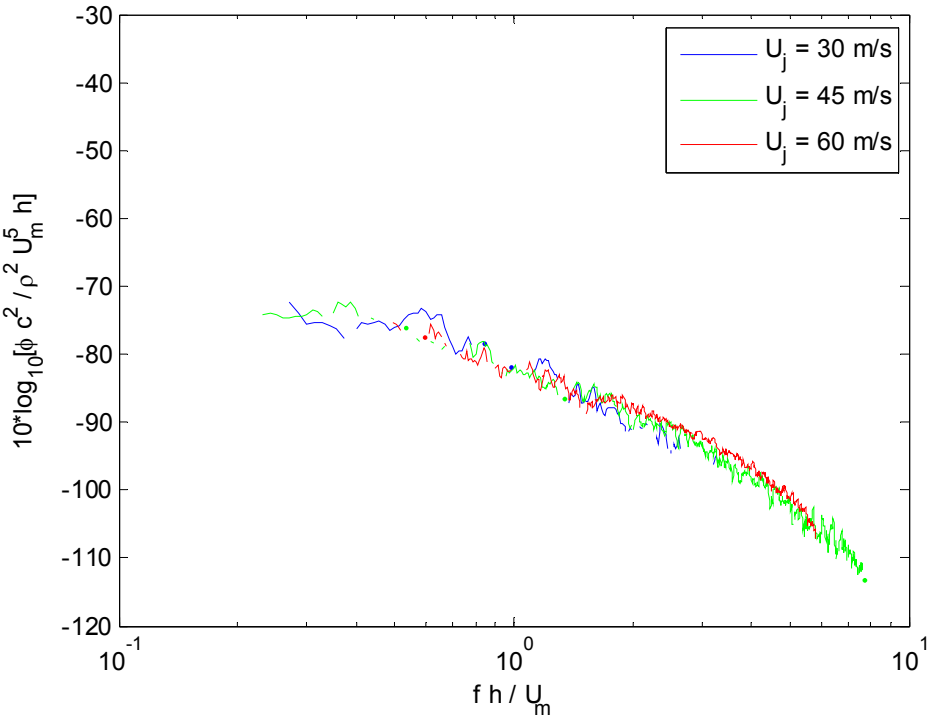

Figure 3.42. Far Field Spectra Normalization for the 6.1 mm Backward Step at $\theta = 123.5^{o}$

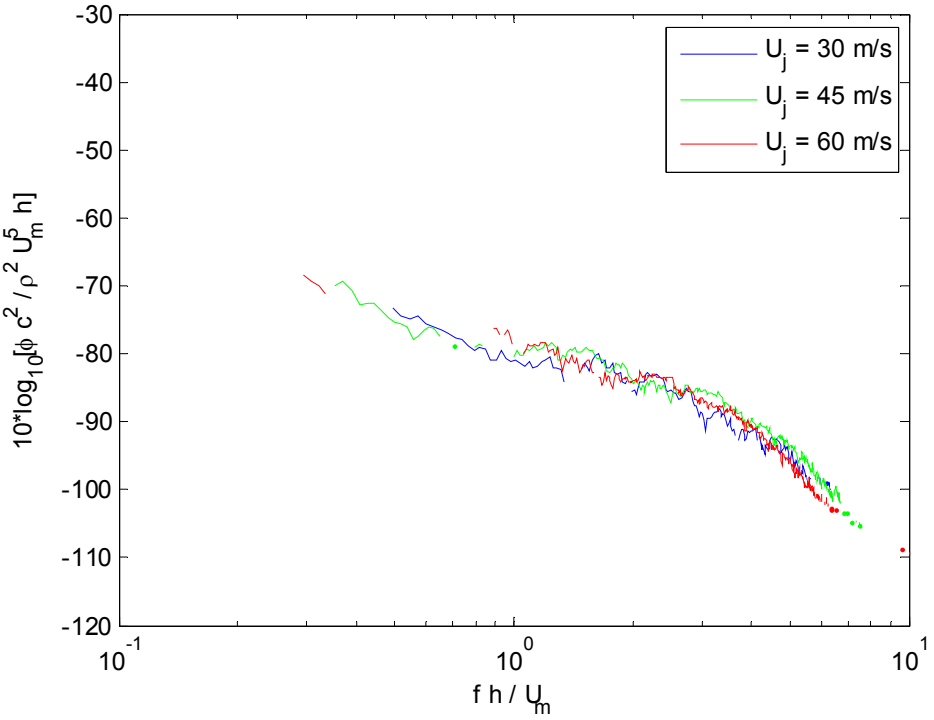

Figure 3.43. Far Field Spectra Normalization for the 11.7 mm Backward Step at $\theta = 123.5^{o}$

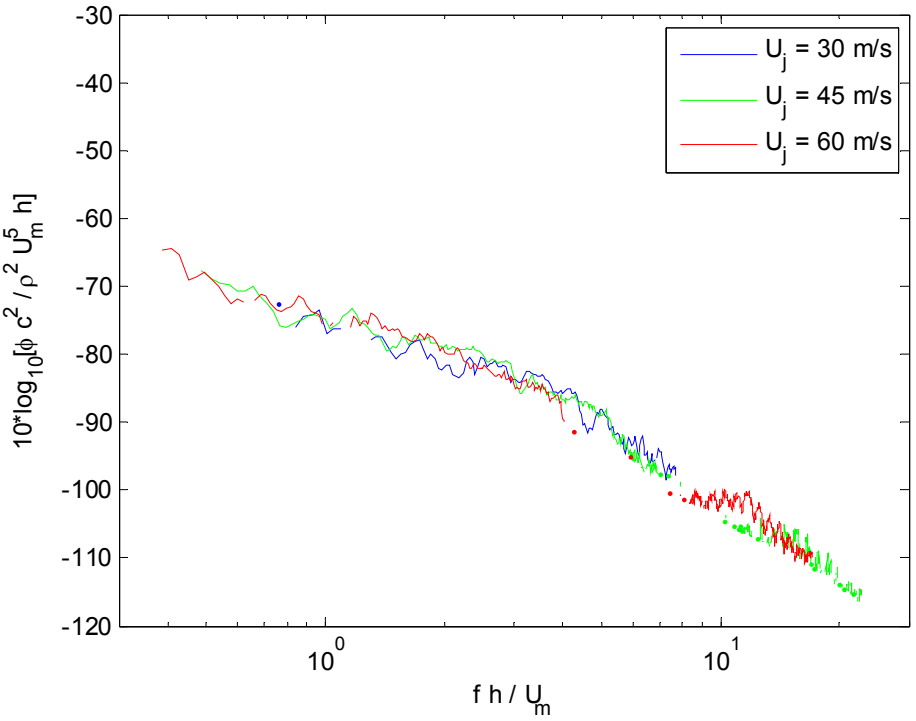

Figure 3.44. Far Field Spectra Normalization for the 18.0 mm Backward Step at θ = 123.5°

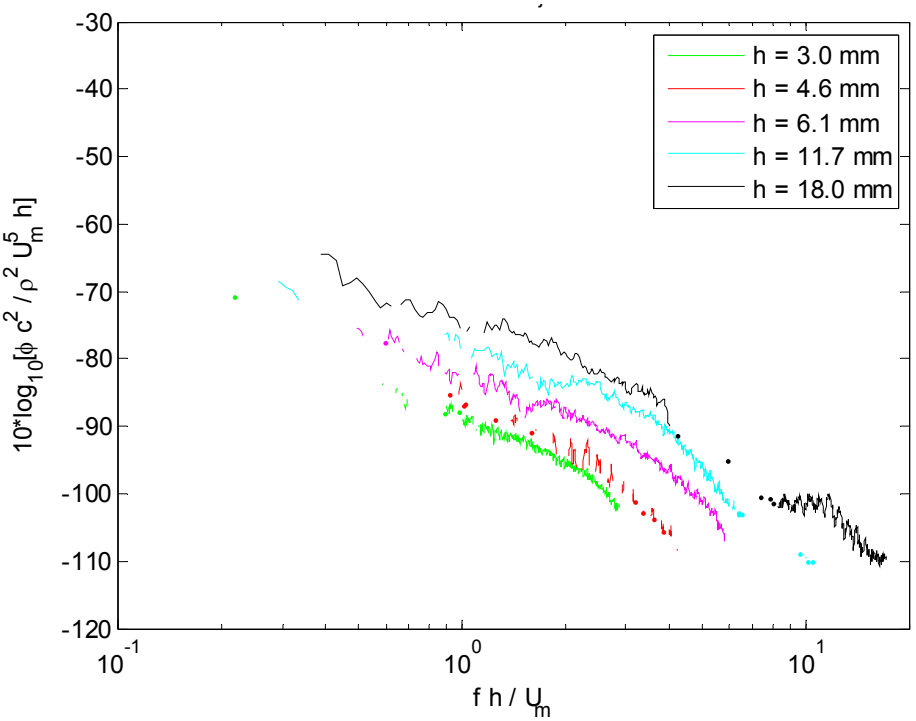

Figure 3.45. Normalized Far Field for Backward Steps at U_j = 60 m/s and θ = 123.5°

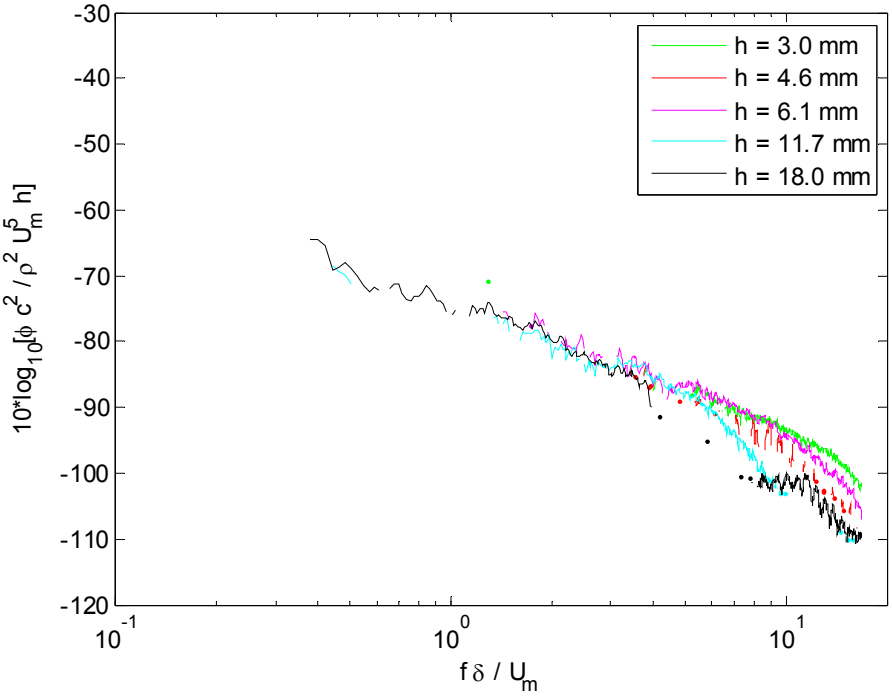

Figure 3.46. Mixed Scaling Normalized Far Field of Backward Steps at U_j = 60 m/s and θ = 123.5°

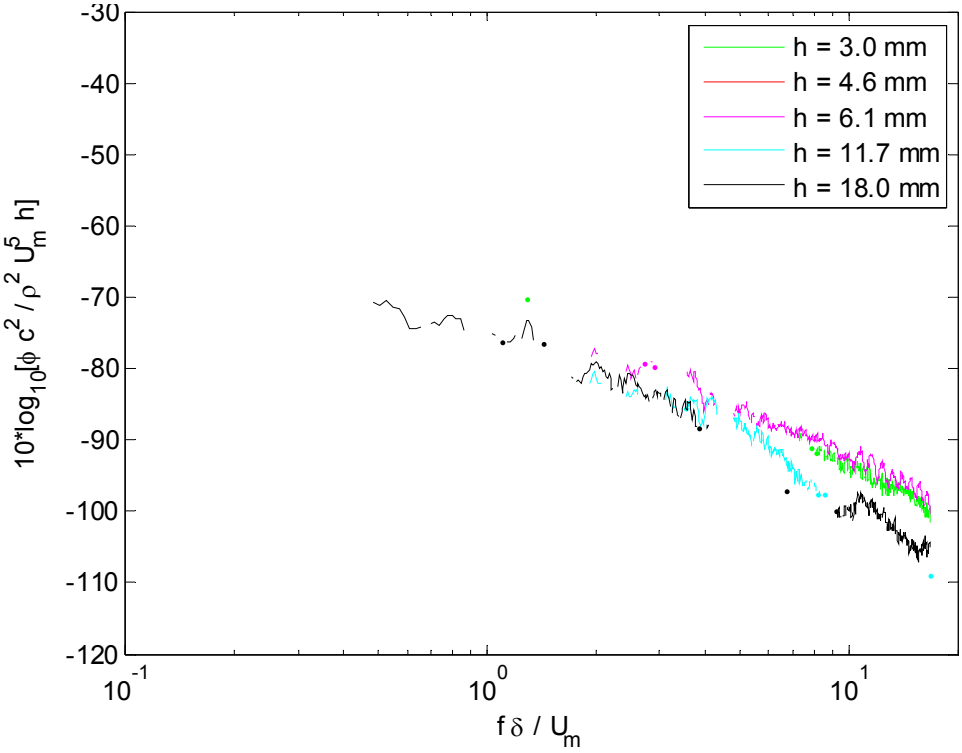

Figure 3.47. Mixed Scaling Normalized Far Field of Backward Steps at U_j = 60 m/s and θ = 97.5°

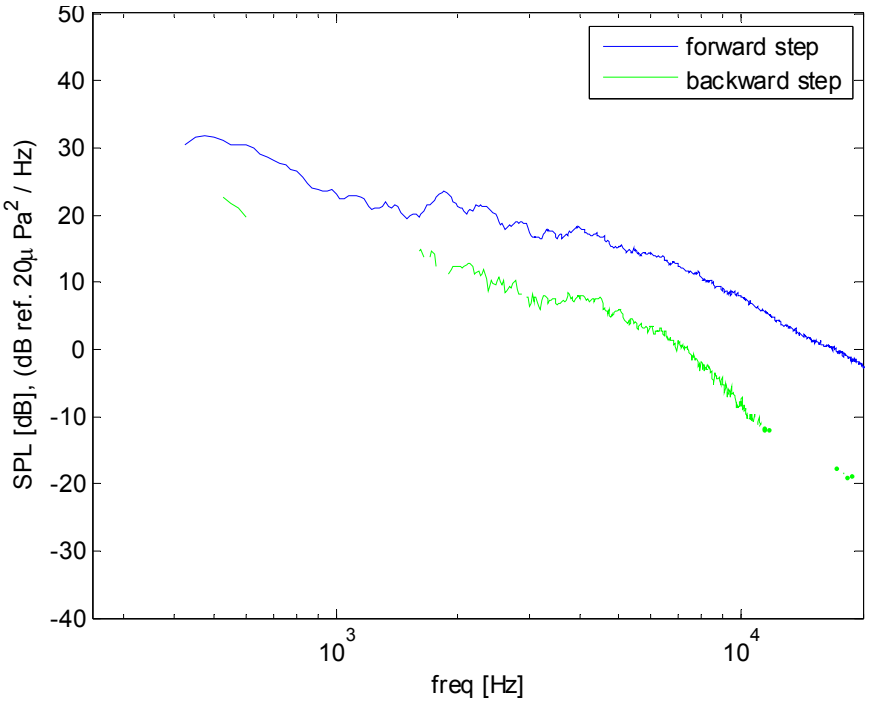

Figure 3.48. Comparison between the Far Field Sound from a Forward and Backward Step of h = 11.7 mm at U_j = 60 m/s and θ = 123.5°

3.3.4 Fluctuating Wall Pressure

The effects of the presence of backward steps on the fluctuating wall pressure field was examined at locations in front of and behind the set of six backward steps at three wall jet exit velocities. With measurement locations detailed in Chapter 2, the wall pressure field was measured at six locations downstream of the full set of six backward step heights. In addition, measurements were made at two locations upstream of the 1.5 and 11.7 mm backward steps. All of these spectral measurements are compared against the corresponding smooth plate spectra measured at the same location for an undisturbed flow surface. All figures for this subsection are presented at the end of the subsection. The distance from the measurement location to the step feature, $(x-x_s)$, has been normalized on the corresponding step height and is present in the legend of each graph.

In order to create the backward steps for this study, material was secured to the top of the wall jet plate. Unlike the forward steps, where the step material was extended to the end of the plate, the backward steps had to be created by placing a ramp connecting the wall jet plate to the step material placed in front of the step location. A ramp was used in attempt to smooth over the resulting forward step created by placing material on the wall jet plate in order to create a backward step. At the time of the experiment, it was thought that any effects on the flow would be less severe if it encountered a smooth ramp as opposed to a sharp forward step.

Figure 3.49 provides the wall pressure spectra measured at two locations in front of the 1.5 and 11.7 mm backward steps at the fastest wall jet exit velocity of 60 m/s. It is clear that the ramp used to transition between the wall jet plate and step material had a significant impact on the measured wall pressure spectra for the two step heights. For the fastest velocity condition at the most upstream measurement location, the wall pressure spectra for both step heights is elevated above the corresponding smooth wall spectra taken at that location over the entire frequency range (as seen in Figure 3.49 b). This behavior is indicative of separated flow. These locations are 165 and 21.2 step heights in front of the step location for the 1.5 and 11.7 mm backward steps, respectively. These same locations are 241 and 13.5 step heights downstream of the end of the ramp for the 1.5 and 11.7 mm step heights, respectively.

The wall pressure spectrum for the smaller step appears to recover to the undisturbed spectrum at the more downstream location of 12.7 step heights in front of the step location, except for a minor discrepancy at a frequency of 5000 Hz. This measurement location is also 394 step heights downstream of the end of the ramp. This running length appears to have been sufficient in allowing any disturbances introduced by the ramp to have dissipated. This was the intended purpose of the ramp which was needed to create a backward step in this facility.

The wall pressure spectrum for the larger step of 11.7 mm does not recover to the corresponding smooth plate levels, and is seen to be affected across the entire frequency range as close as 1.6 step heights in front of the step location. This location is 33 step heights downstream of the end of the ramp. It is clear that enough running length was not provided in order to dissipate the effects of the flow encountering this ramp.

It is notable that such a shallow ramp of angle 6.7^{o} can apparently have the same effect on the wall pressure field as the forward step it was intended to smooth over. This is true to the same extent for the smaller ramp used for the 1.5 mm forward step. This suggests that ramps may be an important area of study for the behavior of the fluctuating wall pressure field.

The same type of behavior is seen in Figures 3.50 and 3.51 for the wall pressure spectra measured at the two slower velocity conditions, however the severity of the disturbances are weaker and appear to dissipate over shorter distances. It should be mentioned again that the jagged upward bend of the spectra at high frequency seen for the slower velocity conditions, and especially at the slowest condition, is not a flow feature but is a result of the pinholes secured to the top of these microphones in order to improve their spatial resolution. As before, the affected data has been dimmed.

Figures 3.52 through 3.54 present the wall pressure spectra measured at the six locations behind the set of six backward steps at the three wall jet exit velocities. As these measurements were made at the same physical location relative to the step location,

the non-dimensional distances downstream of the step are dependent on step height. In this way, the effect of the step on the wall pressure field is seen over different scales as the step height is varied.

As seen in Figure 3.52, at the closest measurement location and fastest velocity condition all of the backward steps have measurable effects which disturb the wall pressure field away from that of the smooth wall pressure spectrum. For the smallest step height of 1.5 mm this location is approximately 21 step heights downstream and the spectrum shows minor elevation across the low to mid frequencies and coincidence with the smooth plate spectrum at frequencies above the high frequency bend occurring at 7 kHz. This is the predicted type of behavior associated with locations downstream of flow reattachment as the wall pressure field relaxes back to the smooth plate levels.

The spectrum for the next largest step height of 3.0 mm exhibits the same behavior as the smaller step with low to mid frequency elevation and high frequency coincidence when compared to the smooth wall spectrum. The difference for this step height is that the elevation of the step spectrum above that of the smooth wall is more severe. This is attributed to the fact that this non-dimensional distance downstream is closer to the step and that this step is larger. It has been shown by past studies that after flow reattachment, the wall pressure field slowly relaxes back to the smooth wall levels; accounting for this behavior. The dependence of the spectral levels on step height is less clear which would need to be determined with more data. The spectrum for the 4.6 mm backward step follows this same trend. More severe low to mid frequency elevation and coincidence with the smooth wall pressure spectrum is witnessed indicative of a measurement made downstream of flow reattachment. The length to flow reattachment was previously presented as 5.65 step heights downstream of the step for this configuration.

The distance to flow reattachment was determined to be 5.2 step heights downstream for the 6.1 mm backward step. This is the same distance downstream of the step that the wall pressure spectrum for this step height was measured. When approaching the step from downstream, this is the first time that the wall pressure spectra is seen to be depressed below that of the smooth plate, and the low to mid frequency elevation is seen to be the most severe than for any other step height. This data supports the findings of past studies that the location of flow reattachment behind a backward step corresponds to the location of maximum wall pressure disturbances as the shear layer impinges back on the flow surface.

As the wall pressure field is probed closer to the step location, the non-dimensional measurement locations for the two largest step heights are inside of the recirculation region behind the step. At the closest location of 1.8 step heights downstream, for the largest step height of 18.0 mm, the wall pressure field is seen to be greatly depressed below the smooth plate levels almost over the entire frequency range. The more downstream location of 2.7 step heights, for the 11.7 mm step height, shows both low frequency elevation and high frequency depression with a cross frequency of approximately 3 kHz. This behavior of the wall pressure field behind a backward step is consistent with the experimental work of Farabee and Casarella (1986).

The spectra taken at the next downstream location for the set of six backward steps portray the same behavior. This location for the 1.5, 3.0, 4.6, and 6.1 mm steps correspond to 38.1, 19.1, 12.4, and 9.4 step heights downstream, respectively.

Accordingly, each spectrum exhibits a slow recovery of the wall pressure field back to the smooth plate values over low to mid frequencies and generally shows coincidence to the high frequency levels. Each spectrum is spaced such that the return to the undisturbed wall pressure field is controlled by downstream distance.

This location corresponds to measurement locations that are just downstream of the mean reattachment line for the 11.7 mm backward step and inside of the recirculation region for the 18.0 mm backward step. These spectra show consistent behavior with what was previously described. Maximum disturbance levels are witnessed in the vicinity of flow reattachment while spectral elevation and depression are seen inside of the recirculation region.

Data collected at the third downstream location continue to exhibit the described behavior. The measured spectra appear to slowly recover back to the undisturbed wall spectrum values with downstream distance away from the step. However, a new trend is seen to occur at this location which is continued through to the other measurement locations further downstream. At high frequency, the measured step spectra are seen to fall below the smooth wall spectrum and not recover with downstream distance, at least over the distances considered in this study. This behavior would suggest three explanations. Either the wall pressure field naturally settles on a new, slightly different equilibrium, the downstream recovery of the high frequency content persists farther downstream than considered here, or this behavior is an effect of the use of a wall jet such that the steps are removing energy from the flow causing this difference between the wall pressure spectra of a smooth wall and behind a backward step. This behavior does not appear to be clearly dependent on step height giving support to the ideas that this is the natural behavior of step flow or that the high frequency recovery persists very far downstream. Additionally, the measurements of Farabee and Casarella (1986) show this same high frequency behavior lasting up to 72 step heights downstream of their single backward step configuration.

Figures 3.53 and 3.54 present this same data for the other two wall jet nozzle exit velocities of 45 and 30 m/s. Consistent behavior as previously discussed for the faster velocity condition is witnessed for these two data sets; with lower overall spectral levels and similar disturbances as a result of the slower flow speed. Once again, aliased data at high frequency for these slower velocity conditions has been dimmed.

3.3.5 Summary of Fluctuating Wall Pressure Results

In summary, the fluctuating wall pressure field was measured in front of and behind a set of backward facing steps in order to determine the effects of the presence of the steps on the wall pressure field and their downstream influence. The ramps needed to create the backward steps in this facility have been shown to significantly affect the downstream wall pressure field in what appears to be separated flow. In terms of the wall pressure field, this disturbance dissipates back to the levels of the undisturbed wall by the step location for the smallest step of 1.5 mm. The wall pressure field measured directly in front of the larger backward step of 11.7 mm shows considerable deviation from the smooth wall levels as a result of the ramp needed to elevate the flow surface. Despite this, the wall pressure field measured downstream of the backward step appears to not be

influenced by this in flow condition because similar behavior is witnessed between the smaller and larger step heights.

The downstream influence of the set of backward steps was seen to follow a general description for all step heights. Spectra measured inside of the separated flow region directly behind the step are seen to be elevated above the corresponding smooth wall levels over low frequencies and suppressed below the smooth wall levels at high frequency. The suppression is most extreme and covers most of the frequency range for locations within approximately 2 step heights downstream. Progressing downstream, the cross frequency of where the spectra are seen to switch from elevated to depressed relative to the smooth wall levels is seen to move to higher frequency. With this movement downstream, the low frequency disturbances are seen to rise while the high frequency disturbances become less severe. The low frequency disturbances are seen to be the most extreme at the location of flow reattachment. Further downstream the wall pressure spectra exhibit a slow, monotonic recovery of the elevated levels back to the levels of the smooth wall spectra. Lasting effects of this kind are seen to persist to upwards of 50 step heights downstream depending on step height. At locations even further downstream, the high frequency levels of the step spectra are seen to slightly drop below the corresponding smooth wall levels. This behavior is similar to what was witnessed for measurements downstream of forward steps and would suggest either a very long oscillatory convergence or settling to a new smooth wall equilibrium wall pressure field. Similar behavior of this kind has been seen in past studies; however it remains inconclusive whether this is a natural flow behavior or is introduced behavior due to the use of a wall jet for this study. To conclude either statement requires additional data aimed specifically at this issue.

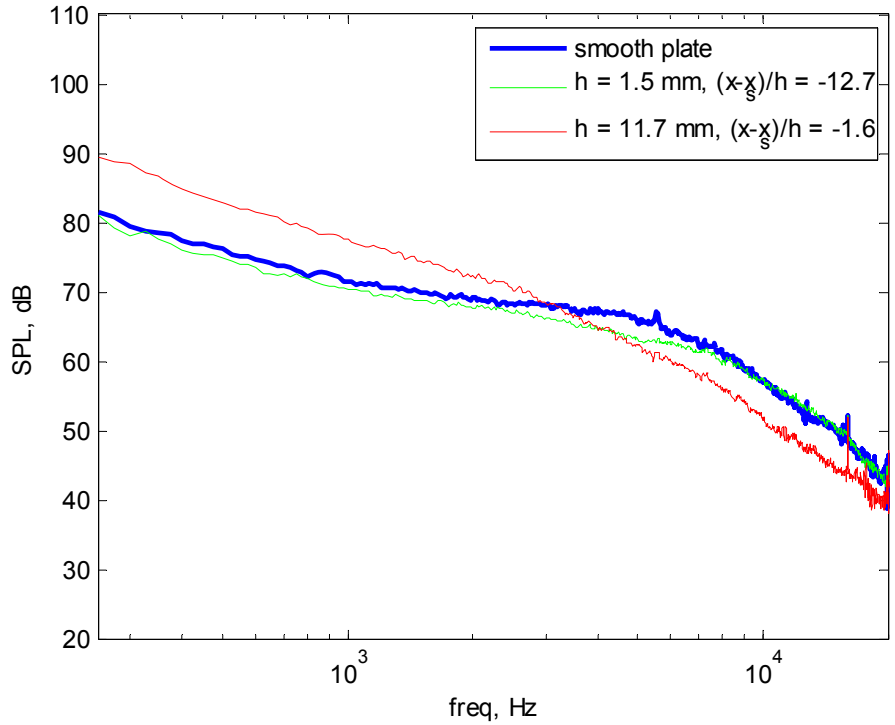

Figure 3.49 a

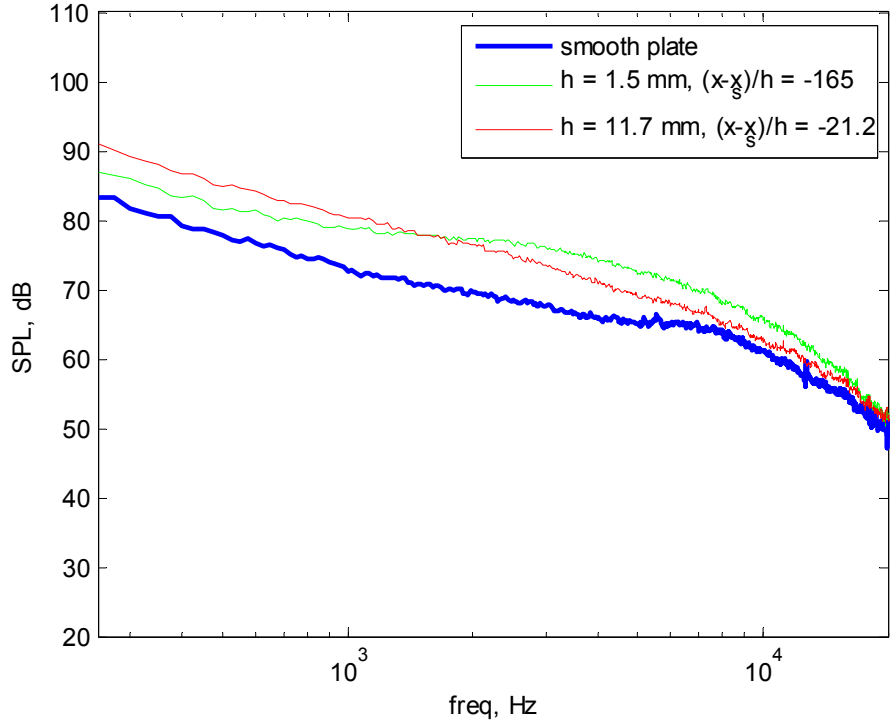

Figure 3.49 b

Figure 3.49 a-b. Wall Pressure Measurements in front of a 1.5 and 11.7 mm Backward Step at U_j = 60 m/s

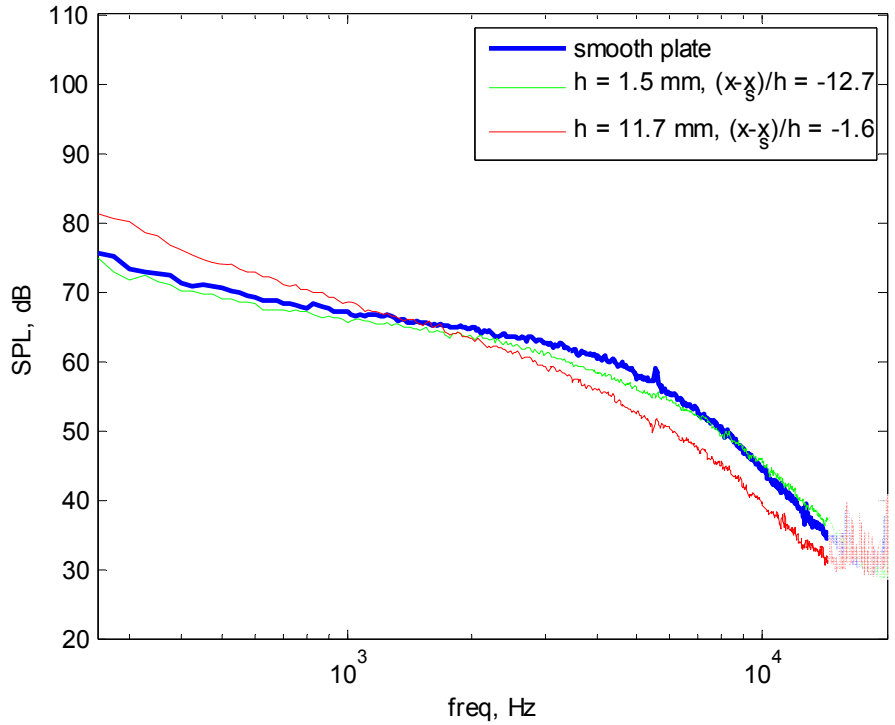

Figure 3.50 a

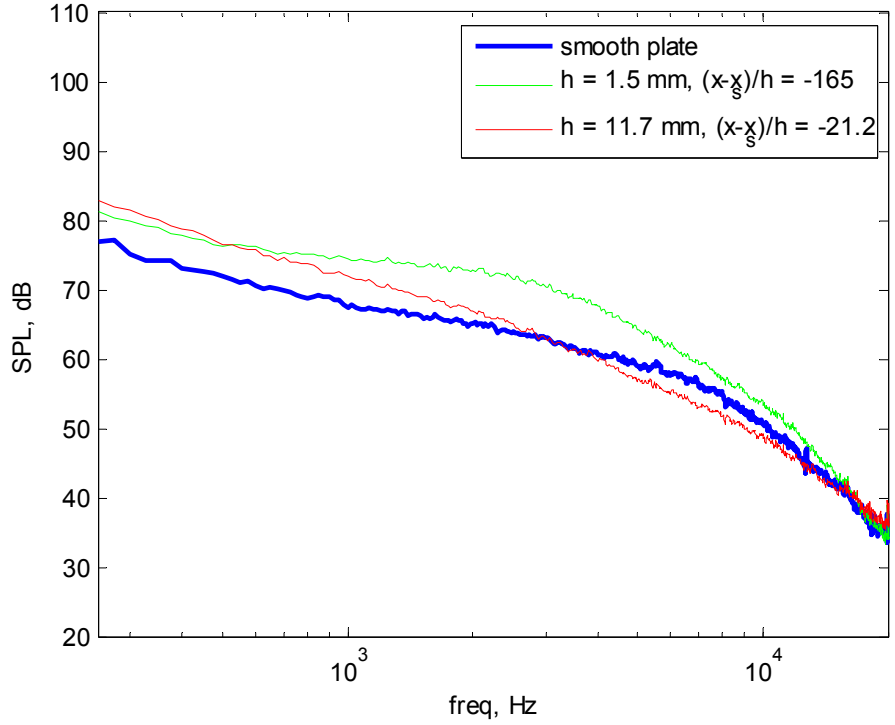

Figure 3.50 b

Figure 3.50 a-b. Wall Pressure Measurements in front of a 1.5 and 11.7 mm Backward Step at U_j = 45 m/s

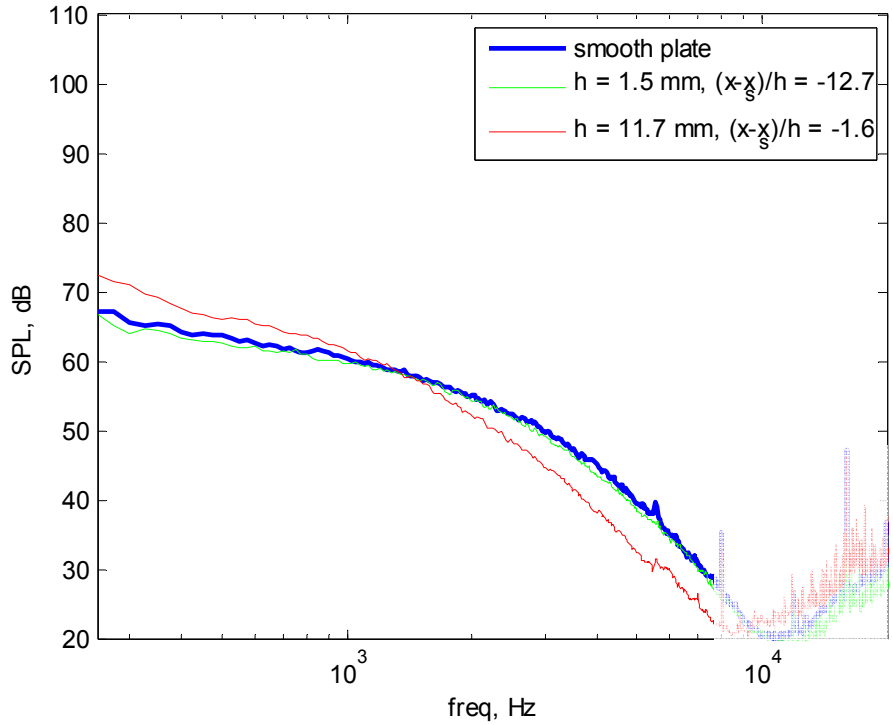

Figure 3.51 a

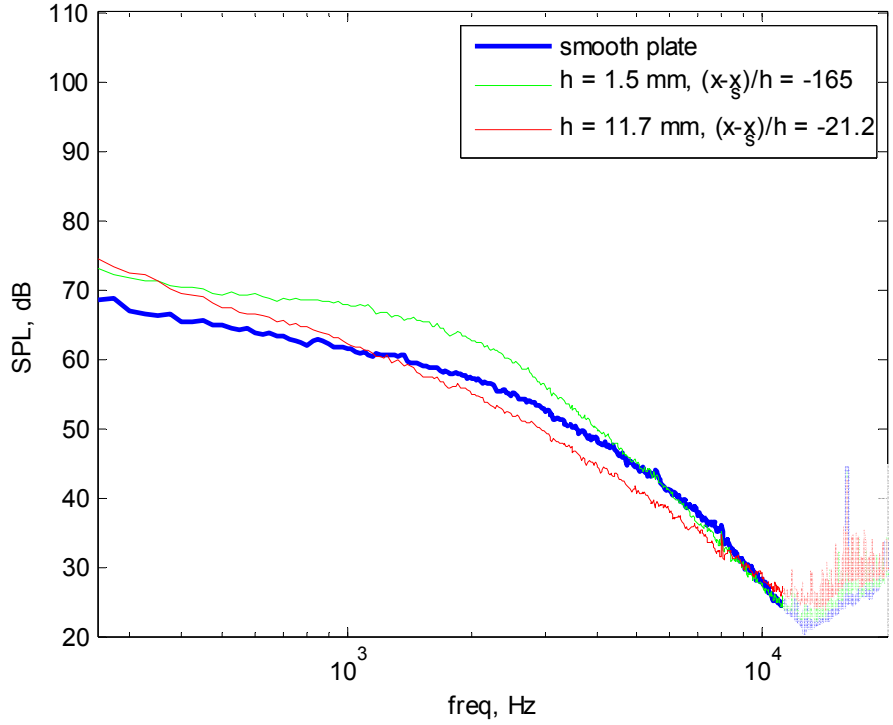

Figure 3.51 b

Figure 3.51 a-b. Wall Pressure Measurements in front of a 1.5 and 11.7 mm Backward Step at U_j = 30 m/s

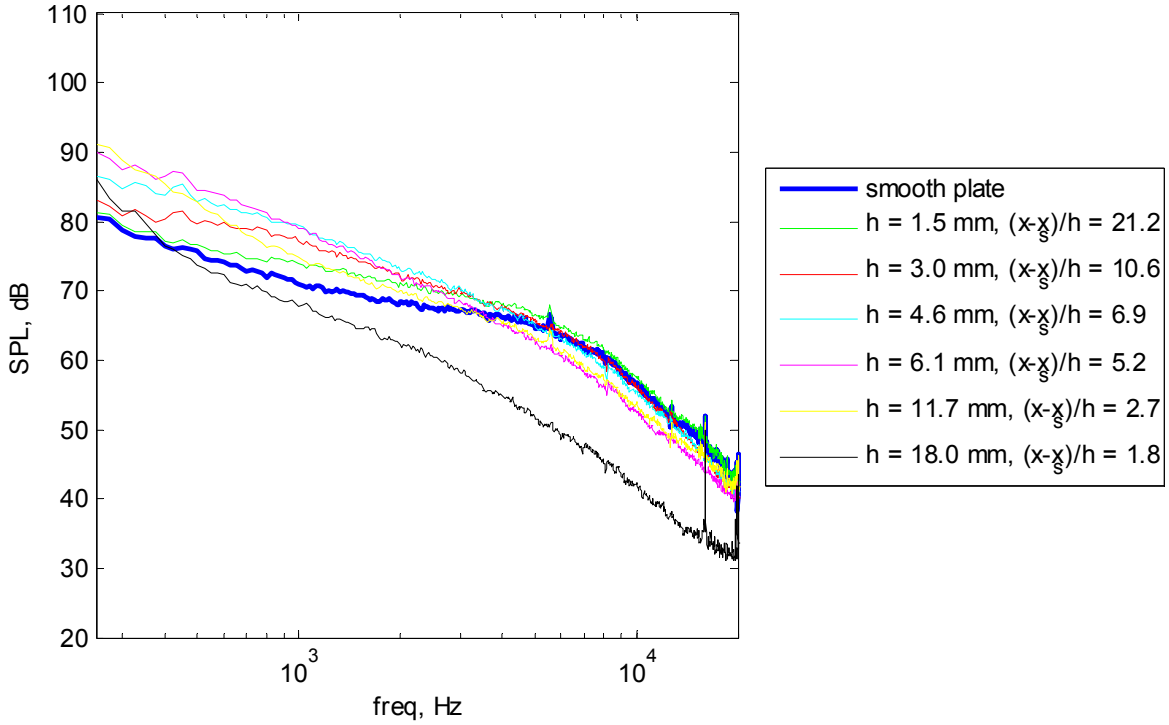

Figure 3.52 a

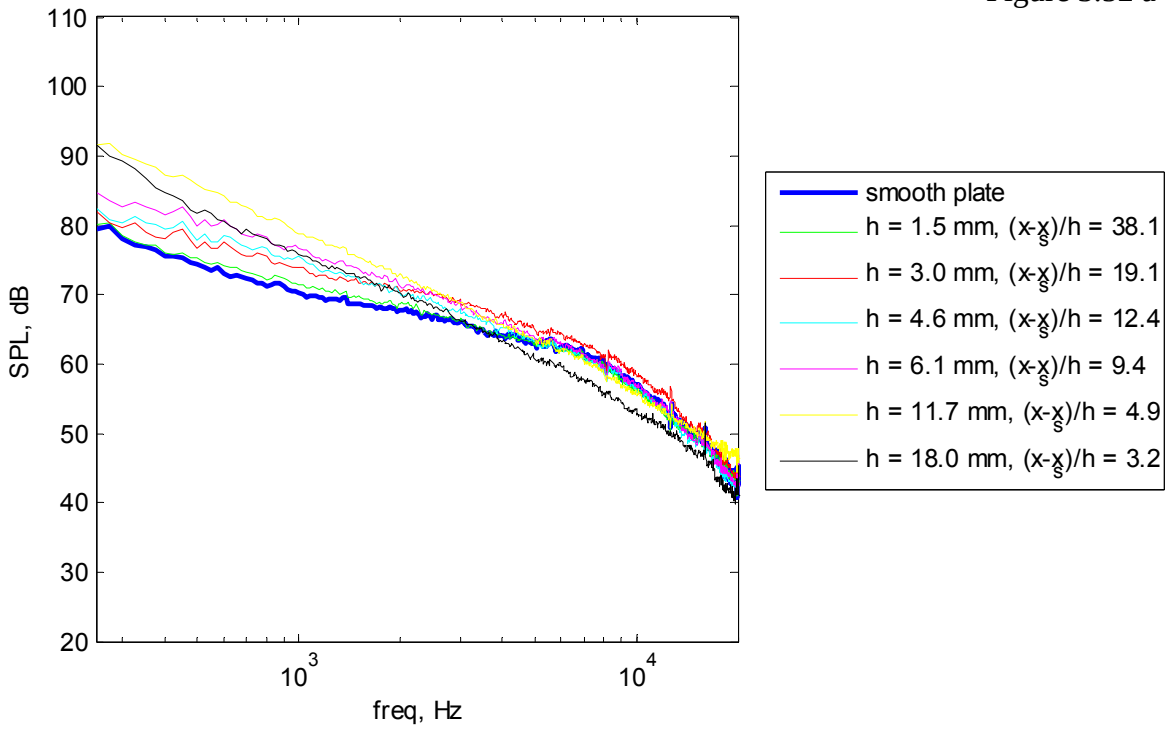

Figure 3.52 b

Figure 3.52 a-f. Wall Pressure Measurements behind All Backward Steps at U_j = 60 m/s

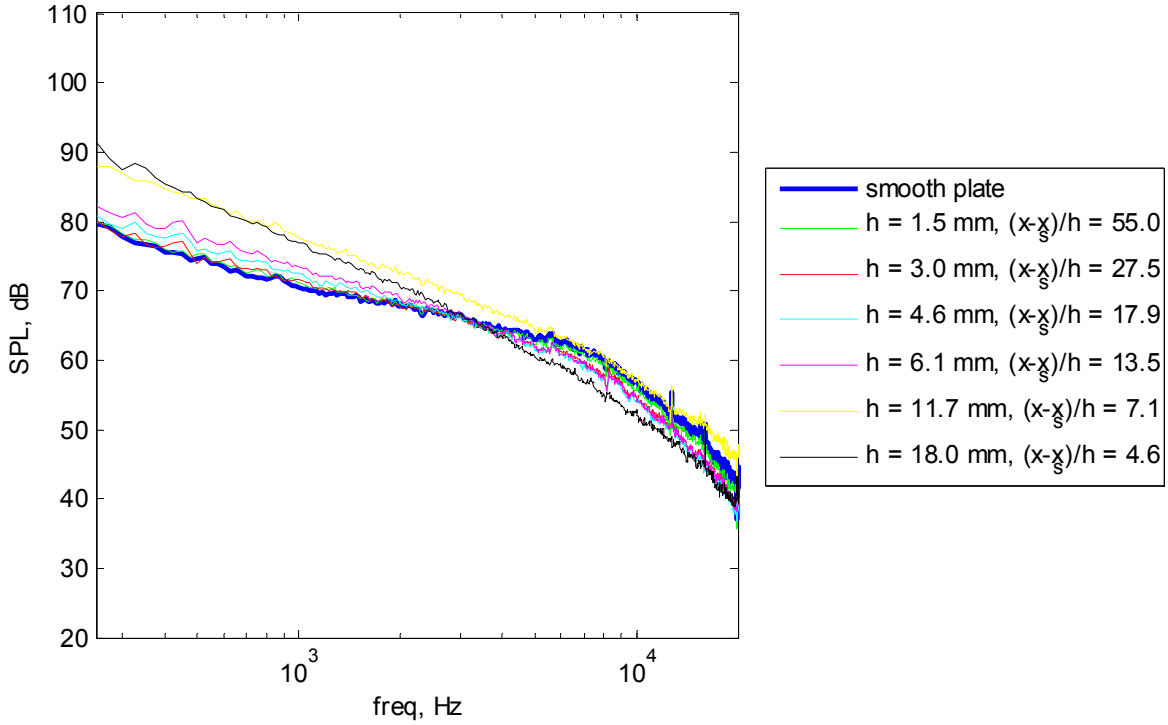

Figure 3.52 c

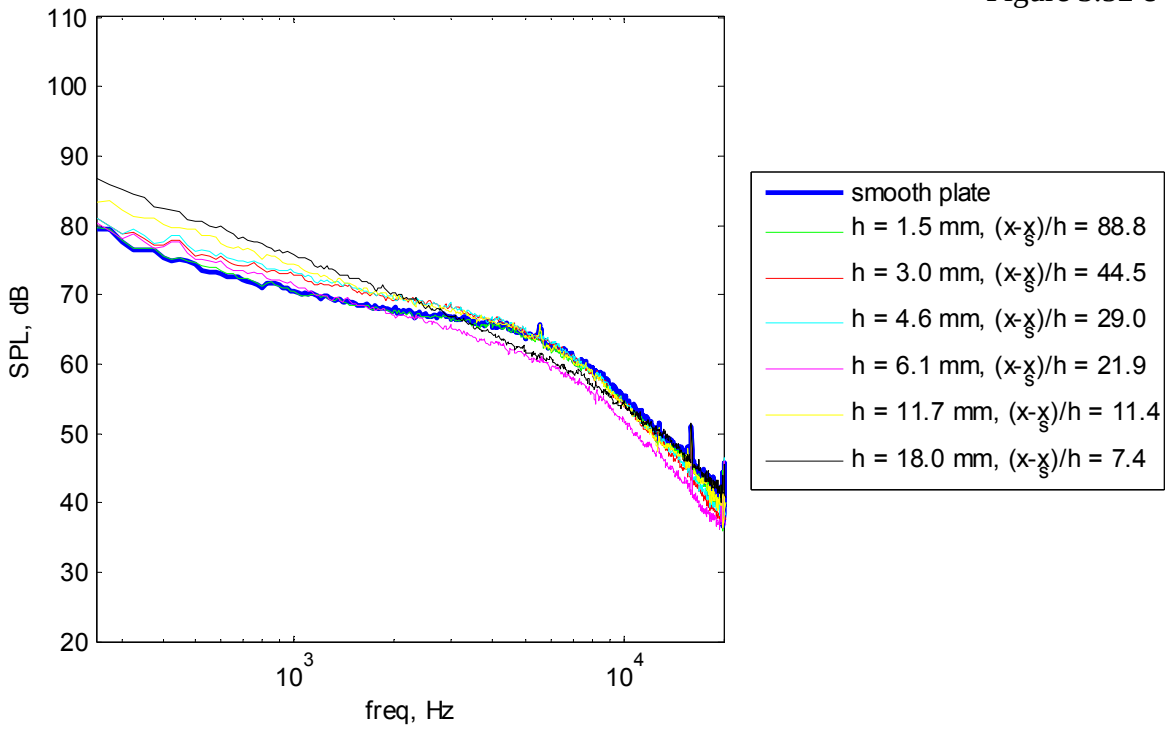

Figure 3.52 d

Figure 3.52 a-f. Wall Pressure Measurements behind All Backward Steps at U_j = 60 m/s

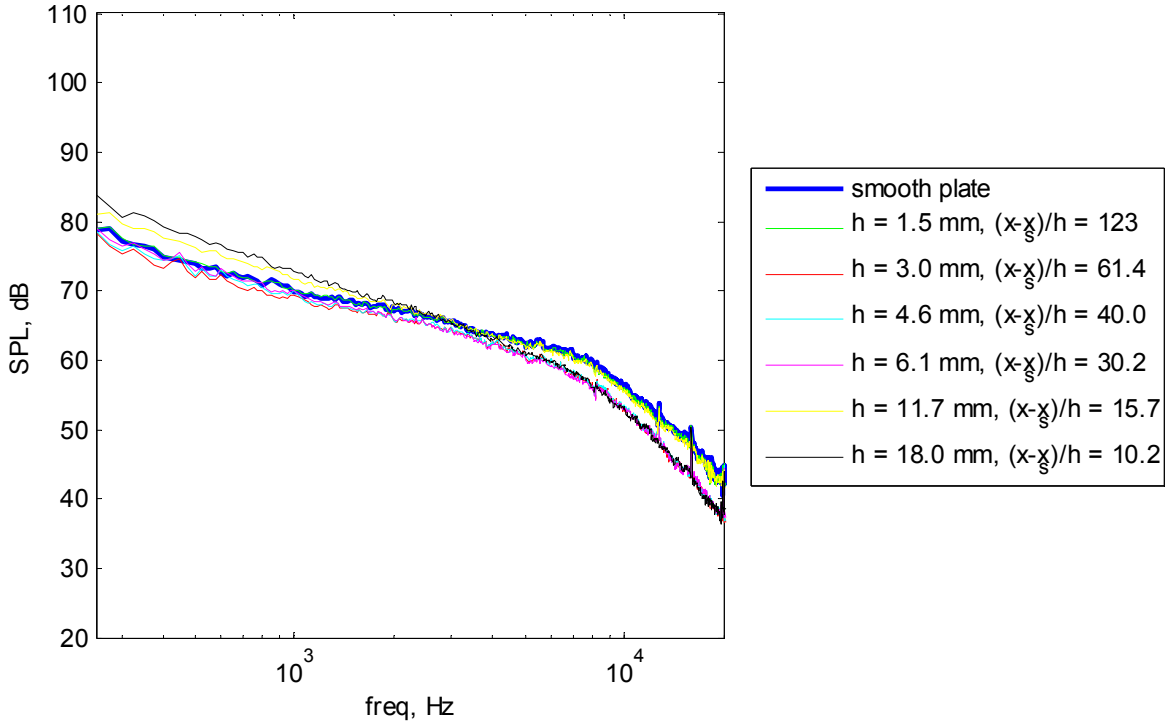

Figure 3.52 e

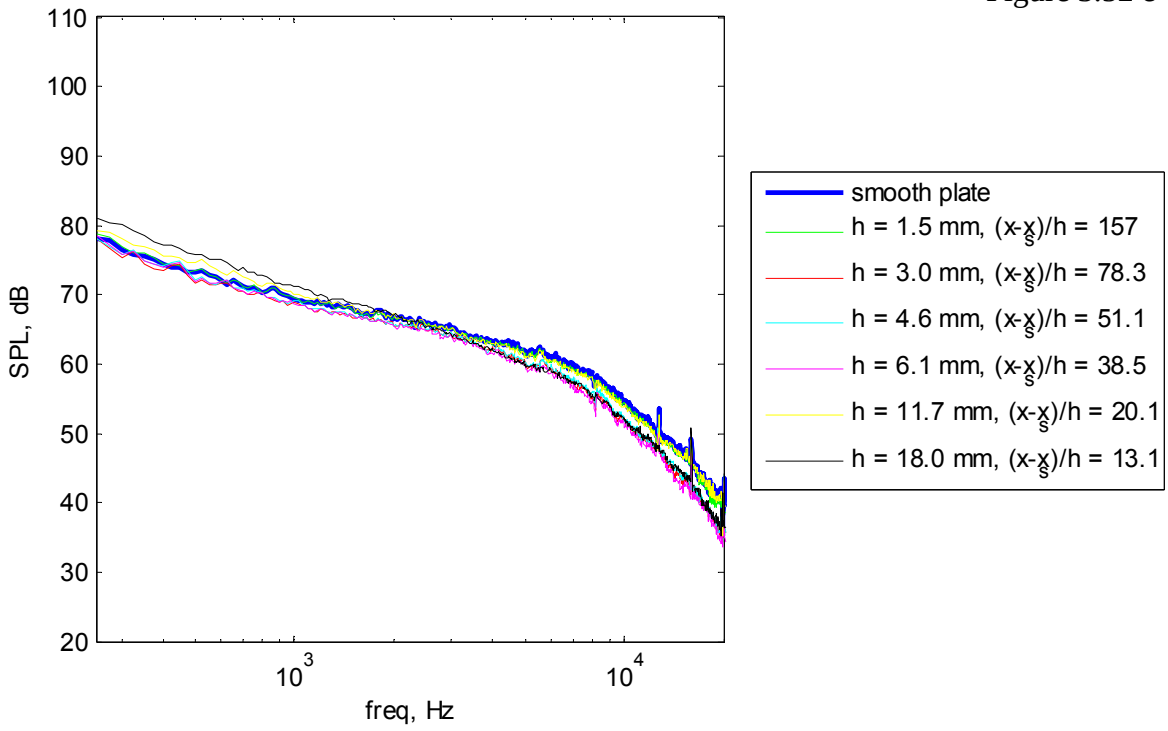

Figure 3.52 f

Figure 3.52 a-f. Wall Pressure Measurements behind All Backward Steps at U_j = 60 m/s

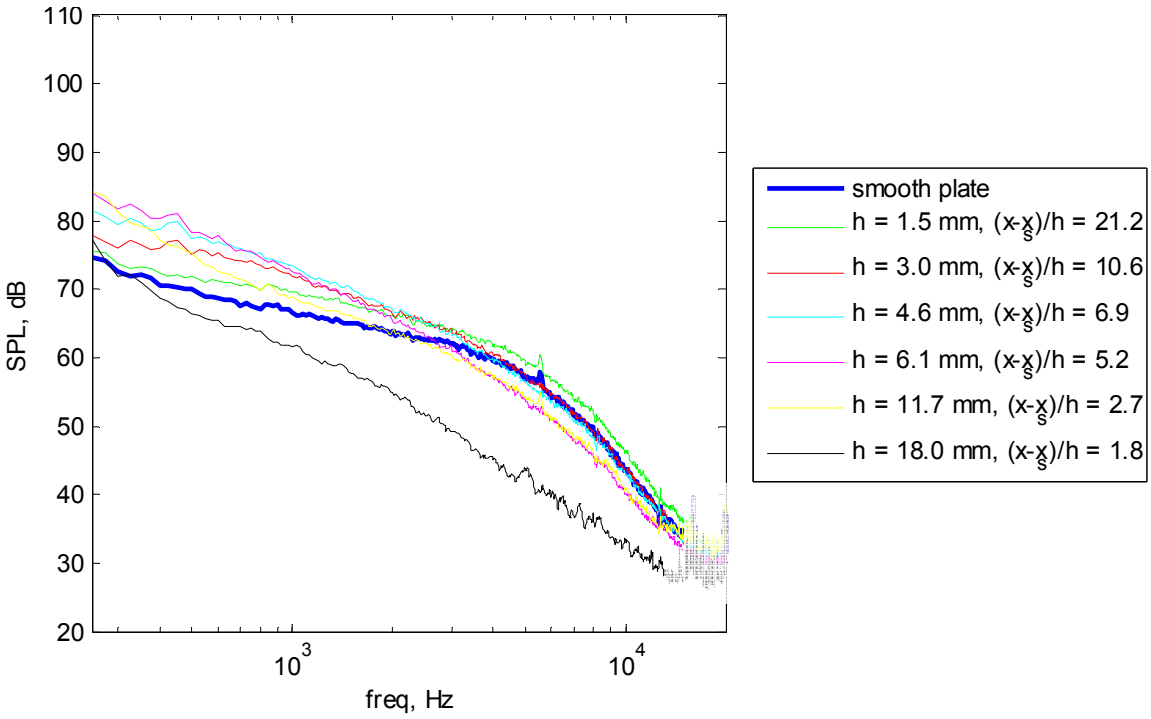

Figure 3.53 a

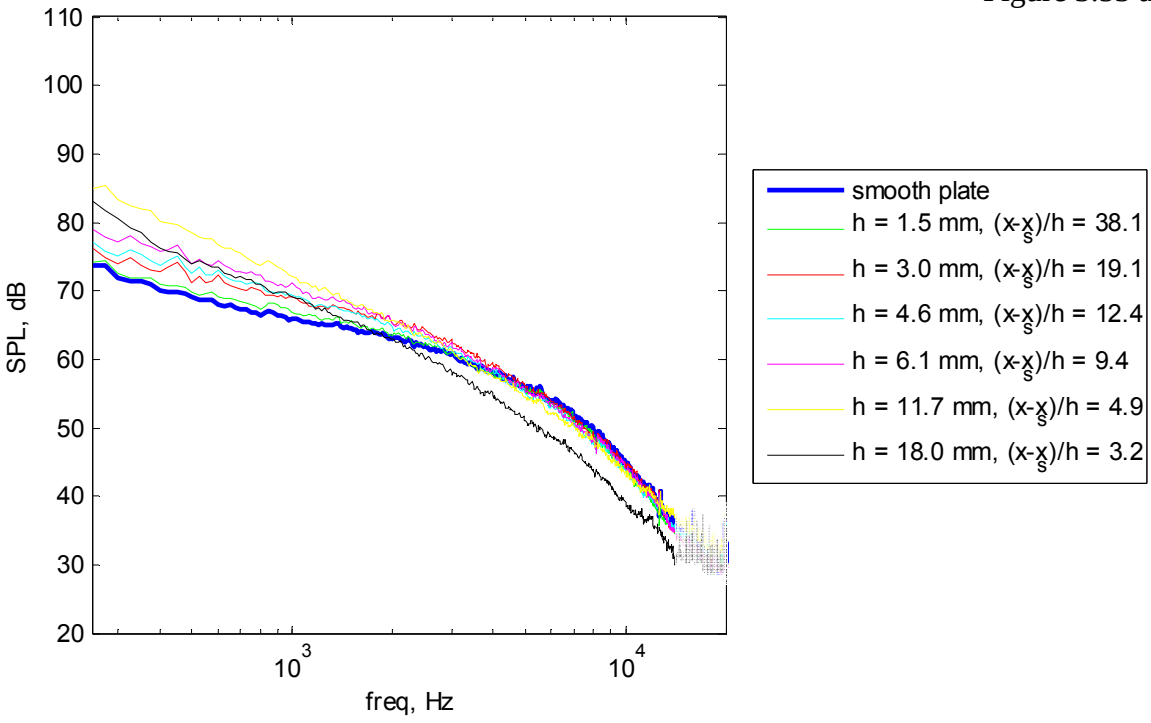

Figure 3.53 b

Figure 3.53 a-f. Wall Pressure Measurements behind All Backward Steps at U_j = 45 m/s

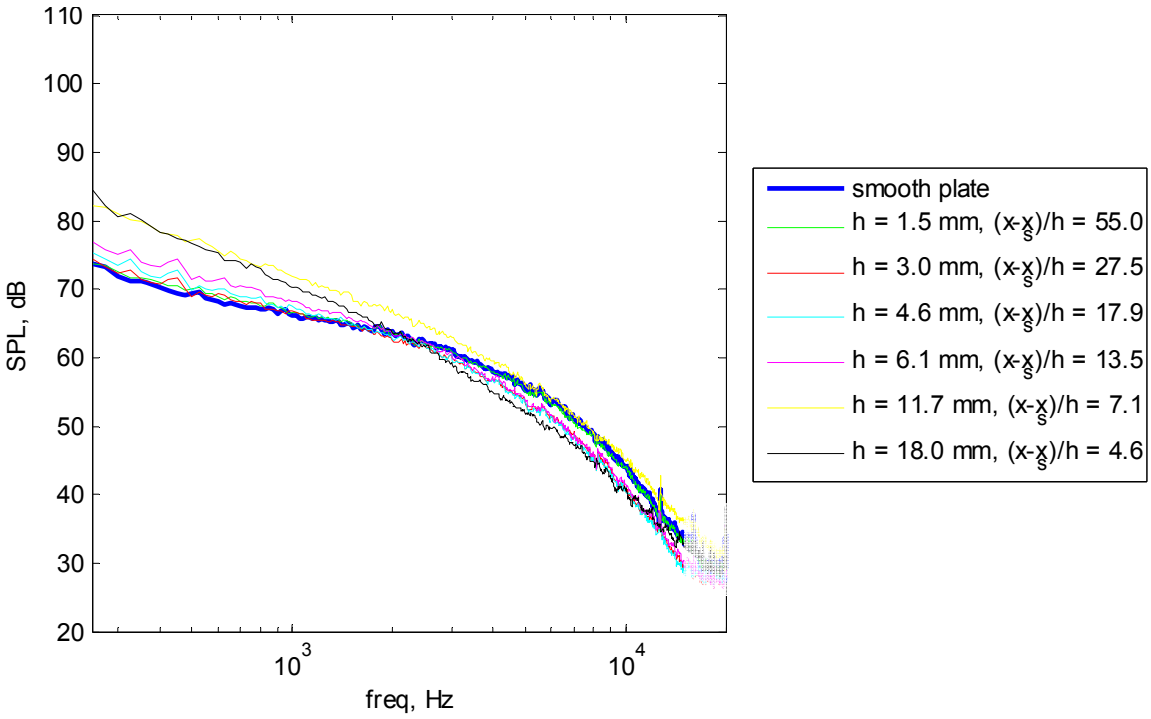

Figure 3.53 c

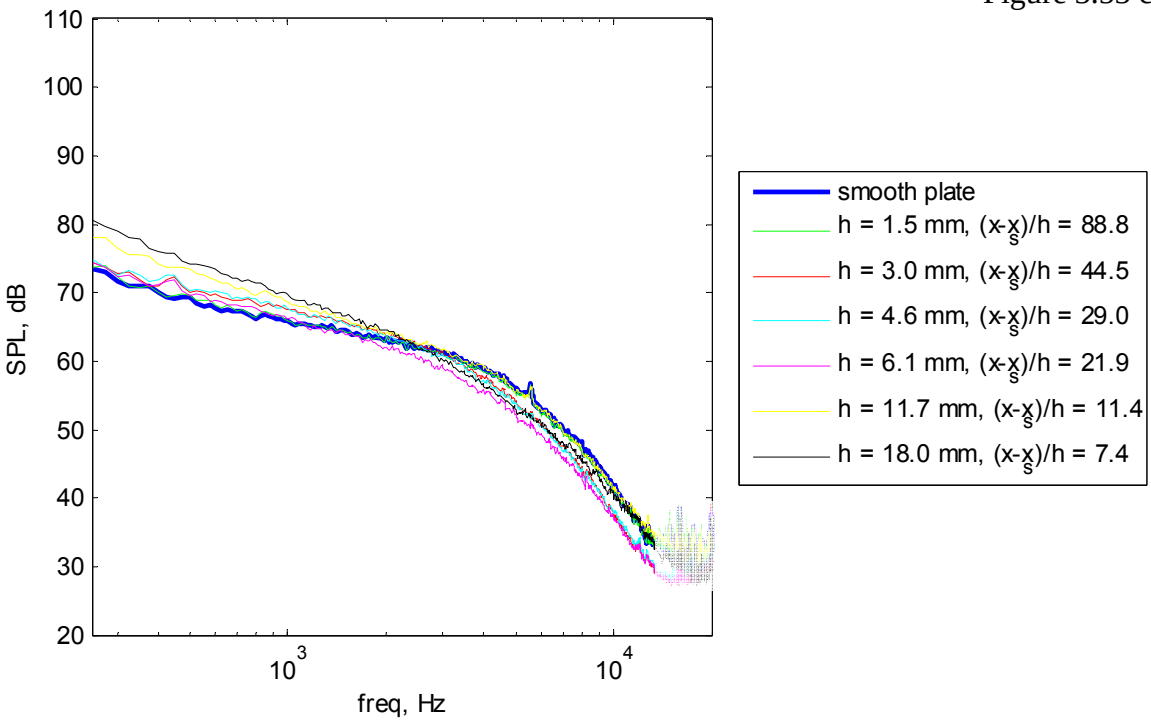

Figure 3.53 d

Figure 3.53 a-f. Wall Pressure Measurements behind All Backward Steps at U_j = 45 m/s

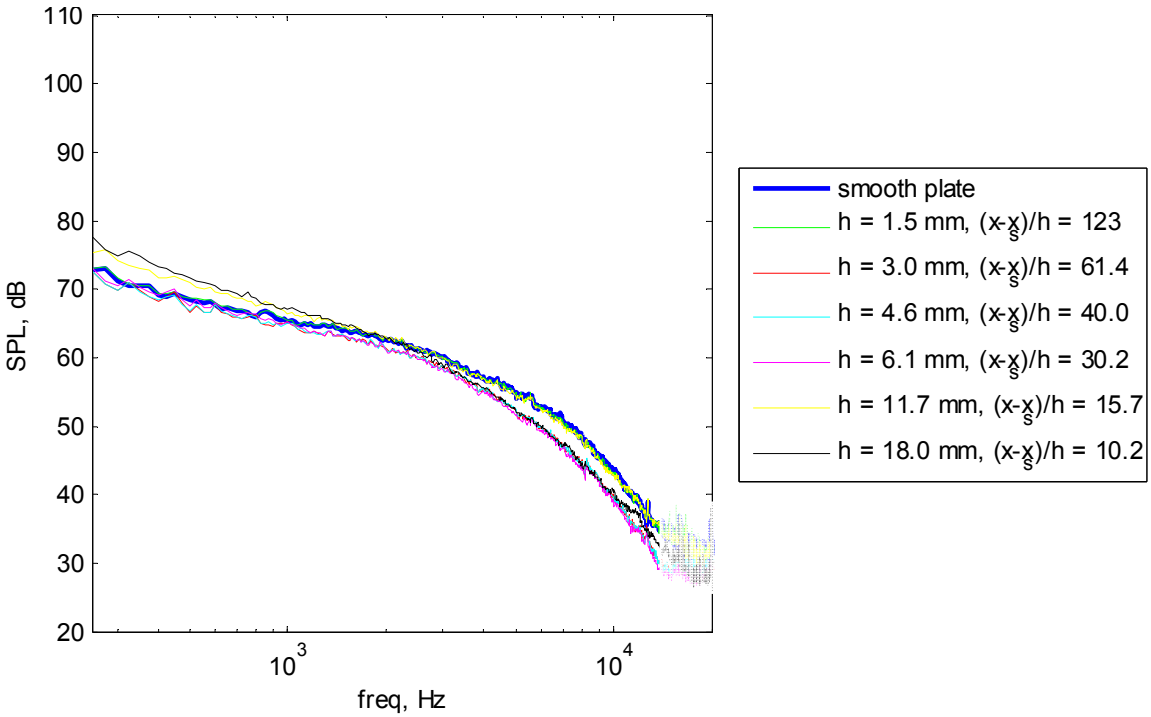

Figure 3.53 e

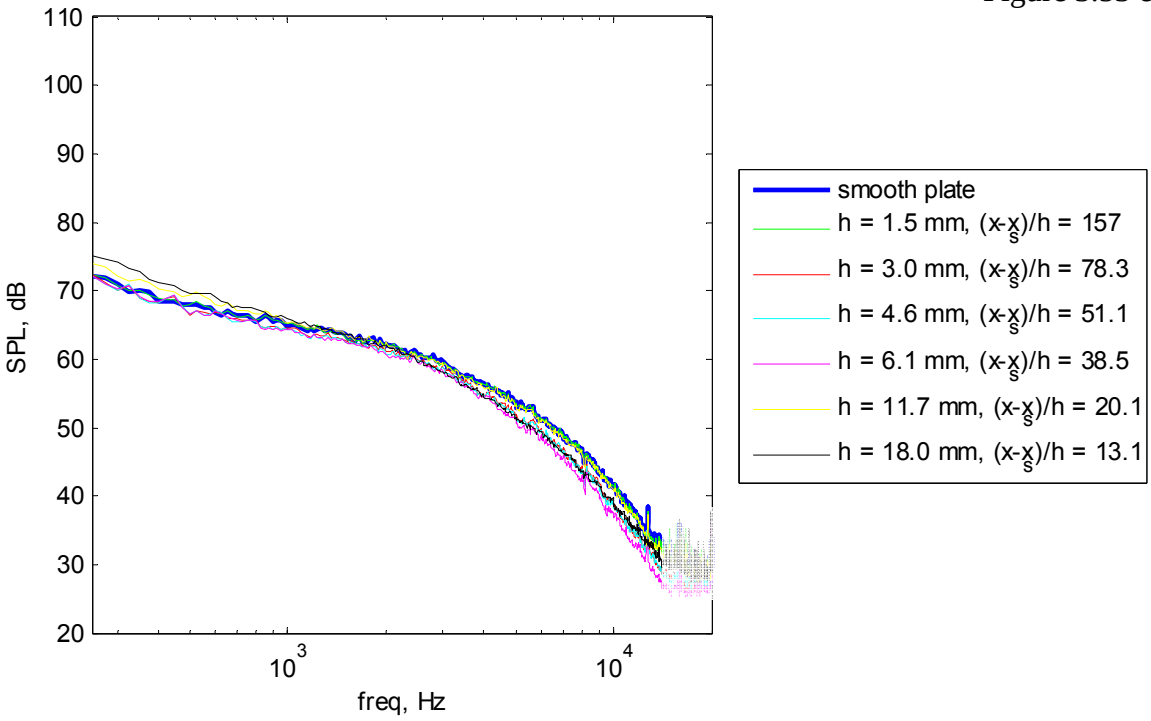

Figure 3.53 f

Figure 3.53 a-f. Wall Pressure Measurements behind All Backward Steps at U_j = 45 m/s

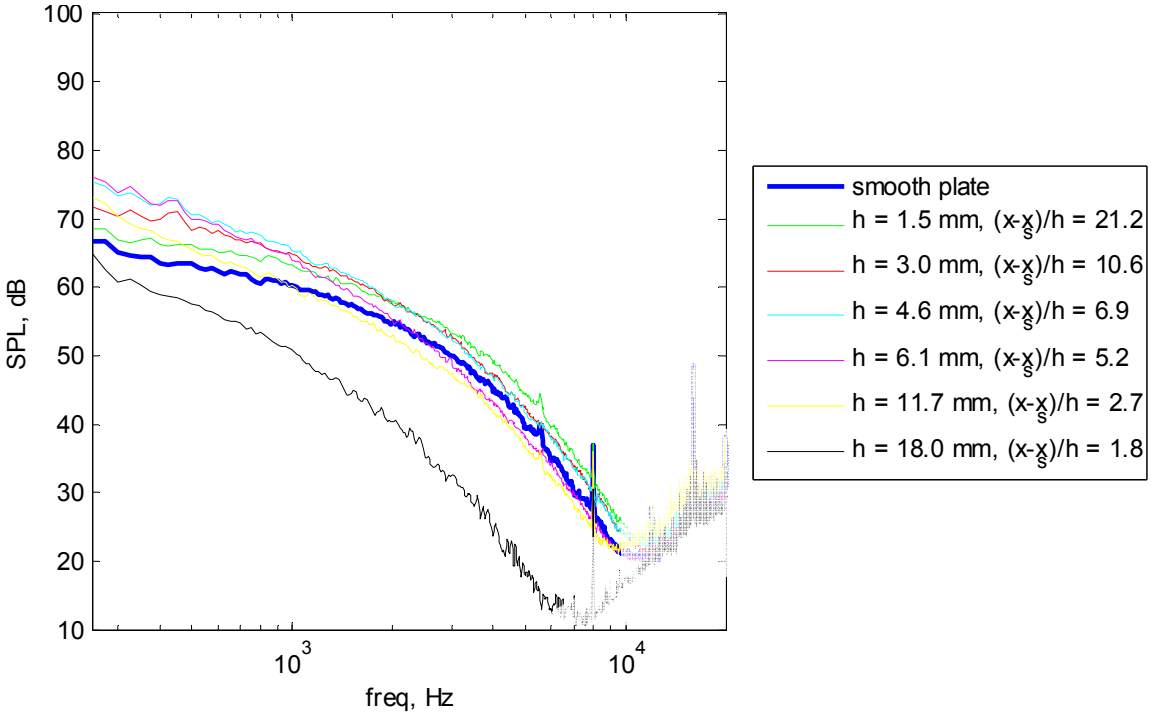

Figure 3.54 a

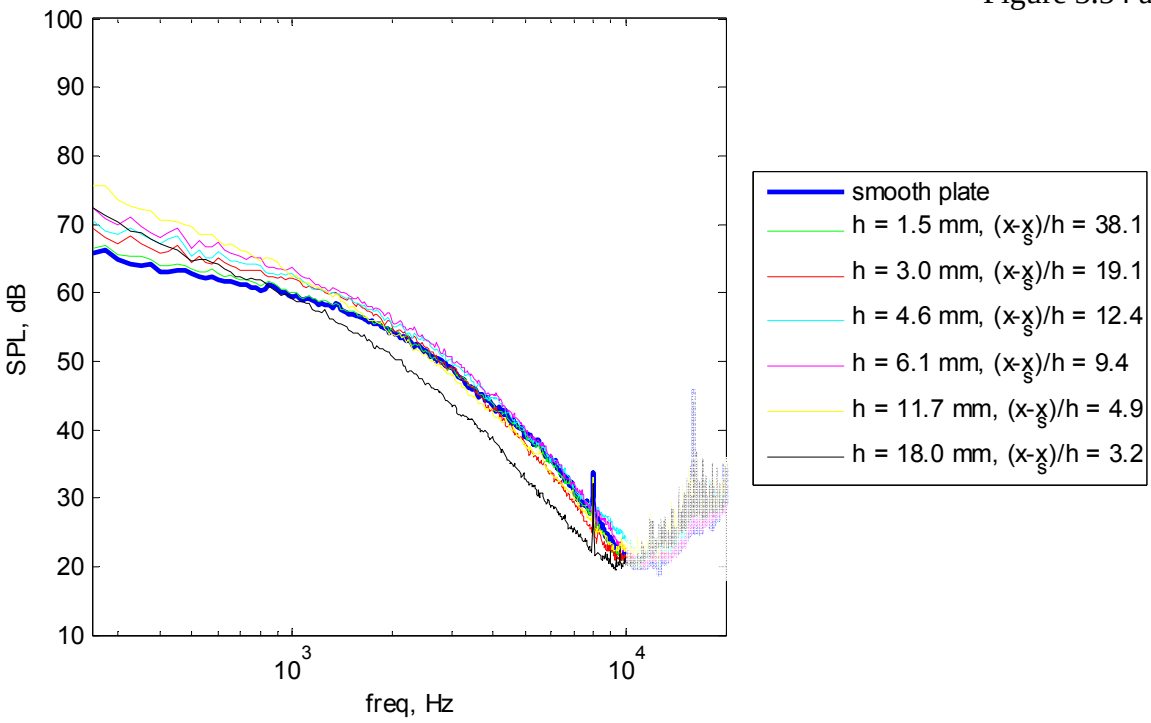

Figure 3.54 b

Figure 3.54 a-f. Wall Pressure Measurements behind All Backward Steps at U_j = 30 m/s

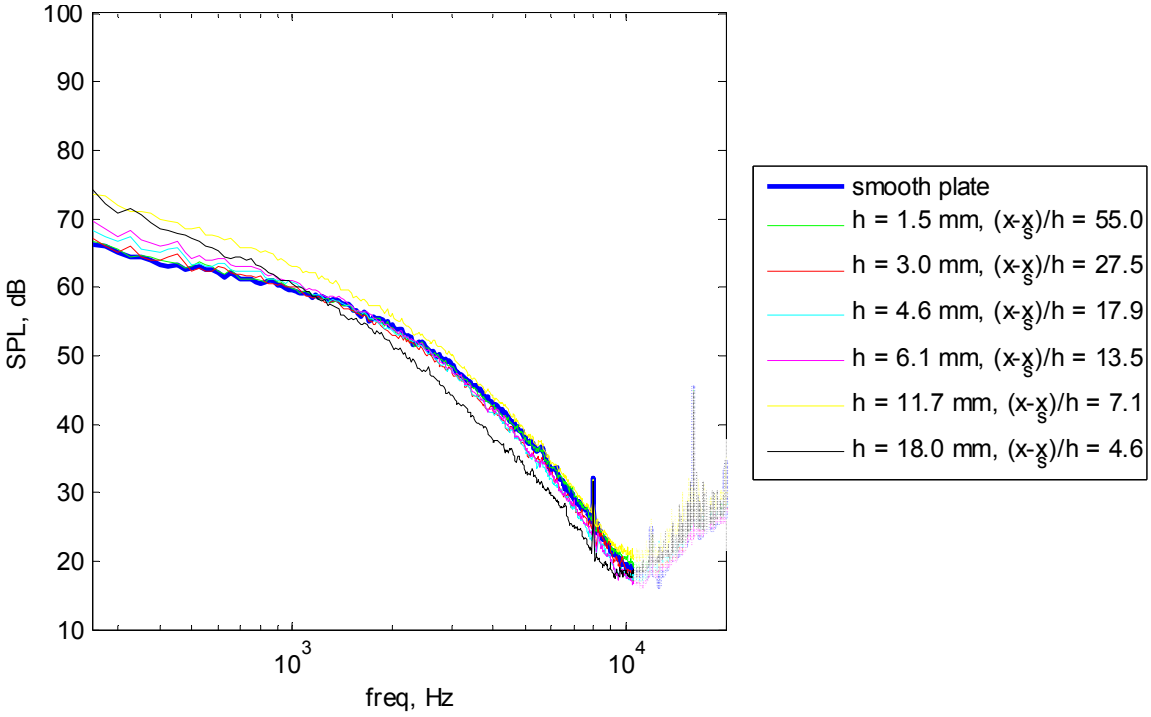

Figure 3.54 c

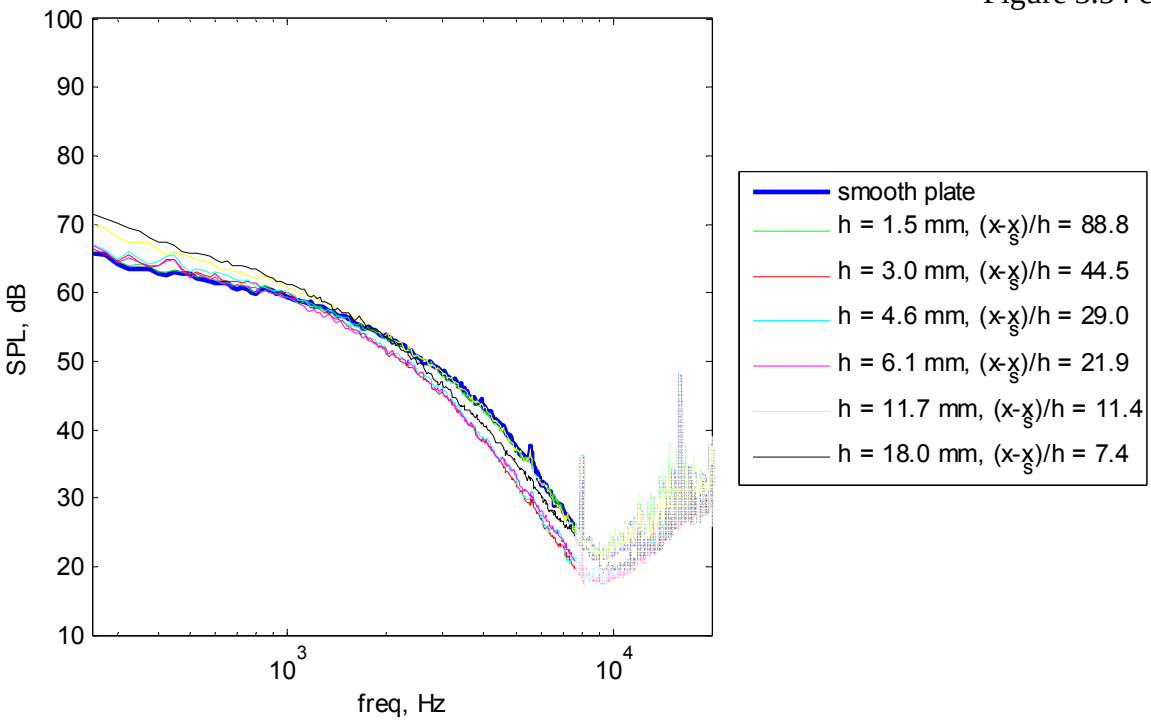

Figure 3.54 d

Figure 3.54 a-f. Wall Pressure Measurements behind All Backward Steps at U_j = 30 m/s

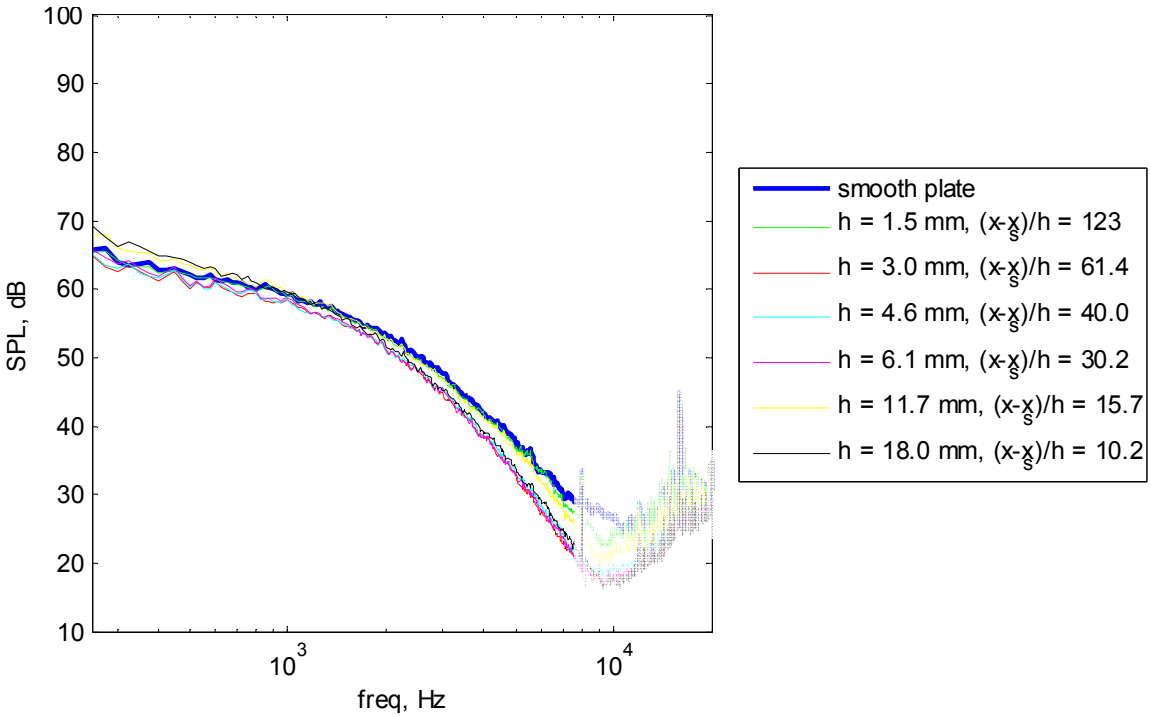

Figure 3.54 e

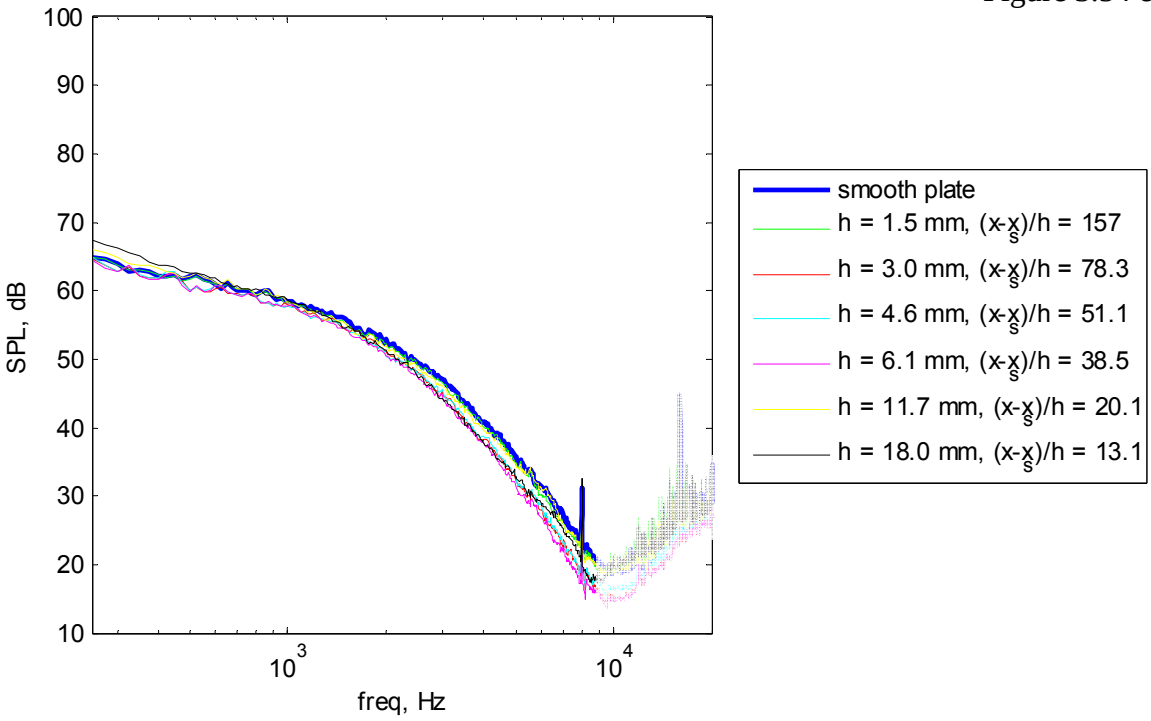

Figure 3.54 f

Figure 3.54 a-f. Wall Pressure Measurements behind All Backward Steps at U_j = 30 m/s

3.4 Far Field Sound Generated By Symmetric Gaps

The radiated far field sound that emanates from a pair of same sized 11.7 mm forward and backward steps, forming a symmetric gap, immersed in flow was studied for four different gap widths, at four stream-wise observation angles, and at three different local maximum velocities. The location of the leading backward step was held constant at the step location, while the forward step was moved downstream to create the different gap widths. The four gap widths considered in this study were 0.5, 1, 2, and 8 step heights in length. All of the definitions and conventions described in Chapter 2 are assumed in the presentation of this data. All figures for this subsection are presented at the end of the subsection.

Figure 3.55 presents the far field spectra from the flow over this set of symmetric gaps for the fastest wall jet exit velocity of 60 m/s at the four observation angles considered. In addition to the far field spectra from the gap flow, the spectra measured from the 11.7 mm forward and backward step at this velocity condition have been overlain for the corresponding observation angles. No backward step spectra were added for the two downstream observation angles as no distinguishable spectra above the background were determined for the backward step. These additional spectra are dark and light grey in color and are identified by arrows and annotations.

It can be seen that these gap spectra are essentially banded above by the spectrum from the forward step and below by the spectrum from the backward step for all observation angles. The gap spectra are structured such that strongest to weakest spectra correspond to the largest to smallest gap widths. This is qualitatively described by larger gaps exposing more of the forward step to the incoming flow, which has been shown to be a stronger producer of sound than a backward step. The quality of the signals is seen to degrade as observation angles move to more downstream angles where the background noise rises.

For an observation angle of 123.5^{o}, the far field spectrum from the largest gap width of eight step heights appears to be completely dominated by the forward step source due to its very similar levels and shape compared to the spectrum of only the forward step. In fact, this gap spectrum is seen to be slightly elevated above the forward step spectrum over the frequencies where the backward step registers a signal. This provides evidence to the idea that the far field sound from this gap configuration is simply an addition of the spectra from the two step configurations. This appears to be a plausible explanation since the forward step is located downstream of the separated flow region of the backward step for this configuration, suggesting they can be treated as independent sources. Figure 3.56 presents the far field spectra from the widest symmetric gap, the 11.7 mm forward step, the 11.7 mm backward step, and a spectrum which is the addition of the power spectral densities of the forward and backward steps. As can be seen, the addition of the forward and backward step spectra does not account for the elevated levels of the gap spectra. This is due to the much weaker backward step signal.

If the gap spectrum for this widest gap is not a simple addition of the forward and backward step contributions, then two possible explanations present themselves. The forward step only configuration encounters the undisturbed wall jet flow, while the forward step composing the gap encounters disturbed flow conditions and likely-elevated

turbulence levels because of the upstream backward step. It is possible that either of these could account for the rise in far field sound. Though not examined in past literature and only speculatively seen in this data, the far field sound dependence on turbulence levels could be significant enough to account for or contribute to the 2dB difference in the spectra.

The far field spectra for the other gaps of shorter width also can not be treated simply as an addition of the steps because the downstream forward step is located inside of what would be the recirculation region of the backward step and is impinged upon by the separated shear layer. As previously stated, as the gap is widened, more of the forward step is exposed to the faster moving flow accounting for the rise in spectral levels.

Spectral dips are seen in the symmetric gap data similar to what has been witnessed for the far field data of step flow. Almost all of the dips appear to be centered on frequencies that imply source locations in the vicinity of the 11.7 mm step heights present. The exception to this is the dip seen at an observation angle of 123.5^{o} for the two step height wide symmetric gap. A smaller, less severe dip is present in the spectrum which suggests acoustic reflections from inside of the gap geometry because the distance implied by the centered frequency corresponds approximately to the gap width.

For this fastest velocity condition, the gap spectra all follow the same trends. Spectral level depends on gap width such that the wake of the upstream backward step shields the forward step. The spectrum for the widest gap is dominated by the forward step source as a result of it being outside of the wake of the backward step. Where available, the far field gap spectrum from the widest gap appears to be an addition of the spectra from the forward and backward steps.

Figures 3.57 and 3.58 present the far field spectra from these gap flows for the two slower wall jet exit velocities of 45 and 30 m/s, respectively. The corresponding forward and backward step spectra have been overlain on the most upstream observation angle of 123.5^{o}. All of the same trends and descriptions are consistent with this data, except that the spectral levels and signal quality is lower due to the slower velocity conditions resulting in weaker sound sources.

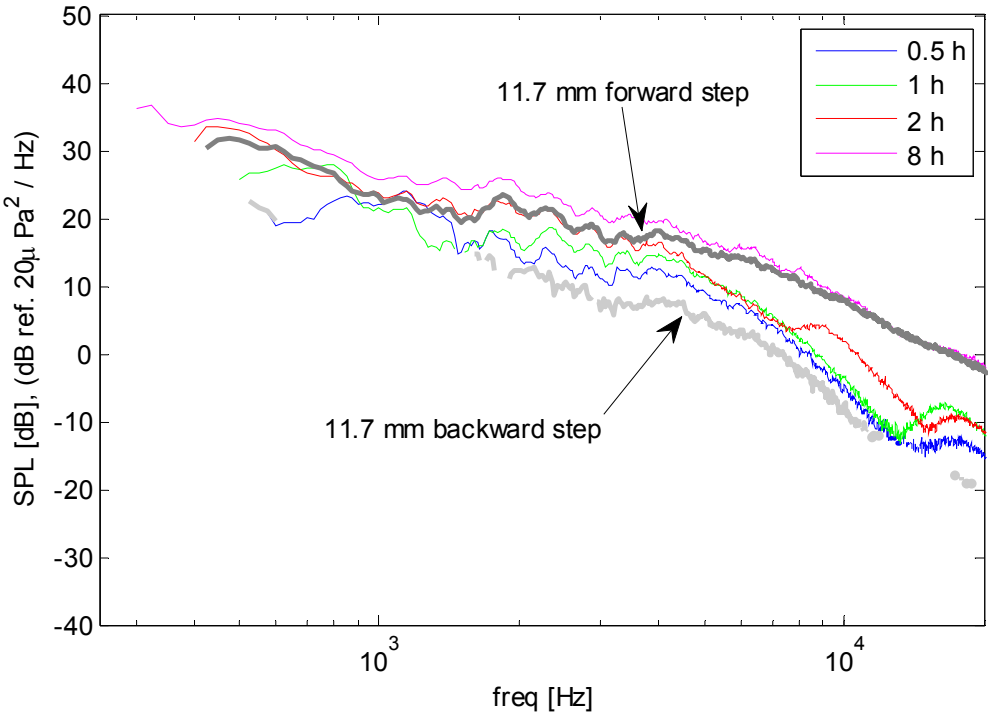

Figure 3.55 a

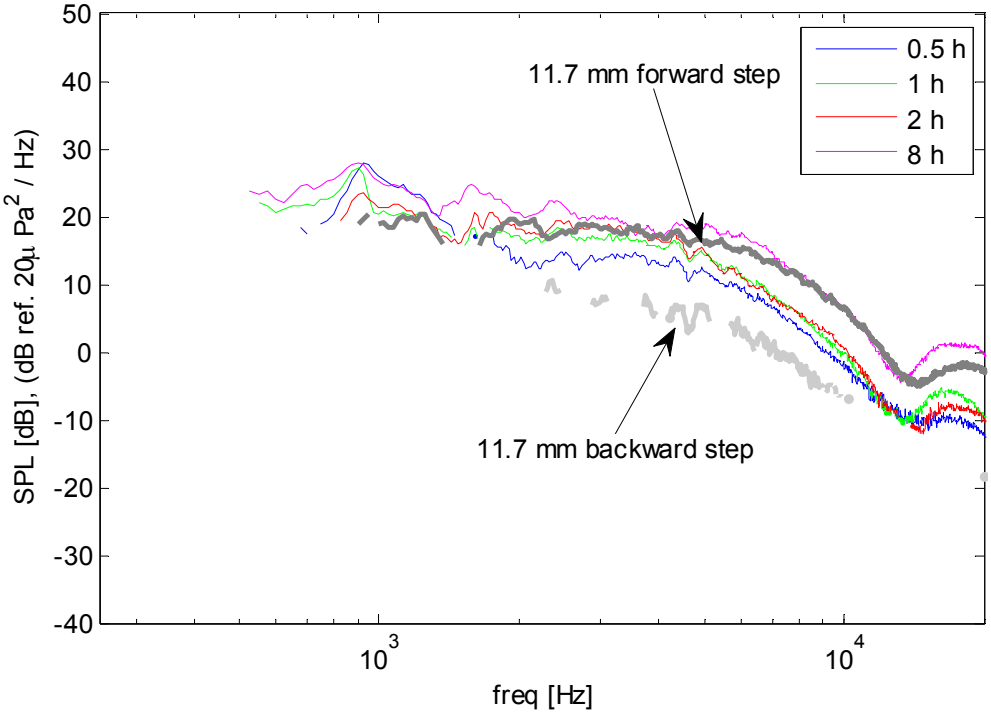

Figure 3.55 b

Figure 3.55 a-d. Far Field Acoustics from Symmetric Gaps at U_j = 60 m/s at the considered Observation Angles; a) θ = 123.5° b) θ = 97.5° c) θ = 74° d) θ = 51.5°

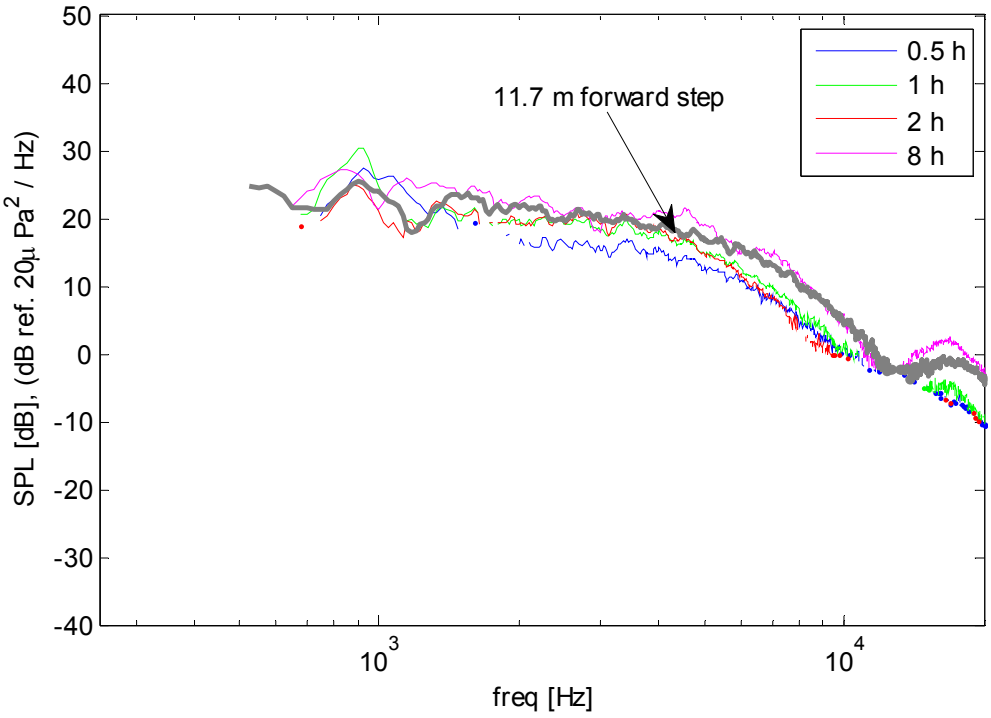

Figure 3.55 c

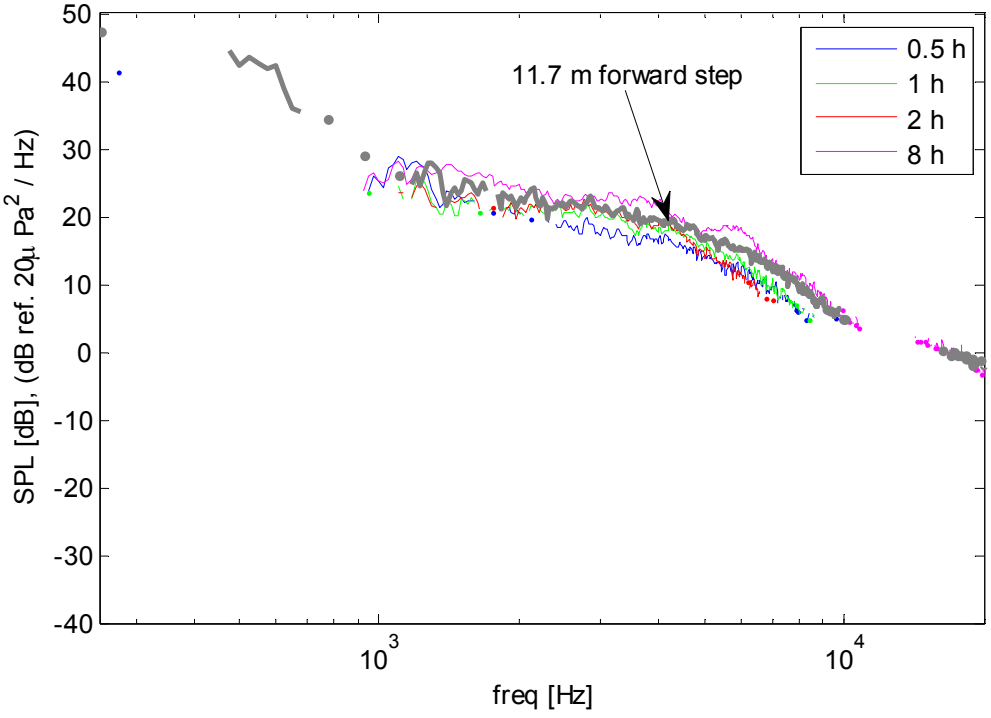

Figure 3.55 d

Figure 3.55 a-d. Far Field Acoustics from Symmetric Gaps at U_j = 60 m/s at the considered Observation Angles; a) θ = 123.5° b) θ = 97.5° c) θ = 74° d) θ = 51.5°

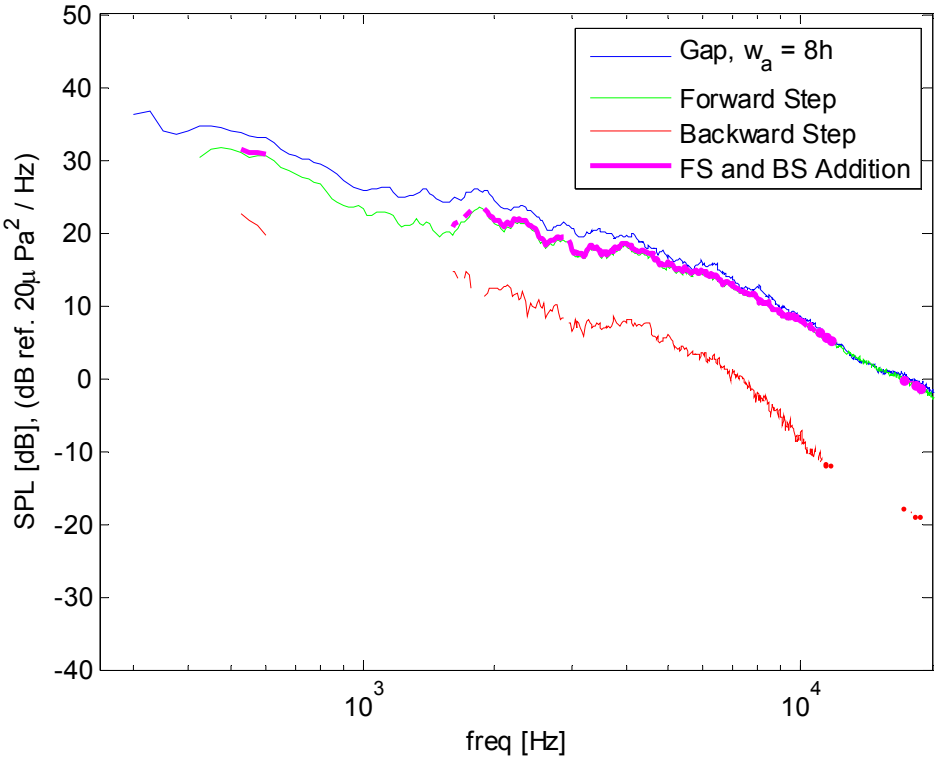

Figure 3.56. Far Field Acoustics from the 11.7 mm Forward and Backward Steps, the 8*h* wide Symmetric Gap, and the Addition of the Forward and Backward Step Power Spectral Densities at U_j = 60 m/s and θ = 123.5°

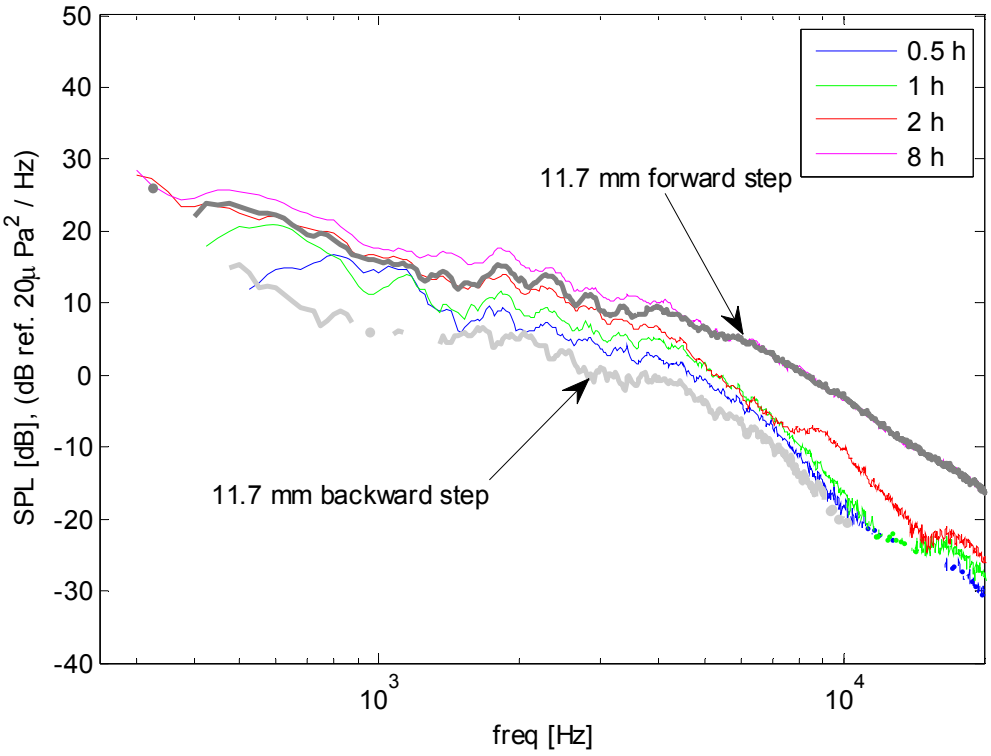

Figure 3.57 a

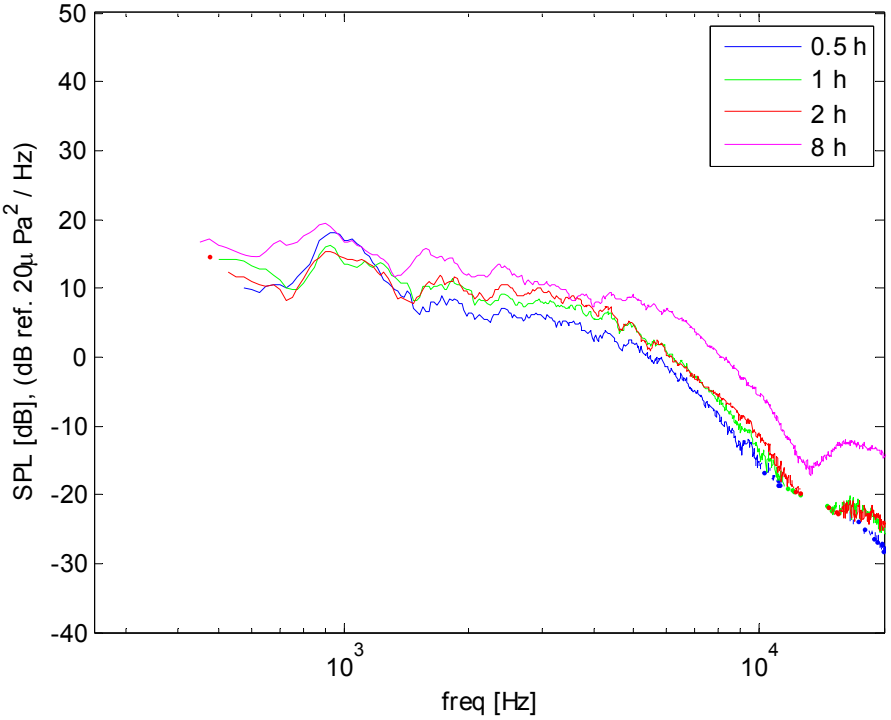

Figure 3.57 b

Figure 3.57 a-d. Far Field Acoustics from Symmetric Gaps at U_j = 45 m/s at the considered Observation Angles; a) θ = 123.5° b) θ = 97.5° c) θ = 74° d) θ = 51.5°

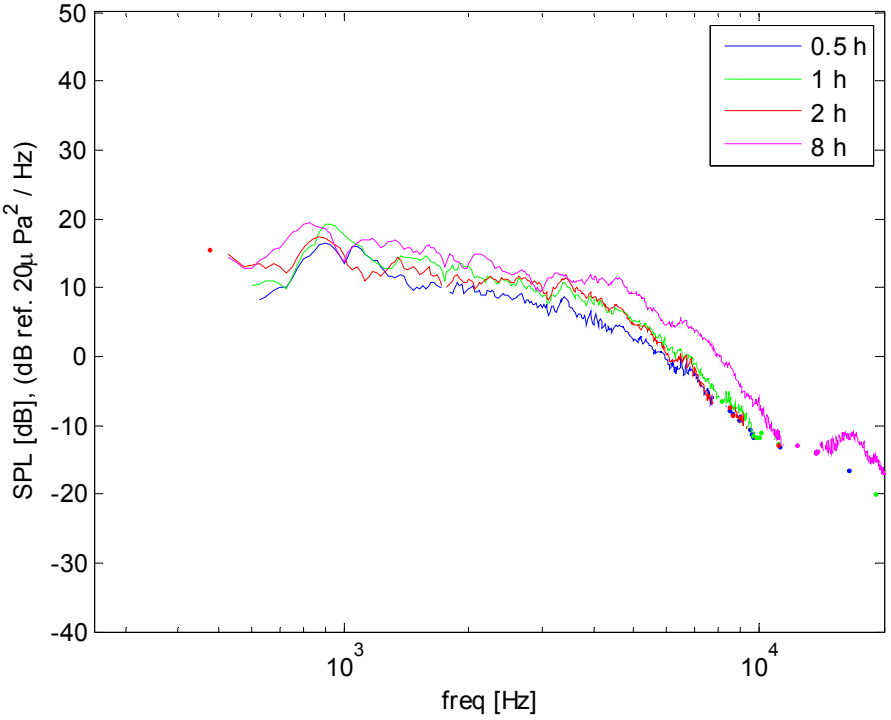

Figure 3.57 c

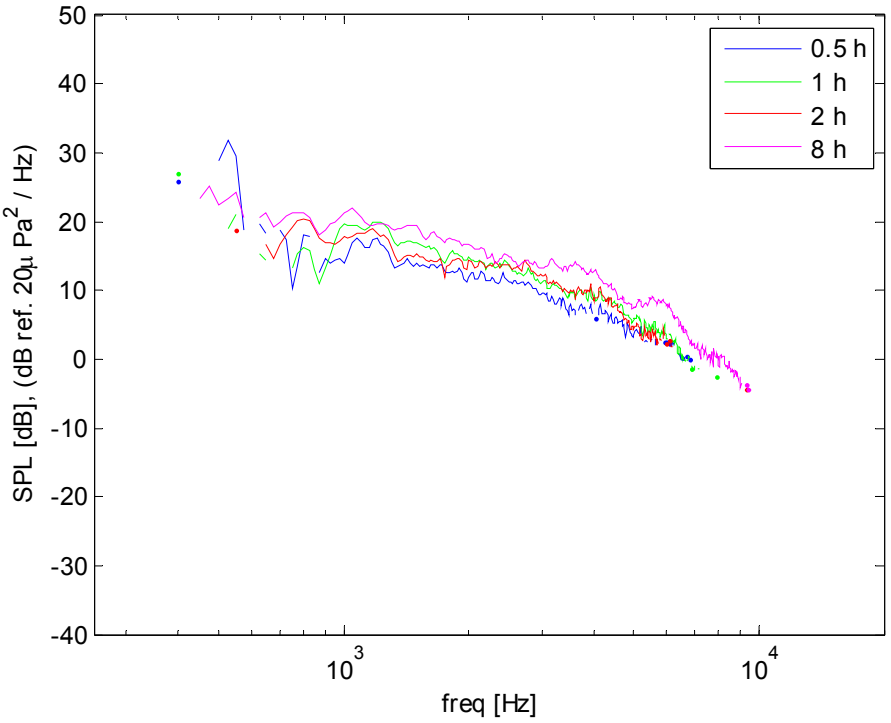

Figure 3.57 d

Figure 3.57 a-d. Far Field Acoustics from Symmetric Gaps at U_j = 45 m/s at the considered Observation Angles; a) θ = 123.5° b) θ = 97.5° c) θ = 74° d) θ = 51.5°

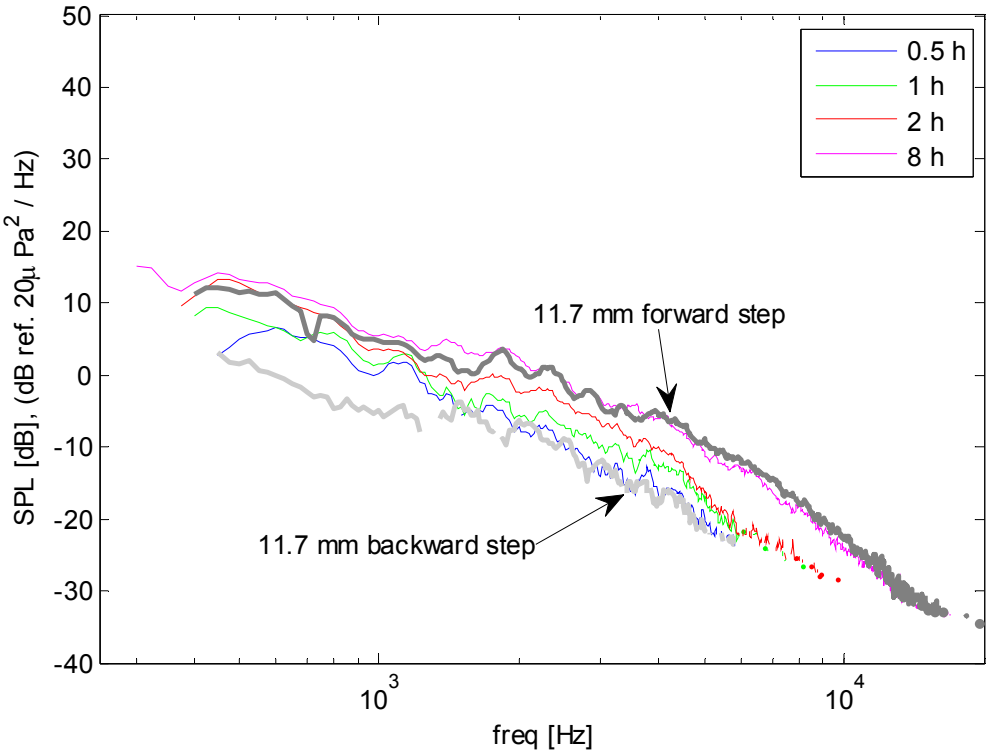

Figure 3.58 a

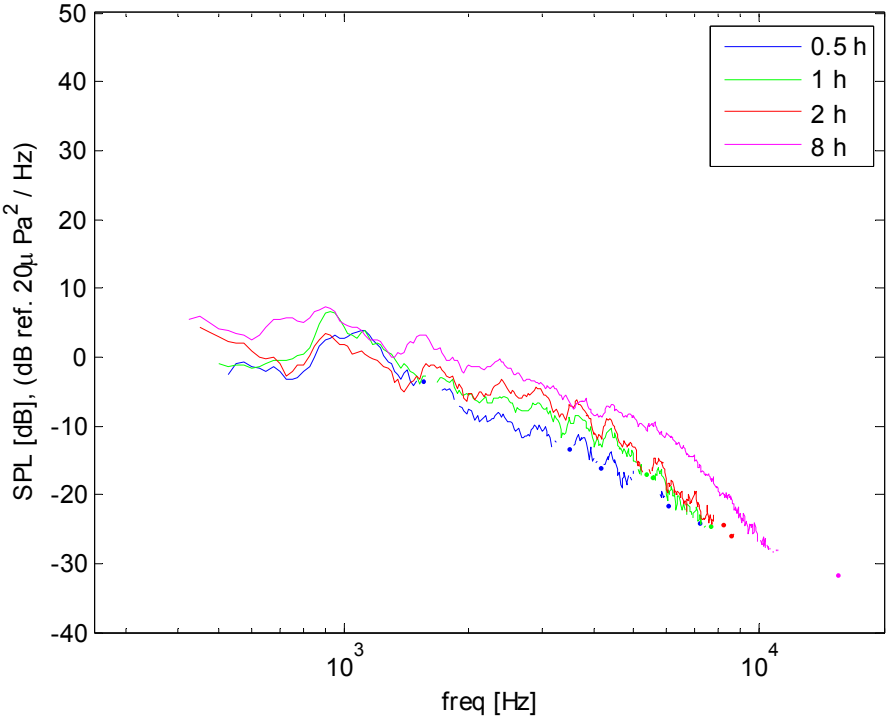

Figure 3.58 b

Figure 3.58 a-d. Far Field Acoustics from Symmetric Gaps at U_j = 30 m/s at the considered Observation Angles; a) θ = 123.5° b) θ = 97.5° c) θ = 74° d) θ = 51.5°

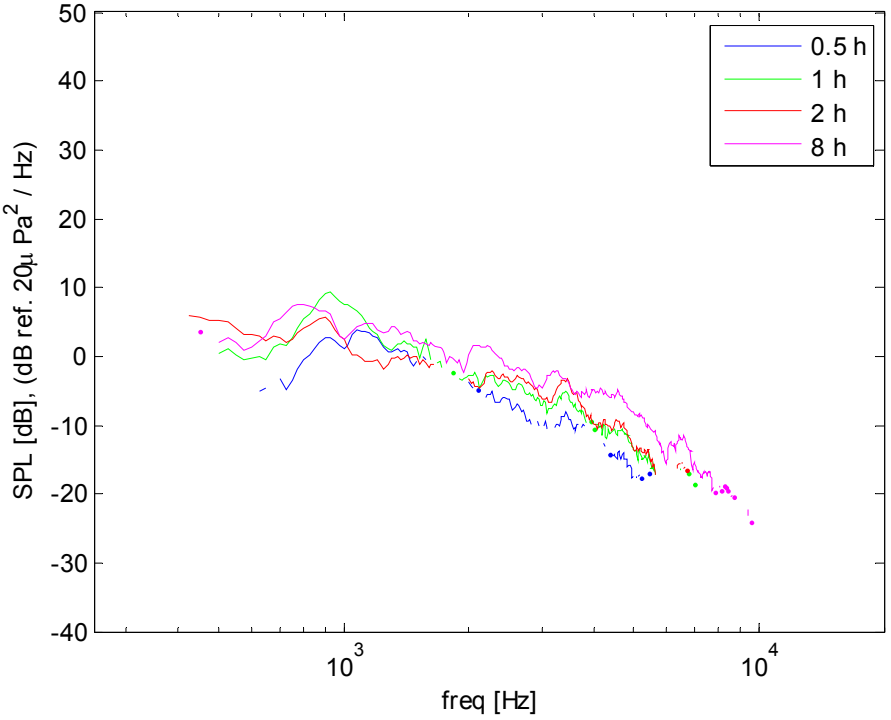

Figure 3.58 c

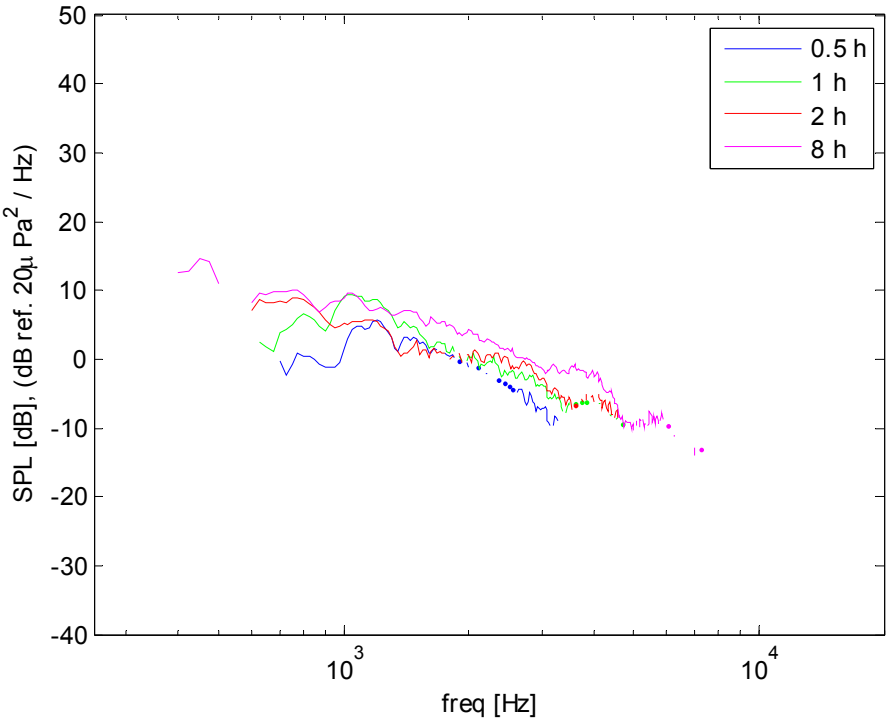

Figure 3.58 d

Figure 3.58 a-d. Far Field Acoustics from Symmetric Gaps at U_j = 30 m/s at the considered Observation Angles; a) θ = 123.5° b) θ = 97.5° c) θ = 74° d) θ = 51.5°

3.5 Far Field Sound Generated By Narrow Asymmetric Gaps

The radiated far field sound that emanates from a set of six narrow asymmetric gaps immersed in flow was collected at four stream-wise observation angles and at three different local boundary layer edge velocities. The narrow asymmetric gaps were created by a single 11.7 mm backward step followed by the set of six forward steps considered in this study at a gap width of 11.7 mm, or one backward step height. All of the definitions and conventions described in Chapter 2 are assumed in the presentation of this data. All figures for this subsection are presented at the end of the subsection.

Figure 3.59 presents the far field spectra from the flow over this set of narrow asymmetric gaps for the fastest wall jet exit velocity of 60 m/s at the four observation angles considered. In addition to the far field spectra from the gap flow, the spectra measured from the 11.7 mm backward step and the 18.0 mm forward step at this velocity condition have been overlain for the corresponding observation angles. No backward step spectra were added for the two downstream observation angles as no distinguishable spectra above the background were determined for the backward step. These additional spectra are dark grey in color and are identified by arrows and annotations.

The spectra from the two upstream observation angles clearly show that the smaller forward steps are essentially shielded by the wake of the upstream backward step. Except at the highest frequencies, the spectra from the four gaps with smaller forward steps than the backward step coincide with the spectra from the backward step only configuration. This behavior is seen for a downstream forward step as large as 6.1 mm, which is approximately half of the height of the upstream backward step. The scalloping that is seen at high frequency for these configurations is centered on frequencies which correspond to source distances away from the flow surface relative to the backward step height of 11.7 mm.

As the forward step height is raised to and above the backward step height, the far field sound levels rise rapidly as more of the forward step is exposed. This behavior is seen for the two largest forward step heights and the far field spectra begin to resemble that of the forward step. For the largest forward step, a new behavior of scalloping is witnessed suggesting acoustic reflections from the gap surfaces in a way that has not been seen for the other step or gap configurations.

The data from the two downstream observation angles exhibit consistent behavior as described for the upstream angles. Because they are shielded by the backward step, little to no far field data is present for the four small forward steps for the same reason as no far field data was registered for the backward step only configuration. The sound levels for these configurations are indistinguishable from the background levels.

Figures 3.60 and 3.61 present this same data for the wall jet exit velocities of 45 and 30 m/s, respectively. Entirely consistent behavior is seen for this data with lower overall levels and signal to noise ratios dependent on the slower velocity conditions. The corresponding 11.7 mm backward step and 18.0 mm forward step far field spectra for the upstream observation angle of 123.5^{o} have been added to illustrate the consistent behavior.

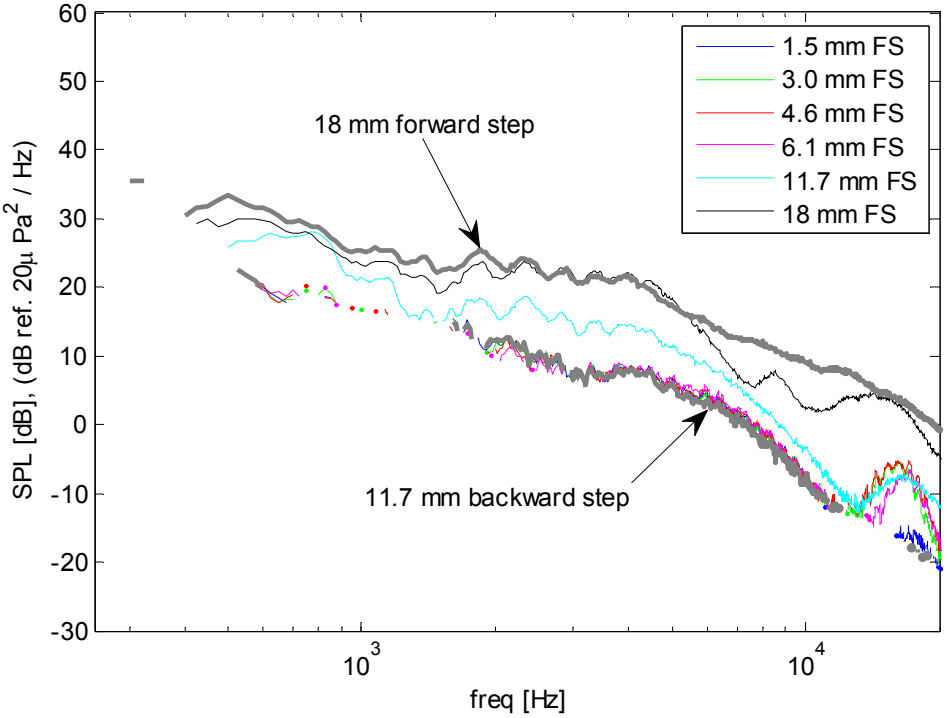

Figure 3.59 a

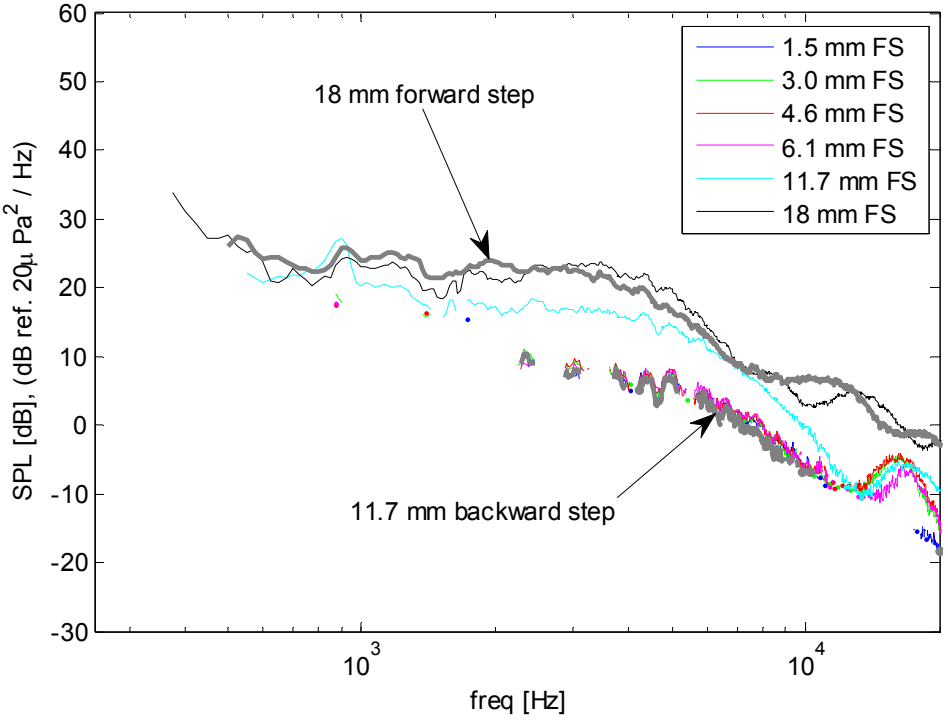

Figure 3.59 b

Figure 3.59 a-d. Far Field Acoustics from Narrow Asymmetric Gaps at U_j = 60 m/s at the considered Observation Angles;
a) θ = 123.5° b) θ = 97.5° c) θ = 74° d) θ = 51.5°

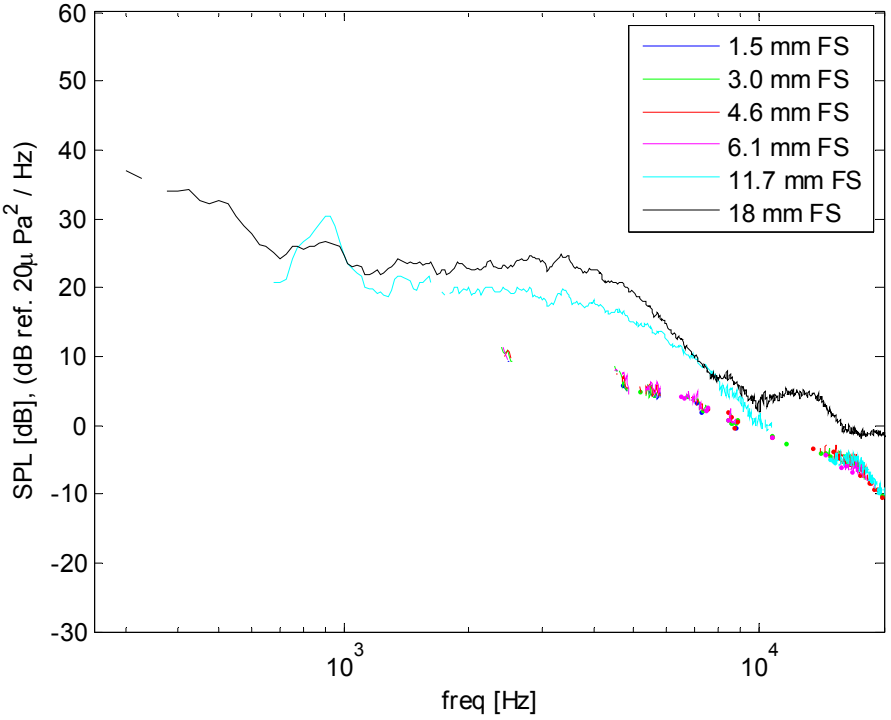

Figure 3.59 c

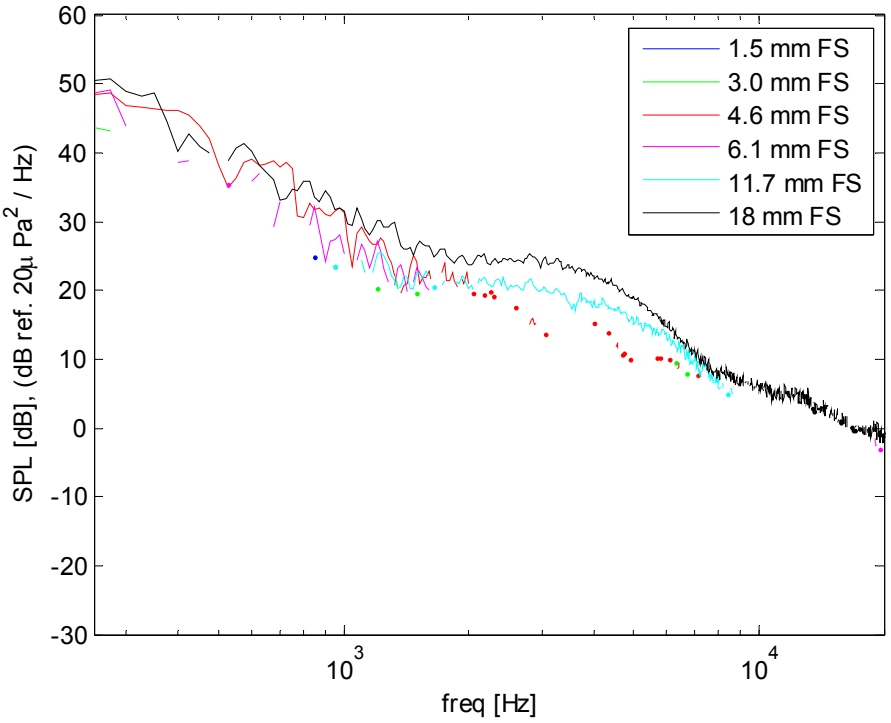

Figure 3.59 d

Figure 3.59 a-d. Far Field Acoustics from Narrow Asymmetric Gaps at U_j = 60 m/s at the considered Observation Angles;
a) θ = 123.5° b) θ = 97.5° c) θ = 74° d) θ = 51.5°

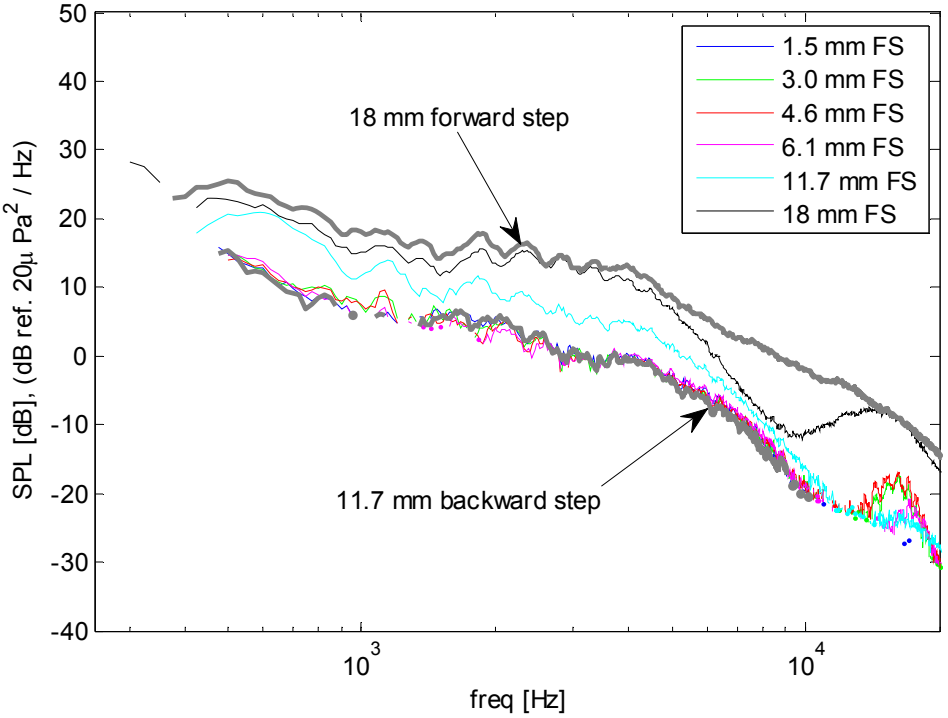

Figure 3.60 a

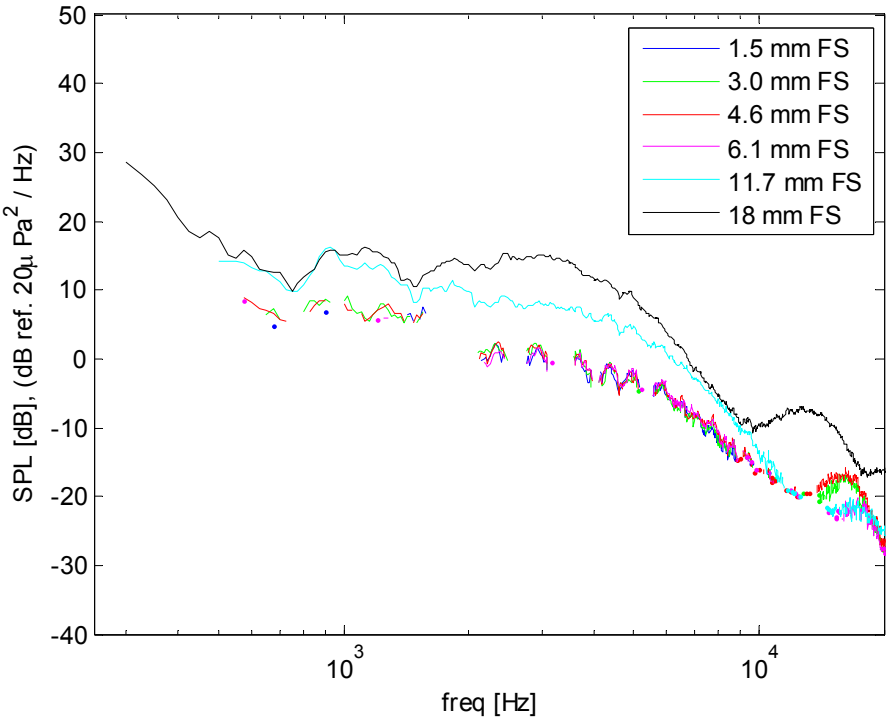

Figure 3.60 b

Figure 3.60 a-d. Far Field Acoustics from Narrow Asymmetric Gaps at U_j = 45 m/s at the considered Observation Angles;
a) θ = 123.5° b) θ = 97.5° c) θ = 74° d) θ = 51.5°

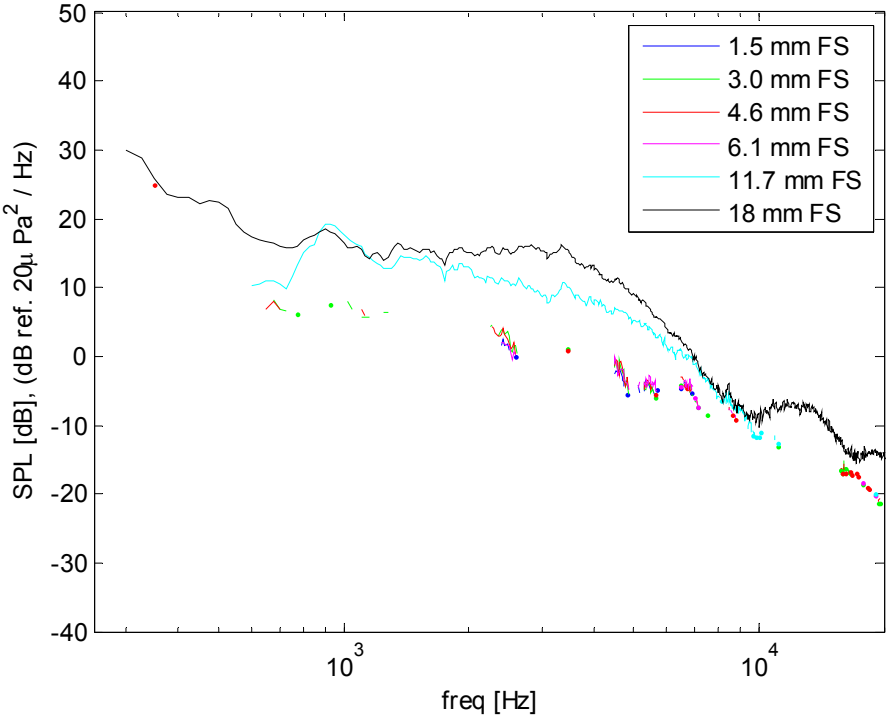

Figure 3.60 c

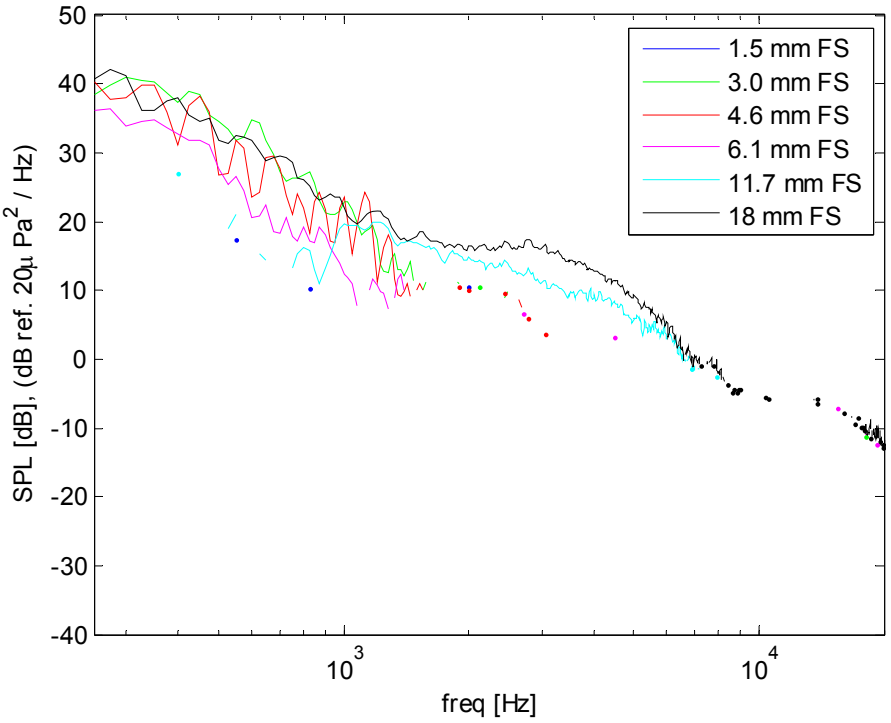

Figure 3.60 d

Figure 3.60 a-d. Far Field Acoustics from Narrow Asymmetric Gaps at U_j = 45 m/s at the considered Observation Angles;
a) θ = 123.5° b) θ = 97.5° c) θ = 74° d) θ = 51.5°

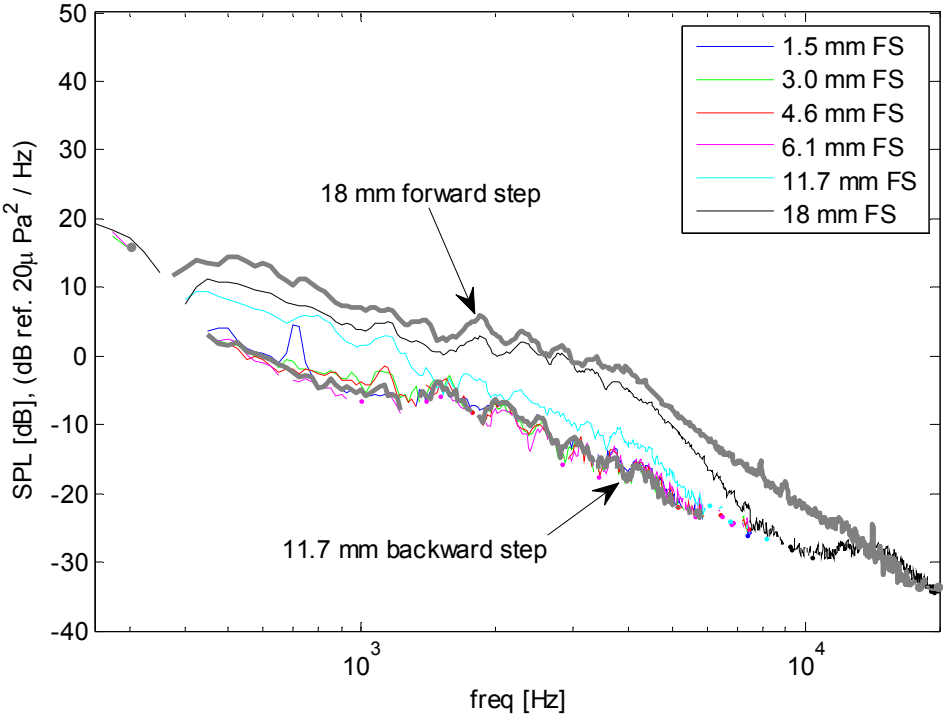

Figure 3.61 a

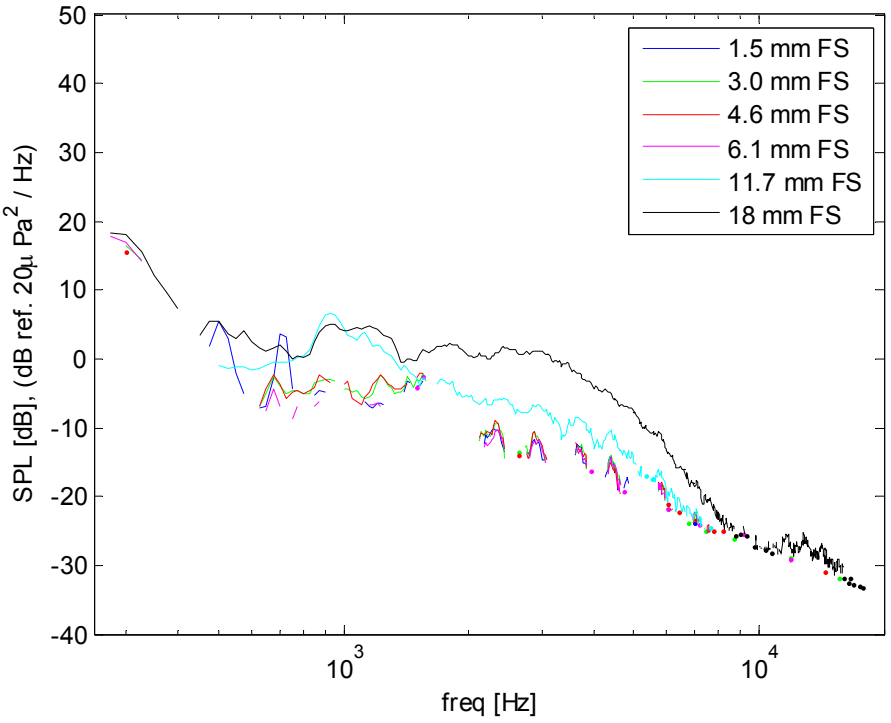

Figure 3.61 b

Figure 3.61 a-d. Far Field Acoustics from Narrow Asymmetric Gaps at U_j = 30 m/s at the considered Observation Angles;
a) θ = 123.5° b) θ = 97.5° c) θ = 74° d) θ = 51.5°

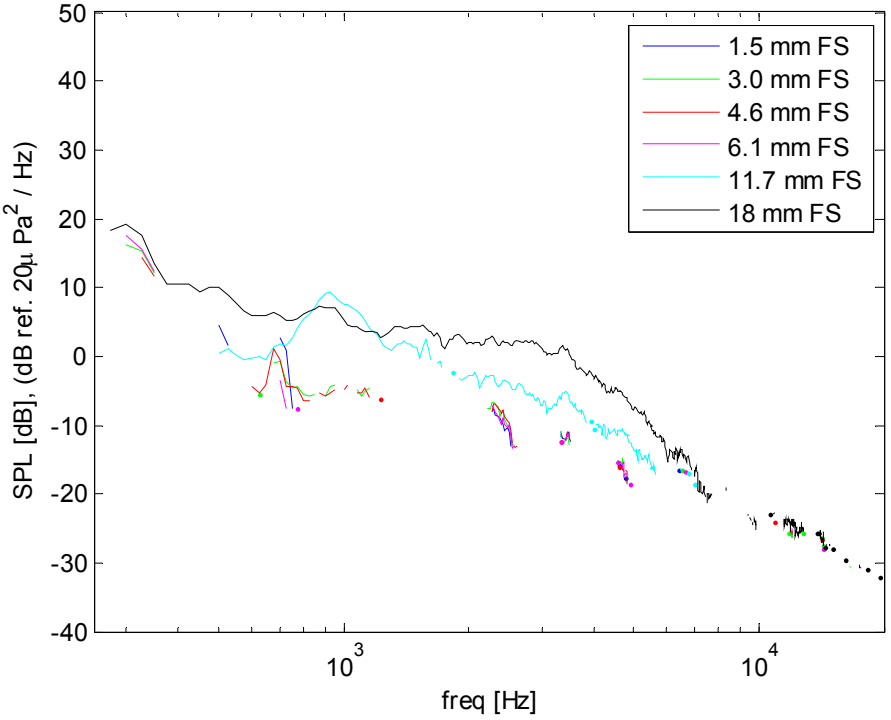

Figure 3.61 c

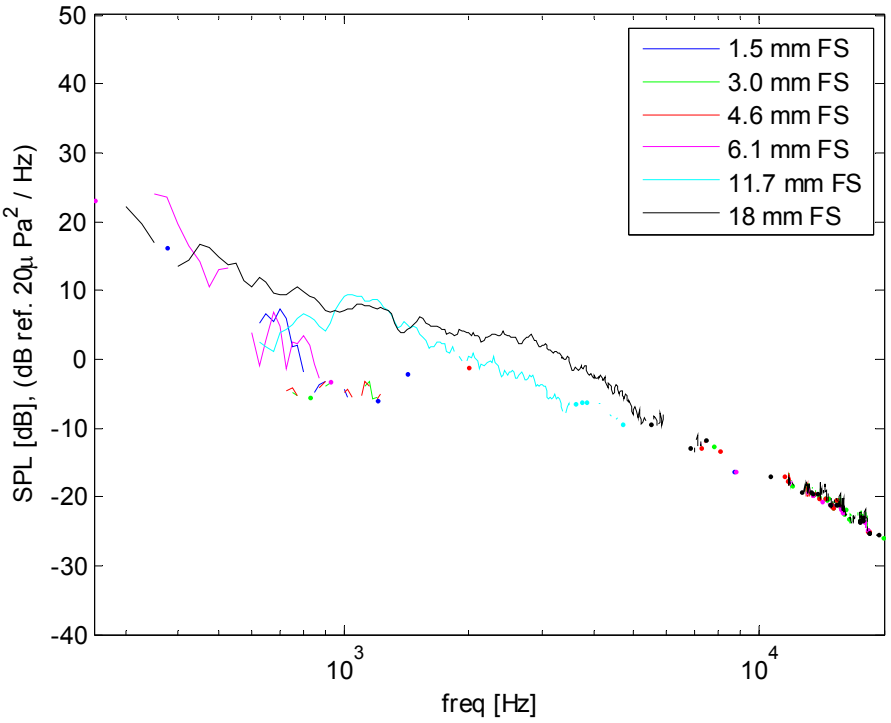

Figure 3.61 d

Figure 3.61 a-d. Far Field Acoustics from Narrow Asymmetric Gaps at U_j = 30 m/s at the considered Observation Angles;
a) θ = 123.5° b) θ = 97.5° c) θ = 74° d) θ = 51.5°

3.6 Far Field Sound Generated By Wide Asymmetric Gaps

The radiated far field sound that emanates from a set of six wide asymmetric gaps immersed in flow was collected at four stream-wise observation angles and at three different local maximum velocities. The wide asymmetric gaps were created by a single 11.7 mm backward step followed by the set of six forward steps considered in this study at a gap width of 93.6 mm, or eight backward step heights. All of the definitions and conventions described in Chapter 2 are assumed in the presentation of this data. All figures for this subsection are presented at the end of the subsection.

Figure 3.62 presents the far field spectra from the flow over this set of wide asymmetric gaps for the fastest wall jet exit velocity of 60 m/s at the four observation angles considered. In addition to the far field spectra from the gap flow, the spectra measured from the 11.7 mm backward step at this velocity condition have been overlain for the corresponding observation angles. No backward step spectra were added for the two downstream observation angles as no distinguishable spectra above the background were determined for the backward step. These additional spectra are dark grey in color and are identified by arrows and annotations.

The far field spectra of these gap flows are very similar to those of the forward step only configurations (seen in Figure 3.8). The far field spectra remain in a cascade structure and exhibit the same spectral dips based on step height. There exists little evidence of the presence of the upstream 11.7 mm backward step in the far field data at first look.

A direct comparison between the forward step spectra and the corresponding spectra from the wide asymmetric gap configuration for the 1.5 and 11.7 mm step heights is given in Figure 3.63 for the two most upstream observation angles. The spectra as seen at both observation angles for the larger forward step of 11.7 mm and its corresponding gap configuration show significant similarity. The spectra deviate by approximately 2dB and experience the same spectral dips at an observation angle of 97.5^{o}. The main difference between the spectra for the 1.5 mm forward step and corresponding gap is that the gap spectra at both observation angles show a slight spectral dip at a frequency that would appear to come from the backward step source. Clearly, this is not seen in the spectra for the forward step only configuration. This comparison shows the minor differences in the spectra, but generally makes clear that the backward step does not significantly contribute to the radiated sound.

This behavior is attributed to the fact that the flow has reattached inside of the width of the gap, and though the flow field is altered, the full face of the forward step is exposed to the incoming flow. Because forward steps have been shown to be significantly more effective at producing far field sound, their contribution dominates the radiated sound. This is evident by the added backward step spectra for the two upstream observation angles of 123.5^{o} and 97.5^{o} in Figure 3.62. At this location, the spectrum for the smallest forward step portion of the gap of 1.5 mm is distinguishable above the spectrum of the 11.7 mm backward step only; which can be thought of as the minimum sound level possible for this gap configuration.

The results for the widest symmetric gap show that the far field is not a simple addition of the independently measured contributions of the two steps that make a gap. In combination with these results though, it has been shown that if the flow has

reattached, then the two steps can be thought of as independent sources. While the backward step will alter the downstream flow field, the forward step will dominate the far field sound because it is a stronger source of flow induced noise.

Figures 3.64 and 3.65 present this same data for the wall jet exit velocities of 45 and 30 m/s, respectively. Entirely consistent behavior is seen for this data with lower overall levels and signal to noise ratios dependent on the slower velocity conditions. The corresponding backward step only far field spectra for the upstream observation angle of 123.5^{o} have been added to illustrate the consistent behavior.

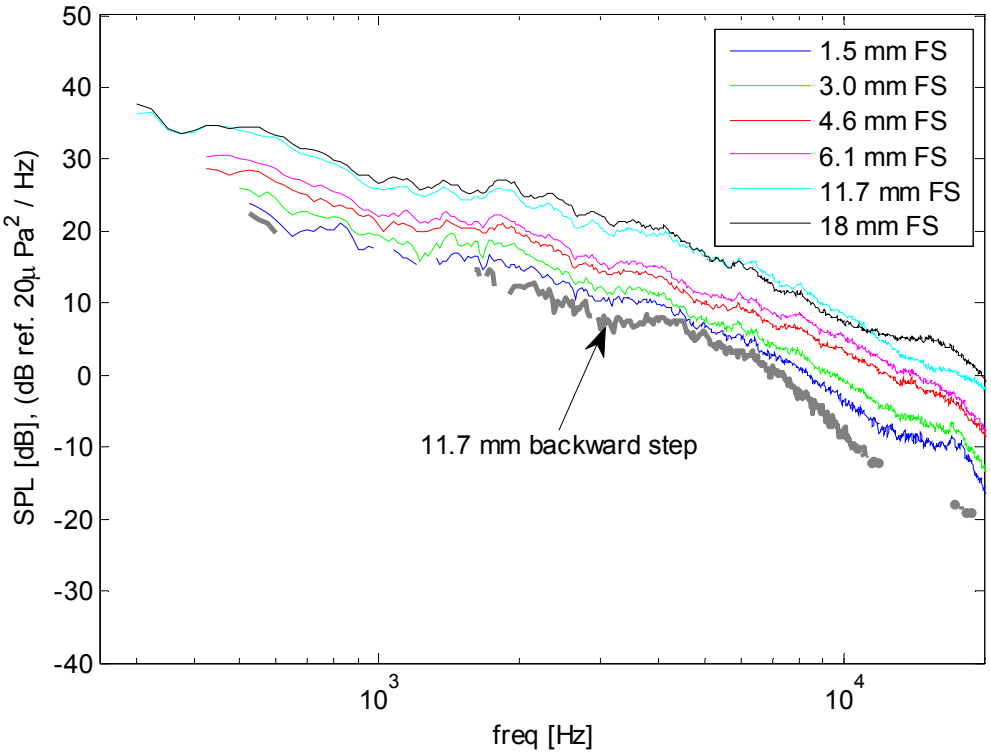

Figure 3.62 a

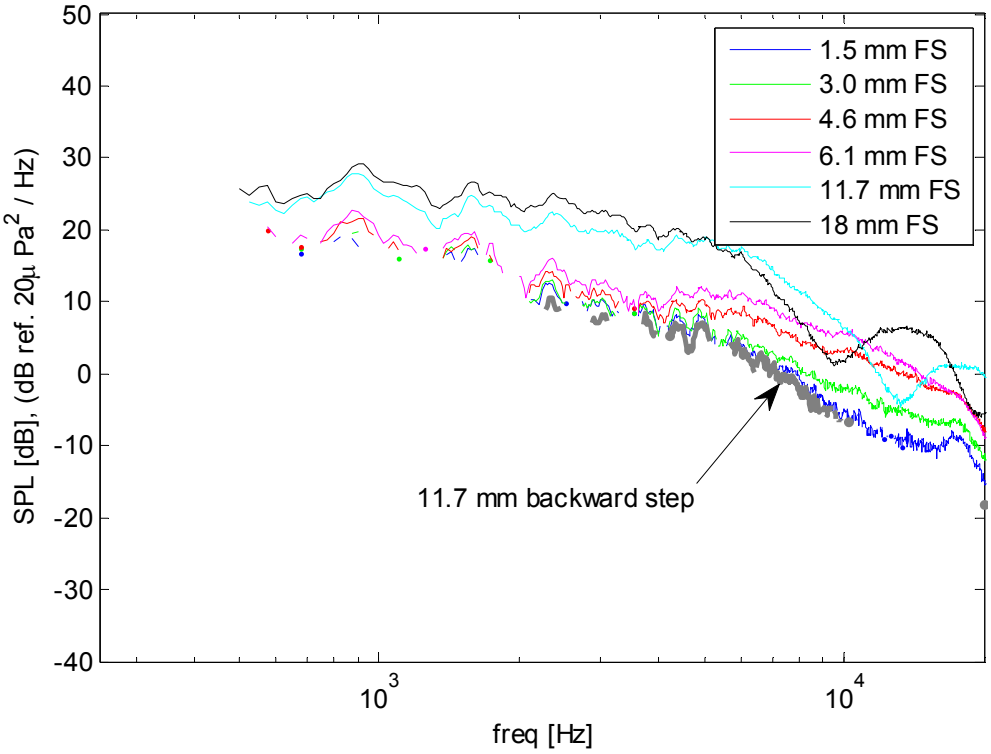

Figure 3.62 b

Figure 3.62 a-d. Far Field Acoustics from Wide Asymmetric Gaps at U_j = 60 m/s at the considered Observation Angles; a) θ = 123.5° b) θ = 97.5° c) θ = 74° d) θ = 51.5°

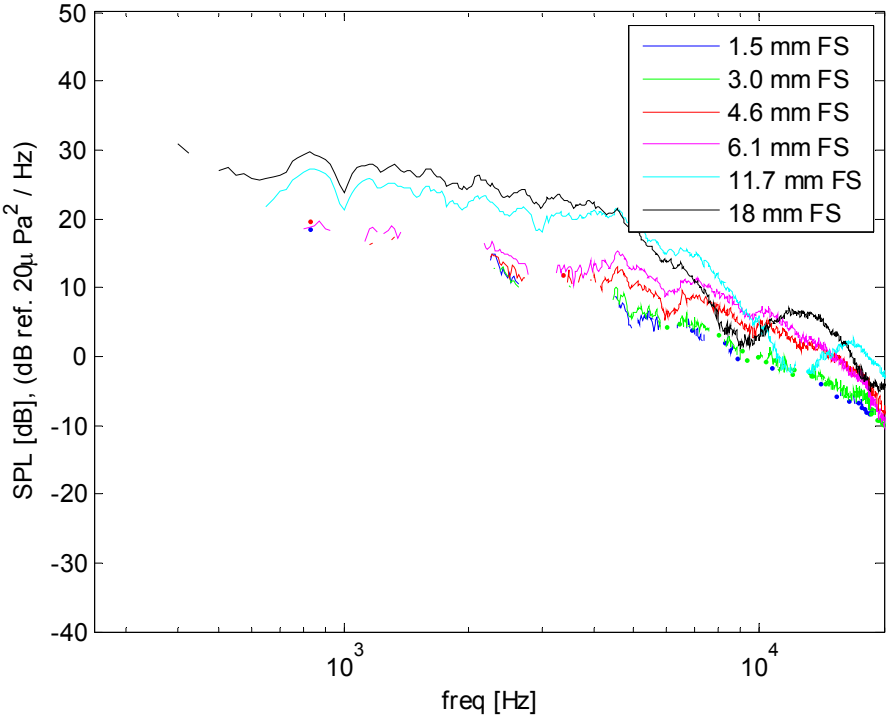

Figure 3.62 c

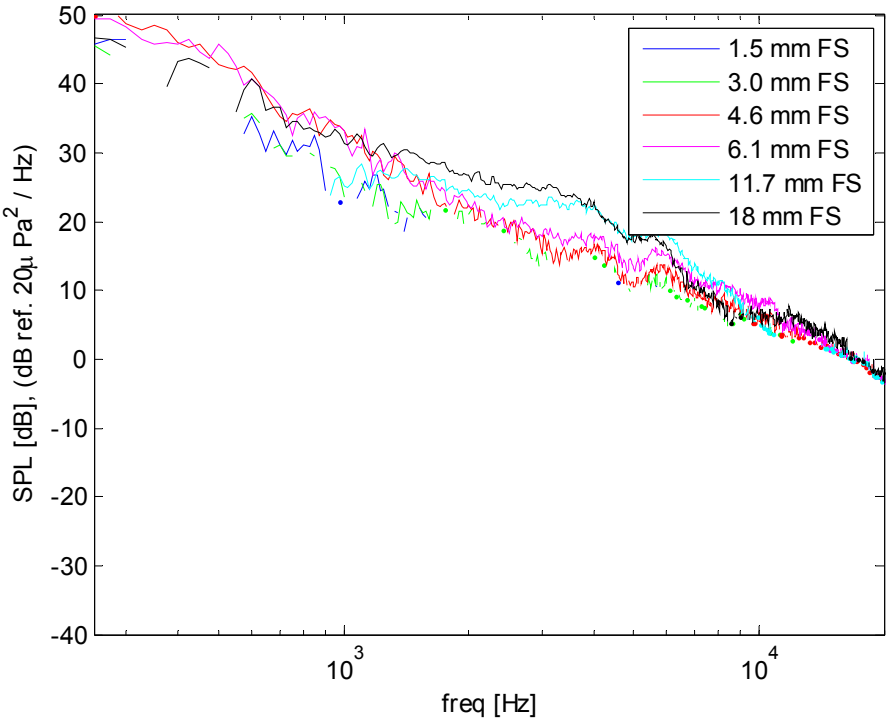

Figure 3.62 d

Figure 3.62 a-d. Far Field Acoustics from Wide Asymmetric Gaps at U_j = 60 m/s at the considered Observation Angles; a) θ = 123.5° b) θ = 97.5° c) θ = 74° d) θ = 51.5°

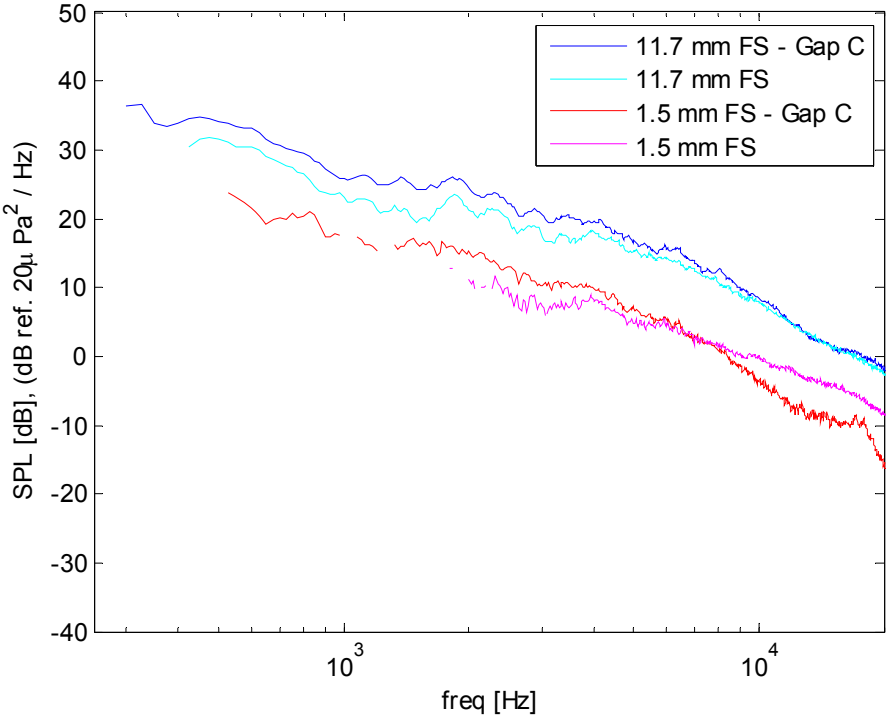

Figure 3.63 a

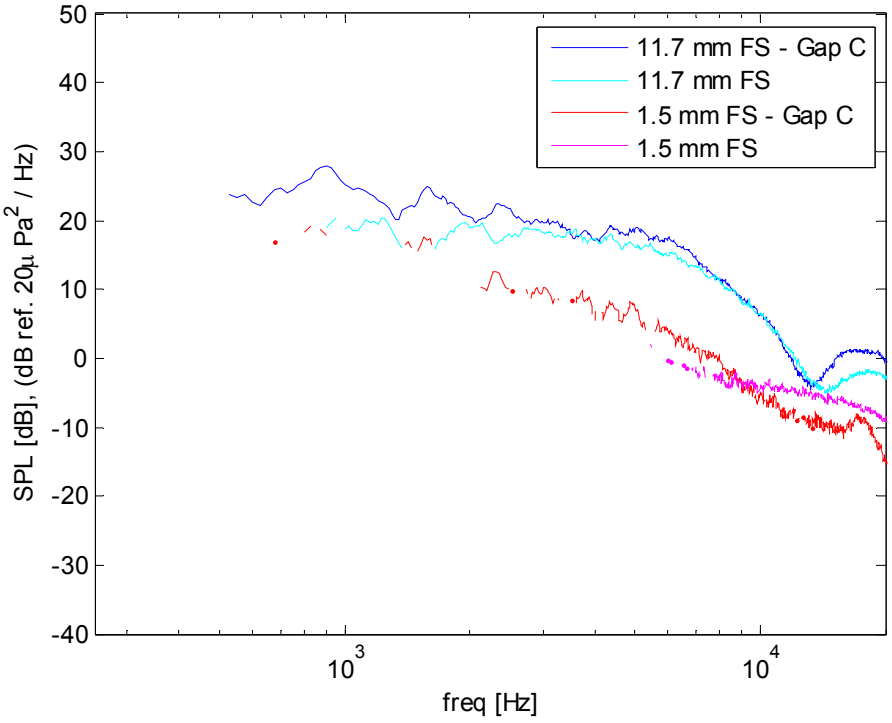

Figure 3.63 b

Figure 3.63 a-b. Far Field Acoustics from Wide Asymmetric Gaps and Forward Steps of 1.5 and 11.7 mm step height at U_j = 60 m/s at the considered Observation Angles; a) θ = 123.5° b) θ = 97.5°

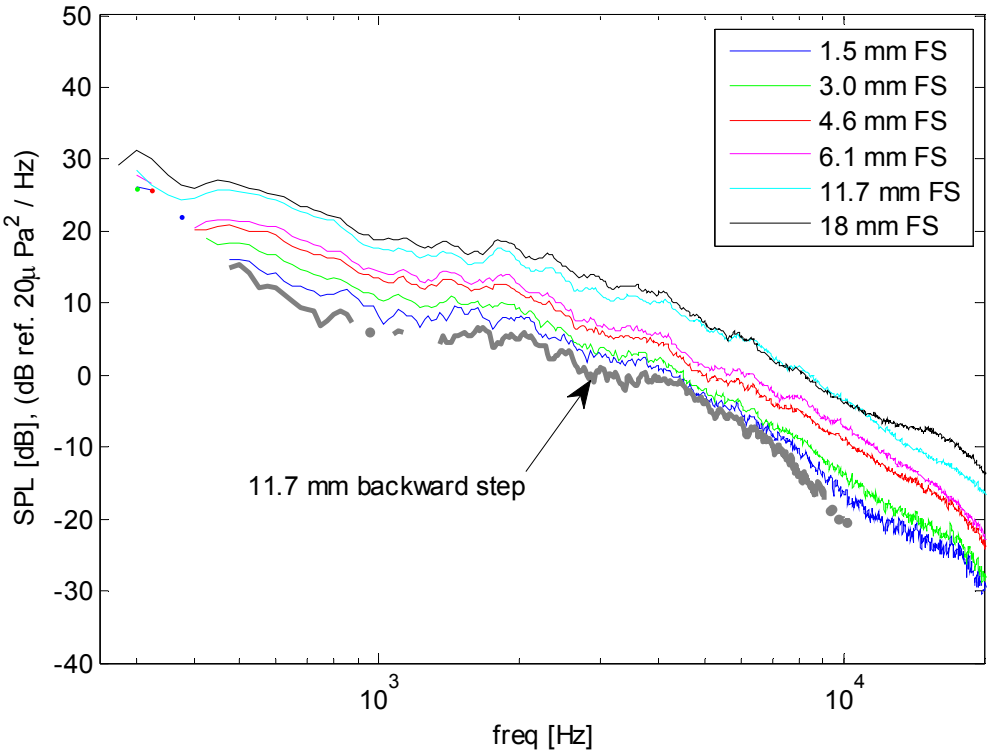

Figure 3.64 a

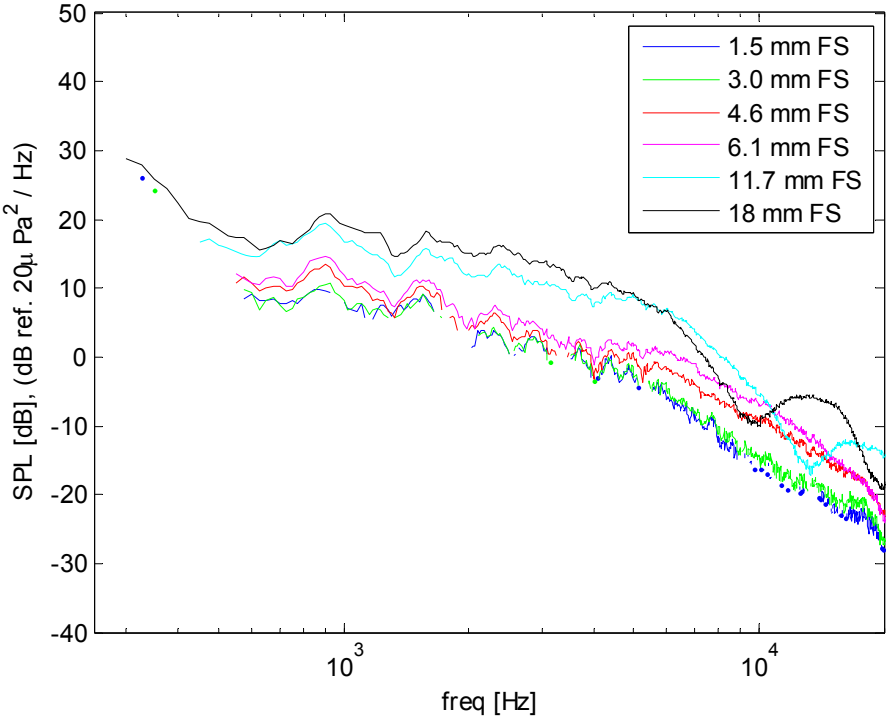

Figure 3.64 b

Figure 3.64 a-d. Far Field Acoustics from Wide Asymmetric Gaps at U_j = 45 m/s at the considered Observation Angles; a) θ = 123.5° b) θ = 97.5° c) θ = 74° d) θ = 51.5°

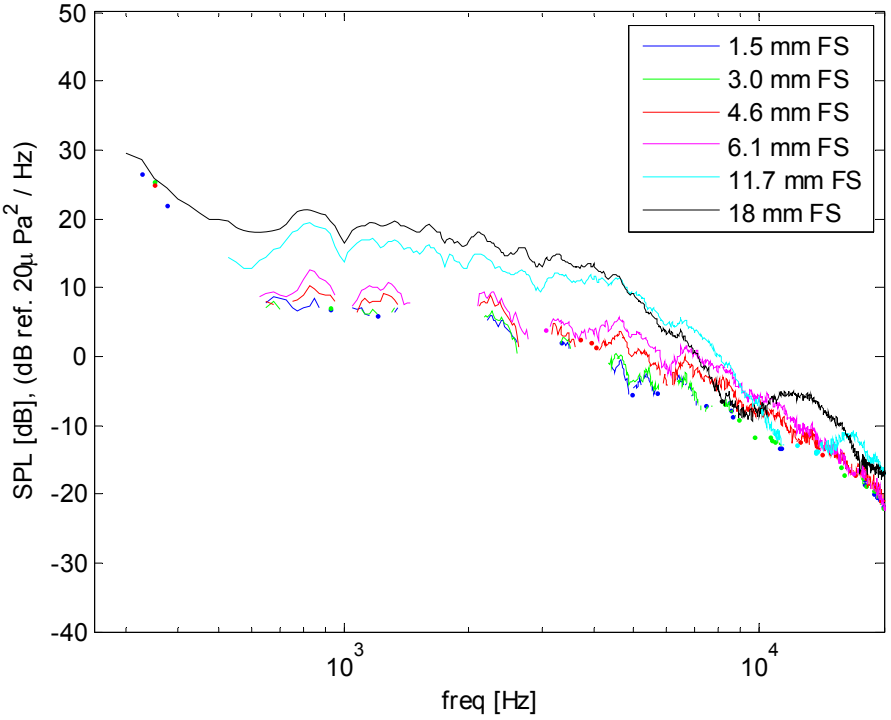

Figure 3.64 c

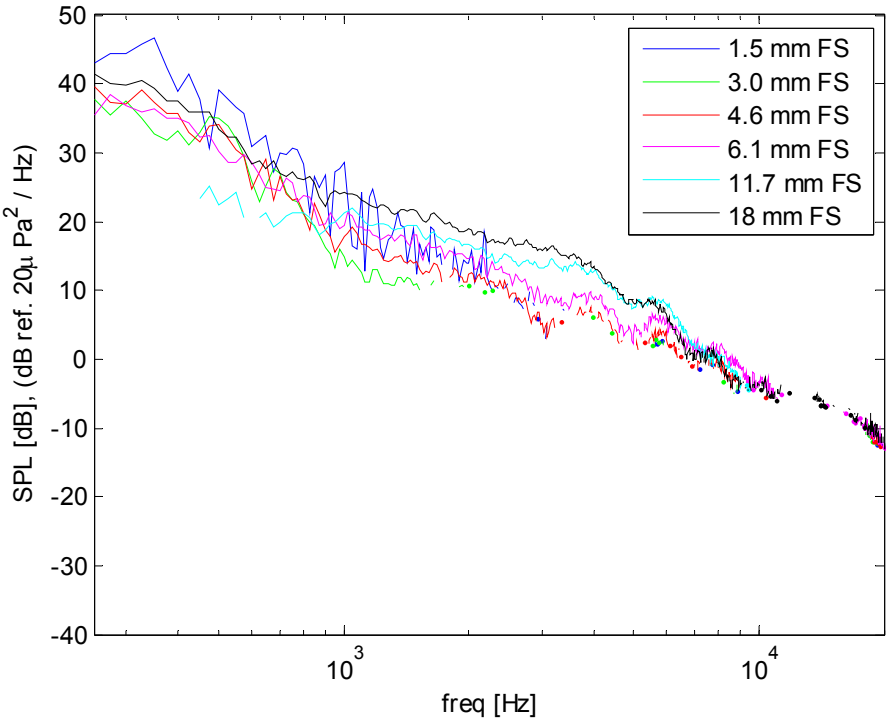

Figure 3.64 d

Figure 3.64 a-d. Far Field Acoustics from Wide Asymmetric Gaps at U_j = 45 m/s at the considered Observation Angles; a) θ = 123.5° b) θ = 97.5° c) θ = 74° d) θ = 51.5°

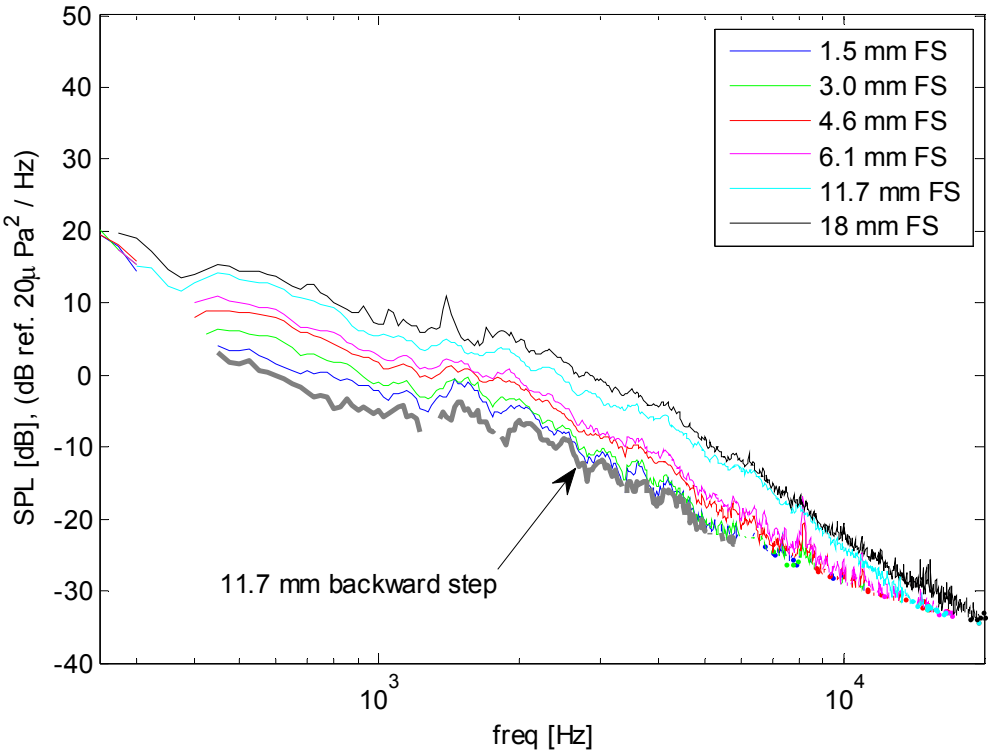

Figure 3.65 a

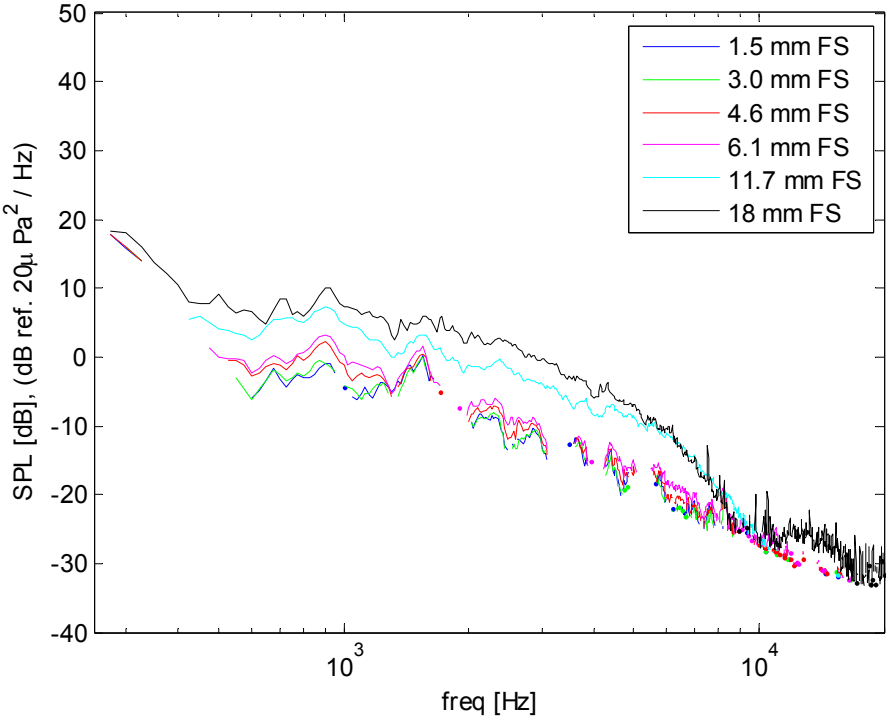

Figure 3.65 b

Figure 3.65 a-d. Far Field Acoustics from Wide Asymmetric Gaps at U_j = 30 m/s at the considered Observation Angles; a) θ = 123.5° b) θ = 97.5° c) θ = 74° d) θ = 51.5°

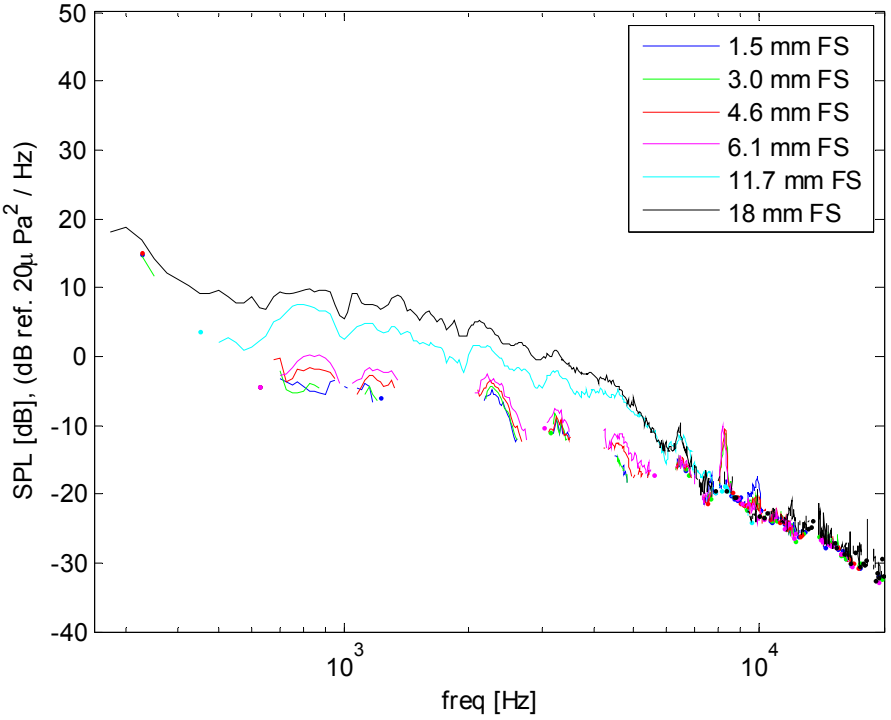

Figure 3.65 c

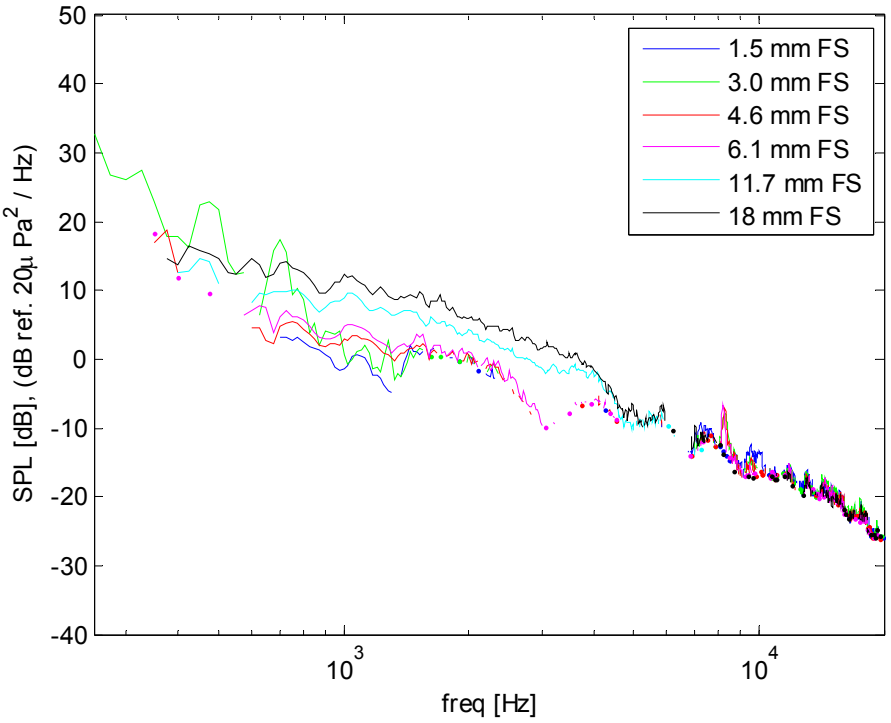

Figure 3.65 d

Figure 3.65 a-d. Far Field Acoustics from Wide Asymmetric Gaps at U_j = 30 m/s at the considered Observation Angles; a) θ = 123.5° b) θ = 97.5° c) θ = 74° d) θ = 51.5°

CHAPTER 4. CONCLUSIONS

The Virginia Tech Anechoic Wall Jet was used to investigate the far field sound and near field fluctuating wall pressure in the presence of surface discontinuities. These discontinuities took the form of forward steps, backward steps, and three different types of gap formations. For each of these configurations the far field sound was measured at multiple observation angles and for multiple velocity conditions. For the two step configurations, the wall pressure field was measured at multiple locations in front of and behind the step features. The following conclusions are made from this study.

Forward Steps

- Forward step noise is seen to increase rapidly with velocity, to be strongly dependent on step height, and shows very little directivity with varying observation angle

- Deconstructive interference in the far field highlights the acoustic non-compactness of large steps and provides further evidence of the source location as in the immediate vicinity of the exposed corner of the step

- A mixed scaling normalization of the far field is introduced which reliably collapses data not influenced by deconstructive interference that is based on step height, boundary layer height, and local maximum velocity as scaling parameters

- This new scaling implies that frequency scales on boundary layer height, δ, and local maximum velocity, U_m; while spectral levels scale on step height, h, and U_m^5

- The most upstream influence of a forward step on the wall pressure field is seen to begin with the forward separation bubble

- The downstream influence of a step was seen at all measurement locations of this study; which was over 100 step heights for the smallest step

- Low to mid frequency elevated disturbances, ranging from 250 to 4,000 Hz, in the fluctuating wall pressure field are seen to slowly recover back to undisturbed levels monotonically

- Evidence of an altered high frequency equilibrium in the wall pressure field, above approximately 4,000 Hz, is seen which needs further investigation

Backward Steps

- Backward step noise is seen to increase rapidly with velocity, to be weakly dependent on step height, and shows very little directivity with varying observation angle

- Deconstructive interference in the far field is witnessed for the largest steps placing the source at a distance relative to the step height

- Noise from a backward step is shown to be significantly weaker than for a similarly sized forward step

- A mixed scaling normalization of the far field is applied which reliably collapse the data from multiple step heights

- This new scaling implies that frequency scales on boundary layer height, δ, and local maximum velocity, U_m; while spectral levels scale on step height, h, and U_m^5

- The behavior of the wall pressure field downstream of backward steps is described, with the most significant low to mid frequency disturbances, between 250 and 4,000 Hz, happening at flow reattachment

- A slow monotonic recovery to the undisturbed wall pressure levels is seen which persists up to 50 step heights downstream; however high frequency behavior, between 4 and 20 kHz, warrants further investigation

Gaps

- Shielding of the acoustic contribution of the forward step portion of the gap geometry is seen if the forward step is buried within the wake of the backward step, leading to radiated sound from only the backward step

- As the forward step portion of the gap becomes more exposed, its contribution to the far field sound rapidly dominates

- The far field sound closely resembles a forward step only configuration for gap geometries where the forward step portion is outside of the separated region behind the backward step

REFERENCES

Addad, Y., Laurence, D., Talotte, C., Jacob, M.C., 2003, "Large Eddy Simulation of a Forward-Backward Facing Step for Acoustic Source Identification", International Journal of Heat and Fluid Flow, vol. 24, ppp. 562-571.

Alexander, N. Rasnick, M. Catlett, M., Devenport, W., and Glegg, S., 2009, "Boundary Layer Noise from Discrete Roughness Elements", AIAA-2009-3310, 15th AIAA/CEAS Aeroacoustics Conference, Miami, Florida, May 11-13, 2009.

Becker, S., Escobar, M., Hahn, C., Ali, M., Kaltenbacher, B., Basel, M., Grunewald, M., 2005, "Experimental and Numerical Investigation of the Flow Induced Noise from a Forward Facing Step", AIAA-2005-3006, 11th AIAA/CEAS Aeroacoustics Conference, Monterey, California, May 23-25, 2005.

Bradshaw, P., and Gee, M.T., 1962, "Turbulent Wall Jets with and without an External Stream", Aeronautical Research Council Reports and Memoranda, R. & M. No. 3252.

Devenport, W.J., Grissom, D., Alexander, W., Smith, B., Glegg, S., 2010, "Measurements of Roughness Noise", submitted to Journal of Sound and Vibration

Efimtsov, B.M., Kozlov, N.M., Kravchenko, S.V., Andersson, A.O., 1999, "Wall Pressure-Fluctuation Spectra at Small Forward-Facing Steps", AIAA-99-1964, 5th AIAA/CEAS Aeroacoustics Conference, Seattle, Washington, May 1999.

Efimtsov, B.M., Kozlov, N.M., Kravchenko, S.V., Andersson, A.O., 2000, "Wall Pressure-Fluctuation Spectra at Small Backward-Facing Steps", AIAA-2000-2053, 6th AIAA/CEAS Aeroacoustics Conference, Lahaina, Hawaii, June 12-14, 2000.

Farabee, T., Cassarella, M., 1986, "Measurements of Fluctuating Wall Pressure for Separated/Reattached Boundary Layer Flows", Journal of Vibration, Acoustics, Stress, and Reliability in Design, vol. 108, pp. 301-307.

Farabee, T., Cassarella, M., 1991, "Spectral features of wall pressure fluctuations beneath turbulent boundary layers", Phys. Fluids A, vol. 3, no. 10, pp. 2410-2420.

Farabee, T. M., and Zoccola, P. J., "Experimental Evaluation of Noise due to Flow over Surface Steps", 1998 ASME International Mechanical Engineering Congress and Exposition.

Grissom, D., 2007, "A Study of Sound Generated by a Turbulent Wall Jet Flow Over Rough Surfaces", Ph.D. Dissertation, AOE Department, Virginia Tech. Avail: http://scholar.lib.vt.edu/theses/available/etd-07192007-123339/ .

Grissom, D., Smith, B., Devenport, W., and Glegg, S., 2007, "Rough Wall Boundary Layer Noise: An Experimental Investigation", AIAA-2007-3418, 13th AIAA/CEAS Aeroacoustics Conference, Rome, Italy, May 20-23, 2007.

Howe, M.S., 1989, "Sound Produced by Turbulent Boundary Layer Flow Over a Finite Region of Wall Roughness, and Over a Forward Facing Step", Journal of Fluids and Structures, 3, pp. 83-96.

Jacob, M., Louisot, A., Juve, D., Guerrand, S., 2001, "Experimental Study of Sound Generated by Backward-Facing Steps Under Wall Jet", AIAA Journal, Vol. 39, No. 7, pp. 1254 – 1260.

Ji, M., and Wang, M., "LES of Turbulent Flow over Steps: Wall Pressure Fluctuations and Flow-Induced Noise", AIAA-2008-3052, 14th AIAA/CEAS Aeroacoustics Conference, Vancouver, BC, May 5-7, 2008.

Leclercq, D., Jacob, M., Louisot, A., 2001, "Forward-Backward Facing Step Pair: Aerodynamic Flow, Wall Pressure and Acoustic Caracterisation", AIAA-2001-2249, 7th AIAA/CEAS Aeroacoustics Conference, Maastricht, Netherlands, May 28-30, 2001.

Lighthill, M.J., 1952, "On Sound Generated Aerodynamically. Part 1. General Theory", Proc. R. Soc., London, vol. A211, pp. 564-587.

Mish, P.F., 2003, "An Experimental Investigation of Unsteady Surface Pressure on Single and Multiple Airfoils", Ph.D. dissertation, Aerospace and Ocean Engineering Dept., Virginia Tech, Blacksburg, VA.

Narasimha, R., Yegna Narayan, K. And Parthasarathy, S., 1973, "Parametric Analysis of Turbulent Wall Jets in Still Air", Aero. J., pp.355-359.

Wygnanski, I., Katz, Y., and Horev, E., 1992, "On the Applicability of Various Scaling Laws to the Turbulent Wall Jet", J. Fluid Mech., vol. 234, pp. 669-690.

Goody, M.C., and Simpson, R.L., 2000, "Surface Pressure Fluctuations Beneath Two- and Three-Dimensional Turbulent Boundary Layers", AIAA Journal, vol. 38, no. 10, pp. 1822-1831

Simpson, R.L., 1985, "Two-Dimensional Turbulent Separated Flow", NATO Advisory Group for Aerospace Research and Development, AGARDograph No. 287 Vol. 1

Smith, B., Alexander, N., Devenport, W.J., Glegg, S., and Grissom, D.L., 2008, "The Relationship Between Roughness Noise and the Near Field Pressure Spectrum", AIAA-2008-2409, 14th AIAA/CEAS Aeroacoustics Conference, Vancouver, BC, May 5-7, 2008.